UNIVERSITY OF CALIFORNIA
RIVERSIDE

The Use of Monocarba-*closo*-dodecaborate Carborane Anion in Catalyst Design

A Dissertation submitted in partial satisfaction
of the requirements for the degree of

Doctor of Philosophy

in

Chemistry

by

Allen L. Chan

March 2017

Dissertation Committee:

Dr. Vincent Lavallo, Chairperson
Dr. Thomas Morton
Dr. Michael Pirrung

The Dissertation of Allen L. Chan is approved:

Committee Chairperson

University of California, Riverside

Acknowledgements

First and foremost, I would like to thank my PI and mentor, Dr. Vincent Lavallo. You always brought out the best in me, and motivated me in achieving things I didn't think possible. Thank you for help making me the person and chemist that I am today.

I would like to also thank my committee members Dr. Thomas Morton and Dr. Michael Pirrung for their enlightening discussions during my Ph.D. career, as well as their input and edits of this thesis. Our collaborator, Dr. Christos Kefalidis at Universite Paul Sabatier, for the lovely computational work that he has done. Furthermore, I wish to thank UCR, in particular the chemistry faculty and staff, with emphasis on Dr. Dan Borchardt, Dr. Fook Tham, Prisciliano Saavedra, and the staff on the second floor for all their hard work.

I'll like to also thank current and former Lavallo lab members: Dr. Matt Asay, Dr. Ahmad El-Hellani, Dr. Gregorio Guisado Barrios, Dr. Hosea Nelson, Uday Chauhan, Javier Fajardo, Jr., David Woen (for weekly emotional support and trauma, as well as reading three drafts of this thesis), Gilbert Moreno, Adam Yu, Dr. James Wright, Sean Quinlivan, David Weinberger, Chris Lugo, Jess Estrada, Steven Fisher, Sarah Lee, Scott McArthur, Jack Kleinsasser, Isaac Banda, and Anton Tomich. Also, I wish to thank the graduate students outside Lavallo group, in particular Jagnandan Kaur, Eddie Laguna, Dr. Hyojik Yang, Andrew Patalano, and Dr. Jay-Ar Bendo for their friendship and collaboration. It

has been quite the adventure and I would like to thank each and every one of you for riding this roller coaster called graduate school with me.

Shout outs to Bob Armstrong (RIP) for being the coolest high school chemistry teacher, to the boricuas at UCSD who made grad school look cool, my parents and brother for all their love and support, and finally to my ride-or-die girl back in the bay: I'm coming home.

The text, figures, and schemes for the following chapters have been reproduced, in part or in their entirety, from the following published or submitted manuscripts:

Chapter 2: "Observation of Room Temperature B-Cl Activation of the $HCB_{11}Cl_{11}^-$ Anion and Isolation of a Stable Anionic Carboranyl Phosphazide." Chan, A. L.; Fajardo Jr., J.; Wright, J. H.; Asay, M.; Lavallo, V. *Inorganic Chemistry* **2013**, *52*, 12308

Chapter 3: "Synthesis and Characterization of Anionic Polybrominated Carboranyl Azides." Fajardo Jr., J.; Chan, A. L.; Tham, F. S.; Lavallo, V. *Inorganica Chimica Acta* **2014**, 422, 206

Chapter 5: "Changing the Charge: Electrostatic Effects in Pd Catalyzed Cross-Coupling" Chan, A. L.; Estrada, J.; Kefalidis, C. E.; Lavallo, V.; *Organometallics* **2016**, 35, 3257

ABSTRACT OF THE DISSERTATION

The Use of Monocarba-*closo*-dodecaborate Carborane Anion in Catalyst Design

by

Allen L. Chan

Doctor of Philosophy, Graduate Program in Chemistry
University of California, Riverside, March 2017
Dr. Vincent Lavallo, Chairperson

Carboranes are polyhedral boron-carbon molecular clusters stabilized by electron-delocalized covalent bonding throughout the skeletal framework. Once thought of as novel curiosities due to their structure and bonding, carboranes have now been applied in many diverse fields, from medicine to nanoscale engineering. Of particular interest is the icosahedral monocarba-*closo*-dodecaborate(-) ($HCB_{11}H_{11}$ anion) carborane and its derivatives due to their many unique properties. This type of carborane is well known for its extremely low nucleophilicity and considered the most weakly coordinating of all known anions. Also, these carboranes are extremely difficult to oxidize and most are stable to the most aggressive reagents. Because of these unique properties, we explore the use of functionalized carboranes as ligand R-groups in transition metal complexes for their eventual application in catalysis.

Organic azides are invaluable building blocks for synthetic chemists. Herein we report the synthesis of various carboranyl azides and some unusual reactivity during the carboranyl azide synthesis. The synthesis and characterization of the parent carboranyl

azide ($Li^+N_3CB_{11}H_{11}^-$) hexabrominated carboranyl azide ($Li^+N_3CB_{11}Br_6^-$), the perbrominated carboranyl azide ($Li^+N_3CB_{11}Br_{11}^-$), and the perchlorinated carboranyl azide ($Li^+N_3CB_{11}Cl_{11}^-$) are reported. We also report unique reactivity involving these new compounds, such as room temperature B-Cl activation of the perchlorinated carba-*closo*-dodecaborate anion.

Though the formation of Schiff bases from amines have long been used in organic chemistry, the condensation of amines to form imines with the carboranyl amine had not yet been reported at the time. Here, we report examples of imine formation with carboranyl amine as well as metal complex formation with carboranyl imines. Also, we report the synthesis of an N-hetereocyclic carbene with the hexabrominated carborane.

Phosphine ligands have been used extensively as ligands in metal catalyzed cross-coupling reactions. Metal catalyzed cross-coupling reactions are a mainstay of synthetic chemistry. Here, we report the synthesis of various carboranyl phosphine ligands and their use as R-ligands in Pd catalyzed coupling reactions. We also disclose on new and previously unreported activity with carboranyl Pd complexes with different substrates.

Table of Contents

List of Figures

List of Schemes

List of Tables

Chapter 1: Introduction

1.1 Background

Carboranes are polyhedral clusters composed of boron and carbon atoms stabilized by electron-delocalized covalent bonding throughout the skeletal framework. The carborane of interest in my projects has been the carba-*closo*-dodecaborate(-) anion, $CB_{11}H_{12}^-$ (Figure 1-1). The parent $CB_{11}H_{12}^-$ carborane was first synthesized by Knoth in 1967[1] from decaborane (synthesized from inexpensive $NaBH_4$)[2]. More than two decades later, the procedure was improved by Stibr[3] in 1984 and Reed[4] in 2010; their methods were used to synthesize the parent carborane throughout this dissertation. More recently, it has been demonstrated that $CB_{11}H_{12}^-$ can also be synthesized from the $B_{11}H_{11}^-$ cluster (also synthesized from $NaBH_4$)[5] via a carbon insertion[6]. Scheme 1-1 and 1-2 illustrate the methods to synthesize the parent carborane. Non-labeled vertices are B-H bonds, and this simplification will be used throughout the thesis. One of the most interesting features of this icosahedral carborane is its unprecedented electronic stability and bonding. The electron counting of carboranyl clusters can be understood through using Wade's rules[7], where the electrons are assigned at the vertices and not at

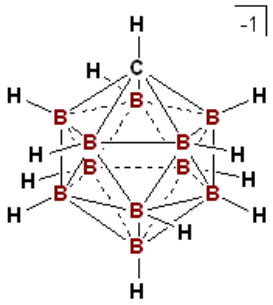

Figure 1-1 Carba-*closo*-dodecaborate(-) anion

the edges or faces[8]. Each BH vertex is an ordinary sigma BH bond, where two electrons are needed to make the bond. Since there are twelve vertices and there are 50 electrons available, the 26 remaining electrons are delocalized throughout the skeletal cage, where the boron atoms form 3-center-2-electron bonds. The negative charge of the carborane is therefore delocalized throughout the carborane cage and is weakly coordinating to its corresponding cation. The parent carborane and its derivatives are extremely stable, and considered some of the most stable clusters in all chemistry[9]. Having delocalized σ bonding throughout the cage, these icosahedral clusters have a very large HOMO-LUMO gap, greater than that of π aromatic systems[10]. The high stability of the carborane cage for many in this class makes it unsusceptible to most oxidants and reductants.

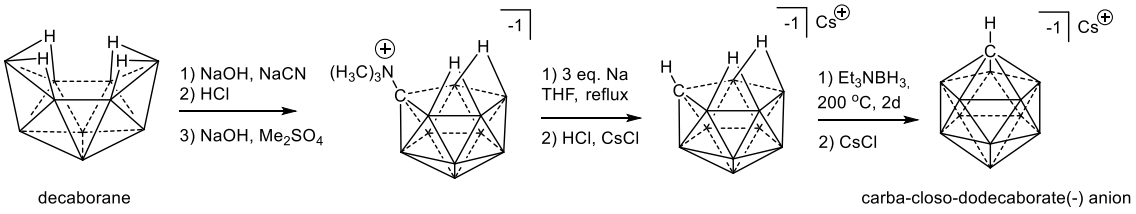

Scheme 1-1 Synthesis of carba-*closo*-dodecaborate(-) anion from decaborane. Note: Non-labeled vertices are B-H bonds

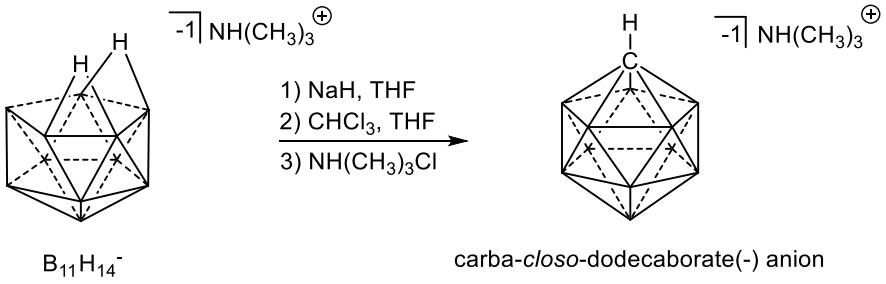

Scheme 1-2 Synthesis of carba-*closo*-dodecaborate(-) anion from $B_{11}H_{14}^-$ cluster. Note: unlabeled vertices are B-H bonds

1.2 B-H substitution

The carborane exhibits interesting electronic properties as the B-H bonds are amenable to electrophilic aromatic substitution in a manner similar to benzene. The parent carborane can be halogenated to useful hexhalo and perhalo derivatives[11] (Scheme 1-3).

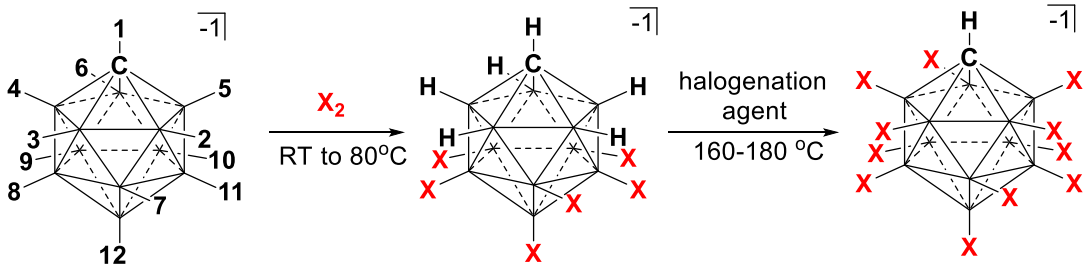

Scheme 1-3 General conditions for halogenation of the carborane cluster. Far left icoshahedran shows numbering vertex numbering of cluster, where in this case each number represents a hydrogen

The carborane cage is polarized such that substitution occurs at the 12th position of the cluster (antipodal to the carbon), followed by the lower pentagonal belt (positions 7-11), and finally the upper pentagonal belt (positions 2-6). Scheme 1-3 shows the general conditions to perform the halogenation. In addition to halogens, the carborane cage can be permethylated[12], and a mixed halogenated and methylated carborane can also be achieved[13]. Cluster halogenation and methylation allows for fine-tuning the electronic properties and the basicity of the carborane system. The parent carborane and its polyhalo and polyalkyl derivatives are among the least nucleophilic species known[14] and their conjugate acids are extremely strong Brønsted acids, where some are found to be strongest to date[15]. The coordinative ability of the parent carborane anion is furthered weakened when the hydrogen atoms are replaced with halogens or alkyl groups; the halogens withdraw electron density from the cage rendering it even less nucleophilic, while the alkyl groups increase solubility in organic solvents without losing its basicity[16]. In addition to electronic tunability, the halogenated carboranes can be useful in preventing cyclometalation in metal complexes, in contrast to the analogous metal complex with the parent carborane, as seen in recent literature[17]. For these reasons, we implement the halogenated cluster in our design of ligands with the goal of making novel catalysts.

After halogenation, the B-X vertices can also be substituted through palladium cross coupling reactions. First demonstrated in 1980[18], the reactions typically involve iodinating the boron vertices followed by palladium catalyzed cross coupling to create B-

C, B-P, B-N, and B-S bonds[19]. Recently, Spokoyny reported B-N, B-O, and B-CN bond by bromination of the boron vertices via Pd cross coupling reactions, the first examples of Pd cross-coupling with a B-bromo-functionalized carborane[20].

1.3 C-H substitution

The acidity of the C-H proton of the parent anion, $CB_{11}H_{12}^-$, is comparable to that of acetylene, and the C-functionalization of the carborane can be done by deprotonation with *n*-butyllithium followed by reaction with electrophiles, such as chlorodiisopropylphosphine or tosyl azide (Scheme 1-4). Many of the carboranes seen in this thesis involve C-H substitution, and will be discussed later in further detail.

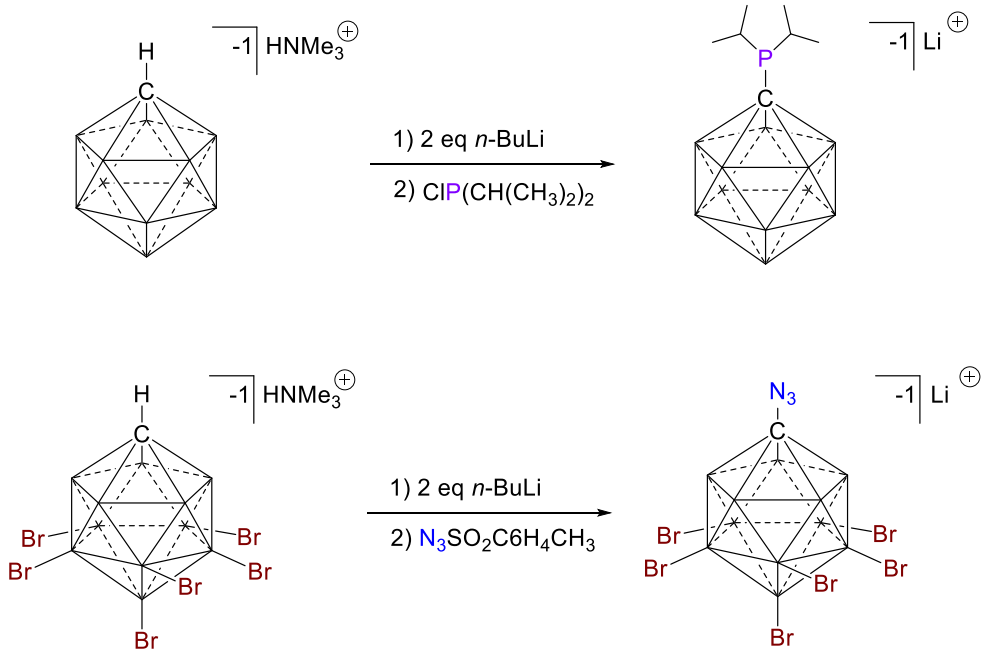

Scheme 1-4 Examples of C functionalization. Note: unlabeled vertices are B-H bonds

1.4 Applications of the Anionic Carborane

The anionic carborane has various applications due to its unique properties. One example is the use of carboranes as stabilizers for highly reactive cations. The anionic carboranes have been used to isolate reactive cations, such as the *t*-butyl cation[21], paracyclophane radical cations[22], and azafullerenes[23,24]. The carborane cluster alone can also be used to catalyze reactions. The $(Ph_3P)Ag^+HCB_{11}H_5Br_6$ can catalyze the hetereo Diels-Alder reaction between N-benzylidene and Danishefsky's diene in quantitative yields[25], as well as Friedel-Crafts proton-catalyzed coupling of fluoroarenes in high yields promoted by R_3Si^+ cation stabilized by the $HCB_{11}H_5Cl_6^-$ counteranion[26]. Furthermore, the anionic carborane has the potential to be used as inert and noncorrosive electrolytes for Mg batteries[27,28]. The purpose of our work is to use the anionic carborane in a novel way as ligand R-groups on metal complexes, and research their effects as catalysts in chemical reactions. The following chapters discuss the journey in pursuit of this goal.

1.5 References

(1) Knoth, W. H. *Journal of the American Chemical Society* **1967**, *89*, 1274.

(2) Miller, H. C.; Miller, N. E.; Muetterties, E. L. *Inorganic Chemistry* **1964**, *3*, 1456.

(3) Plesek, J.; Jelinek, T.; Drdakova, E.; Hermanek, S.; Stibr, B. *Collection of Czechoslovak Chemical Communications* **1984**, *49*, 1559.

(4) Reed, C. A. *Accounts of Chemical Research* **2010**, *43*, 121.

(5) Dunks, G. B.; Ordonez, K. P. *Inorganic Chemistry* **1978**, *17*, 1514.

(6) Andreas Franken, B. T. K., Jens Rudolph, Photon Rao, Bruce C. Noll, Josef Michl *Collection of Czechoslovak Chemical Communications* **2001**, *66*, 1238.

(7) Wade, K. *Electron Deficient Compounds*; Nelson: London, 1971.

(8) Olah, G. A.; Wade, K.; Williams, R. E. *Electron Deficient Boron and Carbon Clusters - General Concepts and Definitions*, 1991.

(9) Grimes, R. N. *Carboranes, 2nd Edition*, 2011.

(10) McKee, M. L. *Inorganic Chemistry* **2002**, *41*, 1299.

(11) Jelinek, T.; Plesek, J.; Hermanek, S.; Stibr, B. *Collection of Czechoslovak Chemical Communications* **1986**, *51*, 819.

(12) King, B. T.; Janoušek, Z.; Grüner, B.; Trammell, M.; Noll, B. C.; Michl, J. *Journal of the American Chemical Society* **1996**, *118*, 3313.

(13) Stasko, D.; Reed, C. A. *Journal of the American Chemical Society* **2002**, *124*, 1148.

(14) Koppel, I. A.; Burk, P.; Koppel, I.; Leito, I.; Sonoda, T.; Mishima, M. *Journal of the American Chemical Society* **2000**, *122*, 5114.

(15) Balanarayan, P.; Gadre, S. R. *Inorganic Chemistry* **2005**, *44*, 9613.

(16) Tsang, C.-W.; Yang, Q.; Sze, E. T.-P.; Mak, T. C. W.; Chan, D. T. W.; Xie, Z. *Inorganic Chemistry* **2000**, *39*, 5851.

(17) Estrada, J.; Lee, S. E.; McArthur, S. G.; El-Hellani, A.; Tham, F. S.; Lavallo, V. *Journal of Organometallic Chemistry* **2015**, *798, Part 1*, 214.

(18) Zakharkin, L. I.; Kovredov, A. I.; Ol'Shevskaya, V. A.; Shaugumbekova, Z. S. *Izvestiya Akademii Nauk SSSR* **1980**, 1691.

(19) Olid, D.; Nunez, R.; Vinas, C.; Teixidor, F. *Chemical Society Reviews* **2013**, *42*, 3318.

(20) Dziedzic, R. M.; Saleh, L. M. A.; Axtell, J. C.; Martin, J. L.; Stevens, S. L.; Royappa, A. T.; Rheingold, A. L.; Spokoyny, A. M. *Journal of the American Chemical Society* **2016**, *138*, 9081.

(21) Nava, M.; Stoyanova, I. V.; Cummings, S.; Stoyanov, E. S.; Reed, C. A. *Angewandte Chemie International Edition* **2014**, *53*, 1131.

(22) Jalilov, A. S.; Han, L.; Nelsen, S. F.; Guzei, I. A. *Journal of Organic Chemistry* **2013**, *78*, 11373.

(23) Kim, K. C.; Hauke, F.; Hirsch, A.; Boyd, P. D. W.; Carter, E.; Armstrong, R. S.; Lay, P. A.; Reed, C. A. *Journal of the American Chemical Society* **2003**, *125*, 4024.

(24) Xie, R. H.; Bryant, G. W.; Sun, G. Y.; Nicklaus, M. C.; Heringer, D.; Frauenheim, T.; Manaa, M. R.; Smith, V. H.; Araki, Y.; Ito, O. *Journal of Chemical Physics* **2004**, *120*, 5133.

(25) Patmore, N. J.; Hague, C.; Cotgreave, J. H.; Mahon, M. F.; Frost, C. G.; Weller, A. S. *Chemistry-a European Journal* **2002**, *8*, 2088.

(26) Allemann, O.; Duttwyler, S.; Romanato, P.; Baldridge, K. K.; Siegel, J. S. *Science* **2011**, *332*, 574.

(27) Tutusaus, O.; Mohtadi, R.; Arthur, T. S.; Mizuno, F.; Nelson, E. G.; Sevryugina, Y. V. *Angewandte Chemie International Edition* **2015**, *54*, 7900.

(28) McArthur, S. G.; Geng, L. X.; Guo, J. C.; Lavallo, V. *Inorganic Chemistry Frontiers* **2015**, *2*, 1101.

Chapter 2: In the Pursuit of Carboranyl Azides: New Reactions and Reactivity, Part 1

2.1 Introduction

Since their discovery in the late 1800s, organic azides have become invaluable building blocks for synthetic chemists[1]. Typical organic azides feature an N_3 moiety linked to a two to four coordinate carbon atom[2,3]. Exceptions to this rule are azides derived from icosahedral carboranes[4-7], where the N_3 fragment is bound to a 6-coordinate carbon center[8-14]. The first C-functionalized carboranyl azide, which was prepared by deprotonation of *ortho*-carborane ($H_2C_2B_{10}H_{10}$) derivatives and subsequent treatment of the carbanion with tosyl azide, was reported by Blanch in 1994[4]. Although the chemistry of such azides remains relatively unexplored, they can be photolyzed to produce transient carboranyl nitrenes and reacted with phosphines[5] to afford Staudinger addition products. We wished to expand on this chemistry by initially focusing our efforts on the perhalogenated carba-*closo*-dodecaborate carborane ($HCB_{11}X_{11}^-$). Perhalogenated carba-*closo*-dodecaborate clusters are exceptionally weakly coordinating anions that have allowed isolation of a variety of fundamentally important and exotic cationic species. The property that distinguishes them from other "non-coordinating" counteranions, such as $B(C_6F_5)_4^-$ and SbF_6^-, is that they are exceptionally resistant to bond cleavage or oxidation by potent electrophilic cations[15]. This combination of poor Lewis basicity and inertness renders these anions ideal for silylium

catalysis and related processes[16-18]. Aside from the anomalous reactivity of $HCB_{11}F_{11}^-$ toward the hydroxide ion[19], the other perhalogenated congeners of the carba-*closo*-dodecaborate cluster are also extremely unreactive toward cluster degradation or B−X bond cleavage by strong Brønsted or Lewis bases. However, the C−H bond of these clusters can be deprotonated with strong bases to generate dianionic species that can be carbon-functionalized with electrophiles[20]. Recently, we reported the first example of a controlled reaction that allows for the nucleophilic substitution of a B-Cl bond of the $HCB_{11}Cl_{11}^-$ anion[21]. Specifically, we disclosed a base-induced cycloaddition reaction between the $HCB_{11}Cl_{11}^-$ anion and simple organic azides that leads to carborane-fused triazoles with unusual aromatic character. Although very thermodynamically favorable, this reaction occurs at temperatures above 100 °C. More recently, we reported that one of these heterocycles can be rendered zwitterionic through alkylation and chemically reduced to form the first isolable triazole radical anion[22]. Here we report the observation of two competing reactions that occur with the $HCB_{11}Cl_{11}^-$ anion at ambient temperature, namely, B-Cl activation/cycloaddition and electrophilic N_3 transfer. Further, we discuss the isolation of an unusual anionic lithium carboranyl phosphazide complex.

2.2 Results and Discussion

We are interested in functionalized perhalogenated carboranes for use as ligand building blocks for catalyst design. An interesting molecule that we have been targeting

is the anionic perchlorinated carba-closo-dodecaborate azide $N_3CB_{11}Cl_{11}^-$, which should be a versatile synthon. Carbon-functionalized azides of the carba-closo-dodecaborate anion are extremely rare. In fact, only a single report exists from Michl et al.[6], in which a permethylated carborane azide is prepared by the trapping of a highly reactive naked C-vertex carborane cluster with N_3^-. We attempted to prepare the perchlorinated carborane azide $N_3CB_{11}Cl_{11}^-$ in a direct route, analogous to Blanch's synthesis of o-carborane azides[4], via deprotonation of **1**, followed by quenching with tosyl azide (Scheme 2-1).

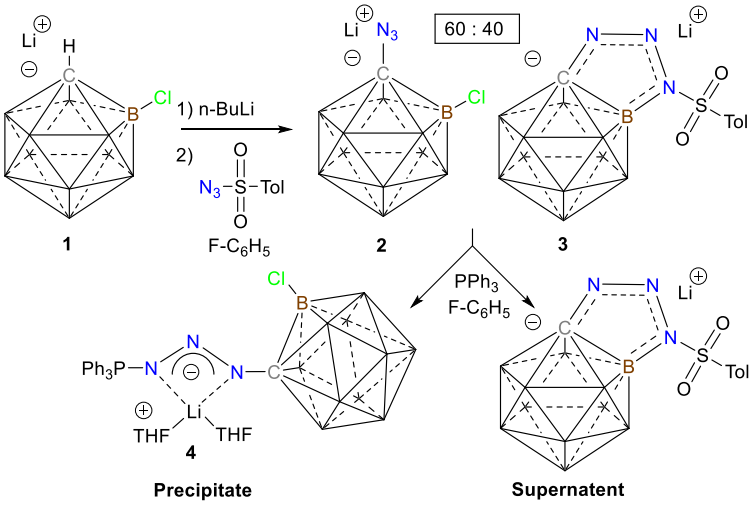

Scheme 2-1 Reaction of **1** with *n*-BuLi and treated with tosyl azide. N_3 transfer is observed to afford azide **2** along with the unexpected formation of heterocycle **3**. Treatment of the mixture with PPh_3 induces precipitation of the anionic phosphazide **4** (unlabeled vertices are B-Cl)

^{11}B NMR spectroscopy monitoring of the reaction indicates the formation of two products in a ratio of approximately 60:40. The minor product displays seven resonances in the ^{11}B NMR, which indicates a disruption of the local C_{5v} symmetry in the cluster. Regardless of the reaction temperature, order of addition, or solvent, the ratio of the two compounds stays approximately the same. Analysis of the mixture by high-resolution mass spectrometry confirmed the formation of $N_3CB_{11}Cl_{11}^-$. IR spectroscopy also confirms the formation of the azide **2** (absorbance at 2143 cm^{-1}). The ionic compounds **2** and **3** have very similar solubility, and all attempts to separate these two species were unsuccessful. However, crystallization of the crude reaction mixture led to a crystal of **3**, which was suitable for a single-crystal X-ray diffraction study (Figure 2-1).

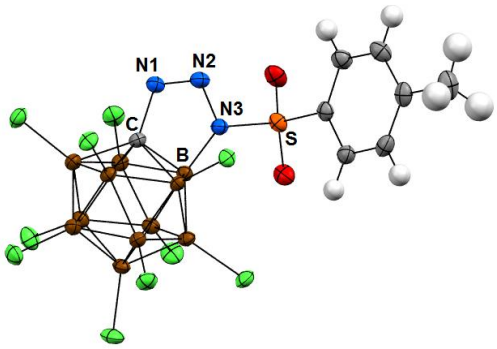

Figure 2-1 Solid state structure of the heterocycle **3** (Color code: C = grey, H = white, N=blue, Cl = green, B = brown, O = red, S = orange)

In the solid state, **3** shows no interaction with any lithium countercations in the lattice (closest contact 4.117 Å). Similar to the analogous phenyl-substituted heterocycle that was recently reported[21], all five atoms of the heterocyclic portion of **3** are coplanar (sum of internal pentagon angles = 540°) and the nitrogen-bearing tosyl group (N_3) is sp^2

- hybridized (sum of angles = 360°). The N1-N2 (1.267(3) Å) and N2-N3 (1.382(2) Å) bond lengths are asymmetric but still significantly shorter than standard N-N single bonds (1.450 Å). The C-B portion of the pentagon is contracted (C1-B1 = 1.679(3) Å) with respect to the other C-B bonds in the cluster (average C-B bond lengths = 1.733 Å), which is close to the phenyl-substituted derivative and a characteristic of exocluster delocalization[21]. In the hopes of altering the solubility of the azide **2**, we sought to derivatize it via a Staudinger reaction to form an iminophosphorane. Typically, N_2 is readily extruded from azides upon contact with a phosphine. However, when the phosphine or azide reaction partner is sterically demanding, the intermediate phosphazide adducts can be isolable species. Kennedy recently reported the preparation of neutral phosphazides from *ortho*-carborane azides[5], which are stable in the absence of light and heat. Thus, the reaction mixture was treated with a solution of triphenylphosphine in fluorobenzene, but no visible sign of N_2 elimination was observed. Over 24 h, large colorless crystals formed in the flask and were isolated. A single-crystal X-ray diffraction study confirmed that N_2 had been retained and revealed the unexpected formation of the anionic lithium phosphazide complex **4**, which exists in the s-trans configuration (Figure 2-2).

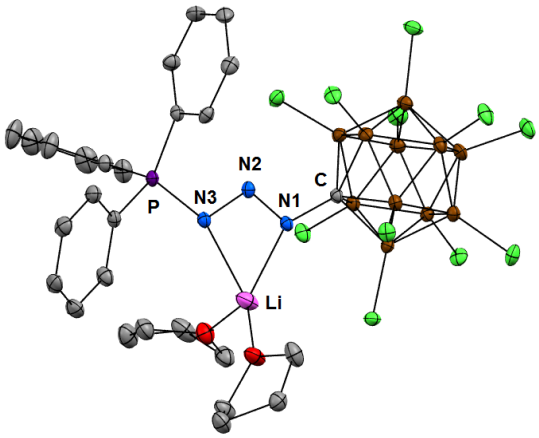

Figure 2-2 Solid state structure of phosphazide **4** (Color code: C = grey, H = white, N=blue, Cl = green, B = brown, O = red, P = purple, Li = pink)

In the solid state, two tetrahydrofuran (THF) molecules are bound to the lithium cation, and **4** acts as a bidentate ligand, coordinating via the terminal nitrogen atoms (N1 and N3) of the N3 unit. Both the N1-N2 (1.284(2) Å) and N2-N3 (1.338(2) Å) distances are short, which suggests π delocalization between the three atoms. Interestingly, even though the carborane anion is acting as a ligand substituent to the N1 atom of the phosphazide core, no intramolecular contacts with the chlorine atoms are observed. Solid-state CPMAS ^{31}P NMR spectroscopy shows a single phosphorus resonance at +38 ppm, attributed to the static structure of **4**. A small shoulder resonance of the main signal might be attributed to a population of the less favorable s-*cis* isomer. Phosphazide **4** is completely insoluble in nonpolar solvents (e.g., hexane, C_6H_6, FC_6H_5) but readily dissolves in THF and CH_2Cl_2. The ^{31}P NMR spectrum of **4** in THF shows a resonance at +21 ppm. The difference in chemical shift between the solution

and solid-state spectra (17 ppm) of **4** might be explained by solvation effects. Interestingly, a signal at -5 ppm corresponding to free PPh_3 is always present in the THF solution of **4** at ambient temperature. Repeated washing of **4** with copious amounts of FC_6H_5, a solvent in which PPh_3 is readily soluble, does not remove the resonance that corresponds to free phosphine. It was postulated that in a THF solution, an equilibrium exists where the PPh_3 moiety dissociates from **4** to reform the azide **2**. Variable-temperature NMR experiments support the presence of an equilibrium between PPh_3, **2**, and **4** in a THF solution and allow for determination of the equilibrium constant at a given temperature. At +60 °C, only PPh_3 can be detected in the ^{31}P NMR spectrum, which is supportive of complete dissociation of the complex at elevated temperatures. Cooling the sample to -35 °C shifts the equilibrium completely to complex **4**, which is evidenced by the presence of only a single resonance in the ^{31}P NMR spectrum (+22 ppm). In contrast, ^{31}P NMR analysis of **4** dissolved in CD_2Cl_2 shows only a single resonance at +33 ppm corresponding to **4**, which is close to the solid-state NMR value (+38 ppm) and suggests the absence of equilibrium in this solvent. IR analysis of the phosphazide **4** in the solid state and in a CH_2Cl_2 solution shows no absorption band for the azide **2** and confirms that complex **4** does not dissociate in this solvent. In contrast, when **4** is dissolved in THF and analyzed by IR, the absorbance for the azide **2** is apparent. The differences in the stability of complex **4** in THF and CH_2Cl_2 can be explained by the stronger coordinative abilities of THF, which likely reversibly sequesters the lithium cation and disrupts the complex. Unlike neutral phosphazides derived from

o-carborane, complex **4** is not light- or air-sensitive. Furthermore, it shows no sign of N_2 loss upon heating for 24 h at 150 °C in FC_6H_5 (at this temperature **4** is soluble). In order to probe whether the stability of the phosphazide was related to its complexation with the lithium ion, we conducted an *in situ* cation metathesis reaction. When **4** is stirred with $N(butyl)_4Br$ in FC_6H_5, it dissolves at ambient temperature, indicating that cation metathesis had occurred. Subsequent heating of the solution at 80 °C for 48 h shows by ^{31}P NMR partial decomposition of the phosphazide to unidentified phosphorus-containing species. The lithium cation likely brings enhanced stability to the phosphazide by preventing formation of the four-membered P-N-N-N ring transition state necessary for N_2 extrusion.

2.3 Conclusion

A surprising reaction where a B-Cl bond of one of the least reactive anions is cleaved and substituted at room temperature is reported. Similar reactions under mild conditions with 1,3-dipoles other than tosyl azide might be possible. The competing reaction to form the anionic azide **2** demonstrates that such perhalogenated azides are stable entities and accessible in a direct manner. Isolation of the phosphazide **4** is the first example of an anionic phosphine azide adduct and opens up the possibility of preparing other charged carborane-containing

phosphazide derivatives. The preparation of such species is actively under investigation.

2.4 Experimental

Unless otherwise stated, all manipulations were carried out using standard Schlenk or glovebox techniques (O_2, H_2O < 1ppm) under a dinitrogen or argon atmosphere. Solvents were dried on K or CaH_2, and distilled under argon before use. Trimethylammonium carborane[11] ($HNMe_3HCB_{11}Cl_{11}$) and tosyl azide[5] were prepared by literature methods. Reagents were purchased from commercial vendors and used without further purification. NMR spectra were recorded on Bruker Avance 300 MHz, Varian Inova 300 MHz, Varian Inova 400 MHz, Varian Inova 500 MHz, or Bruker Avance 600 MHz spectrometers. NMR chemical shifts are reported in parts per million (ppm). The CPMAS ^{31}P NMR was done on the Bruker Avance 600 MHz with a spin rate of 10 KHz in a 4mm rotor using the CP-MAS probe. ^{1}H NMR chemical shifts and ^{13}C NMR chemical shifts were referenced to residual protio solvent. ^{11}B NMR chemical shifts were externally referenced to BF_3OEt_2. ^{31}P NMR chemical shifts were externally referenced to 80% H_3PO_4 in H_2O and PPh_3 for the Bruker Avance 300 MHz and Bruker Avance 600 MHz, respectively. The infrared spectra were collected on Bruker Equinox 55 FTIR and Pike Technologies GladiATR MB3000 instruments. The mass spectra were collected on an Agilent LCTOF Multimode-ESI/APCI with direct injection.

Synthesis and Spectroscopic Data

Mixture of $N_3CB_{11}Cl_{11}^-$ (2) and $C_7H_7O_2SN_3CB_{11}Cl_{10}^-$ (3)

$HNMe_3HCB_{11}Cl_{11}$ (5 g, 8.59 mmol) was first deprotonated with *n*-butyllithium (2.7 eq., 9.3 mL, 23.2 mmol, 2.5 M in hexanes) in THF and allowed to stir overnight. The solvent was removed under vacuum, and the precipitate was washed twice with hexanes. The solid was re-dissolved in $F\text{-}C_6H_5$ and immediately treated with a $F\text{-}C_6H_5$ solution of tosyl azide (1.1 eq., 1.86 g, 9.45 mmol) at -35°C over 15 minutes. The reaction mixture was stirred and allowed to slowly warm to room temperature overnight, where a precipitate of $LiO_2SC_7H_7$/LiCl formed. The mixture was filtered to remove the salt byproduct and the solution concentrated under vacuum. The residue was washed with hexanes (2 x 10 mL) and dried to afford a white residue containing **2** and **3**. **Note:** the two compounds could not be separated. Although the ^1H and ^{13}C NMR spectra of the mixture appear to correspond to the pure heterocycle **3**, the ^{11}B NMR spectrum reveals the presence of **2** (azide **2** has no protons and the carborane carbon is not observed).

^1H NMR (400 MHz, THF-d_8, 25°C): $\delta =$ 7.91 (d, $^3J(H,H)$ = 8.2 Hz, 2H, aryl), 7.34 (d, $^3J(H,H)$ = 8.2 Hz, 2H, aryl), 2.36 (s, 3H, CH_3); ^{13}C NMR (101 MHz, THF-d_8, 25°C): $\delta =$ 146.9 (C, aryl), 136.1 (C, aryl), 130.6 (CH, aryl), 129.7 (CH, aryl), 84.0 (C, Carborane), 67.7 (CH_2, THF), 25.3 (CH_2, THF), 21.9 (CH_3); ^{11}B NMR (96 MHz, $F\text{-}C_6H_5$, 25°C): $\delta =$ -4.1, -7.2, -10.6, -11.7, -16.5. HRMS calculated for **2** ($[M]^-$) 562.7697, found: 562.7695. HRMS calculated for **3**

([M]$^-$) 681.8195, found: 681.8177. Solid-state IR: N_3 azide stretch = 2087, 2143 cm^{-1}. THF solution IR spectrum: N_3 azide stretch = 2090, 2143 cm^{-1}.

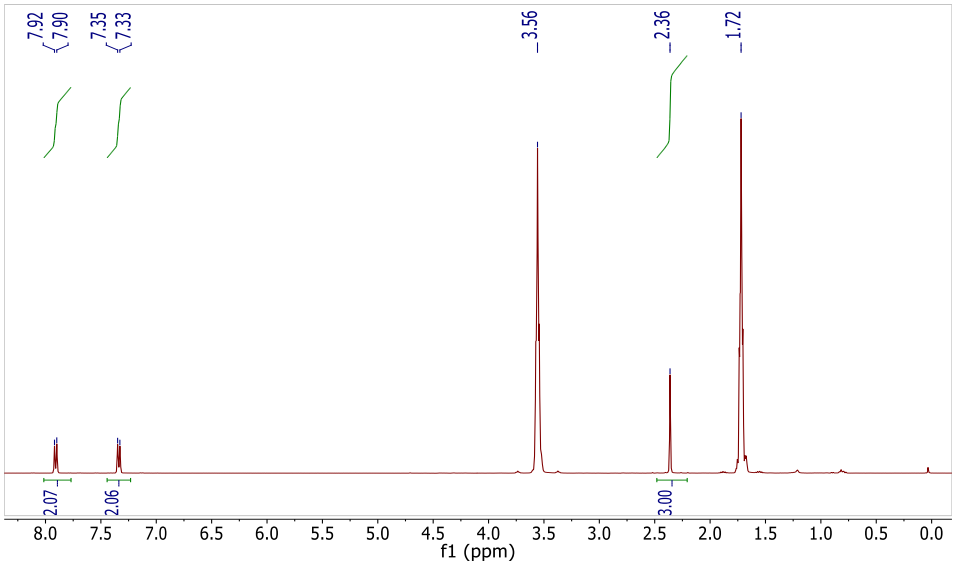

Figure 2-3 ^{1}H NMR spectrum of the mixture of compounds **2** and **3** (25°C, 400 MHz, THF-d_8)

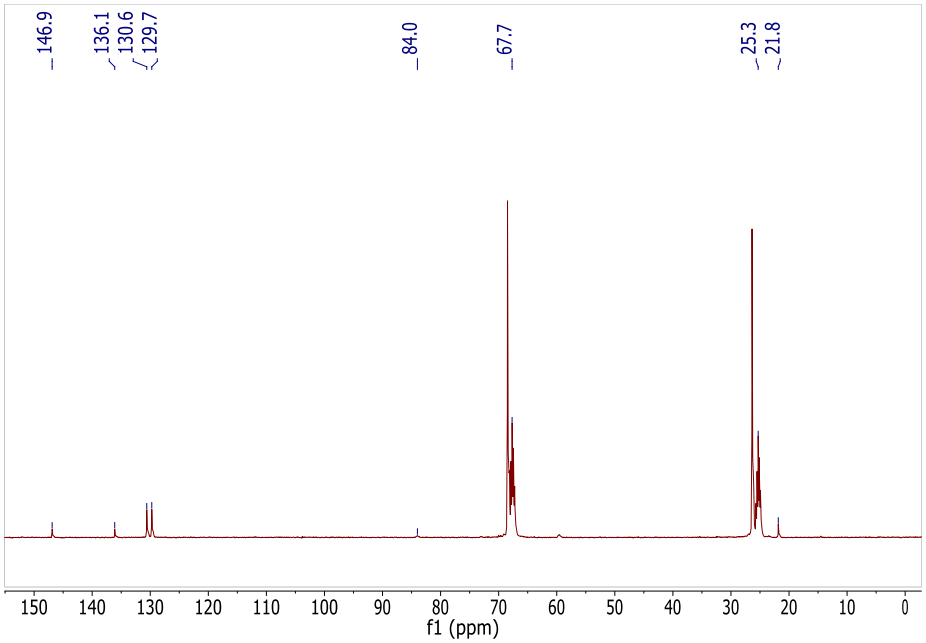

Figure 2-4 ^{13}C NMR spectrum of the mixture of compounds **2** and **3** (25°C, 101 MHz, THF-d_8)

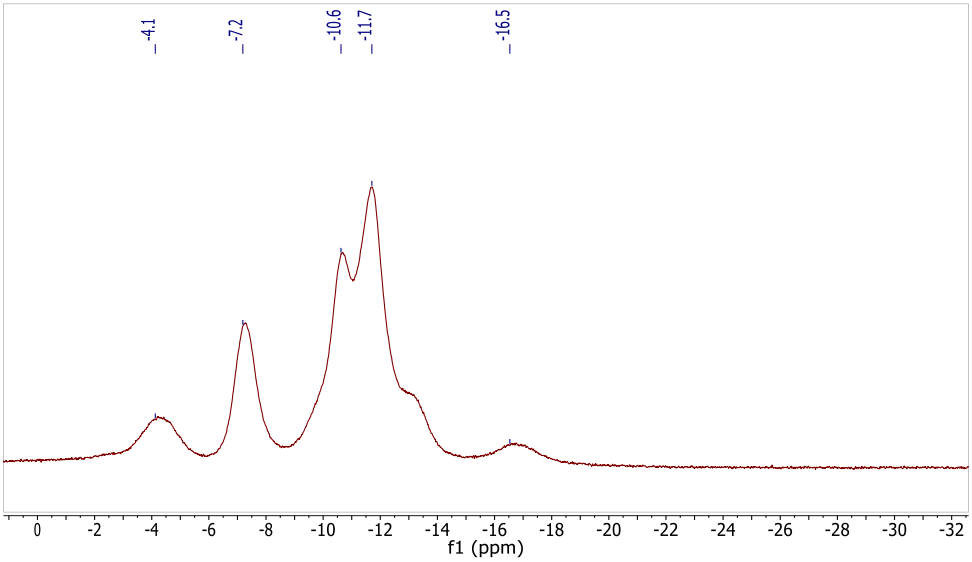

Figure 2-5 ^{11}B NMR spectrum of the mixture of compounds **2** and **3** (25°C, 96 MHz, F-C_6H_5)

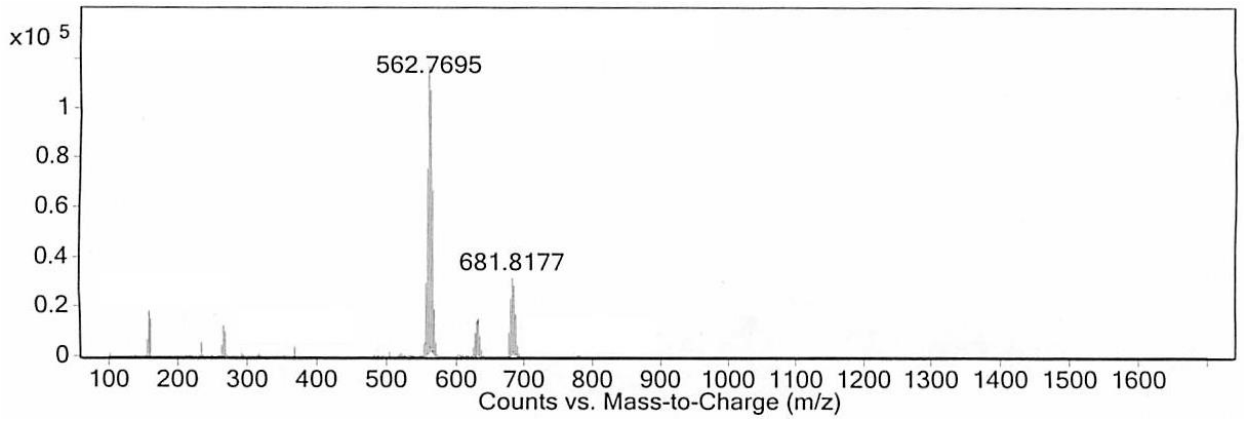

Figure 2-6 HRMS of the mixture of compounds **2** and **3**; (Multimode-ESI/APCI) $[M]^-$ Calculated **2** 562.7697; Calculated **3** 681.8195

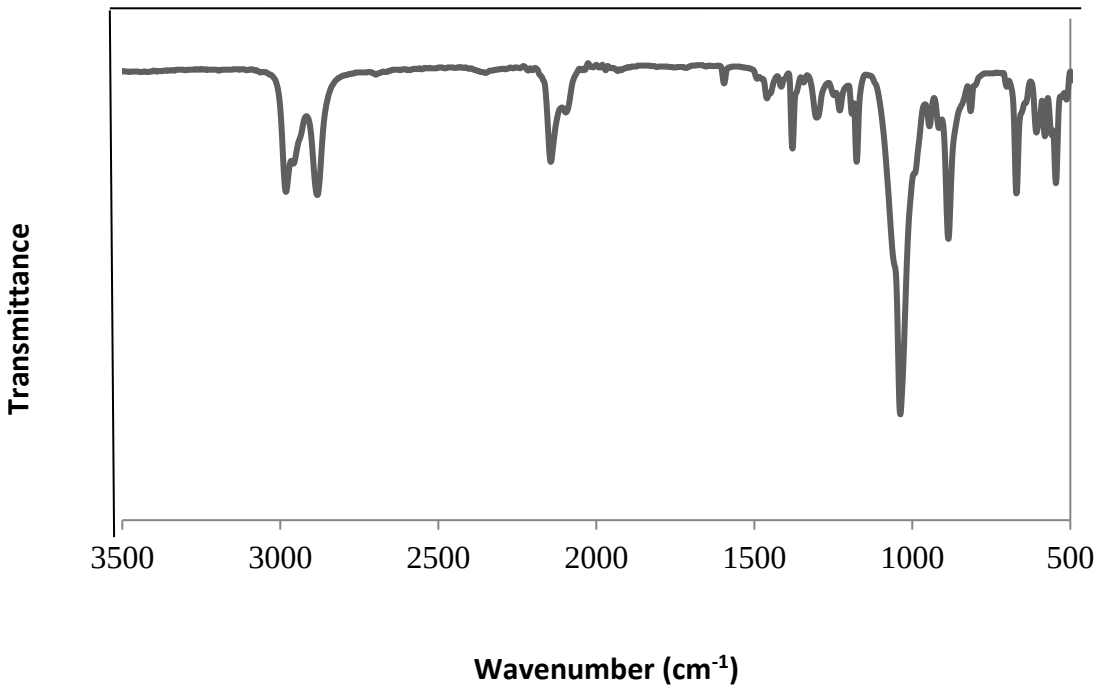

Figure 2-7 Solid-state IR spectrum of the mixture of compounds **2** and **3**

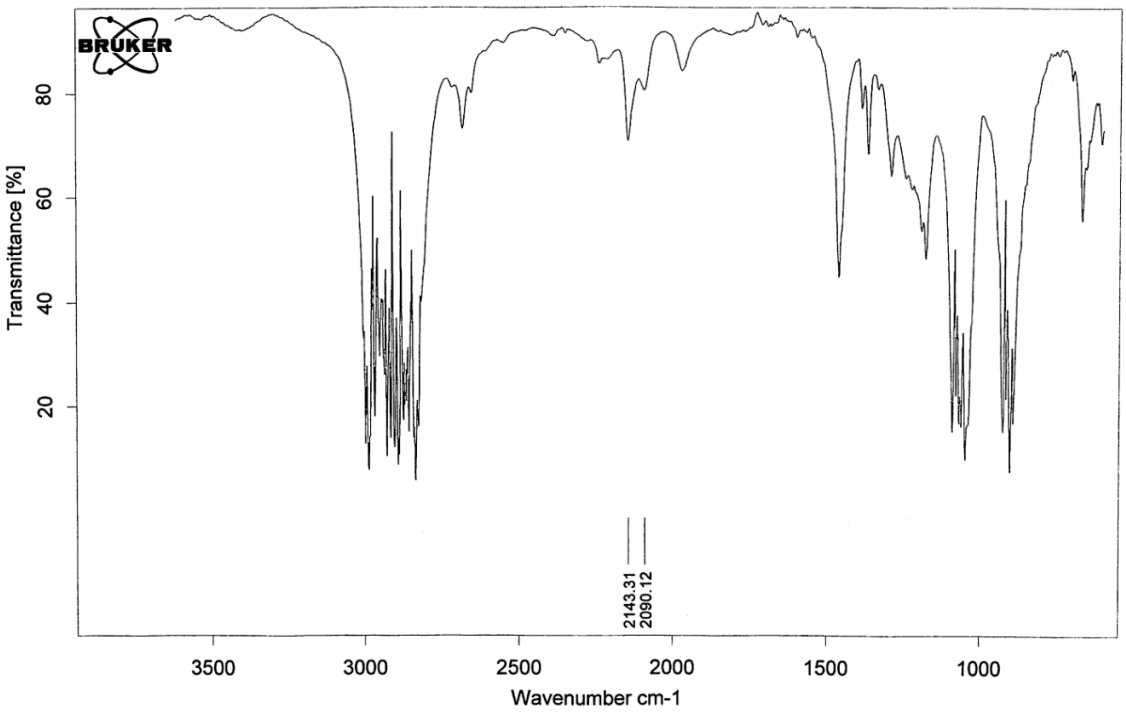

Figure 2-8 IR spectrum of the mixture of compounds **2** and **3** in THF

$Li(THF)_2[Ph_3PN_3CB_{11}Cl_{11}]$ (4)

After dissolving the mixture of compounds **2** and **3** in 20 mL of F-C_6H_5, triphenylphosphine (1.1 eq., 2.48 g, 9.45 mmol) was added to the solution. The mixture was quickly stirred to dissolve the PPh_3 and then stirring was stopped. The reaction was left undisturbed overnight, at which point **4** crystallized from the solution. The crystals were collected and washed twice with F-C_6H_5 to give **4** (4.98 g, 5.10 mmol) in 59% yield. ^{1}H NMR (500 MHz, THF-d_8, 25°C): $\delta = 7.22$ - 7.69 (m, bounded PPh_3 + free PPh_3); ^{1}H NMR (500 MHz, THF-d_8, -40°C): $\delta = 7.69$ (m, 6H, aryl), 7.60 (m, 3H, aryl), 7.48 (m, 6H, aryl); ^{1}H NMR (400 MHz, CD_2Cl_2, 25°C):

δ = 7.77 (m, 3H, aryl), 7.60 (m, 12H, aryl), 3.67 (m, 6.8H, THF), 1.81 (m, 6.8H, THF); ^{13}C NMR (126 MHz, CD_2Cl_2, 25°C): δ = 134.80 (CH, *p*-aryl), 133.84 (^{3}J(P,C) = 9.2 Hz, CH, *m*-aryl), 131.37 (^{2}J(P,C) = 11.1 Hz, CH, *o*-aryl), 124.90 (^{1}J(P,C) = 98.7 Hz, C, *ipso*-aryl), 70.55 (CH_2, THF), 27.15 (s, CH_2, THF); ^{11}B NMR (96 MHz, CD_2Cl_2, 25°C): δ = -3.4, -11.0, -12.1; ^{31}P NMR (121 MHz, THF-d_8, 25°C): δ = 21.1, -4.9; ^{31}P NMR (243 MHz, THF-d_8, -45°C): δ = 23.1; ^{31}P NMR (162 MHz, CD_2Cl_2, 25°C): δ = 33.5; CPMAS ^{31}P NMR (243 MHz, 25°C): δ = 38.4. HRMS ($[M]^-$) (Figure 2-18) does not show the mass of the phosphazide **4**, but fragmentation into the azide **2**. IR of **4** in THF (Figure 2-19) shows N_3 azide stretch at 2143 cm^{-1}; IR of **4** in CD_2Cl_2 (Figure 2-20) shows the absence of an N_3 functionality. Elemental Analysis for $Ph_3PN_3CB_{11}Cl_{11}\cdot Li\cdot 1.7$ THF (confirmed by ^{1}H NMR): Experimental (C: 32.46%, H: 3.02%, N: 4.40%). Calculated (C: 32.05%, H: 3.03%, N: 3.97%).

In order to perform the cation exchange, $N(Butyl)_4Br$ (1.0 eq.) was added to **4** in F-C_6H_5 and stirred overnight at ambient temperature. The mixture was then filtered. Subsequent heating of the solution at 80°C for 16 hours showed decomposition of product. Before decomposition: ^{31}P NMR (121 MHz, F-C_6H_5, 25°C): δ = 32.0. After heating: ^{31}P NMR (121 MHz, F-C_6H_5, 25°C): δ = 76.5, 42.9, 32.0, -4.7.

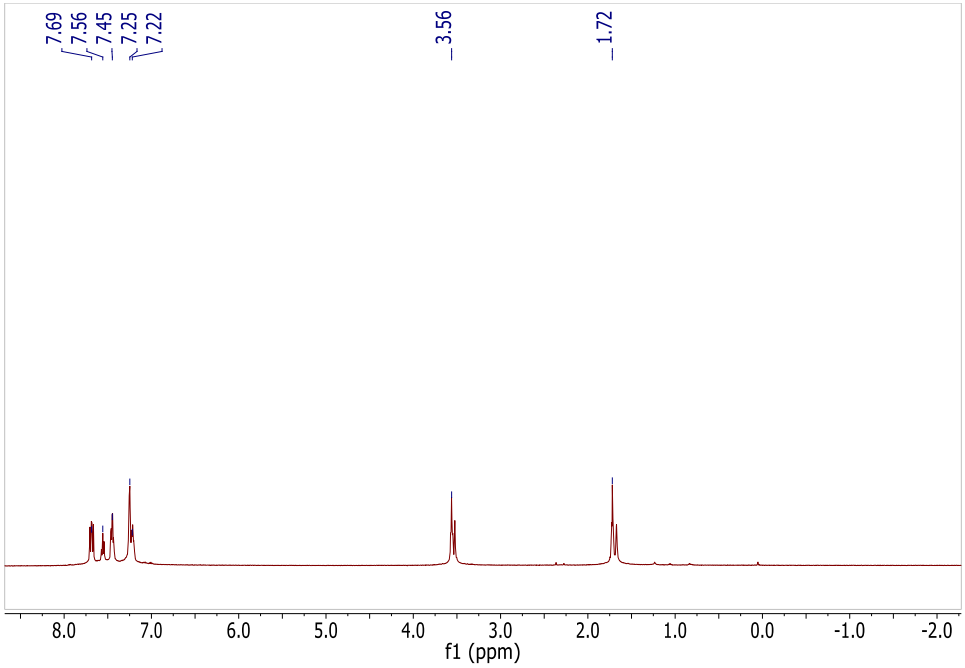

Figure 2-9 ^{1}H NMR of **4** showing phosphazide and free PPh_3 (25°C, 500 MHz, THF-d_8)

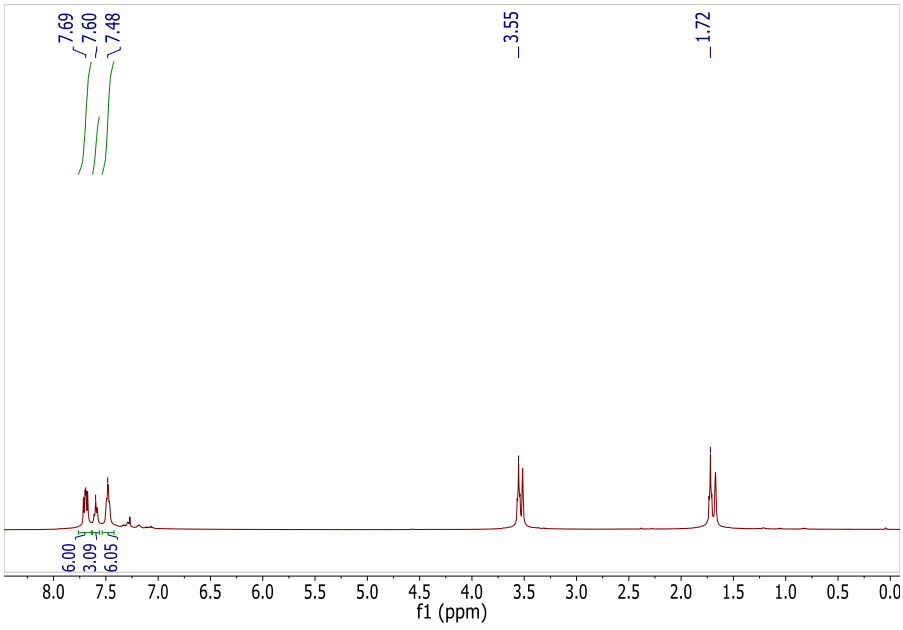

Figure 2-10 ^{1}H NMR of **4** showing only phosphazide (-40°C, 500 MHz, THF-d_8)

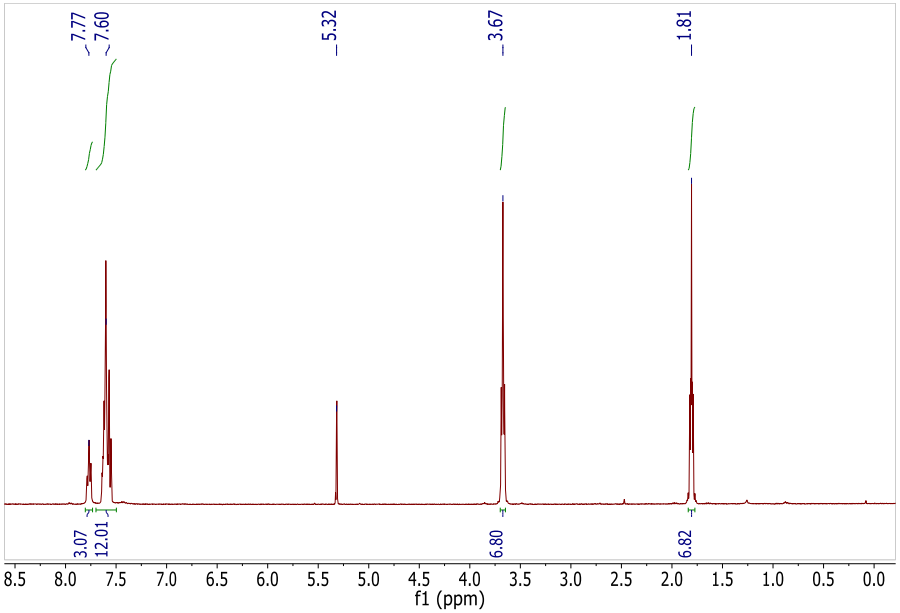

Figure 2-11 ^{1}H NMR of **4** (25°C, 500 MHz, CD_2Cl_2)

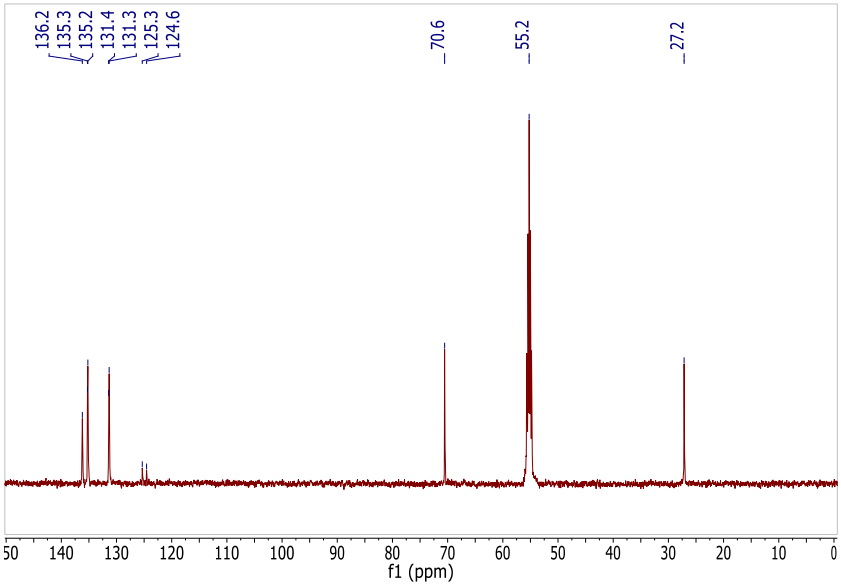

Figure 2-12 ^{13}C NMR of the **4** (25°C, 126 MHz, CD_2Cl_2)

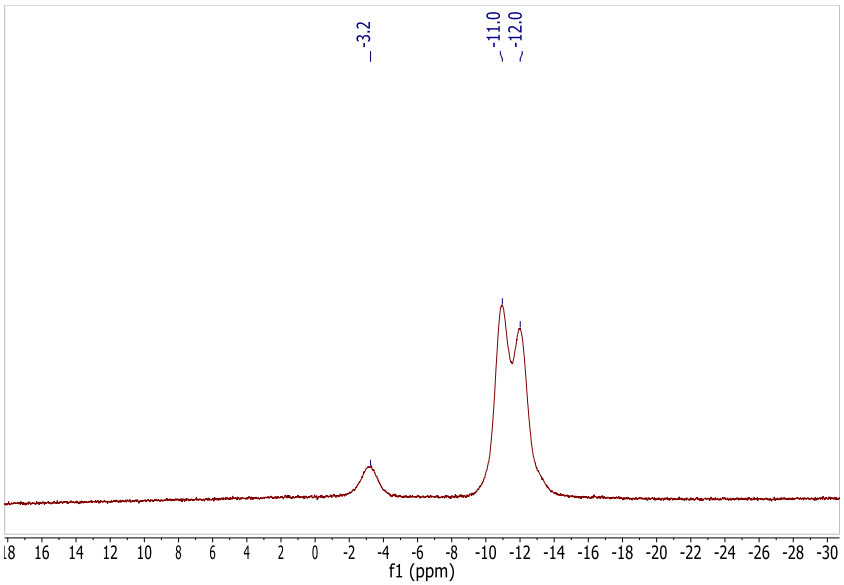

Figure 2-13 ^{11}B NMR of **4** (25°C, 96 MHz, CD_2Cl_2)

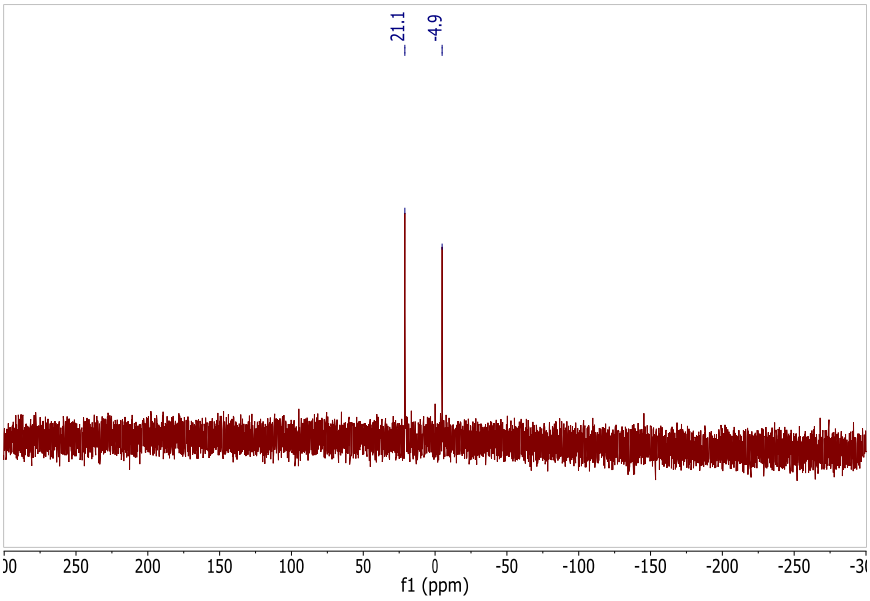

Figure 2-14 ^{31}P NMR of **4** showing phosphazide and free PPh_3 (25°C, 121 MHz, THF-d_8)

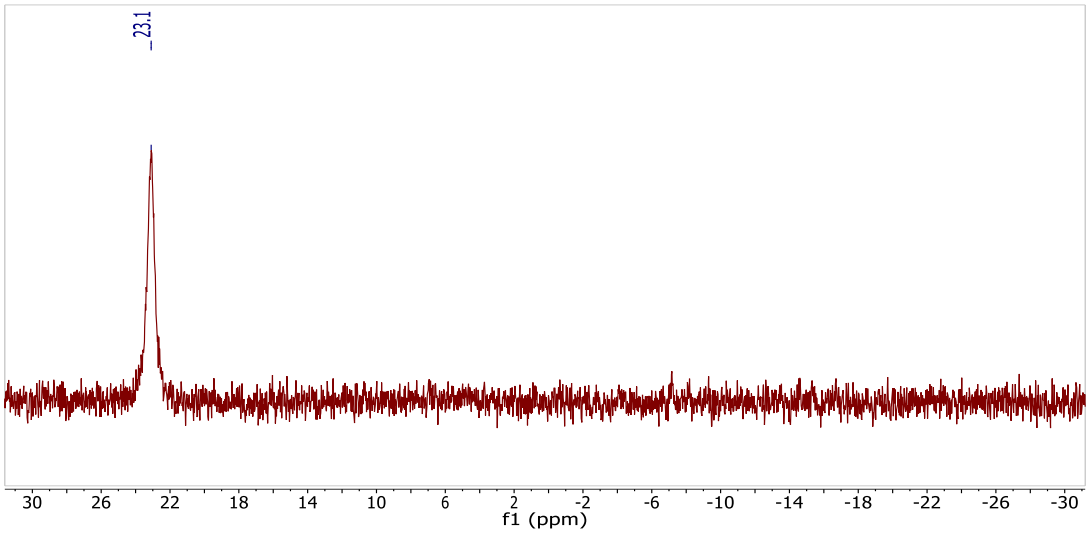

Figure 2-15 ^{31}P NMR of **4** showing only phosphazide 4 (-45°C, 243 MHz, THF-d_8)

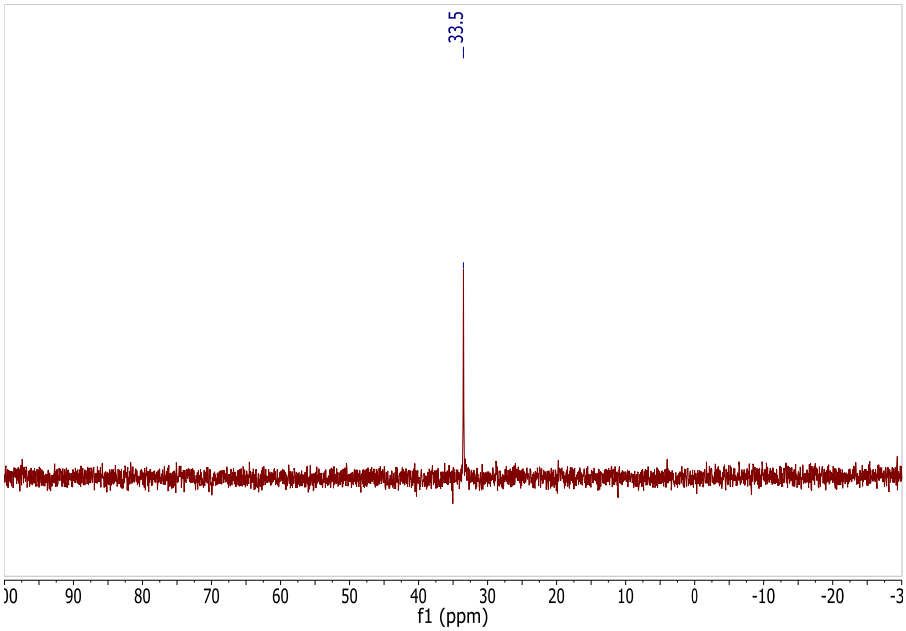

Figure 2-16 ^{31}P NMR spectrum of **4**(25°C, 162 MHz, CD_2Cl_2)

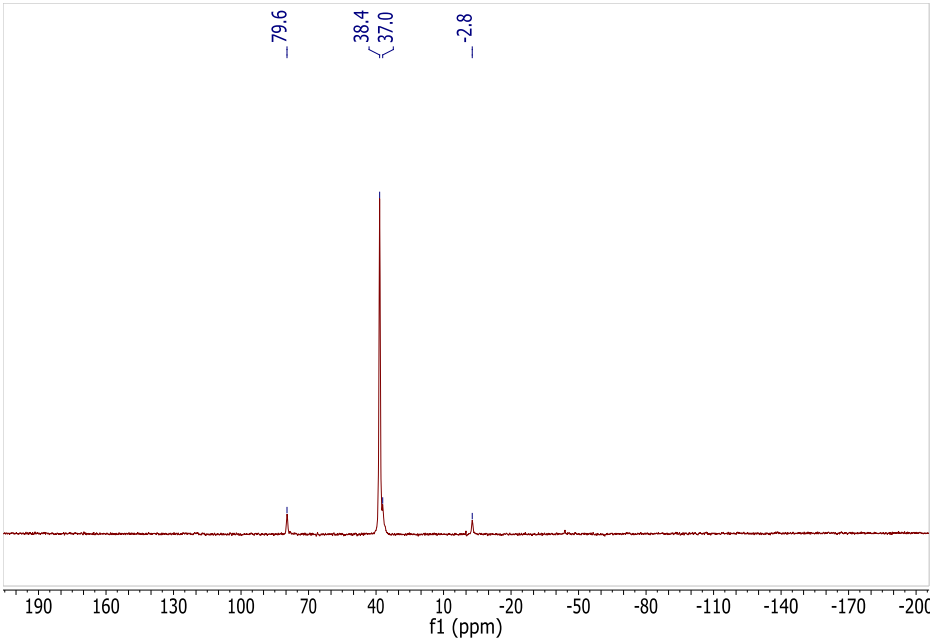

Figure 2-17 CPMAS ^{31}P NMR spectrum of **4** (243 MHz), where the resonances at 79.57 ppm and -2.75 ppm correspond to the spinning sidebands

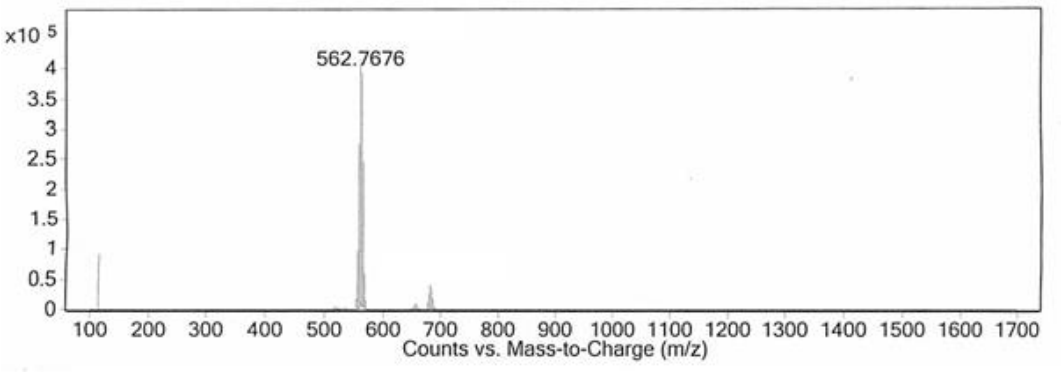

Figure 2-18 HRMS of **4** showing fragmentation into the azide **2** (Multimode-ESI/APCI) $[M]^-$ Calculated 2 562.7697

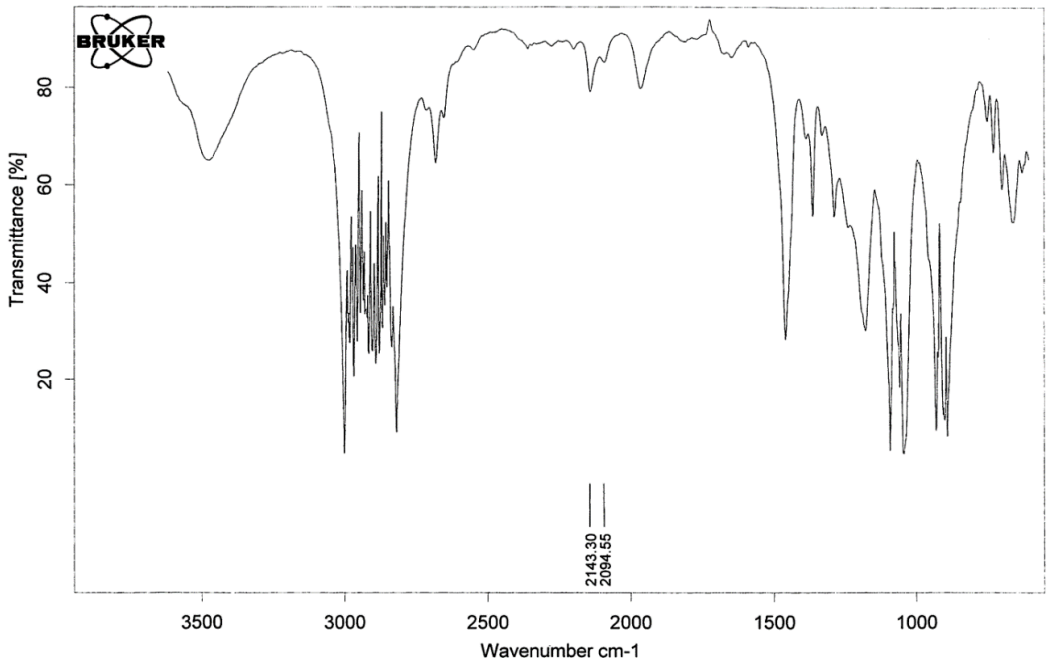

Figure 2-19 IR spectrum of **4** in THF

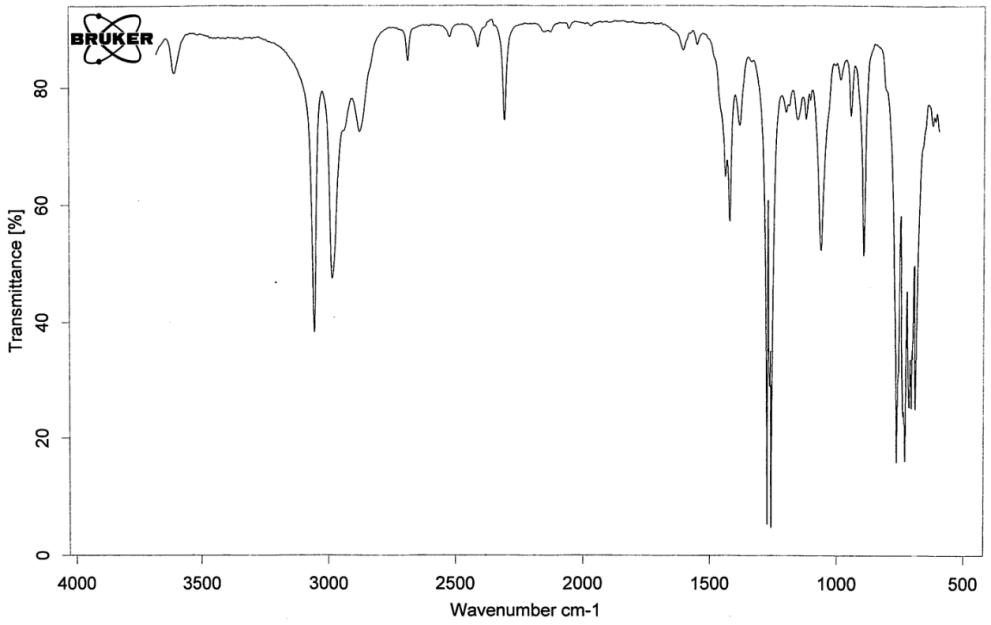

Figure 2-20 IR spectrum of **4** in CD_2Cl_2

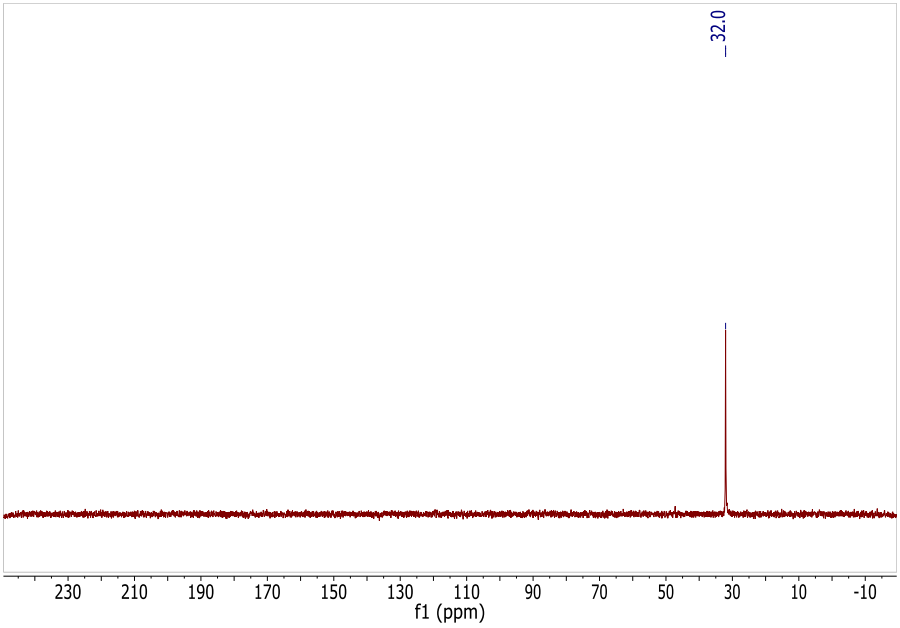

Figure 2-21 ^{31}P NMR spectrum of the tetrabutylammonium salt of **4** (25°C, 121 MHz, F-C_6H_5**)**

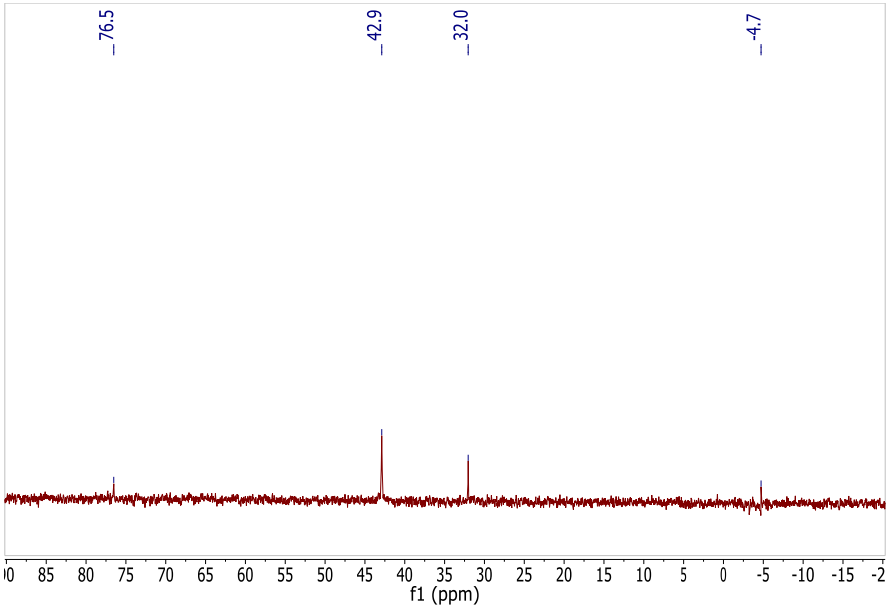

Figure 2-22 ^{31}P NMR spectrum of the tetrabutylammonium salt of **4** after heating (25°C, 121 MHz, F-C_6H_5)

Variable Temperature (VT) NMR Studies

The VT NMR study was carried out on the Varian Inova 500 MHz and Avance 600 MHz NMR instruments. The experiment started at room temperature (25°C), then proceeded to increase temperature in increments of ~5°C until reaching 64°C. The sample was then cooled back to 25°C, and spectra were recorded in decrements of 5°C or 10°C until reaching -45°C. Below are the spectra obtained at various temperatures. The populations of the two sites at various temperatures were used to find K_{eq} (in M). Given that $\Delta G = \Delta H - T\Delta S$ and $\Delta G = -RT\ln K_{eq}$, $\ln K_{eq} = \Delta H/(-RT) + \Delta S/R$. By plotting, $\ln K_{eq}$ vs. 1/T, ΔH and ΔS were found using a linear regression graph. ΔH and ΔS were found to be 8.8 kcal/mol and 29.7 cal/(mol*K), respectively.

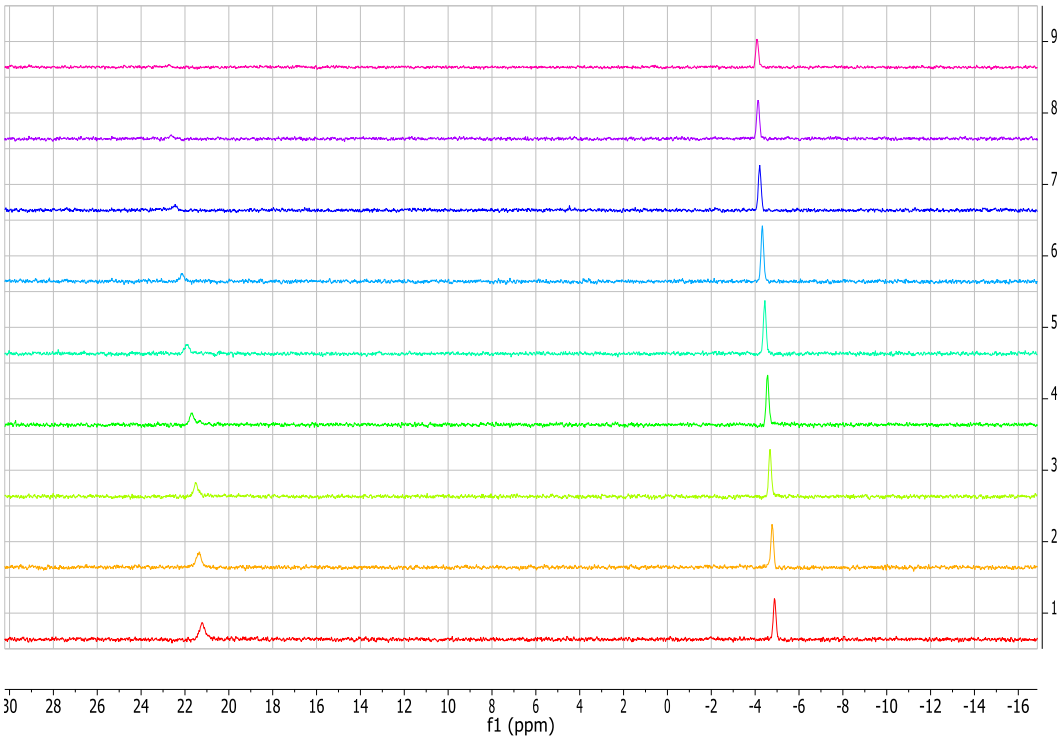

Figure 2-23 Variable Temperature ^{31}P NMR of phosphazide **4** Pink = 65°C, purple = 63°C, blue = 60°C, light blue = 55°C, cyan = 50°C, green = 45°C, light green = 40°C, yellow = 35°C, and red = 30°C (202.4 MHz, THF)

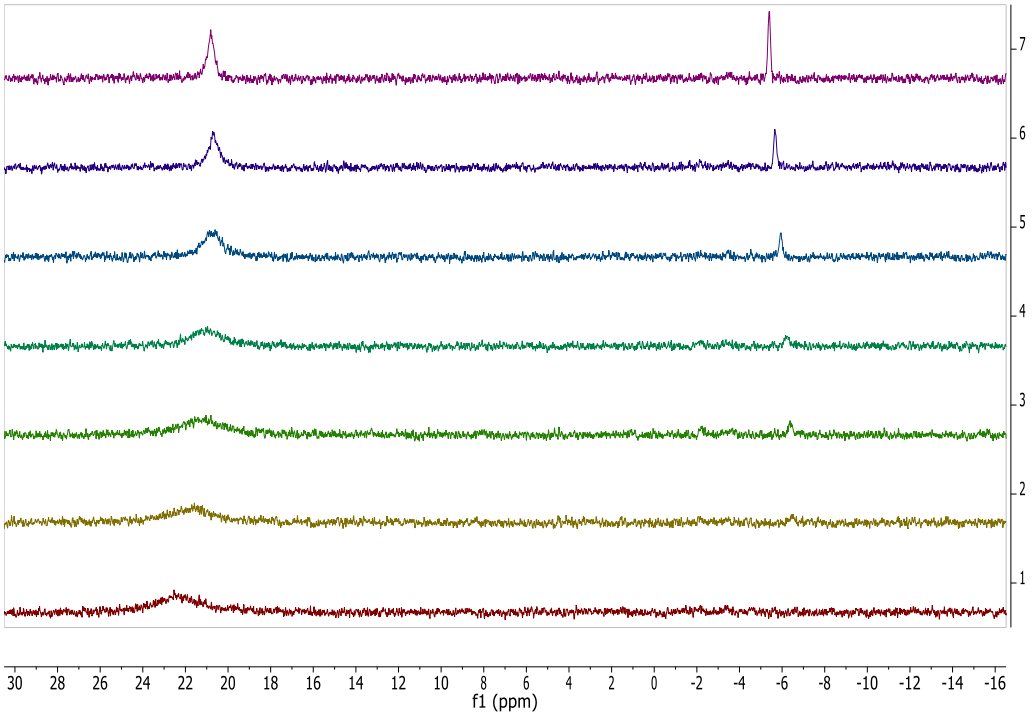

Figure 2-24 Variable Temperature ^{31}P NMR of phosphazide **4** (continued) Purple = 15°C, indigo corresponds to 5°C, blue = -5°C, dark green = -15°C, light green = -20°C, yellow = -25°C, and red = -30°C (202.4 MHz, THF)

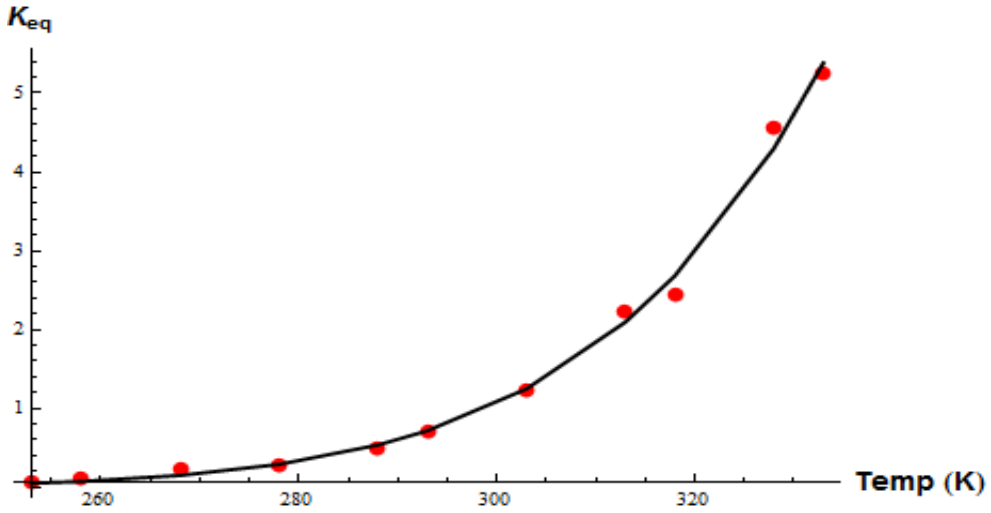

Figure 2-25 Graph of K_{eq} vs. Temp (K)

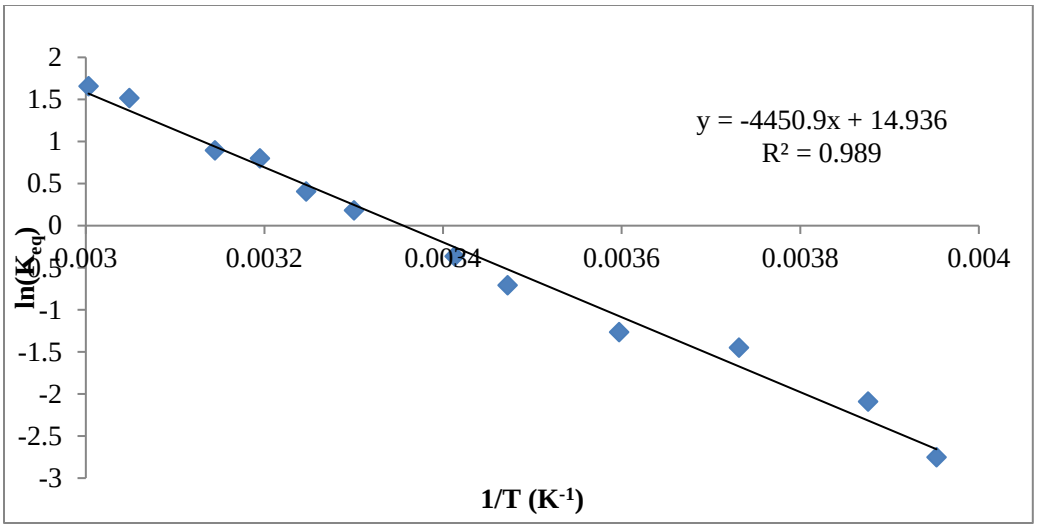

Figure 2-26 Graph of $\ln(K_{eq})$ vs. $1/T$ (K^{-1})

X-Ray Diffraction Studies

X-Ray Structure Determination of **3:** A colorless needle fragment (0.54 x 0.09 x 0.05 mm^3) was used for the single crystal x-ray diffraction study of $[[C_4H_8O]_4Li]^+[C_7H_7N_3O_2SCB_{11}Cl_{10}]^-$ (sample vL6r2_0m). The crystal was coated with perfluoropolyethers (PFPE) oil and mounted on to a cryo-loop glass fiber. X-ray intensity data were collected at 100(2) K on a Bruker platform-CCD x-ray diffractometer system (fine focus x-ray tube, Mo-radiation, λ = 0.71073 Å, 50KV/30mA power). The CCD detector was placed at a distance of 5.0600 cm from the crystal.

A total of 2400 frames were collected for a hemisphere of reflections (with scan width of 0.3° in ω, starting ω and 2θ angles at -30°, and ϕ angles of 90°, 120°, 180°, and 270° for every 600 frames, 60 sec/frame exposure time). The frames were integrated

using the Bruker SAINT software package and using a narrow-frame integration algorithm. Based on an orthorhombic crystal system, the integrated frames yielded a total of 112850 reflections at a maximum 2θ angle of 56.56° (0.75 Å resolution), of which 10810 were independent reflections (R_{int} = 0.0675, R_{sig} = 0.0335, redundancy = 10.4, completeness = 100%) and 7638 (70.7%) reflections were greater than $2\sigma(I)$. The unit cell parameters were, **a** = 17.771(2) Å, **b** = 19.490(2) Å, **c** = 25.163(3) Å, $\alpha = \beta = \gamma$ = 90°, V = 8715.7(18) Å^3, Z = 8, calculated density D_c = 1.491 g/cm^3. Absorption corrections were applied (absorption coefficient μ = 0.729 mm^{-1}; max/min transmission = 0.9624/0.6930) to the raw intensity data using the SADABS program.

The Bruker SHELXTL software package[6] was used for phase determination and structure refinement. The distribution of intensities (E^2-1 = 0.997) and systematic absent reflections indicated one possible space group, Pbca. The space group Pbca (#61) was later determined to be correct. Direct methods of phase determination followed by two Fourier cycles of refinement led to an electron density map from which most of the non-hydrogen atoms were identified in the asymmetry unit of the unit cell. With subsequent isotropic refinement, all of the non-hydrogen atoms were identified. There was one cation of $[C_4H_8O]_4Li]^+$ and one anion of $[C_7H_7N_3O_2SCB_{11}Cl_{10}]^-$ present in the asymmetry unit of the unit cell. Three of the four THF molecules attached to the Li-atom were disordered (disordered site occupancy ratios were 70%/30%, 61%/39%, and 81%/19%).

Atomic coordinates, isotropic and anisotropic displacement parameters of all the non-hydrogen atoms were refined by means of a full matrix least-squares procedure on

F^2. The H-atoms were included in the refinement in calculated positions riding on the atoms to which they were attached. The refinement converged at R1 = 0.0349, wR2 = 0.0704, with intensity, I>2σ(I). The largest peak/hole in the final difference map was 0.461/-0.395 e/$Å^3$.

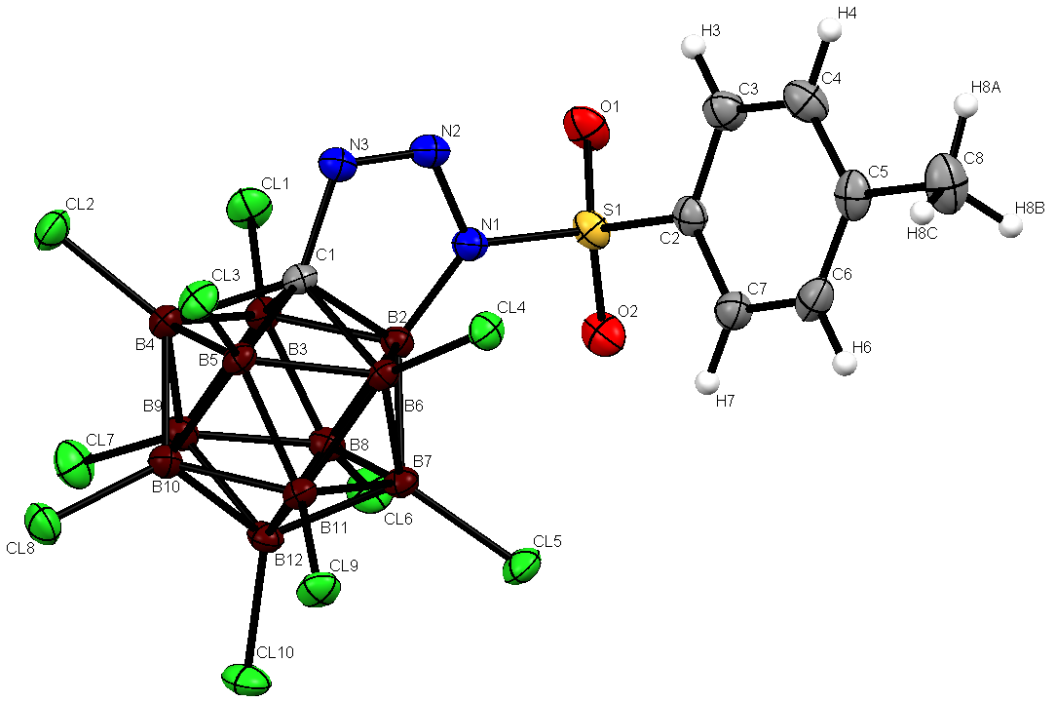

Figure 2-27 Crystal structure of **3** (CCDC 940701), where the lithium countercation has been omitted for clarity

Crystal data and structure refinement for compound **3**

Identification code	vl6r2_0m
Empirical formula	C24 H39 B11 Cl10 Li N3 O6 S
Formula weight	977.99

Temperature	100(2) K	
Wavelength	0.71073 Å	
Crystal system	Orthorhombic	
Space group	Pbca	
Unit cell dimensions	a = 17.771(2) Å	α = 90°.
	b = 19.490(2) Å	β = 90°.
	c = 25.163(3) Å	γ = 90°.
Volume	8715.7(18) $Å^3$	
Z	8	
Density (calculated)	1.491 Mg/m^3	
Absorption coefficient	0.729 mm^{-1}	
F(000)	3968	
Crystal size	0.54 x 0.09 x 0.05 mm^3	
Theta range for data collection	1.75 to 28.28°.	
Index ranges	-23<=h<=23, -25<=k<=25, -33<=l<=33	
Reflections collected	112850	
Independent reflections	10810 [R(int) = 0.0675]	
Completeness to theta = 28.28°	100.0 %	
Absorption correction	Semi-empirical from equivalents	
Max. and min. transmission	0.9624 and 0.6930	

Refinement method	Full-matrix least-squares on F^2
Data / restraints / parameters	10810 / 294 / 599
Goodness-of-fit on F^2	1.081
Final R indices [I>2sigma(I)]	R1 = 0.0349, wR2 = 0.0704
R indices (all data)	R1 = 0.0702, wR2 = 0.0876
Largest diff. peak and hole	0.461 and -0.395 e.Å^{-3}

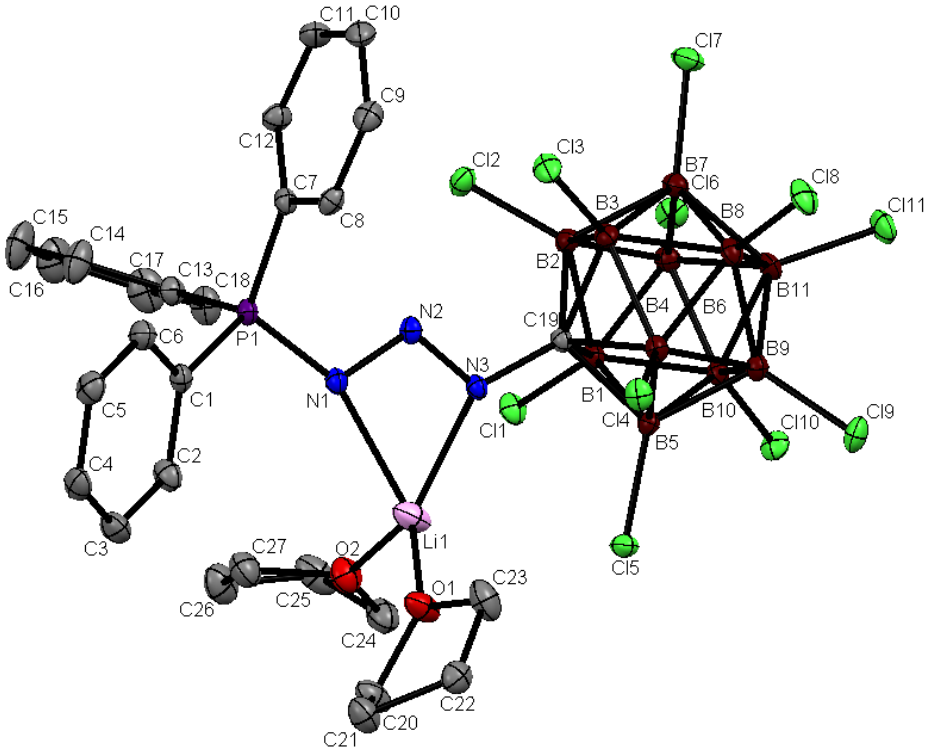

Figure 2-28 Crystal structure of **4** (CCDC 940702)

Crystal Data and Structure Analysis Details for vcl53

Empirical formula	C27 H31 B11 Cl11 Li N3 O2 P
Formula weight	976.32
Crystallization solvent	Fluorobenzene
Crystal shape	blade
Crystal color	colorless
Crystal size	0.04 x 0.07 x 0.41 mm

Data Collection

Preliminary photograph(s)	rotation	
Type of diffractometer	Bruker APEX-II CCD	
Wavelength	0.71073 Å MoK	
Data collection temperature	100 K	
Theta range for 9920 reflections used		
in lattice determination	2.38 to 31.75°	
Unit cell dimensions	a = 12.7459(3) Å	α= 90°
	b = 16.8796(4) Å	β= 98.934(2)°
	c = 19.9589(5) Å	γ = 90°
Volume	4241.97(18) Å^3	
Z	4	
Crystal system	monoclinic	
Space group	P 1 21/c 1 (# 14)	

Density (calculated)	1.529 g/cm^3
F(000)	1960
Theta range for data collection	2.0 to 35.0°
Completeness to theta = 25.000°	100.0%
Index ranges	-20 <= h <= 19, -26 <= k <= 27, -31 <= l <= 31
Data collection scan type	and scans
Reflections collected	151789
Independent reflections	18000 [R_{int}= 0.1157]
Reflections > 2□(I)	10920
Average □(I)/(net I)	0.0816
Absorption coefficient	0.79 mm^{-1}
Absorption correction	Semi-empirical from equivalents
Max. and min. transmission	1.0000 and 0.9474

Structure Solution and Refinement

Primary solution method	dual
Secondary solution method	?
Hydrogen placement	geom
Refinement method	Full-matrix least-squares on F^2
Data / restraints / parameters	18000 / 0 / 505

Treatment of hydrogen atoms	constr
Goodness-of-fit on F^2	1.10
Final R indices [I>2□(I), 10920 reflections]	R1 = 0.0488, wR2 = 0.0904
R indices (all data)	R1 = 0.1089, wR2 = 0.1055
Type of weighting scheme used	calc
Weighting scheme used	
Max shift/error	0.002
Average shift/error	0.000
Extinction coefficient	n/a
Largest diff. peak and hole	1.23 and -0.60 e·$Å^{-3}$

Programs Used

Cell refinement	SAINT V8.27B (Bruker-AXS, 2007)
Data collection	APEX2 2010.7-0, APEX2 2013.2-0 (Bruker-AXS, 2007)
Data reduction	SAINT V8.27B (Bruker-AXS, 2007)
Structure solution	SHELXT (Sheldrick, 2012)
Structure refinement	SHELXL-2013/2 (Sheldrick, 2013)
Graphics	DIAMOND 3 (Crystal Impact, 1999)

2.5 References

(1) Brase, S.; Gil, C.; Knepper, K.; Zimmermann, V. *Angewandte Chemie International Edition* **2005**, *44*, 5188.

(2) Banert, K.; Arnold, R.; Hagedorn, M.; Thoss, P.; Auer, A. A. *Angewandte Chemie International Edition* **201**, *51*, 7515.

(3) Jung, N.; Braese, S. *Angewandte Chemie International Edition* **2012**, *51*, 12169.

(4) Blanch, R. J.; Bush, L. C.; Jones, M. *Inorganic Chemistry* **1994**, *33*, 198.

(5) Kennedy, R. D. *Chemical Communications* **2010**, *46*, 4782.

(6) Vyakaranam, K.; Havlas, Z.; Michl, J. *Journal of the American Chemical Society* **2007**, *129*, 4172.

(7) Chan, A. L.; Fajardo, J., Jr.; Wright, J. H.; Asay, M.; Lavallo, V. *Inorganic Chemistry* **2013**, *52*, 12308.

(8) Spokoyny, A. M. *Pure and Applied Chemistry* **2013**, *85*, 903.

(9) Brusselle, D.; Bauduin, P.; Girard, L.; Zaulet, A.; Vinas, C.; Teixidor, F.; Ly, I.; Diat, O. *Angewandte Chemie International Edition* **2013**, *52*, 12114.

(10) Olid, D.; Nunez, R.; Vinas, C.; Teixidor, F. *Chemical Society Reviews* **2013**, *42*, 3318.

(11) Reed, C. A. *Accounts of Chemical Research* **2010**, *43*, 121.

(12) Scholz, M.; Hey-Hawkins, E. *Chemical Reviews* **2011**, *111*, 7035.

(13) Douvris, C.; Michl, J. *Chemical Reviews* **2013**, *113*, PR179.

(14) Farras, P.; Juarez-Perez, E. J.; Lepsik, M.; Luque, R.; Nunez, R.; Teixidor, F. *Chemical Society Reviews* **2012**, *41*, 3445.

(15) Matthews, S. L.; Heinekey, D. M. *Inorganic Chemistry* **2011**, *50*, 7925.

(16) Douvris, C.; Nagaraja, C. M.; Chen, C.-H.; Foxman, B. M.; Ozerov, O. V. *Journal of the American Chemical Society* **2010**, *132*, 4946.

(17) Gu, W.; Haneline, M. R.; Douvris, C.; Ozerov, O. V. *Journal of the American Chemical Society* **2009**, *131*, 11203.

(18) Douvris, C.; Ozerov, O. V. *Science* **2008**, *321*, 1188.

(19) Ivanov, S. V.; Rockwell, J. J.; Polyakov, O. G.; Gaudinski, C. M.; Anderson, O. P.; Solntsev, K. A.; Strauss, S. H. *Journal of the American Chemical Society* **1998**, *120*, 4224.

(20) Ramirez-Contreras, R.; Ozerov, O. V. *Dalton Transactions* **2012**, *41*, 7842.

(21) Wright, J. H., II; Kefaidis, C. E.; Tham, F. S.; Maron, L.; Lavallo, V. *Inorganic Chemistry* **2013**, *52*, 6223.

(22) Asay, M.; Kefalidis, C. E.; Estrada, J.; Weinberger, D. S.; Wright, J.; Moore, C. E.; Rheingold, A. L.; Maron, L.; Lavallo, V. *Angewandte Chemie International Edition* **2013**, *52*, 11560.

Chapter 3: In the Pursuit of Carboranyl Azides: New Reactions and Reactivity, Part 2

3.1 Introduction

As previously reported, the perchlorinated carborane anion showed unusual activity, and the azide $N_3CB_{11}Cl_{11}^-$ **2** could not be isolated due to a competitive cycloaddition reaction which we believe to be explained, in part, by the formation of a favorable aromatic system (Scheme 3-1)[1]. In our continued search for carboranyl azides, we are interested in utilizing the inert and weakly coordinative properties of carba-*closo*-dodecaborate anion derivatives in ligand and catalyst design[2-4]. Also, we wanted to see if the carboranyl azide behave like typical organic azides and are able to undergo a Staudinger reaction in order to form the carboranyl amine, a useful building block for ligand design. Here, we report the selective synthesis of the parent, per-, and hexabrominated carboranyl azides, as well as the first single-crystal X-ray diffraction studies of such azides. We also disclose the ability of the hexabrominated carboranyl azide to undergo a Staudinger reaction, creating a new method for creating the synthetically useful carboranyl amine synthon.

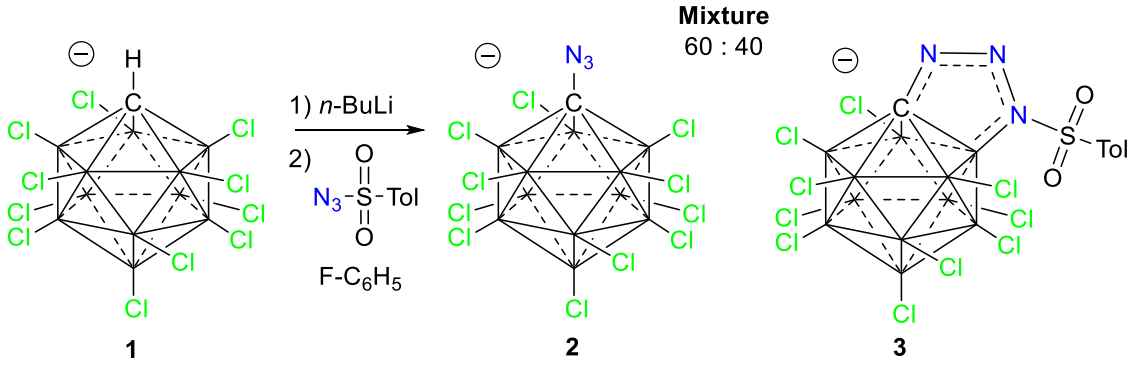

Scheme 3-1 Synthesis of the perchlorinated anionic carboranyl azide **2** and carborane-fused triazole **3** byproduct (unlabeled vertices = B)

3.2 Results and Discussion

With the desire to gain access to halogenated anionic carboranyl azides in pure form, we wondered if per- and hexabrominated carba-*closo*-dodecaborate anions as well as the parent carborane anion were amenable to N_3 functionalization without the formation of carborane-fused triazoles. Our previous calculations[1] indicate that the observed cycloaddition reactions with the $HCB_{11}Cl_{11}^-$ anion and azides follow an associative substitution pathway, and hence the increased size of the halide substituents of the $HCB_{11}Br_{11}^-$ cluster might retard B-Br cleavage. With respect to the hexabrominated carborane anion and the parent carborane anion, the cyclization should not occur at all because the pentagonal belt of boron atoms adjacent to the carbon center all have hydride substituents (Scheme 3-2).

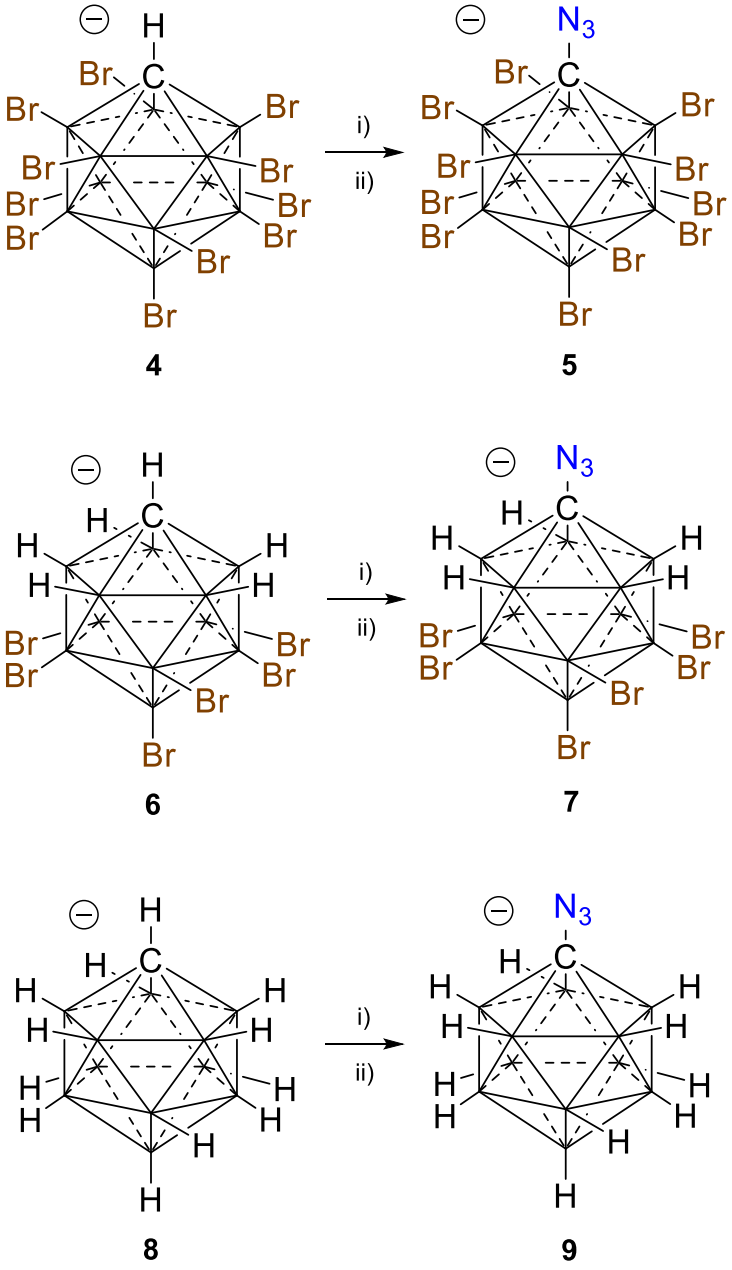

Scheme 3-2 Scheme showing the synthesis of the anionic carboranyl azides $[N_3CB_{11}Br_{11}]^-$ **5**, $[N_3CB_{11}H_5Br_6]^-$ **7**, and $[N_3CB_{11}H_{11}]^-$ **9** by addition of *n*-BuLi (**i**) and tosyl azide (**ii**) (unlabeled vertices = B)

Thus, we prepared the perbrominated carborane anion **4** from the parent hydrido carborane $HCB_{11}H_{11}^-$ by bromination under Ozerov's conditions[5]. Deprotonation

of **4** with *n*-BuLi and subsequent treatment of the dianionic intermediate with tosyl azide affords the targeted azide **5** as the sole product (Scheme 3-2). Similarly, treatment of the hexabrominated carborane anion **6** with base followed by addition of the N_3 transfer agent produced the azide **7**. Furthermore, the parent carborane behaved in a similar fashion after the addition of base and tosyl azide to yield the corresponding carboranyl azide **9**. The identity of **5** and **7** were confirmed by HRMS and ^{11}B NMR spectroscopy, and the identity of **9** was confirmed by ^{11}B NMR spectroscopy. ^{1}H NMR of all compounds were obtained in which the observed signals correspond to coordinated solvent. The ^{13}C resonances of **5** and **7** could not be observed, which can be explained by broadening of the signal induced by the attached quadrupolar nitrogen and boron atoms. Analysis of the IR spectra of **5** and **7** shows N_3 stretches at 2135 cm^{-1} and 2119 cm^{-1}, respectively, which is similar to that observed for the previously reported perchlorinated azide **2** (2143 cm^{-1})[6]. These azides are soluble in polar solvents (H_2O, H_3CCN, F-C_6H_5), but insoluble in hydrocarbons. Azides **5** and **7** are not shock sensitive and thermally stable up to 185^{o}C and 190^{o}C, respectively, where they begin to decompose. Regardless of the reaction conditions, the formation of a brominated carborane-fused heterocycle analogous to **3** was not observed.

No crystallographic data has ever been reported for either *ortho*-carborane azides or azides derived from the carba-*closo*-dodecaborate anion. Thus, we sought to investigate the solid-state structures of **5**/**7**, and for comparison, the previously reported *ortho*-carboranyl azide **10** (1-N_3-2-Ph-$C_2B_{10}H_{10}$)[7] (Figure 3-1). Although the

formation of azide **5** was confirmed by X-ray crystallography (Figure 3-17), all of our attempts at obtaining data for an accurate discussion of bond lengths and angles were hampered by significant disorder in the crystals. In contrast, the hexabrominated carboranyl azide **7** crystallized in an ordered fashion via slow evaporation of an acetone solution. Although azide **10** derived from *ortho*-carborane is an oil at room temperature, crystals suitable for a single-crystal X-ray diffraction study were obtained at -40^{o}C from a saturated hexane solution. The N-N-N bond lengths for both **7** and **10** are nearly identical (**7**: N1-N2 = 1.248(5), N2-N3 = 1.129(5) Å; **10**: N1-N2 = 1.2584(13), N2-N3 = 1.1219(14) Å) and indicate a significant amount of double and triple bond character between N1-N2 and N2-N3, respectively. Interestingly the C1-N1 bond length for **7** (C1-N1 = 1.455(5) Å) is slightly longer than that of **10** (C1-N1 = 1.4282(13) Å), which suggests that the *o*-carborane core of **10** is engaged in a degree of exo-π-conjugation[1,8] with the N_3 moiety. Indeed, the bond length (1.725(5) Å) between the two cluster carbons of **10** is stretched compared to a closely related phosphazide adduct (1.680(2) Å)[7], which is indicative of an interaction between the skeletal electrons and the N_3 substituent[8]. Although the slightly elongated C1-N1 bond length of **7** cannot be explained by steric arguments, it might be attributed to Coulombic repulsion between the charged carborane and the dipolar N_3 moiety. The cluster C-B bonds of **7** (C-B average = 1.708(5) Å) and **10** (C-B average = 1.715(15) Å) are in the typical range (1.700-1.735 Å) for carba-*closo*-dodecaborate[9] and *ortho*-carborane[10] derivatives.

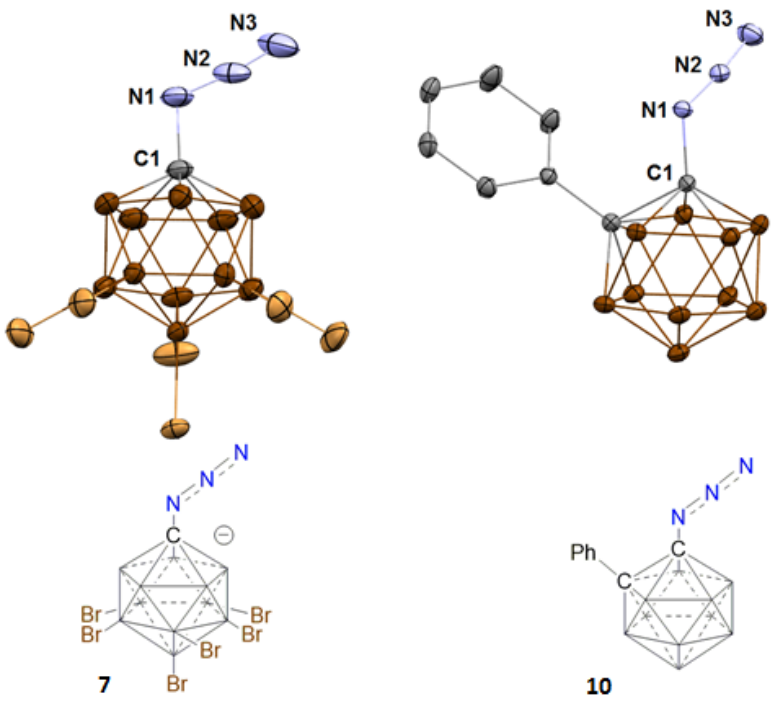

Figure 3-1 Crystal structure of the hexabrominated carboranyl azide **7** $[Li]^+[N_3CB_{11}H_5Br_6]^-$ (CCDC: 995208, Li^+ omitted) and the previously reported *ortho*-carboranyl azide **10** (1-N_3-2-Ph-$C_2B_{10}H_{10}$) (CCDC: 995207). Unlabeled vertices = B and hydrogen atoms omitted for clarity

After the synthesis of the carboranyl azides, we wished to attempt further reactivity to compare with their organic counterparts. We attempted to do a Staudinger reaction on the hexabrominated carboranyl azide as a proof of concept. Surprisingly there was no reaction with the addition of triphenylphosphine, the standard phosphorus reagent for azide hydrolysis to the amine[11]. Because of weakly coordinative ability of the carboranyl cage, we postulated that a more nucleophilic phosphine was necessary for azide coordination. Indeed, after the addition of PMe_3, we see an immediate change in the ^{11}B NMR and MS. After addition of HCl and H_2O followed by

basic workup, full conversion to the carboranyl amine was seen in the ^{11}B NMR and confirmed by MS. Though carboranyl amines have been synthesized from decaborane in high yields[12], there have not been reported condensation reactions with aldehydes or ketones at the time this research occurred. The carboranyl amine **11** was then dissolved in excess salicylaldehyde and full conversion to the corresponding imine product **12** was indicated by MS. Scheme 3-3 shows the overall reaction to carboranyl imine **12**.

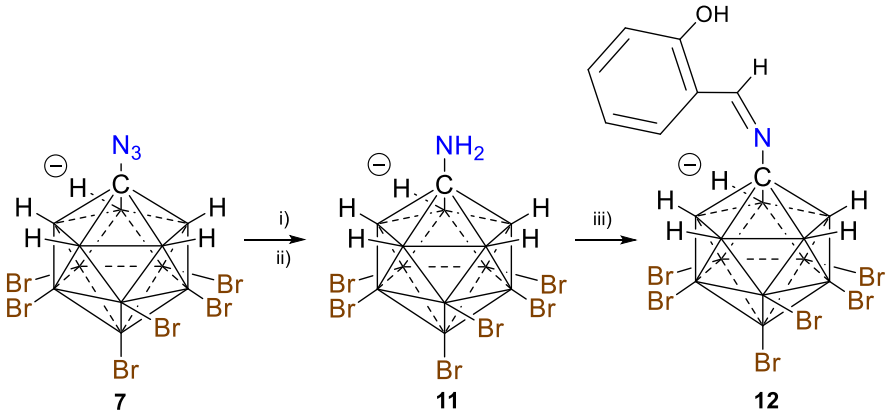

Scheme 3-3 Scheme showing the synthesis of the carboranyl imine **12** by addition of PMe_3 and HCl/H_2O(i) followed by LiOH(ii), and salicylaldehyde (**iii**) (unlabeled vertices = B)

3.3 Conclusion

We have demonstrated that anionic C-functionalized parent and polybrominated carba-*closo*-dodecaborate azides are readily accessible in pure form. In contrast to the $[HCB_{11}Cl_{11}]^-$ anion **1**, no competitive B-Br substitution reaction is observed, suggesting that its parent and brominated congener **4** is more inert to nucleophilic attack. The chemical reactivity of these azides, such as their potential to undergo Staudinger

reduction has also been shown to be possible, albeit with a more nucleophilic phosphorus reagent than the typical organic azides. The carboranyl amine also undergoes condensation with salicylaldehyde, which was unknown at the time the research was being done.

3.4 Experimental

Unless otherwise stated, all manipulations were carried out using standard Schlenk or glovebox techniques (O_2, H_2O < 1ppm) under a N_2 or Ar atmosphere. Solvents were dried over K or CaH_2, and distilled under argon before use. Tosyl azide and carborane salts $[HNMe_3]^+[HCB_{11}Br_{11}]^-$, $[HNMe_3]^+[HCB_{11}H_5Br_6]^-$, and $[HNMe_3]^+[HCB_{11}H_{11}]^-$ were prepared by literature methods. Reagents were purchased from commercial vendors and used without further purification. NMR spectra were recorded on Bruker Avance 300 MHz, Varian Inova 300 MHz, or Varian Inova 400 MHz spectrometers, and NMR chemical shifts are reported in ppm. ^1H NMR chemical shifts and ^{13}C NMR chemical shifts were referenced to residual protio solvent. ^{11}B NMR chemical shifts were externally referenced to BF_3OEt_2. The IR spectra were collected on Bruker Alpha FTIR and Pike Technologies GladiATR MB3000 instruments. The mass spectra were collected on an Agilent LCTOF Multimode-ESI/APCI with direct injection.

Synthesis and Spectroscopic Data

$[Li]^+[N_3CB_{11}Br_{11}]^-$ (5)

$[HNMe_3]^+[HCB_{11}Br_{11}]^-$ (**4**) (2.48 g, 2.31 mmol) was dissolved in THF (20 mL), deprotonated with 2.5 M *n*-butyllithium (3.0 eq., 2.8 mL, 7.0 mmol), and stirred for 14 hours. After removing the solvent *in vacuo*, the residue was washed with hexanes (2 x 20 mL). The solid was then dissolved in F-C_6H_5 (40 mL) and treated dropwise with an F-C_6H_5 (5 mL) solution of tosyl azide (1.8 eq., 0.82 g, 4.16 mmol). The reaction mixture was stirred for 14 hours and a precipitate of $LiO_2SC_7H_7$ formed. The mixture was filtered to remove the salt byproduct and the solution concentrated under vacuum. The residue was washed with hexanes (2 x 10 mL) and dried to afford **5** as an off-white powder (1.95 g, 66% yield). ^{1}H NMR (300 MHz, $CDCl_3$, 25°C): $\delta =$ 2.00 (m, coord. THF), 3.84 (m, coord. THF); ^{13}C NMR (101 MHz, acetone-d_6, 25°C): $\delta =$ 26.2 (CH_2, coord. THF), 68.1 (CH_2, coord. THF); ^{11}B NMR (96 MHz, F-C_6H_5, 25°C): $\delta =$ -1.2, -8.2. HRMS calculated for **5** ($[M]^-$) 1051.2109, found: 1051.2137. Solid-state IR: N_3 azide stretches= 2135.0 cm^{-1} and 2086.0 cm^{-1}. IR of **5** in $CHCl_3$: 2135.2 cm^{-1} (N_3). mp = 185-190°C (dec).

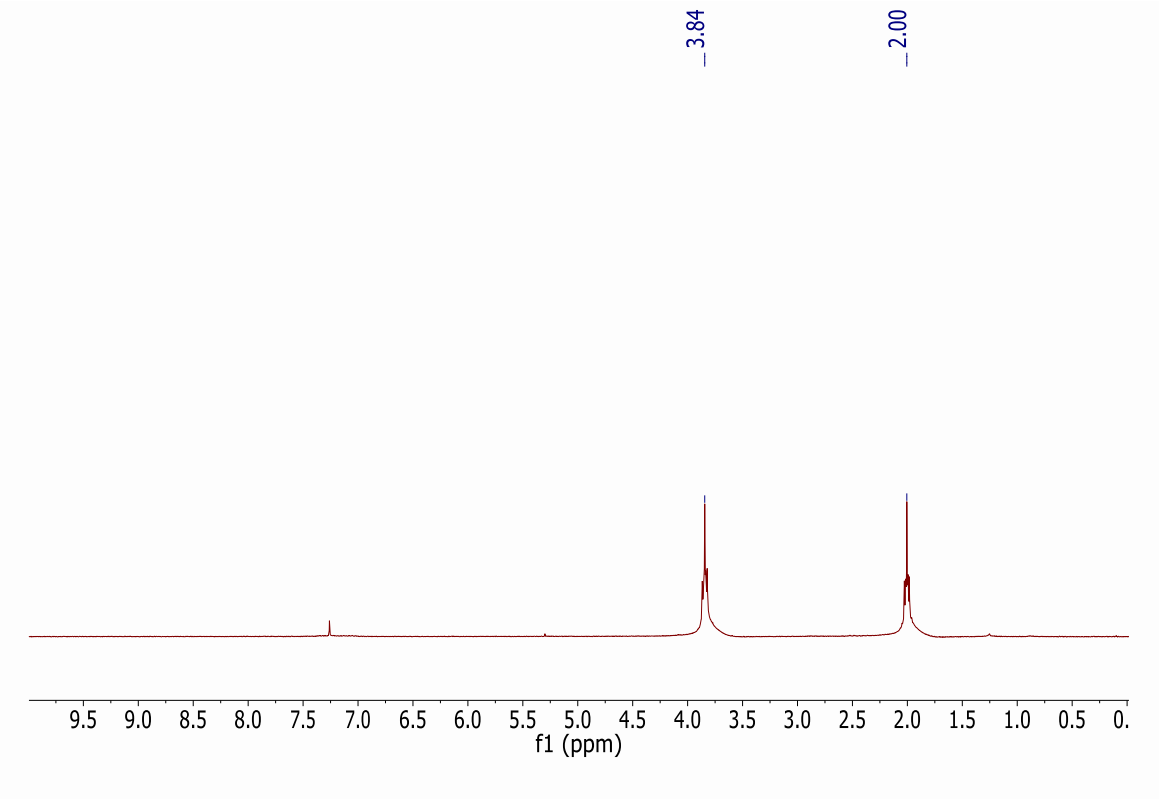

Figure 3-2 ^{1}H NMR spectrum of **5**, showing coordinated THF (25°C, 300 MHz, $CDCl_3$)

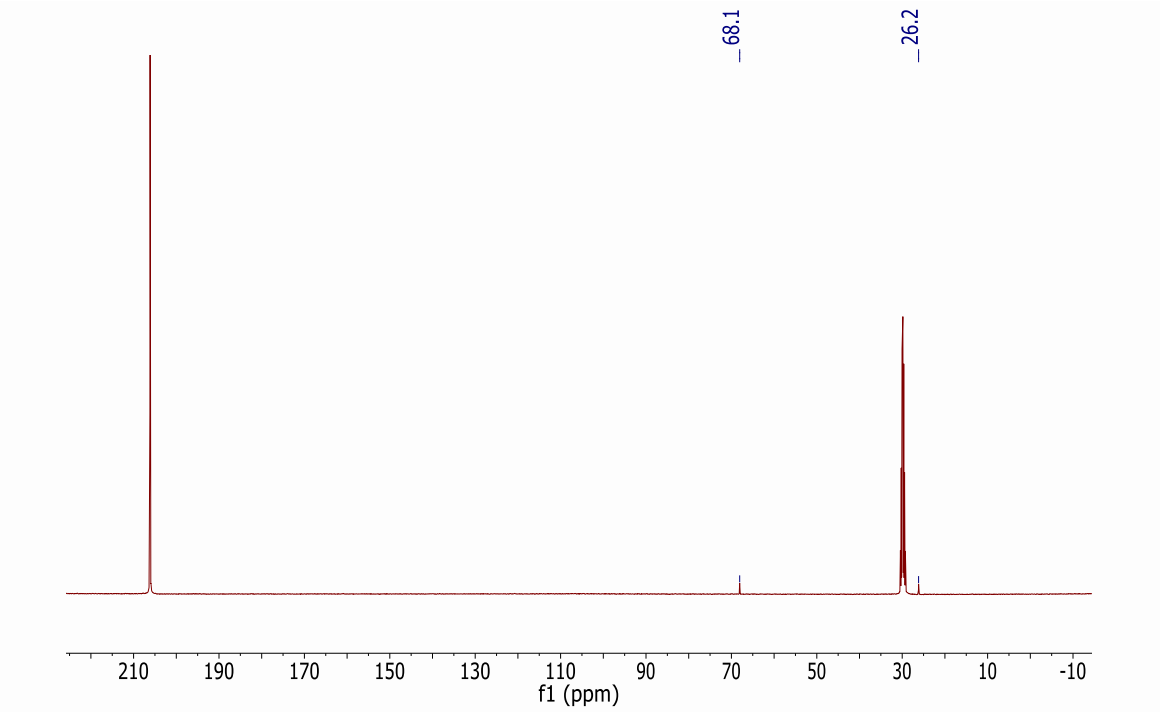

Figure 3-3 ^{13}C NMR spectrum of **5**, showing coordinated THF. Carborane carbon is not observed, due to quadrupolar broadening of the signal (25^{o}C, 101 MHz, acetone-d_6)

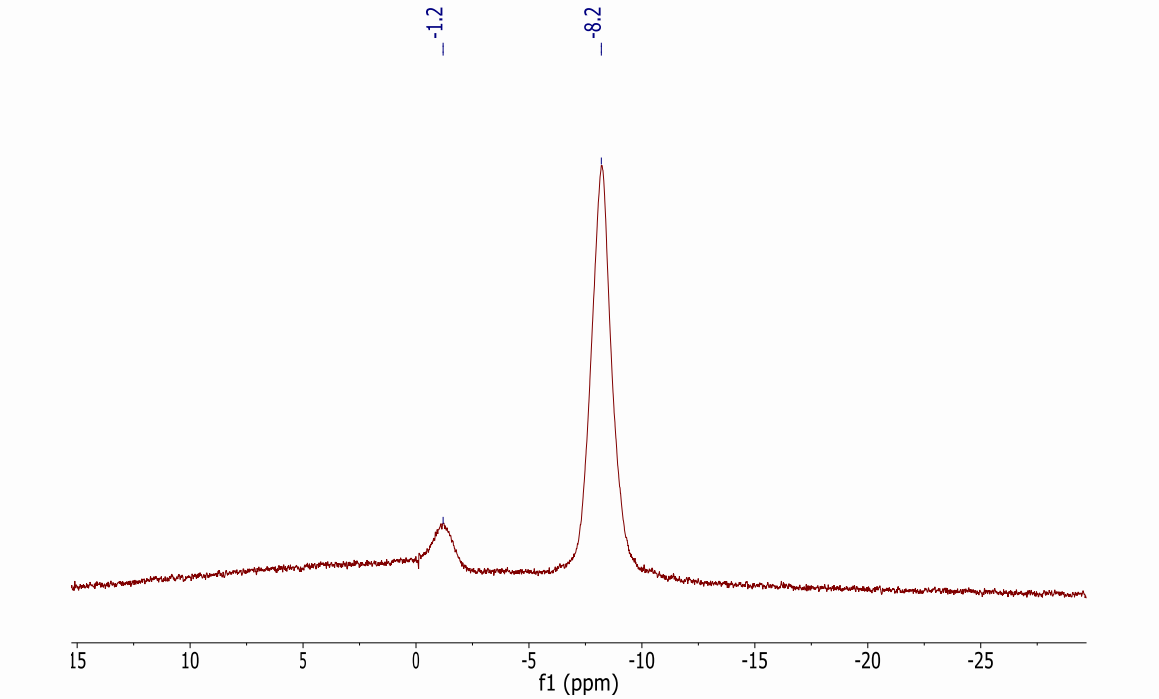

Figure 3-4 ^{11}B NMR spectrum of **5** (25°C, 96 MHz, F-C_6H_5)

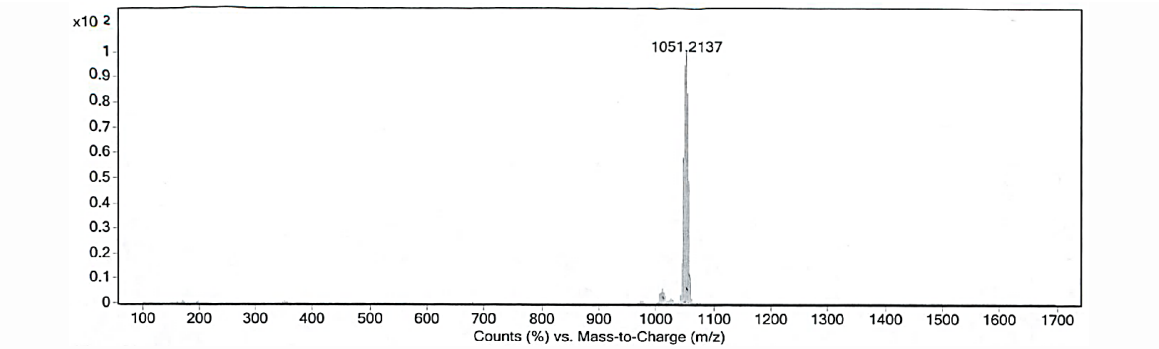

Figure 3-5 HRMS **5** (Multimode-ESI/APCI) $[M]^-$; Calculated **5** 1051.2109

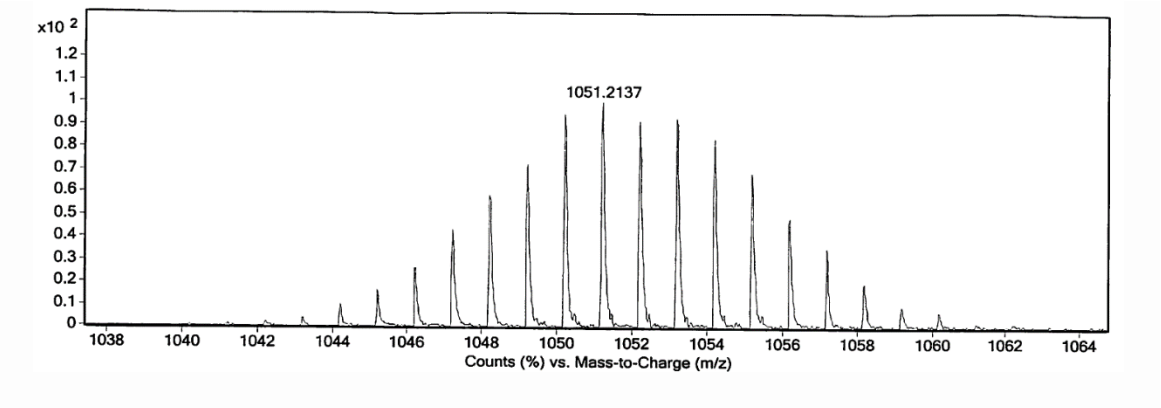

Figure 3-6 HRMS **5** (Multimode-ESI/APCI) [M]- Close-up of isotope pattern

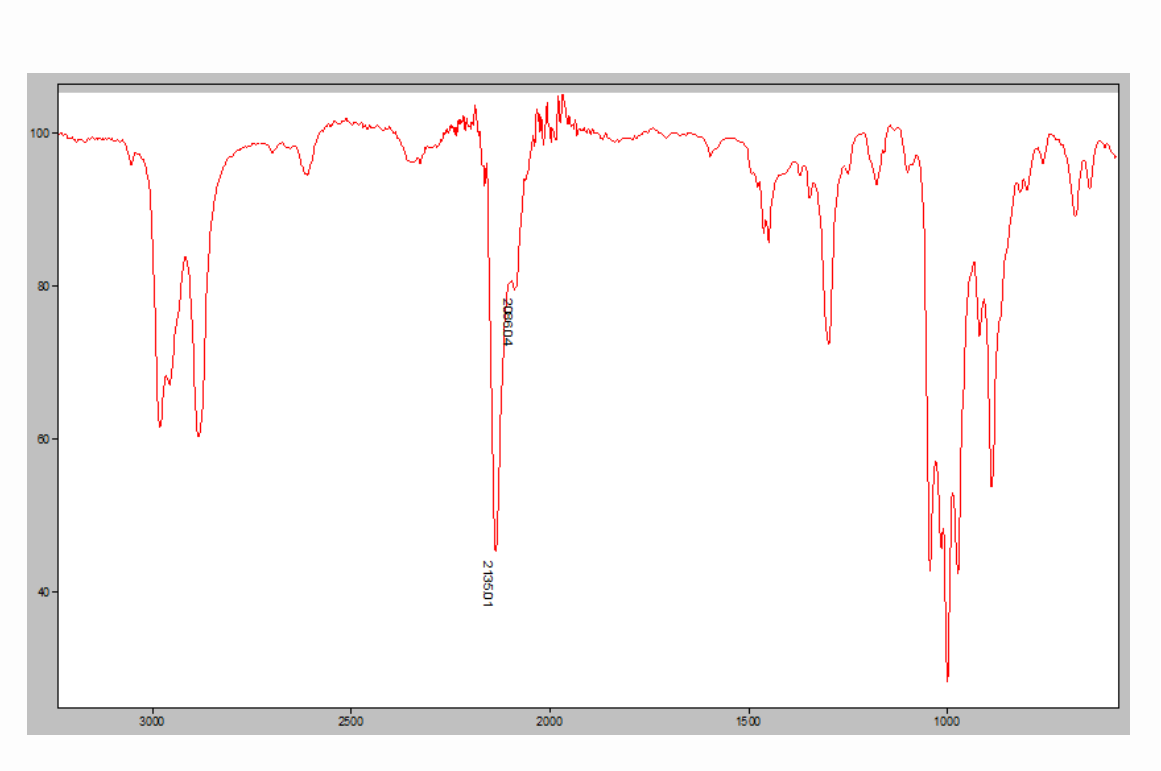

Figure 3-7 Solid-state IR spectrum of **5**

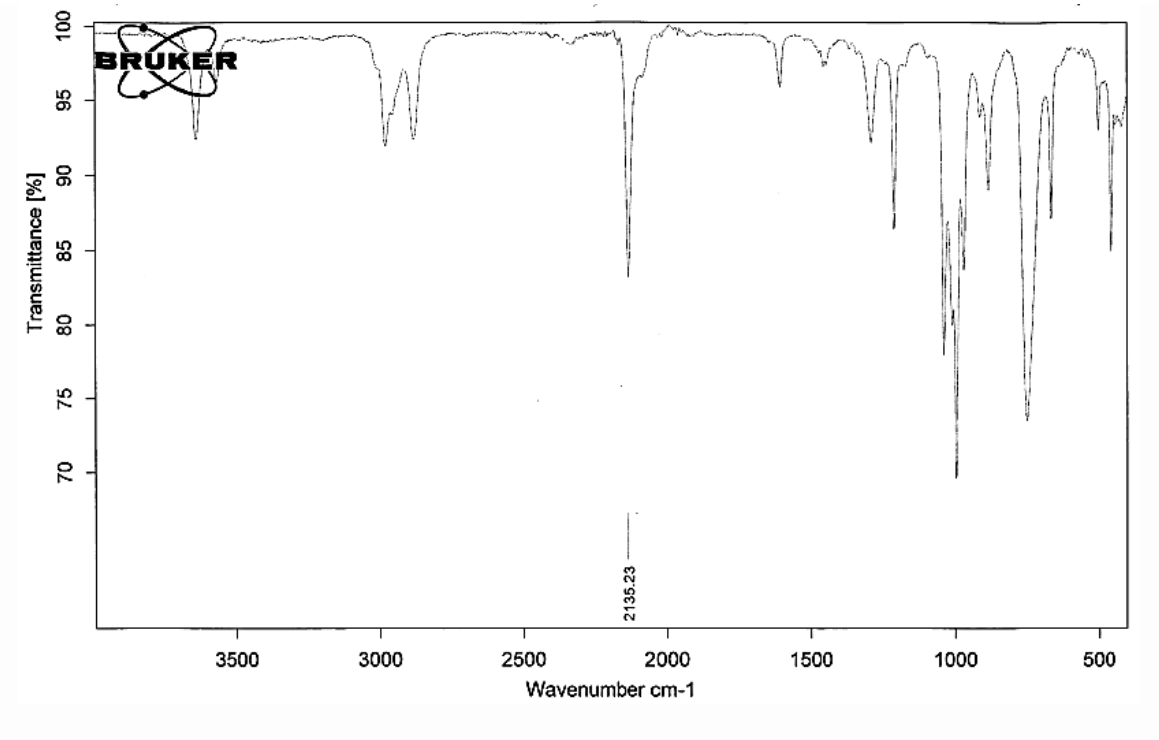

Figure 3-8 IR spectrum of **5** in $CHCl_3$

$[Li]^+[N_3CB_{11}H_5Br_6]^-$ (7)

$[HNMe_3]^+[HCB_{11}H_5Br_6]^-$ (**6**) (74 mg, 0.11 mmol) was dissolved in THF, deprotonated with 2.5 M *n*-butyllithium (2.7 eq., 0.13 mL, 0.30 mmol), and allowed to stir for 14 hours. After removing the solvent *in vacuo*, the precipitate was washed with hexanes (2 x 5 mL). The solid was then re-dissolved in THF (Note: in contrast to $[CB_{11}Br_{11}]^{2-}$, the $[CB_{11}H_5Br_6]^{2-}$ dianion deprotonates F-C_6H_5, and hence, THF was utilized) and immediately treated with a THF (5 mL) solution of tosyl azide (1.1 eq., 22 mg, 0.11 mmol) at -35°C over 15 minutes. The reaction mixture was stirred overnight at ambient temperature, upon which a precipitate of $LiO_2SC_7H_7$ formed. The mixture was cooled to -

35°C (Note: at this temperature $LiO_2SC_7H_7$ is completely insoluble in THF) and filtered to remove the salt byproduct and the solution concentrated under vacuum. The residue was washed with hexanes (2 x 5 mL) and dried to afford **7** as a white solid (82 mg, 78% yield).^{1}H NMR (300 MHz, $CDCl_3$, 25°C): $\delta =$ 1.97 (m, coord. THF), 3.83 (m, coord. THF); ^{13}C NMR (126 MHz, $CDCl_3$, 25°C): $\delta =$ 25.7 (CH_2, coord. THF), 68.8 (CH_2, coord. THF); ^{11}B NMR (96 MHz, THF, 25°C): $\delta =$ -15.1, -6.9, -0.1. HRMS calculated for **7** ($[M]^-$) 657.6627, found: 657.6613. IR of **7** in $CHCl_3$: 2118.6 cm^{-1} (N_3). mp = 192-200 °C (dec).

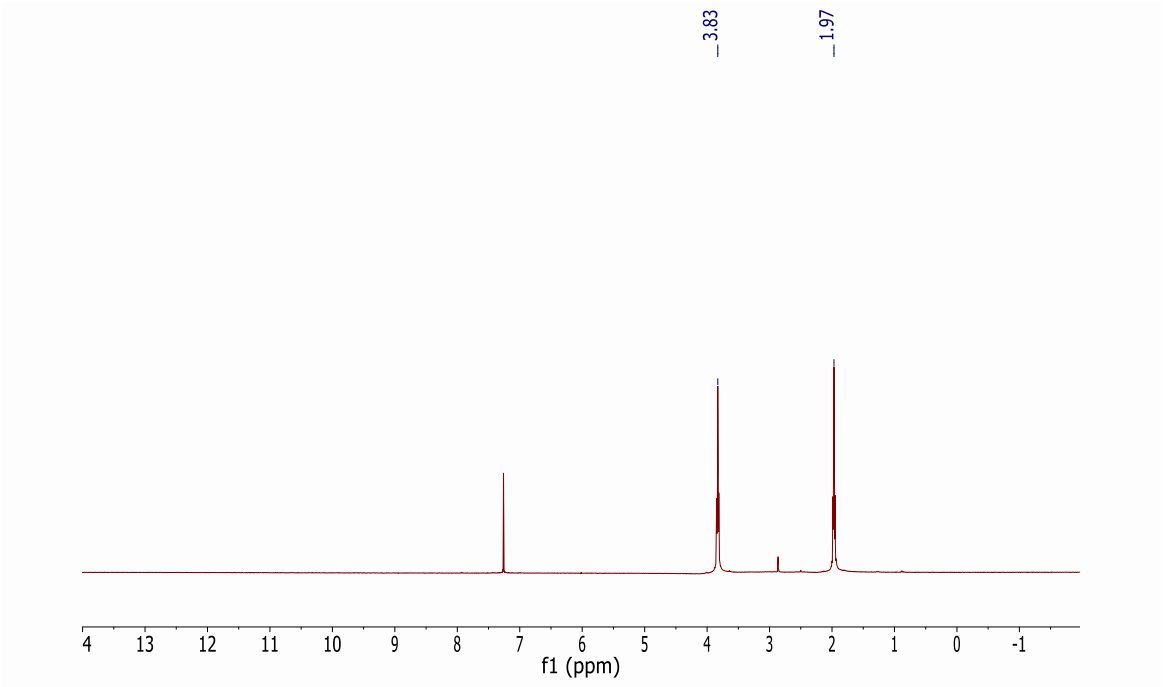

Figure 3-9 ^{1}H NMR spectrum of **7** (25°C, 300 MHz, $CDCl_3$)

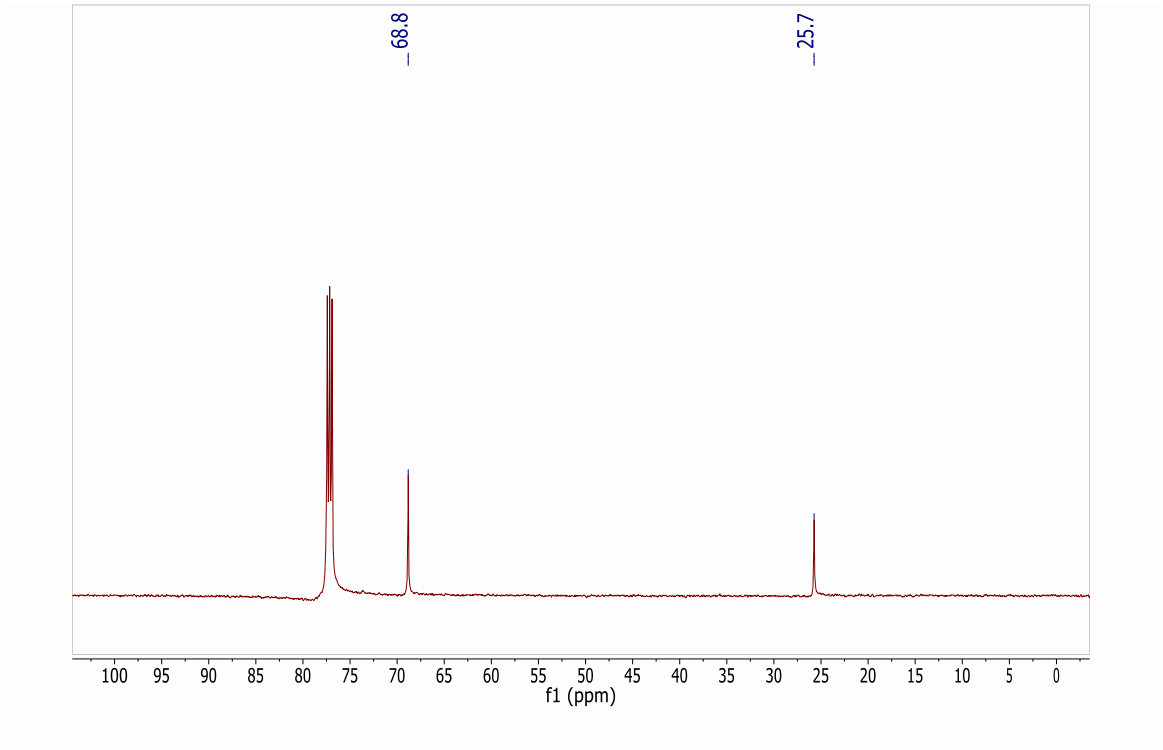

Figure 3-10 ^{13}C NMR spectrum of **7** (25°C, 126 MHz, $CDCl_3$)

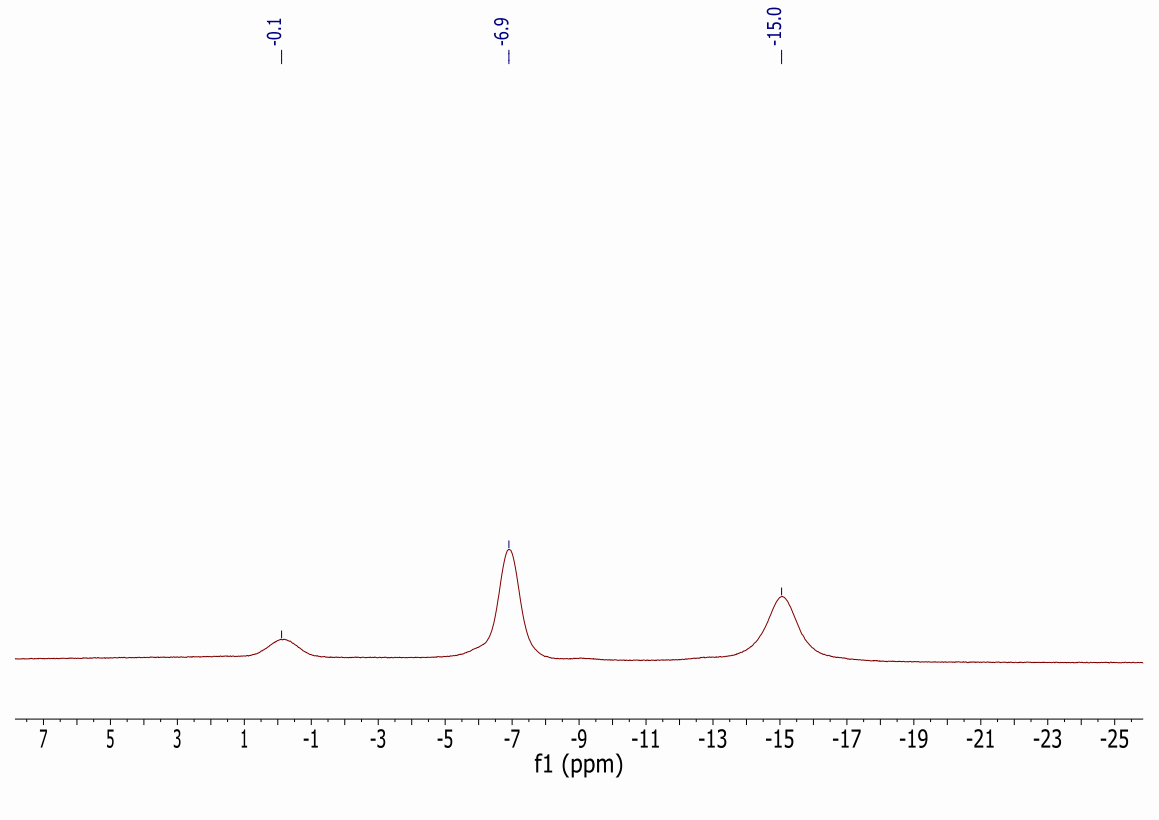

Figure 3-11 ^{11}B NMR spectrum of **7** (25°C, 96 MHz, THF)

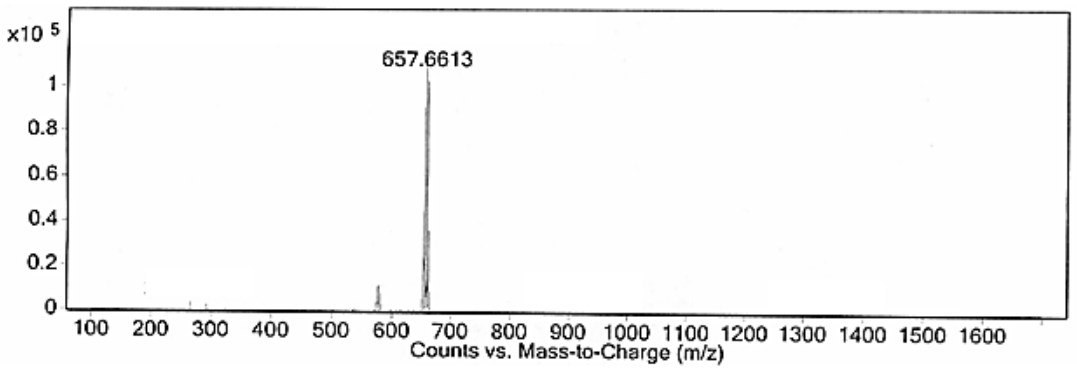

Figure 3-12 HRMS **7** (Multimode-ESI/APCI) $[M]^-$; Calculated **7** 657.6627

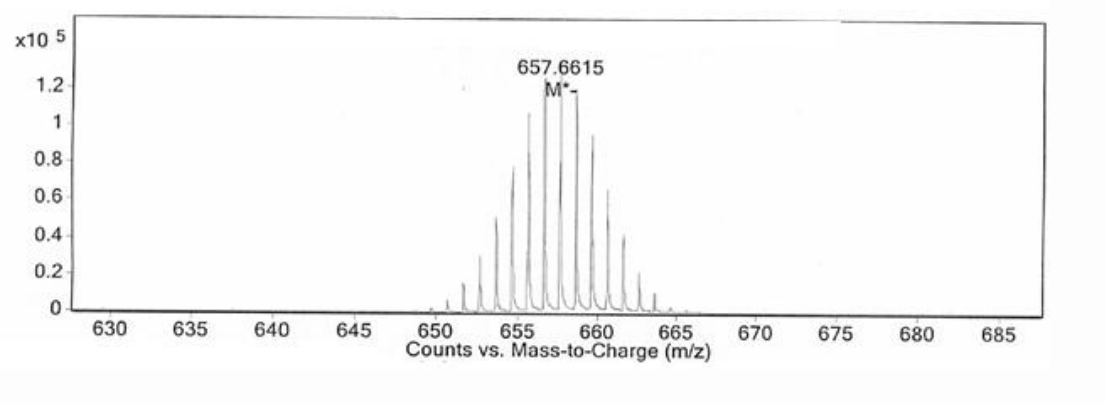

Figure 3-13 HRMS **7** (Multimode-ESI/APCI) $[M]^-$ Close-up of isotope pattern

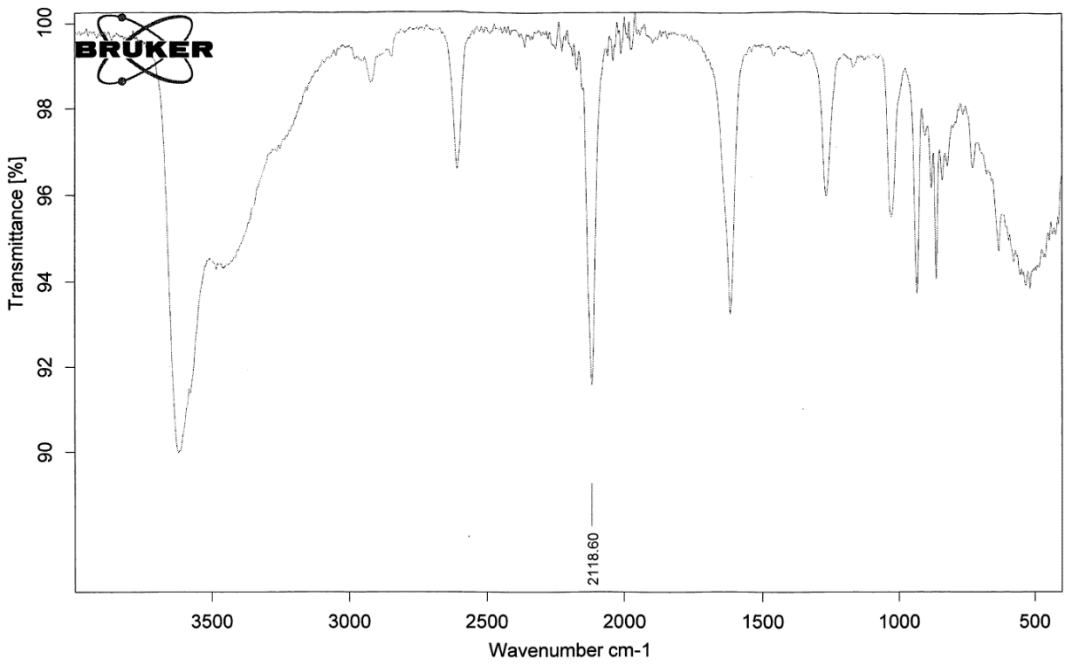

Figure 3-14 IR spectrum of **7** in $CHCl_3$

$[Li]^+[N_3CB_{11}H_{11}]^-$ (9)

$[HNMe_3]^+[HCB_{11}H_{11}]^-$ (**8**) (125 mg, 0.615 mmol) was dissolved in THF, deprotonated with 2.5 M *n*-butyllithium (2.7 eq., 0.66 mL, 1.66 mmol), and allowed to stir for 14 hours. After removing the solvent *in vacuo*, the precipitate was washed with hexanes (2 x 5 mL). The solid was then re-dissolved in THF and immediately treated with a THF (5 mL) solution of tosyl azide (1.1 eq., 133 mg, 0.677 mmol) at -35°C over 15 minutes. The reaction mixture was stirred overnight at ambient temperature, upon which a precipitate of $LiO_2SC_7H_7$ formed. The mixture was cooled to -35°C (Note: at this temperature $LiO_2SC_7H_7$ is completely insoluble in THF) and filtered to remove the salt byproduct and the solution concentrated under vacuum. The residue was washed with hexanes (2 x 5 mL) and dried to afford **9** as a white solid (163 mg, 65% yield).^{1}H NMR (300 MHz, $CDCl_3$, 25°C): $\delta = 1.94$ (m, coord. THF), 3.79 (m, coord. THF); ^{11}B NMR (96 MHz, THF, 25°C): $\delta =$ -11.8, -14.2.

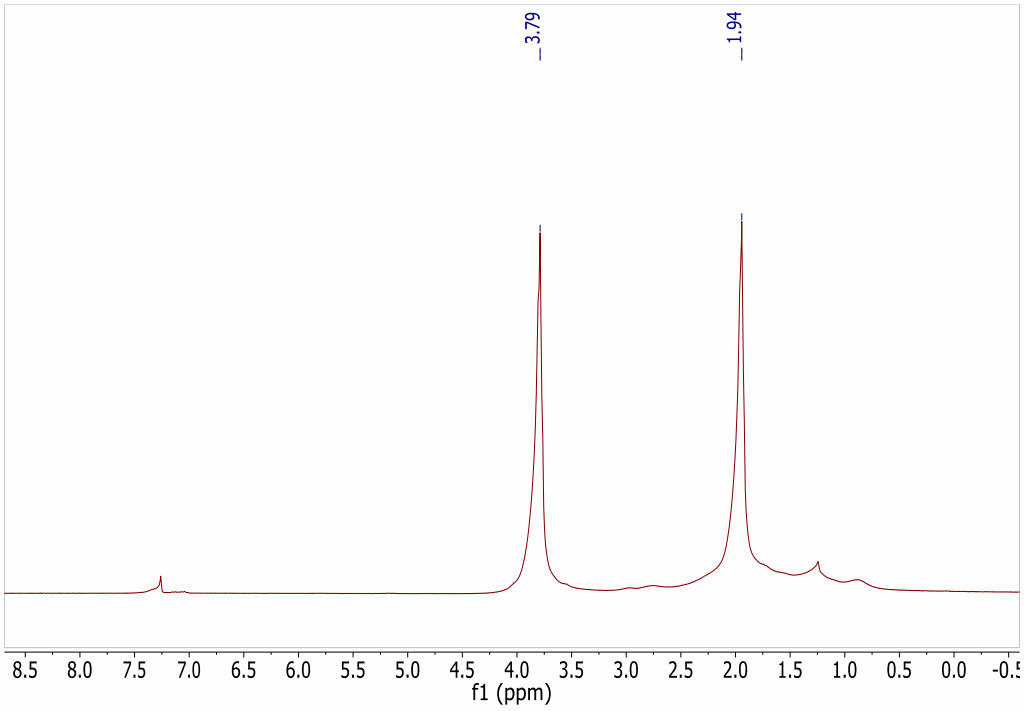

Figure 3-15 ^{1}H NMR spectrum of **9** (25°C, 300 MHz, $CDCl_3$)

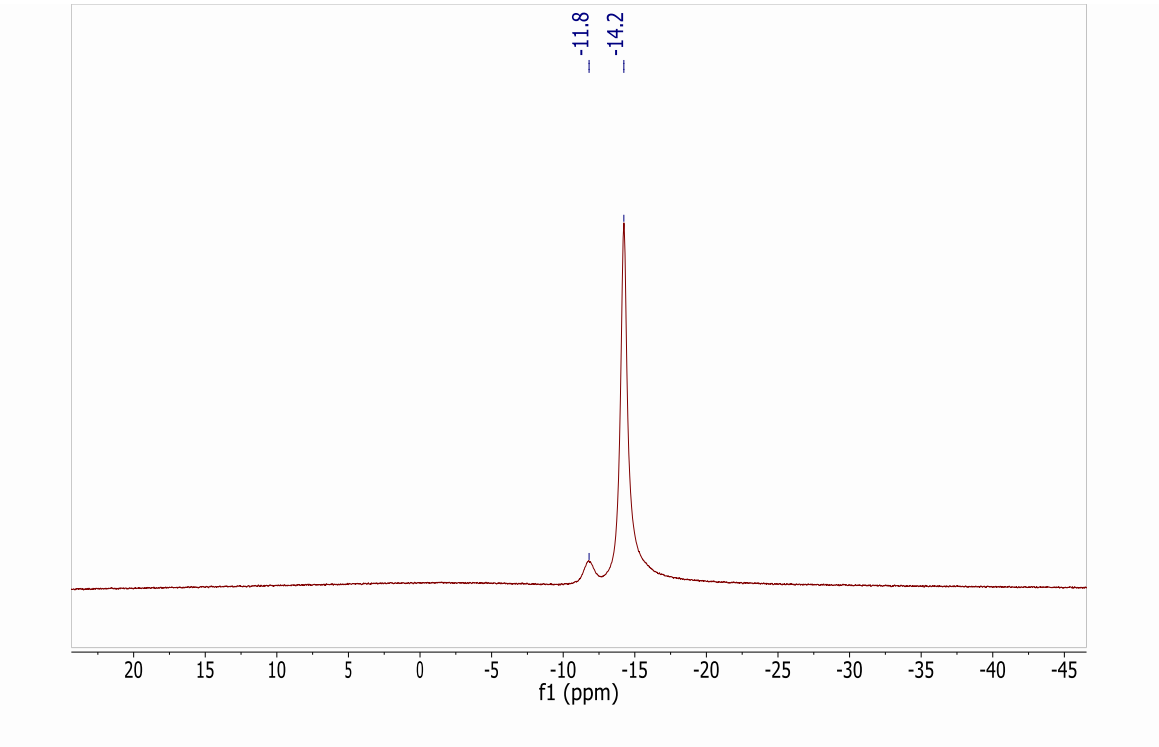

Figure 3-16 ^{11}B NMR spectrum of **9** (25°C, 96 MHz, $CDCl_3$)

$[Li]^+[NH_2CB_{11}H_5Br_6]^-$ (11)

$[Li]^+[N_3CB_{11}H_5Br_6]^-$ (**8**) (100 mg, 0.153 mmol) was dissolved in THF where 1 eq of PMe_3 was added dropwise to form the carboranyl iminophosphorane **11** and carboranyl amine **12**. After addition of a few drops of HCl and H_2O (2 mL). The mixture was then extracted with ether (5 mL x 3). To the ether, LiOH was then added to deprotonate the carboranyl ammonium species. The amine was extracted with H_2O (5 mL x 3) where the water was then pumped down. The resultant residue was washed with hexanes (2 x 5 mL) and dried to afford **11** as a white solid (58 mg, 60% yield). ^{11}B NMR (96 MHz, THF, 25°C): $\delta =$ 0.7, -6.8, -15.8. HRMS calculated for **11** ($[M]^-$) 631.6714, found: 631.6880.

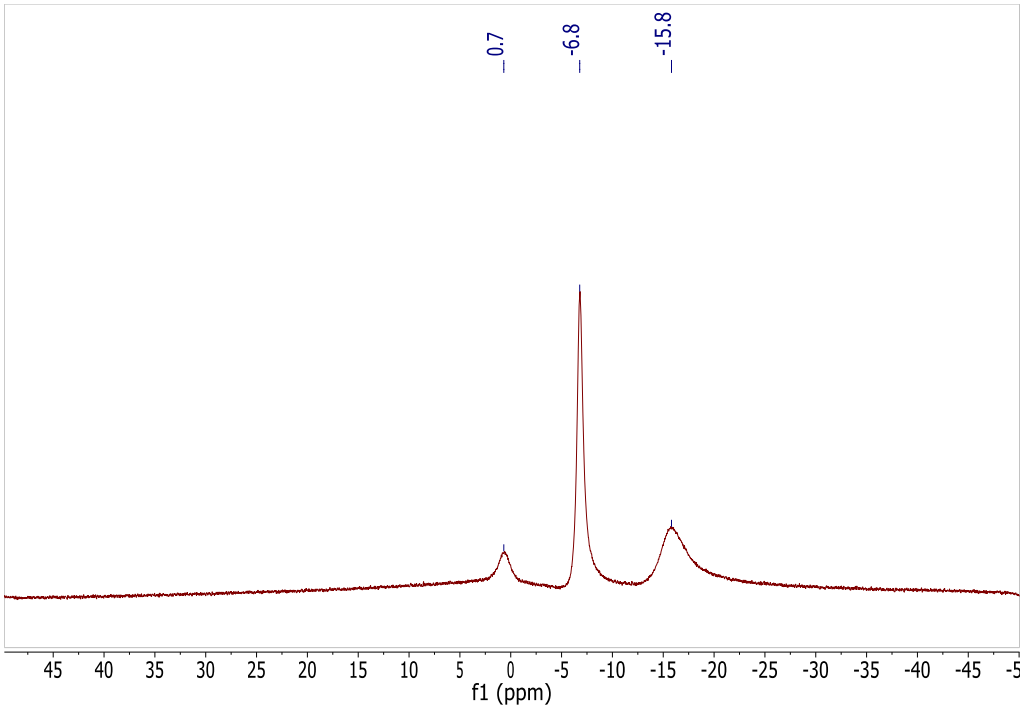

Figure 3-17 ^{11}B NMR spectrum of **11** (25°C, 96 MHz, THF)

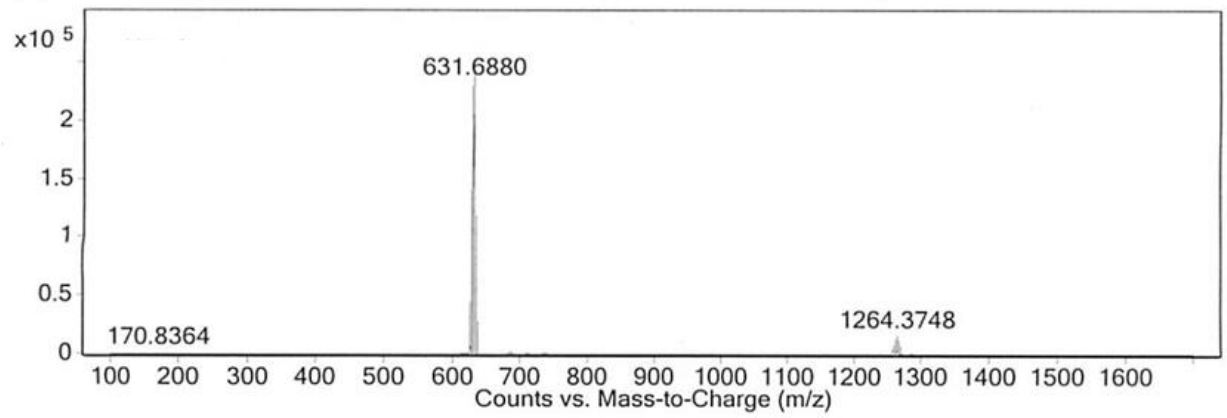

Figure 3-18 HRMS **11** (Multimode-ESI/APCI) $[M]^-$; Calculated **11** 631.6714

$[Li]^+[C_6H_4OHCNCB_{11}H_5Br_6]^-$ (12)

$[Li]^+[NH_2CB_{11}H_5Br_6]^-$ (**11**) (58 mg, 0.092 mmol) was dissolved in 1 mL of salicylaldehyde. After stirring for 2 hours, MS was taken to confirm conversion to imine product **12**.

HRMS calculated for **12**($[M]^-$) 735.6976, found: 735.7046.

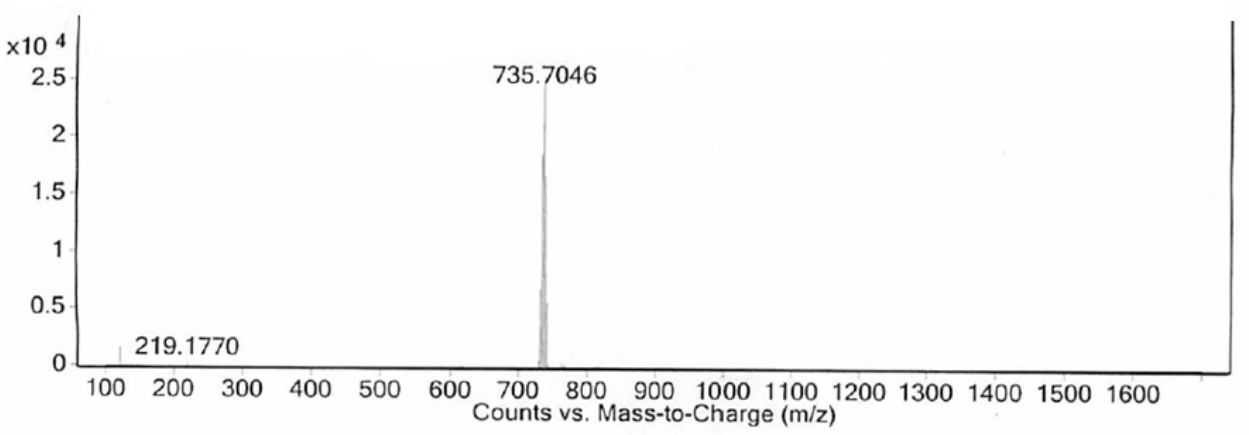

Figure 3-19 HRMS **12** (Multimode-ESI/APCI) $[M]^-$; Calculated **12** 735.6976

X-Ray Diffraction Studies

X-Ray Structure Determination for **5** (CCDC 996113)

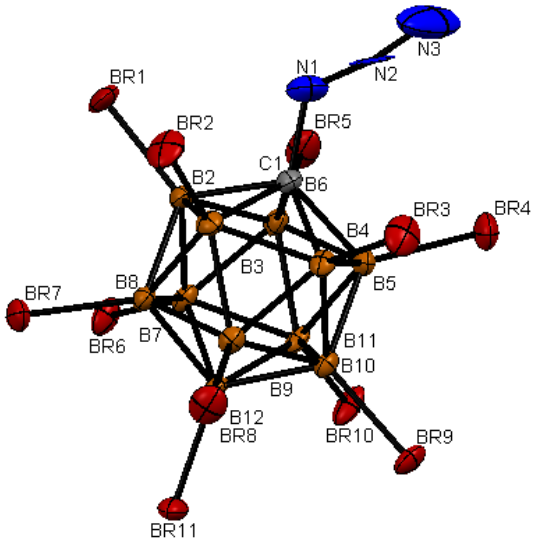

Figure 3-20 Crystal Structure of **5** (CCDC 996113), where the lithium countercation has been omitted for clarity

A colorless fragment of a prism (0.282 x 0.264 x 0.109 mm^3) was used for the single crystal x-ray diffraction study of $[CN_3B_{11}Br_{11}]^-_2[C_{22}H_{34}N_6O_8S_2Li_2]^+.C_6H_5F$ (sample vL40_0mP-1). The crystal was coated with paratone oil and mounted on to a cryo-loop glass fiber. X-ray intensity data were collected at 100(2) K on a Bruker APEX2 platform-CCD x-ray diffractometer system (fine focus Mo-radiation, λ = 0.71073 Å, 50KV/30mA power). The CCD detector was placed at a distance of 5.1200 cm from the crystal.

A total of 4800 frames were collected for a sphere of reflections (with scan width of 0.3° in ω and ϕ, starting ω and 2θ angles of -30°, and ϕ angles of 0°, 90°, 120°, 180°, 240°, and 270° for every 600 frames, and 1200 frames with ϕ-scan from 0-360°, 10

sec/frame exposure time). The frames were integrated using the Bruker SAINT software package and using a narrow-frame integration algorithm. Based on a triclinic crystal system, the integrated frames yielded a total of 58596 reflections at a maximum 2θ angle of 59.142° (0.72 Å resolution), of which 11823 were independent reflections (R_{int} = 0.0311, R_{sig} = 0.0249, redundancy = 5.0, completeness = 99.9%) and 9722 (82.2%) reflections were greater than $2\sigma(I)$. The unit cell parameters were, **a** = 12.7713(5) Å, **b** = 13.1886(5) Å, **c** = 14.7026(6) Å, α = 78.141(1), β = 65.380(1)°, γ = 69.750(1) V = 2106.70(15) Å^3, Z = 1, calculated density D_c = 2.274 g/cm^3. Absorption corrections were applied (absorption coefficient μ = 10.550 mm^{-1}; max/min transmission = 0.393/0.155) to the raw intensity data using the SADABS program.

The Bruker SHELXTL software package was used for phase determination and structure refinement. The distribution of intensities (E^2-1 = 1.027) and no systematic absent reflections indicated two possible space groups, P-1and P1. The space group P-1 (#2) was later determined to be correct. Direct methods of phase determination followed by two Fourier cycles of refinement led to an electron density map from which most of the non-hydrogen atoms were identified in the asymmetric unit of the unit cell. With subsequent isotropic refinement, all of the non-hydrogen atoms were identified. There were one cation of $[C_{22}H_{34}N_6O_8S_2Li_2]^+$, one anion of $[CN_3B_{11}Br_{11}]^-$, one disordered solvent molecule of C_6H_5F (disordered site occupancy factor ratio was 61%/39%), and one water molecule present in the asymmetric unit of the unit cell. The N_3-group attached to the C-atom of the carborane was modeled as a rigid group restraint. The A

and B level alerts reported in the checkcif file are probably due to the carborane N_3-group disorder that could not be clearly modeled. Attempts to model the possible N_3 disorder group failed. The possible cause of the N_3-group disorder is most likely due to the solvent of crystallization (fluorobenzene) disorder and an estimate of 3-5 percent of partially occupied water in the vicinity of the N_3-group.

Atomic coordinates, isotropic and anisotropic displacement parameters of all the non-hydrogen atoms were refined by means of a full matrix least-squares procedure on F^2. The H-atoms were included in the refinement in calculated positions riding on the atoms to which they were attached. The refinement converged at R1 = 0.336, wR2 = 0.0791, with intensity $I>2\sigma$ (I). The largest peak/hole in the final difference map was 2.906/-2.021 e/Å^3. The high peak/hole in the difference electron density in the vicinity of all the Br-atoms is probably due to limitation of the absorption correction errors calculated.

Crystal Data and Structure Refinement for **5**

Identification code	vL40_0mP-1
Empirical formula	C36 H44 B22 Br22 F2 Li2 N12 O8 S2
Formula weight	2884.67
Temperature	100(2) K
Wavelength	0.71073 Å
Crystal system	Triclinic
Space group	P -1

Unit cell dimensions	a = 12.7713(5) Å	α= 78.141(1)°.
	b = 13.1886(5) Å	β= 65.380(1)°.
	c = 14.7026(6) Å	γ = 69.750(1)°.
Volume	2106.70(15) Å^3	
Z	1	
Density (calculated)	2.274 Mg/m^3	
Absorption coefficient	10.550 mm^{-1}	
F(000)	1344	
Crystal size	0.282 x 0.264 x 0.109 mm^3	
Theta range for data collection	1.527 to 29.571°.	
Index ranges	-17<=h<=17, -18<=k<=18, -20<=l<=20	
Reflections collected	58596	
Independent reflections	11823 [R(int) = 0.0311]	
Completeness to theta = 25.242°	100.0 %	
Absorption correction	Semi-empirical from equivalents	
Refinement method	Full-matrix least-squares on F^2	
Data / restraints / parameters	11823 / 276 / 525	
Goodness-of-fit on F^2	1.039	
Final R indices [I>2sigma(I)]	R1 = 0.0336, wR2 = 0.0791	
R indices (all data)	R1 = 0.0450, wR2 = 0.0834	

Extinction coefficient	n/a
Largest diff. peak and hole	2.906 and -2.021 e.Å^{-3}

X-Ray Structure Determination of **7** (CCDC 995208)

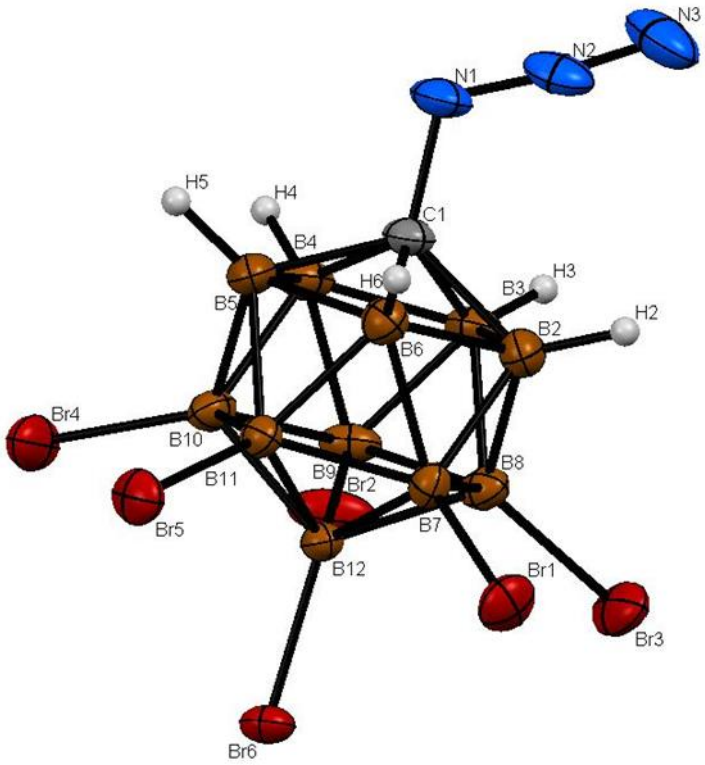

Figure 3-21 Crystal Structure of **7** (CCDC 995208), where the lithium counteraction has been omitted for clarity

A colorless plate fragment (0.27 x 0.23 x 0.05 mm^3) was used for the single crystal x-ray diffraction study of $[Li_2[C_4H_8O]_6]^{2+}[N_3CH_5B_{11}Br_6]_2^-$. The crystal was coated

with paratone oil and mounted on to a cryo-loop glass fiber. X-ray intensity data were collected at 100(2) K on a Bruker APEX2 platform-CCD x-ray diffractometer system (fine focus Mo-radiation, λ = 0.71073 Å, 50KV/35 mA power). The CCD detector was placed at a distance of 5.1000 cm from the crystal.

A total of 2400 frames were collected for a hemisphere of reflections (with scan width of 0.3° in ω, starting ω and 2θ angles at -30°, and ϕ angles of 0°, 90°, 180°, and 270° for every 600 frames, 20 sec/frame exposure time). The frames were integrated using the Bruker SAINT software package and using a narrow-frame integration algorithm. Based on a monoclinic crystal system, the integrated frames yielded a total of 45593 reflections at a maximum 2θ angle of 60.06° (0.71 Å resolution), of which 8658 were independent reflections (R_{int} = 0.0502, R_{sig} = 0.0394, redundancy = 5.3, completeness = 100%) and 6497 (75.0%) reflections were greater than 2σ(I). The unit cell parameters were, **a** = 11.4585(3) Å, **b** = 21.0377(6) Å, **c** = 12.4213(4) Å, β = 98.660(1)°, V = 2960.15(15) Å^3, Z = 2, calculated density D_c = 1.882 g/cm^3. Absorption corrections were applied (absorption coefficient μ = 8.156 mm^{-1}; max/min transmission = 0.6955/0.2176) to the raw intensity data using the SADABS program.

The Bruker SHELXTL software package was used for phase determination and structure refinement. The distribution of intensities (E^2-1 = 0.940) and systematic absent reflections indicated one possible space group, P2(1)/n. The space group P2(1)/n (#14) was later determined to be correct. Direct methods of phase determination followed by two Fourier cycles of refinement led to an electron density map from which most of the

non-hydrogen atoms were identified in the asymmetry unit of the unit cell. With subsequent isotropic refinement, all of the non-hydrogen atoms were identified. There was one half of a cation of $[Li_2[C_4H_8O]_6]^{2+}$ and one anion of $[N_3CH_5B_{11}Br_6]^-$ present in the asymmetry unit of the unit cell.

Atomic coordinates, isotropic and anisotropic displacement parameters of all the non-hydrogen atoms were refined by means of a full matrix least-squares procedure on F^2. The H-atoms were included in the refinement in calculated positions riding on the atoms to which they were attached. The refinement converged at R1 = 0.0376, wR2 = 0.0822, with intensity $I>2\sigma$ (I). The largest peak/hole in the final difference map was 1.937/-1.237 e/Å^3. The high electron density peaks (1.95-1.72) near the Br-atoms are probably due to absorption correction error.

Crystal Data and Structure Refinement for **7**

Identification code	vl30_0m	
Empirical formula	C20 H46 B22 Br12 Li2 N6 O6	
Formula weight	1677.25	
Temperature	100(2) K	
Wavelength	0.71073 Å	
Crystal system	Monoclinic	
Space group	P2(1)/n (#14)	
Unit cell dimensions	a = 11.4585(3) Å	$\alpha = 90°$.
	b = 21.0377(6) Å	$\beta = 98.660(1)°$.

	c = 12.4213(4) Å $\gamma = 90°$.
Volume	2960.15(15) $Å^3$
Z	2
Density (calculated)	1.882 Mg/m^3
Absorption coefficient	8.156 mm^{-1}
F(000)	1584
Crystal size	0.27 x 0.23 x 0.05 mm^3
Theta range for data collection	1.92 to 30.03°.
Index ranges	-16<=h<=16, -29<=k<=29, -17<=l<=17
Reflections collected	45593
Independent reflections	8658 [R(int) = 0.0502]
Completeness to theta = 30.03°	100.0 %
Absorption correction	Semi-empirical from equivalents
Max. and min. transmission	0.6955 and 0.2176
Refinement method	Full-matrix least-squares on F^2
Data / restraints / parameters	8658 / 0 / 313
Goodness-of-fit on F^2	1.027
Final R indices [I>2sigma(I)]	R1 = 0.0376, wR2 = 0.0822
R indices (all data)	R1 = 0.0606, wR2 = 0.0904
Largest diff. peak and hole	1.937 and -1.237 $e.Å^{-3}$

X-Ray Structure Determination of **8** (CCDC 995208)

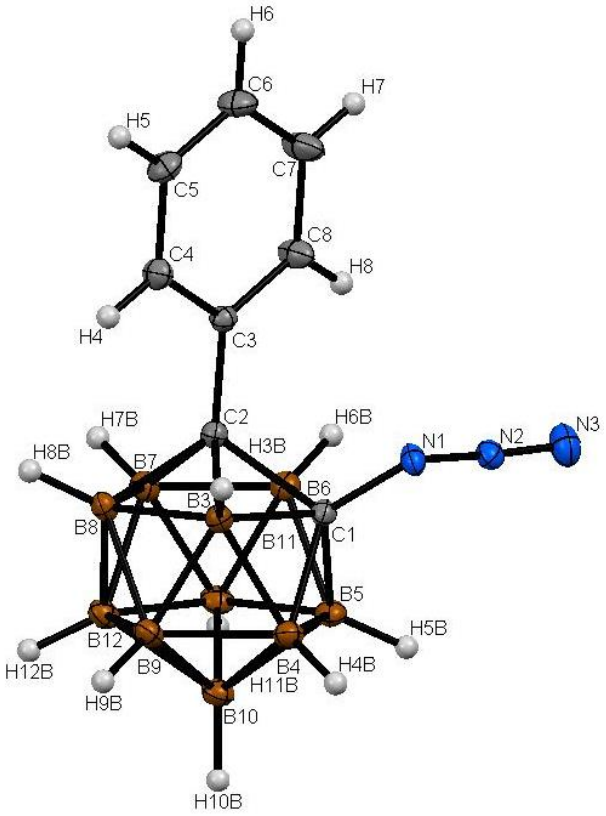

Figure 3-22 Crystal Structure of **8** (CCDC 995207)

A colorless thin plate fragment (0.484 x 0.221 x 0.027 mm^3) was used for the single crystal x-ray diffraction study of $C_8H_{15}B_{10}N_3$ (sample vL5_0m). The crystal was coated with paratone oil and mounted on to a cryo-loop glass fiber. X-ray intensity data were collected at 100(2) K on a Bruker APEX2 platform-CCD x-ray diffractometer system (fine focus Mo-radiation, λ = 0.71073 Å, 50KV/30mA power). The CCD detector was placed at a distance of 5.0600 cm from the crystal.

A total of 3130 frames were collected for a sphere of reflections (with scan width of 0.3° in ω, starting ω and 2θ angles at -30°, and ϕ angles of 0°, 90°, 120°, 180°, and

270° for every 600 frames, 130 frames for ϕ at 240°, 30 sec/frame exposure time). The frames were integrated using the Bruker SAINT software package and using a narrow-frame integration algorithm. Based on a monoclinic crystal system, the integrated frames yielded a total of 27400 reflections at a maximum 2θ angle of 31.012° (0.70 Å resolution), of which 4309 were independent reflections (R_{int} = 0.0429, R_{sig} = 0.0282, redundancy = 6.4, completeness = 100%) and 3367 (78.1%) reflections were greater than $2\sigma(I)$. The unit cell parameters were, **a** = 10.4809(10) Å, **b** = 10.3180(10) Å, **c** = 13.5712(13) Å, β = 105.304(2)°, V = 1415.6(2) Å^3, Z = 4, calculated density D_c = 1.226 g/cm^3. Absorption corrections were applied (absorption coefficient μ = 0.064 mm^{-1}; max/min transmission = 0.970/0.998) to the raw intensity data using the SADABS program.

The Bruker SHELXTL software package was used for phase determination and structure refinement. The distribution of intensities (E^2-1 = 0.980) and systematic absent reflections indicated one possible space group, P2(1)/c. The space group P2(1)/c (#14) was later determined to be correct. Direct methods of phase determination followed by two Fourier cycles of refinement led to an electron density map from which most of the non-hydrogen atoms were identified in the asymmetric unit of the unit cell. With subsequent isotropic refinement, all of the non-hydrogen atoms were identified. There was one molecule of $C_8H_{15}B_{10}N_3$ present in the asymmetric unit of the unit cell. The alerts level B, and G reported in the checkcif is due to the long C-C bond and 6-coordination of the C-atom in carborane structure.

Atomic coordinates, isotropic and anisotropic displacement parameters of all the non-hydrogen atoms were refined by means of a full matrix least-squares procedure on F^2. The H-atoms were included in the refinement in calculated positions riding on the atoms to which they were attached. The refinement converged at R1 = 0.0426, wR2 = 0.1082, with intensity I>2σ (I). The largest peak/hole in the final difference map was 0.355/-0.324 e/Å^3.

Crystal Data and Structure Refinement for **8**

Identification code	vL5_0m	
Empirical formula	C8 H15 B10 N3	
Formula weight	261.33	
Temperature	100(2) K	
Wavelength	0.71073 Å	
Crystal system	Monoclinic	
Space group	P 21/c (#14)	
Unit cell dimensions	a = 10.4809(10) Å	α= 90°.
	b = 10.3180(10) Å	β= 105.304(2)°.
	c = 13.5712(13) Å	γ = 90°.
Volume	1415.6(2) Å^3	
Z	4	
Density (calculated)	1.226 Mg/m^3	

Absorption coefficient	0.064 mm^{-1}
F(000)	536
Crystal size	0.484 x 0.221 x 0.027 mm^3
Theta range for data collection	2.015 to 30.506°.
Index ranges	-14<=h<=14, -14<=k<=14, -19<=l<=19
Reflections collected	27400
Independent reflections	4309 [R(int) = 0.0429]
Completeness to theta = 25.242°	100.0 %
Absorption correction	Semi-empirical from equivalents
Refinement method	Full-matrix least-squares on F^2
Data / restraints / parameters	4309 / 0 / 190
Goodness-of-fit on F^2	1.041
Final R indices [I>2sigma(I)]	R1 = 0.0426, wR2 = 0.1082
R indices (all data)	R1 = 0.0597, wR2 = 0.1189
Extinction coefficient	n/a
Largest diff. peak and hole	0.355 and -0.324 e.$Å^{-3}$

3.4 References

(1) Wright, J. H., II; Kefaidis, C. E.; Tham, F. S.; Maron, L.; Lavallo, V. *Inorganic Chemistry* **2013**, *52*, 6223.

(2) El-Hellani, A.; Kefalidis, C. E.; Tham, F. S.; Maron, L.; Lavallo, V. *Organometallics* **2013**, *32*, 6887.

(3) El-Hellani, A.; Lavallo, V. *Angewandte Chemie International Edition* **2014**, *53*, 4489.

(4) Lavallo, V.; Wright, J. H., II; Tham, F. S.; Quinlivan, S. *Angewandte Chemie International Edition* **2013**, *52*, 3172.

(5) Gu, W.; McCulloch, B. J.; Reibenspies, J. H.; Ozerov, O. V. *Chemical Communications* **2010**, *46*, 2820.

(6) Chan, A. L.; Fajardo, J., Jr.; Wright, J. H.; Asay, M.; Lavallo, V. *Inorganic Chemistry* **2013**, *52*, 12308.

(7) Kennedy, R. D. *Chemical Communications* **2010**, *46*, 4782.

(8) Fox, M. A.; Peace, R. J.; Clegg, W.; Elsegood, M. R. J.; Wade, K. *Polyhedron* **2009**, *28*, 2359.

(9) Douvris, C.; Michl, J. *Chemical Reviews* **2013**, *113*, PR179.

(10) Scholz, M.; Hey-Hawkins, E. *Chemical Reviews* **2011**, *111*, 7035.

(11) Gololobov, Y. G.; Kasukhin, L. F. *Tetrahedron* **1992**, *48*, 1353.

(12) T. Jelinek, J. P., S. Hermanek, B. Stıbr *Collection of Czechoslovak Chemical Communications* **1986**, *51*, 819.

Chapter 4: Carboranyl Amines and Imines: Caboranyl Ligands for Metal Complexes

4.1 Introduction

In order to utilize the unique properties of the carborane as ligand R-groups on metal complexes, we delved into incorporating carborane ligands into Schiff bases. Recently, Schiff bases have been a source of ligand design for metal complexes[1-3]. Due to the relative ease of synthesizing certain classes of these ligands[4], as well as observed catalytic activity of Schiff base complexes in the synthesis of important branched[5] and linear polyethylenes[6-8], the oxidation of hydrocarbons[9], the ring opening polymerization of large cycloalkenes[10], and the alkylation of allylic substrates[11], we wished to explore this synthetic avenue of incorporating the carborane cluster into this ligand class.

Another interesting and intersecting motif that we wanted to pursue is the synthesis of N-heterocyclic carbenes with carborane anions. NHCs are well known for their utility as ligands for catalysts[12,13], and we have also previously shown interesting chemical behavior of NHCs fused with the parent carborane anions when deprotonated with various bases at different temperatures[14]. Prompted by these results, we were interested in making analogous NHCs starting from the hexabrominated and perhalogenated carboranyl amine to compare with the NHCs made with the parent carboranyl amine.

4.2 Results and Discussion

Using carboranyl amine synthesized via Stibr's method[15], we attempted to do a simple condensation reaction with salicylaldehyde. Overnight, the carboranyl amine is fully converted to the Schiff base, as indicated by ^{1}H NMR. We then added NaH in THF, where we see a change in the ^{1}H NMR and ^{11}B NMR. Various metals are currently being screened for this new carborane based ligand.

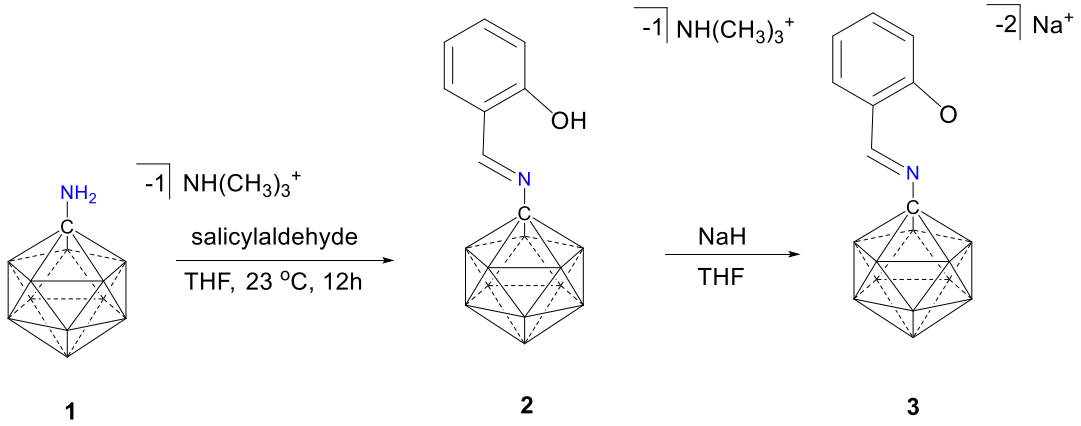

1 **2** **3**

Scheme 4-1 Synthesis of imine **2** and **3**

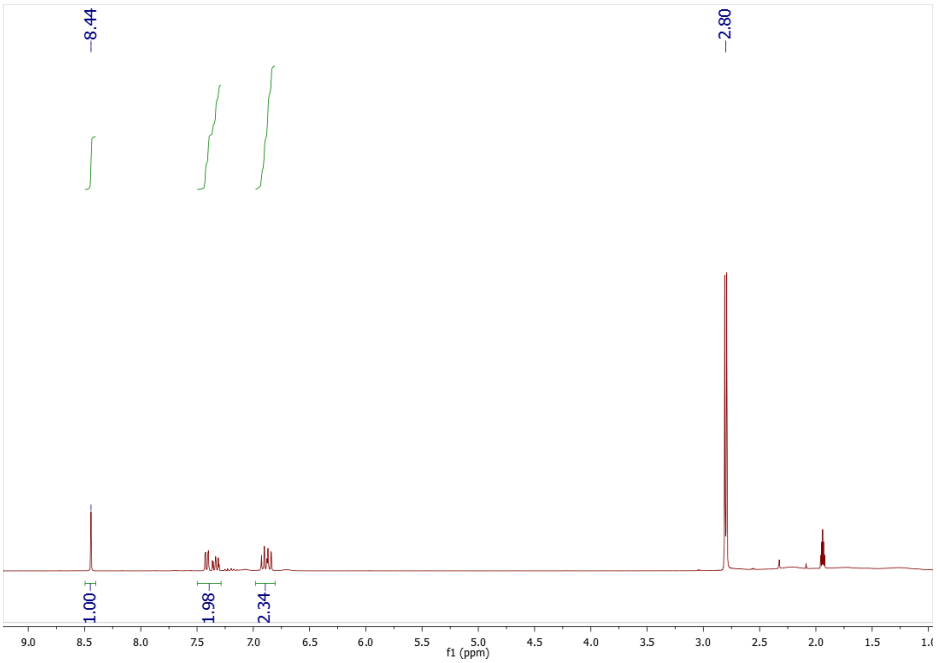

Figure 4-1 ^{1}H NMR of imine **2** (25°C, 300 MHz, THF-d_8)

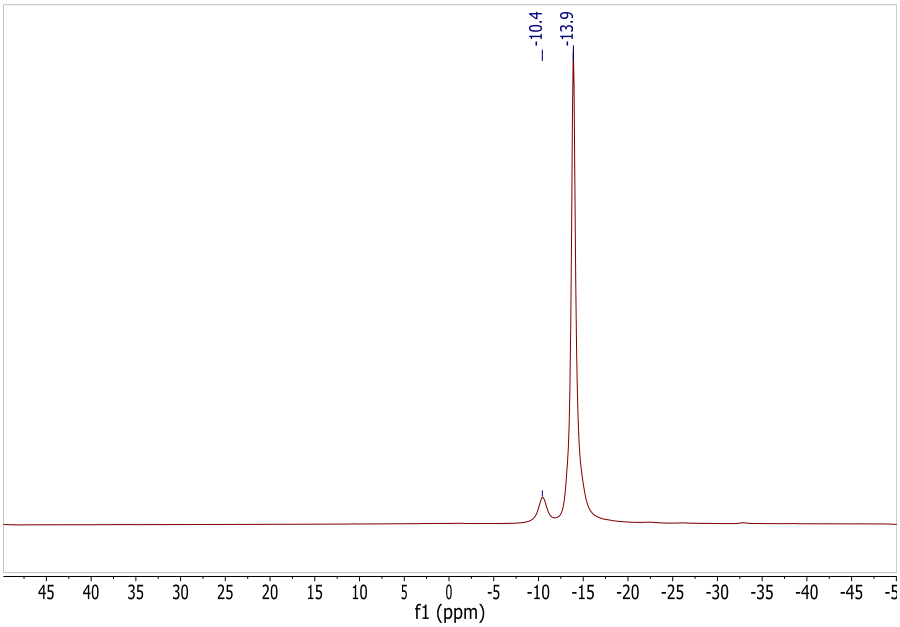

Figure 4-2 ^{11}B NMR of imine **2** (25°C, 96 MHz, THF-d_8)

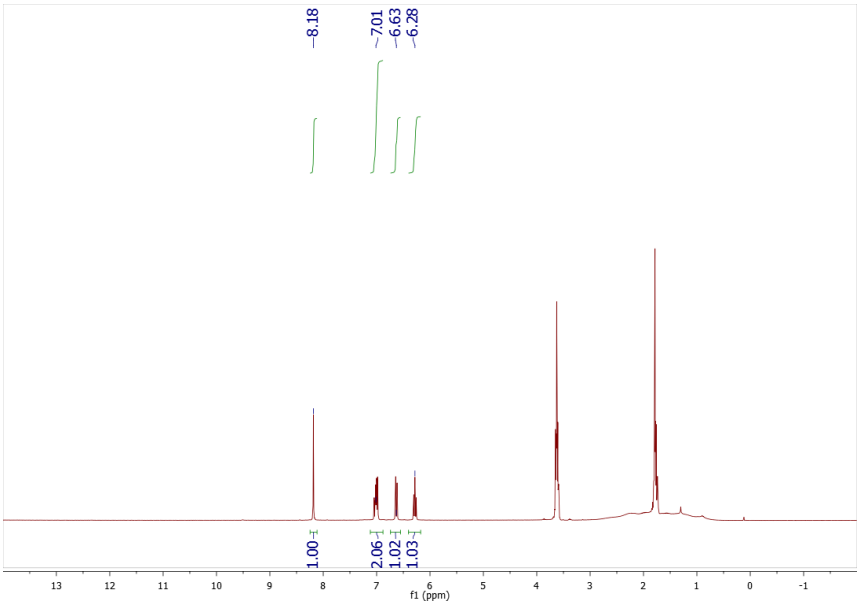

Figure 4-3 ^{1}H NMR of imine **3** (25^{o}C, 300 MHz, THF-d_8)

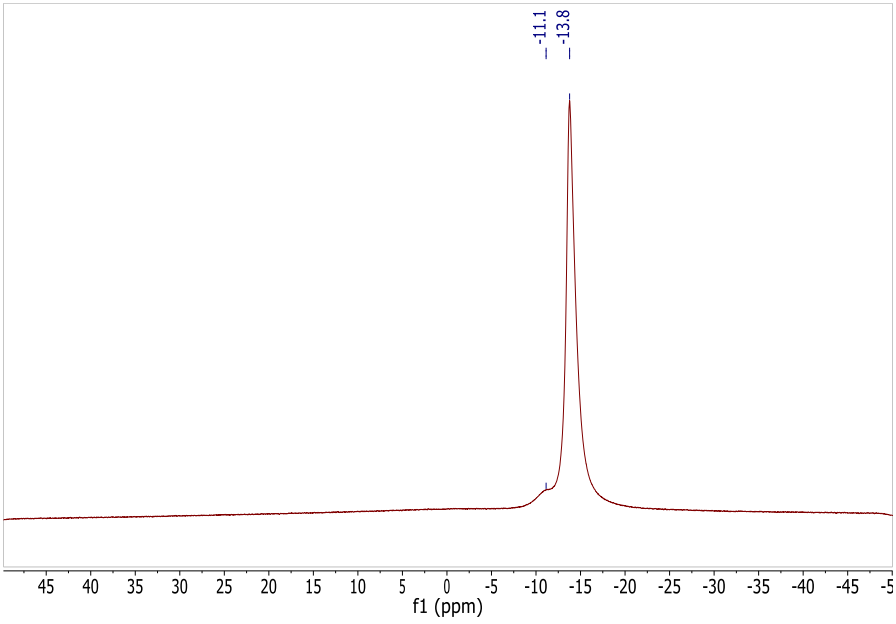

Figure 4-4 ^{11}B NMR of imine **3** (25^{o}C, 96 MHz, THF-d_8)

With the desire to generate another avenue to the hexabrominated carboranyl amine, we attempted to brominate the perhydrogenated carboranyl amine synthesized via Stibr's synthesis[15]. Initially, we attempted to use Reed's method of brominating the parent carborane[16] to brominate the carboranyl amine. However, we see amide formation with the acetic acid. By adding bromine neat to the parent carboranyl amine, we see full conversion to the Br_6 carboranyl amine after several days. With the hexabrominated carboranyl amine in hand, we wished to synthesize an N-heterocyclic carbene analogous to previously published work on N-heterocyclic carbenes derived from the parent carboranyl amine[14]. Scheme 4-1 shows the synthesis to the carbene **6**. Preliminary results show the formation of the NHC by ^{1}H and ^{13}C NMR. We are currently looking into various metals to coordinate to this new carbene based ligand.

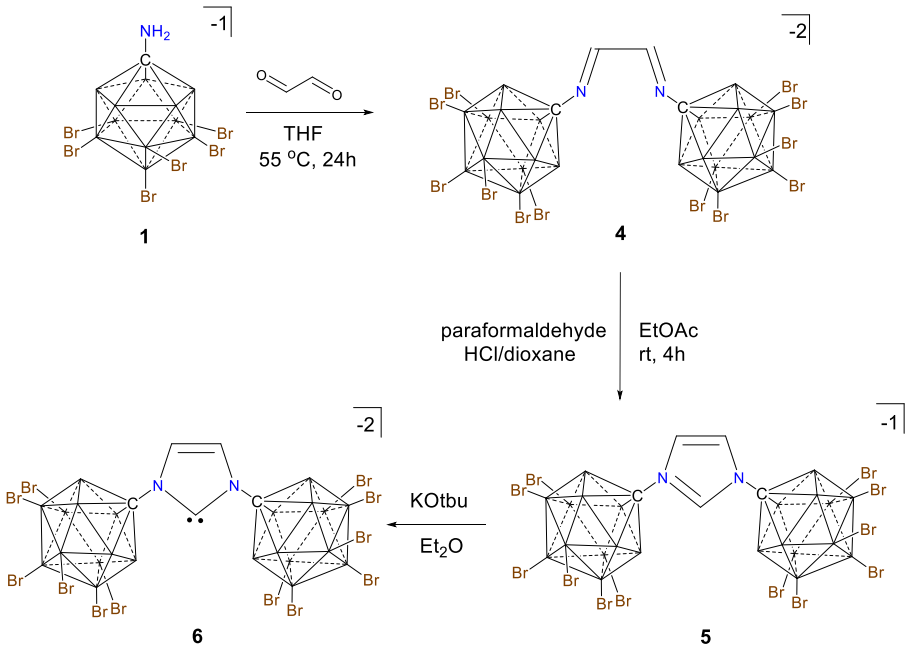

Scheme 4-2 Reaction scheme for the synthesis of carbene **6**

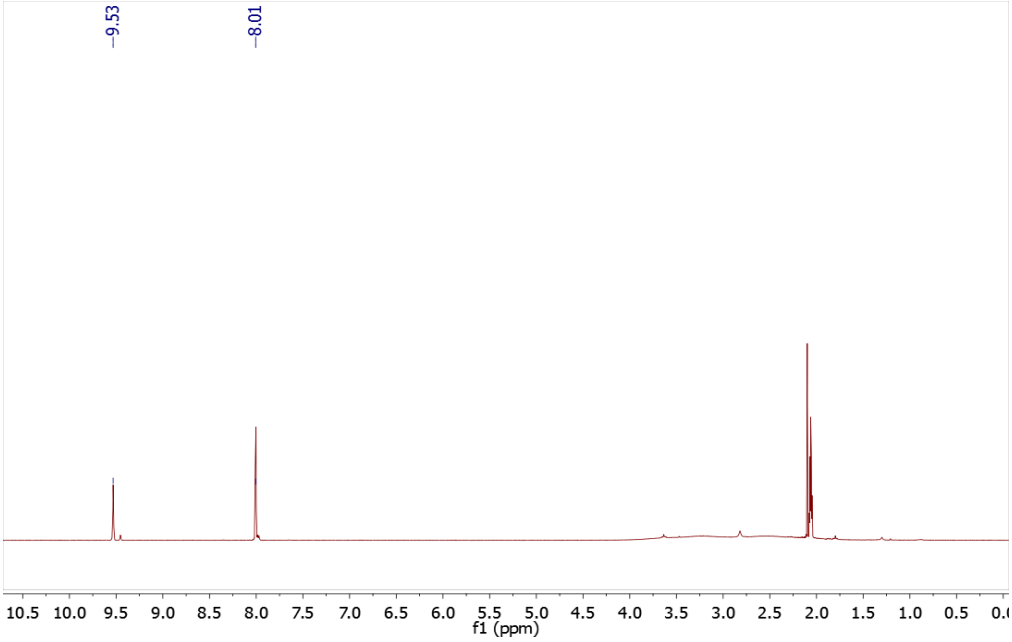

Figure 4-5 ^{1}H NMR of imidazolium **5** (25°C, 300 MHz, acetone-d_6)

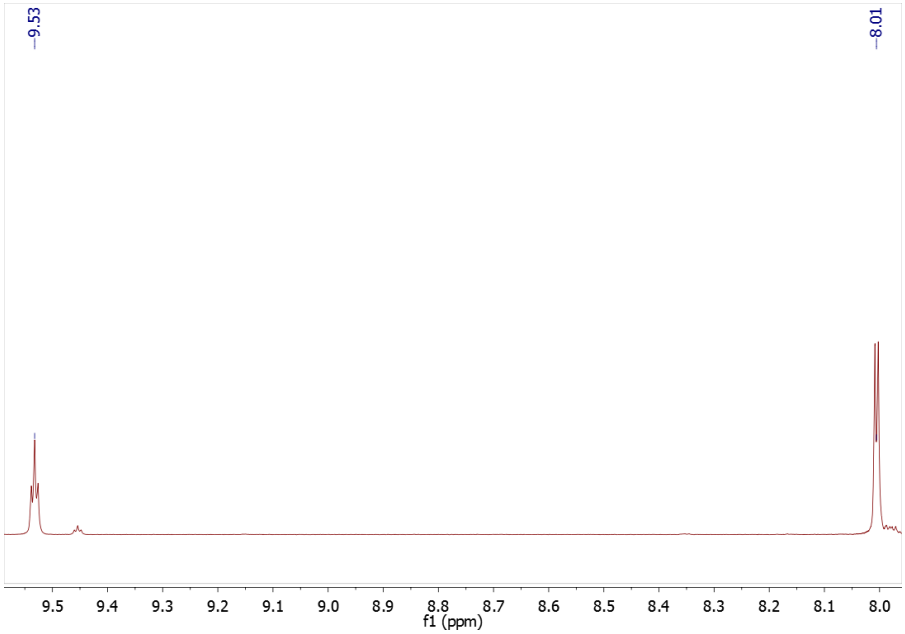

Figure 4-6 close up of the Figure 4-6 showing splitting pattern

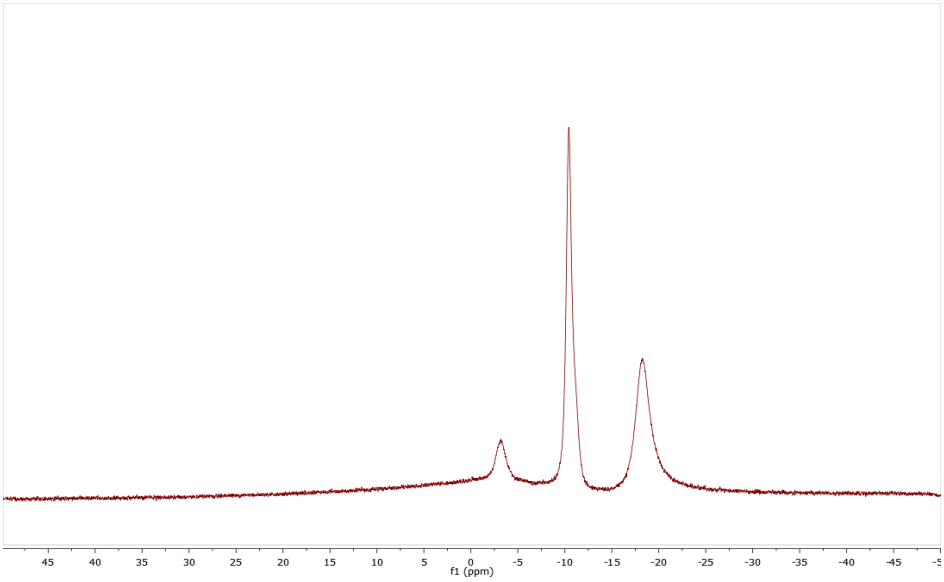

Figure 4-7 ^{11}B NMR of imidazolium **5** (25^{o}C, 96 MHz, acetone-d_6)

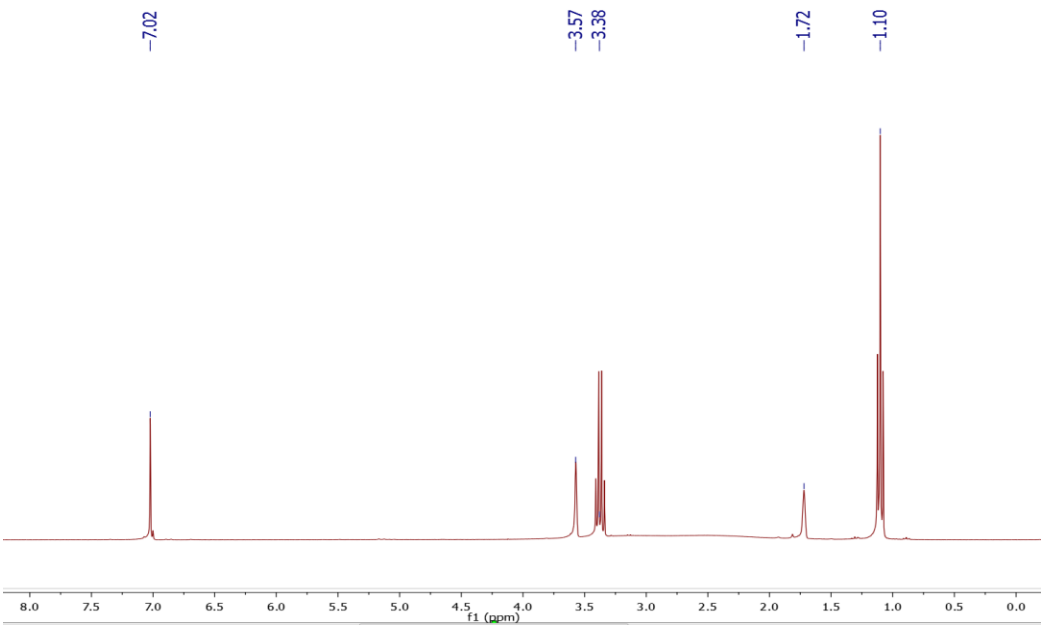

Figure 4-8 ^{1}H NMR of carbene **6** (25°C, 600 MHz, THF-d_6)

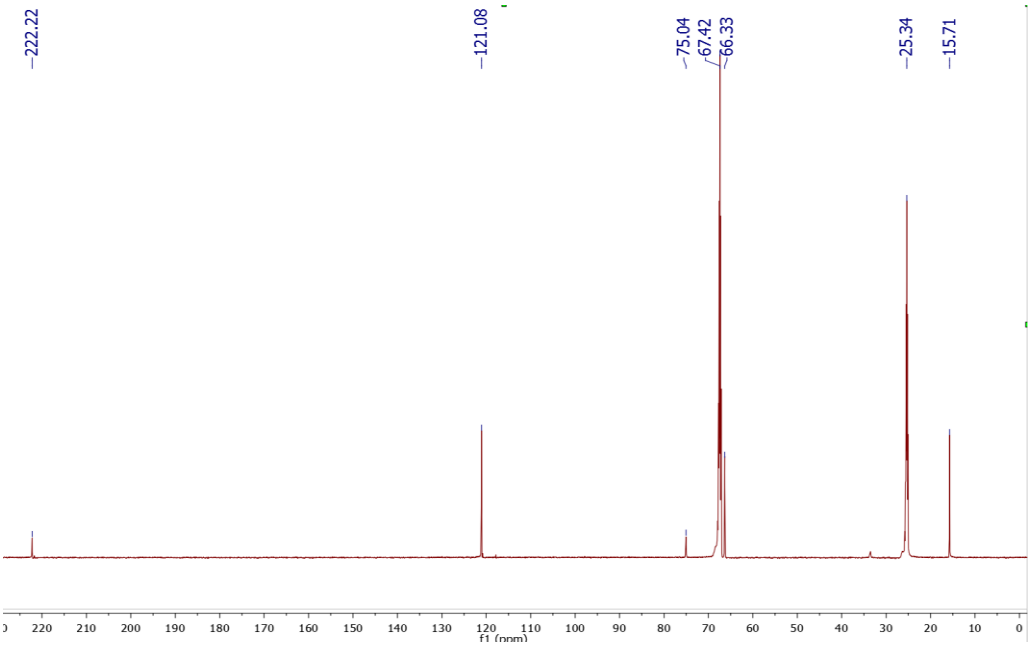

Figure 4-9 ^{13}C NMR of carbene 6 (25°C, 121 MHz, THF-d_8)

4.3 Conclusion

Here we report on two new carboranyl ligand design. For the carboranyl Schiff base, we are investigating various metals, particularly nickel and palladium for use as polymerization catalysts. For the NHC with carborane, we are investigating the effects of various bases to imidazolium **5** as well as electron rich metals such as gold and silver to form metal complexes due to the reduced electron density of the NHC from the 12 bromines compared to the NHC composed derived from the parent carborane.

4.4 X-Ray Diffraction Studies

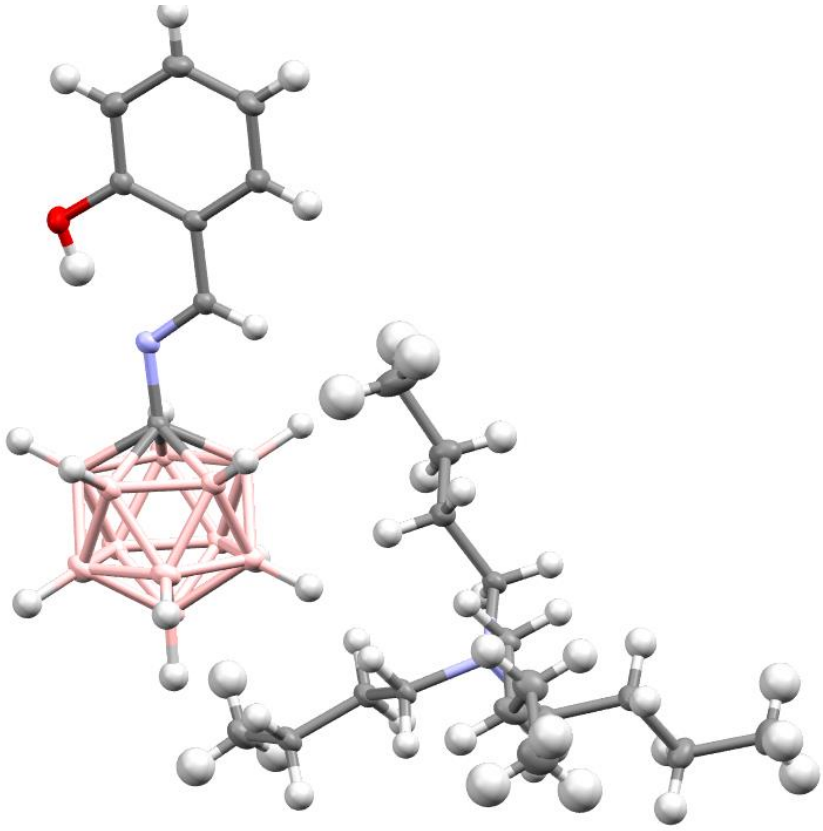

Figure 4-10 Solid-state structure of imine **2** with a tetrabutylammonium cation

A light brown needle fragment (0.42 x 0.17 x 0.14 mm^3) was used for the single crystal x-ray diffraction study of $[N[C_4H_9]_4]^+[C_7H_5OHNCB_{11}H_{11}]^-$ (sample vL86r_0m). The crystal was coated with paratone oil and mounted on to a cryo-loop glass fiber. X-ray intensity data were collected at 100(2) K on a Bruker APEX2 platform-CCD x-ray diffractometer system (fine focus Mo-radiation, λ = 0.71073 Å, 50KV/35mA power). The CCD detector was placed at a distance of 5.0600 cm from the crystal.

A total of 2160 frames were collected for a sphere of reflections (with scan width of 0.5° in ω, starting ω and 2θ angles at -30°, and ϕ angles of 0°, 90°, 120°, 180°, 240°, and 270° for every 360 frames, 10 sec/frame exposure time). The frames were integrated using the Bruker SAINT software package and using a narrow-frame integration algorithm. Based on a monoclinic crystal system, the integrated frames yielded a total of 72869 reflections at a maximum 2θ angle of 59.14° (0.72 Å resolution), of which 9125 were independent reflections (R_{int} = 0.0659, R_{sig} = 0.0385, redundancy = 8.0, completeness = 100%) and 6695 (73.4%) reflections were greater than $2\sigma(I)$. The unit cell parameters were, **a** = 10.2335(3) Å, **b** = 15.5702(4) Å, **c** = 20.7433(6) Å, β = 99.694(1)°**,** V = 3257.99(16) Å^3, Z = 4, calculated density D_c = 1.029 g/cm^3. Absorption corrections were applied (absorption coefficient μ = 0.056 mm^{-1}; max/min transmission = 0.9925/0.9769) to the raw intensity data using the SADABS program.

The Bruker SHELXTL software package was used for phase determination and structure refinement. The distribution of intensities (E^2-1 = 0.968) and systematic absent reflections indicated one possible space group, P2(1)/c. The space group P2(1)/c (#14) was later determined to be correct. Direct methods of phase determination followed by two Fourier cycles of refinement led to an electron density map from which most of the non-hydrogen atoms were identified in the asymmetric unit of the unit cell. With subsequent isotropic refinement, all of the non-hydrogen atoms were identified. There were one cation of $[N[C_4H_9]_4]^+$ and one anion of $[C_7H_5OHNCB_{11}H_{11}]^-$ present in the asymmetric unit of the unit cell. There was intra-molecular hydrogen bonding between

the OH-group and the N-atom. Table 7 shows the bond angle and distances of the OH...N intra-molecular hydrogen bond.

Atomic coordinates, isotropic and anisotropic displacement parameters of all the non-hydrogen atoms were refined by means of a full matrix least-squares procedure on F^2. The H-atoms were included in the refinement in calculated positions riding on the atoms to which they were attached, except the OH hydrogen was refined unrestrained. The refinement converged at R1 = 0.0497, wR2 = 0.1184, with intensity $I>2\sigma$ (I). The largest peak/hole in the final difference map was 0.343/-0.228 e/$Å^3$.

Table 1. Crystal data and structure refinement for vL86r_0m.

Identification code	vl86r_0m	
Empirical formula	C24 H53 B11 N2 O	
Formula weight	504.59	
Temperature	100(2) K	
Wavelength	0.71073 Å	
Crystal system	Monoclinic	
Space group	P2(1)/c	
Unit cell dimensions	a = 10.2335(3) Å	α= 90°.
	b = 15.5702(4) Å	β= 99.694(1)°.
	c = 20.7433(6) Å	γ = 90°.
Volume	3257.99(16) $Å^3$	
Z	4	
Density (calculated)	1.029 Mg/m^3	
Absorption coefficient	0.056 mm^{-1}	

F(000)	1096
Crystal size	0.42 x 0.17 x 0.14 mm^3
Theta range for data collection	1.64 to 29.57°.
Index ranges	-14<=h<=14, -21<=k<=21, -28<=l<=28
Reflections collected	72869
Independent reflections	9125 [R(int) = 0.0659]
Completeness to theta = 29.57°	100.0 %
Absorption correction	Semi-empirical from equivalents
Max. and min. transmission	0.9925 and 0.9769
Refinement method	Full-matrix least-squares on F^2
Data / restraints / parameters	9125 / 0 / 350
Goodness-of-fit on F^2	1.029
Final R indices [I>2sigma(I)]	R1 = 0.0497, wR2 = 0.1184
R indices (all data)	R1 = 0.0738, wR2 = 0.1329
Largest diff. peak and hole	0.343 and -0.228 e.$Å^{-3}$

4.5 References

(1) Larrow, J. F.; Jacobsen, E. N.; Gao, Y.; Hong, Y.; Nie, X.; Zepp, C. M. *The Journal of Organic Chemistry* **1994**, *59*, 1939.

(2) Rue, E. L.; Bruland, K. W. *Marine Chemistry* **1995**, *50*, 117.

(3) Hernández-Molina, R.; Mederos, A. In *Comprehensive Coordination Chemistry II*; Meyer, T. J., Ed.; Pergamon: Oxford, 2003, p 411.

(4) Gupta, K. C.; Sutar, A. K. *Coordination Chemistry Reviews* **2008**, *252*, 1420.

(5) Guan, Z.; Cotts, P. M.; McCord, E. F.; McLain, S. J. *Science* **1999**, *283*, 2059.

(6) Small, B. L.; Brookhart, M.; Bennett, A. M. A. *Journal of the American Chemical Society* **1998**, *120*, 4049.

(7) Britovsek, G. J. P.; Gibson, V. C.; Kimberley, B. S.; Maddox, P. J.; McTavish, S. J.; Solan, G. A.; White, A. J. P.; Williams, D. J. *Chemical Communications* **1998**, 849.

(8) Britovsek, G. J. P.; Bruce, M.; Gibson, V. C.; Kimberley, B. S.; Maddox, P. J.; Mastroianni, S.; McTavish, S. J.; Redshaw, C.; Solan, G. A.; Stromberg, S.; White, A. J. P.; Williams, D. J. *Journal of the American Chemical Society* **1999**, *121*, 8728.

(9) Xi, Z. W.; Wang, H. P.; Sun, Y.; Zhou, N.; Cao, G. Y.; Li, M. *Journal of Molecular Catalysis a-Chemical* **2001**, *168*, 299.

(10) Claverie, J. P.; Soula, R. *Progress in Polymer Science* **2003**, *28*, 619.

(11) Hayashi, T. *Journal of Organometallic Chemistry* **1999**, *576*, 195.

(12) Hahn, F. E.; Jahnke, M. C. *Angewandte Chemie International Edition* **2008**, *47*, 3122.

(13) Diez-Gonzalez, S.; Marion, N.; Nolan, S. P. *Chemical Reviews* **2009**, *109*, 3612.

(14) El-Hellani, A.; Lavallo, V. *Angewandte Chemie International Edition* **2014**, *53*, 4489.

(15) T. Jelinek, J. P., S. Hermanek, B. Stıbr *Collection of Czechoslovak Chemical Communications* **1986**, *51*, 819.

(16) Reed, C. A. *Accounts of Chemical Research* **2010**, *43*, 121.

Chapter 5: A Study of Pd(0) complexes with Carboranyl Phosphines

5.1 Introduction

Pd-catalyzed cross-coupling is an indispensable method in the chemist's tool box[1-12]. The most common ligands utilized in cross-coupling protocols are neutral phosphines appended with alkyl or aryl groups. To achieve high activity, particularly with challenging substrates such as aryl-chlorides, bulky electron rich phosphines are implemented. With respect to electronics, such ligands render the metal more electron rich, promoting oxidative addition. The steric influence of the ligand promotes the formation of mono-phosphine ligated species that are required to effect efficient C-X oxidative addition. Among the state-of-the-art phosphine ligands[13,14], biaryl phosphines[12,15,16], such as S-phos, are often the go-to ligands for the cross-coupling of aryl-chlorides and other difficult substrates. It is believed that the high activity of these systems arises from metal π-arene interactions, which stabilize the low-coordinate resting state of the catalysts[17].

Over the last few years we have developed a variety of phosphine[18-23] and N-heterocyclic carbene[24-26] ligands, such as **1** (Scheme 5-1), featuring weakly coordinating *closo*-carborane anion[27-33] substituents. Attaching these primarily inorganic clusters bestows L-type ligands with an anionic charge. The charge is delocalized throughout the closed polyhedral Δ*H* structure, which disposes the charge close to the metal center

regardless of conformation. This fact, coupled with the carborane anions's chemical stability[31,32,34], makes our systems distinct from ligands appended with tetra-coordinate borate moieties[35-39]. We are particularly interested in utilizing the weak coordinative abilities and charge of the cluster to induce electrostatic effects in the coordination sphere of metals. In gold catalysis, we have demonstrated that it is possible to create highly active and well defined single component systems for C-N bond forming reactions[22].

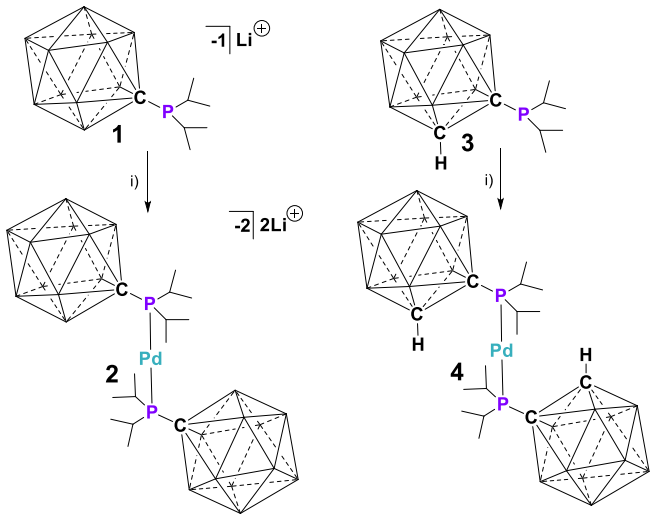

Scheme 5-1 Synthesis of isosteric/electronic dianionic and neutral Pd(0) complexes **2** and **4**, respectively. i) = $(TMSCH_2)_2Pd(COD)$ 0.5 eq., C_6D_6, R.T., 5 min. Unlabeled vertices = B-H

Herein, we report our initial findings relevant to Pd-catalyzed cross-coupling chemistry by preparing a stable dianionic 14-electron Pd(0) species **2** that readily reacts with chloroarenes at room temperature. Implementing an isosteric ligand **3**, featuring

the neutral *o*-carborane ligand substituent, yields an isoelectronic but neutral complex **4** that is not competent for the activation of chloro-arenes or catalysis. We provide both experimental and computational evidence that the high reactivity of **2** is the result of electrostatic effects that facilitate both phosphine dissociation and stabilization of the transition state during the oxidative addition process. This mode of stabilization is distinct from the well-known π-arene interactions of biaryl phosphines, **4** in that it occurs both on and off cycle.

5.2 Results and Discussion

We have recently determined the σ-inductive effects of both 10 and 12-vertex *closo*-carborane anions[18]. In contrast to neutral C-functionalized *o*-carborane[28,40], these anionic clusters are strong donors similar to alkyl groups. Ligand **1** is just slightly less donating than $P(iPr)_3$. Given our understanding of the donor ability of **1** and its steric parameters we chose to utilize it to investigate the possibility of preparing a dianionic two coordinate Pd(0) species **2** for reactivity studies (Figure 5-1). At the same time, we wished to investigate a sterically identical but neutral ligand **3**, featuring an *o*-carboranyl group, and its PdL_2 complex **4** (Scheme 5-1). Analogous neutral derivatives supported by classical phosphines are convenient for solution based reactivity and mechanistic studies because they contain no additional ligands, which might complicate interpretation of the spectroscopic data. Thus, ligands **1** and **3** were reacted

independently with half an equivalent of $(TMSCH_2)_2Pd(COD)$ in C_6D_6 (Scheme 5-1). Analysis of the reaction mixtures by ^{31}P NMR spectroscopy showed the rapid consumption of the ligands (**1**: 45.0 ppm; **3**: 54.2 ppm) and the clean formation of the new products (**2**: 65.5 ppm; **4**: 81.1 ppm) containing symmetrical phosphines. ^{1}H NMR spectroscopy showed resonances for the new phosphine complexes as well as the expected signature for 1,2-bistrimethysilyl ethane formed via reductive elimination. For the dianionic complex **2** the ^{11}B NMR spectrum shows three resonances (1:5:5 ratio) demonstrating that the cluster is intact and retains its local C_{5v} symmetry. The ^{11}B NMR spectrum of the neutral complex **4** is more complicated due to the lower symmetry of the *o*-carborane. Complex **2** can be isolated in pure form by precipitation of the mixture in hexane. Complex **4** can be isolated by recrystallization from acetonitrile. Interestingly, the dianionic complex **2** is soluble and stable in degassed D_2O (Figure 4-4), while the neutral complex **4** is insoluble.

The structure of **2** and **4** were unambiguously determined by single crystal X-ray diffraction studies (Figure 5-1). In the solid-state both complexes are dicoordinate and essentially linear (P- Pd-P angles: **2** = 172.1°; **4** = 170.8°). Aside from the two spectator lithium countercations tetrahedrally coordinated by four THF molecules, the Pd fragment in **2** has very similar geometric parameters compared to **4** (Figure 5-1).

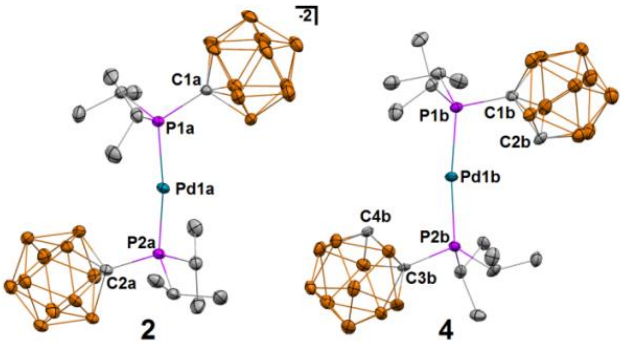

Figure 5-1 Solid-state structures of **2** and **4**. Selected bond lengths in Å. **2**: Pd1a-P1a = 2.2615(10), Pd1a-P2a = 2.2688(10), P1a-C1a = 1.875(4) P2a-C2a = 1.872(3); **4**: Pd1b-P1b = 2.2661(17), Pd1b-P2b = 2.2774(17), P1b-C1b = 1.869(7); P2b-C3b = 1.880(7). Hydrogens and countercations of **2** are omitted for clarity. Color code: B = brown, C = grey, Pd = blue, P = violet

With these two charge-differentiated but isosteric/electronic complexes in hand, we sought to probe their reactivity with Cl-C_6H_5. Hence, we independently dissolved complexes **2** and **4** in neat Cl-C_6H_5 and monitored the reactions by ^{31}P NMR spectroscopy. Within 9 minutes complex **2** was completely consumed, to afford two new products in a ratio of 9:1 (Scheme 5-2, A). The primary product, which displays a singlet resonance, was assigned as the monoanionic bisphosphine Pd(II) Aryl complex **5**. The structure of isolated **5** was corroborated by multinuclear NMR spectroscopy as well as a single crystal x-ray diffraction study (see *X-Ray Diffraction Studies*). The formation of **5** can be explained by an oxidative addition of Cl-C_6H_5 with subsequent elimination of LiCl (recall complex **2** has two Li^+ counter cations). The minor product **6** displays two coupled doublets (50.2 and 8.9 ppm, J = 323.5 Hz) in the ^{31}P NMR spectrum, indicating the formation of an unsymmetrical bisphosphine complex. Complex **6** was isolated and

determined by multinuclear NMR spectroscopy, as well as a single crystal x-ray diffraction study (see *X-Ray Diffraction Studies*), to be the B-cyclometalated Pd(II) complex **6**. The formation of **6** can be rationalized by an oxidative addition/sigma bond metathesis sequence which results in the elimination of benzene and LiCl, *vide infra*. In contrast complex **4** reacted very sluggishly, with approximately 90% of complex **4** intact after 24 hours at R.T. Aside from the starting material **4** an intractable mixture of numerous ^{31}P containing complexes was detected (Figure 5-18). Even after refluxing **4** in neat Cl-C_6H_5 for 24 hours a significant amount of starting material remains (Figure 5-19). The fast oxidative addition of **2** with Cl-C_6H_5 at R.T. is remarkable. Comparable dicoordinate PdL_2 systems featuring standard phosphines like $P(Cy)_3$ and $P(t\text{-}Bu)_3$, which we independently prepared[41] and subjected to identical reaction conditions, react sluggishly ($Pd(PCy_3)_2$ **8**: 70% conversion/24h) or not at all ($Pd(P(t\text{-}Bu)_3$ **9**: no reaction) (Figures 5-30 and 5-32). That being said, state-of-the-art biaryl-phosphines like S-phos can form transient[17] L_2Pd complexes in solution, which show comparable rates of oxidative addition[42]. Considering that ligand **1** is less electron donating than $P(i\text{Pr})_3$[18], and more electron rich ligands like $P(Cy)_3$ and $P(t\text{-}Bu)_3$ do not promote the rapid oxidative addition of Cl-C_6H_5 at ambient temperature, it is clear that the observed reactivity cannot be explained by the electron donor ability of **1**. Likewise, the fast oxidative addition cannot be explained by steric arguments, since the isosteric complex **4**, featuring the neutral *o*-carborane, does not behave the same as complex **2**. Therefore, we propose that the rapid oxidative addition is the result of electrostatic

effects. Perhaps, the binding of two ligands that bear a pendant negative charge to the same transition metal center favors ligand dissociation, based on a coulombic argument (Figure 5-2). If **2** behaves similarly to standard L_2Pd systems, this effect would favor the formation of the required L-Pd(solvent) complexes. Indeed, the addition of excess phosphine **1** to solutions of **2** strongly retards the rate of oxidative addition, which is in line with a dissociative pathway prior to oxidative addition. To further probe the lability of phosphine **1** we treated a solution of **2** with 1 equivalent of $P(Cy_3)_3$. Ligand **1** is quite labile as we observe a distribution of **1**, **2**, monosubstituted product **7**, and the double ligand substitution product $Pd(PCy_3)_2$ **8** (Figure 5-33).

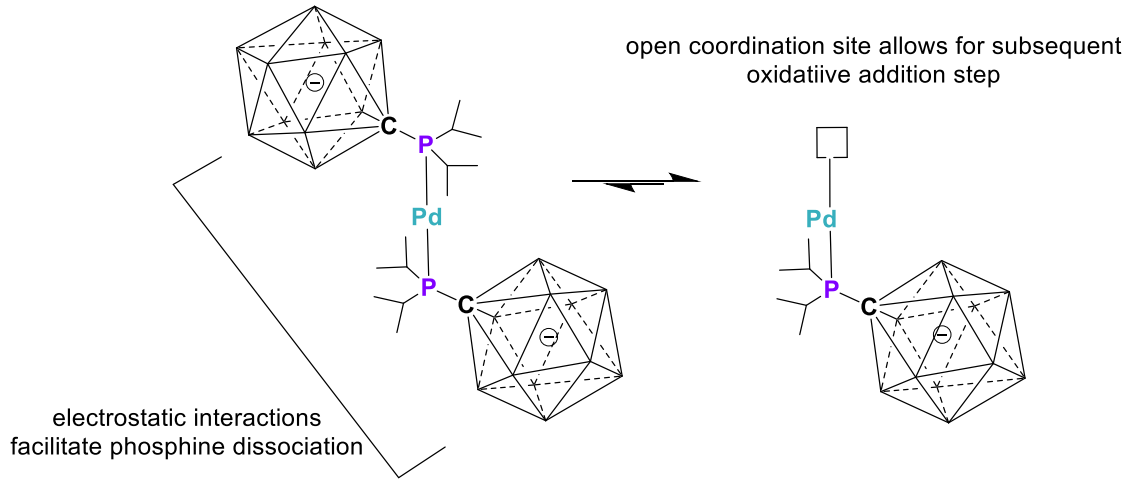

Figure 5-2 Proposed rapid oxidation via a dissociation step facilitated by electrostatic repulsion

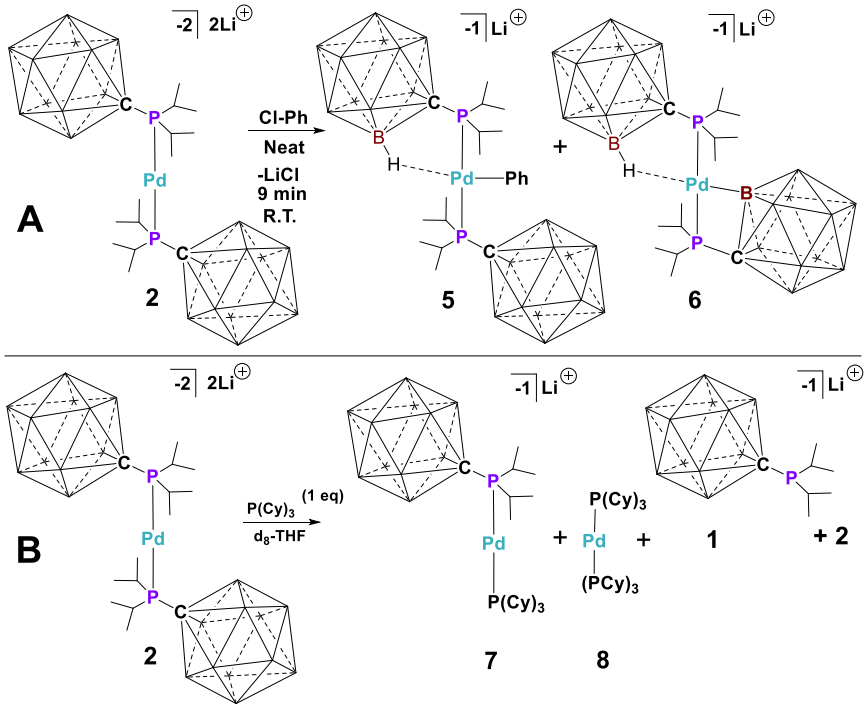

Scheme 5-2 Complex **2** reacts rapidly with Cl-Ph at R.T. to afford a 9:1 ratio of species **5** and **6**, respectively (A) and stoichiometric addition of $P(Cy)_3$ to afford a distribution of mono and di substitution products (B), showing the lability of the phosphines bound to **2**

To probe the possibility that the oxidative addition was the result of interactions between the Li^+ cations and the $Cl\text{-}C_6H_5$ substrate, we examined the behavior of system **2** with Na^+, K^+ countercations (see *Synthesis and Spectroscopic Data* section). These complexes were formed *in situ* by implementing Na^+ and K^+ phosphine salts of **1** and $(TMSCH_2)_2Pd(COD)$. The presence of Na^+ and K^+ does not change the rate of oxidative addition, suggesting the countercations do not participate in the ligand dissociation or oxidative addition steps of the reaction sequence.

In order to gain support for our hypothesis we investigated the ligand substitution and oxidative addition process computationally (see *Computational Details* section). As depicted in Figure 5-3, complex **2** can undergo a dissociative phosphine substitution with Cl-C_6H_5 to afford intermediate **II**. The latter undergoes a low barrier (**TS_{II-III}:** $\Delta H^{\ddagger}$= 7.4 kcal/mol) oxidative addition to afford the monoanionic Pd(II) intermediate **III**, which is in line with our experimental conditions. Interestingly, in intermediate **II, TS_{II-III},** and **III** there is a weak interaction between the cluster and the Pd center. This interaction stabilizes both the intermediates and transition state during the oxidative addition process. A Quantum Theory Atoms in Molecules (QTAIM) analysis of both intermediates as well as the transition state confirms that this interaction is essentially purely electrostatic. Such stabilizing interactions are unique and distinct from the π-arene interactions of biaryl phosphines, which occur only during the catalyst resting state[17]. For comparison, the isoelectronic and neutral *o*-carborane supported Pd(0) complex **4** displays an endothermic (12.2 kcal/mol) ligand substitution with Cl-C_6H_5(see *Computational Details*). In addition, the activation barrier for the oxidative addition is +10.8 kcal/mol, with the sum of the two processes being +23.1 kcal/mol uphill. The latter observation serves as a direct explanation of the absence of such reactivity experimentally.

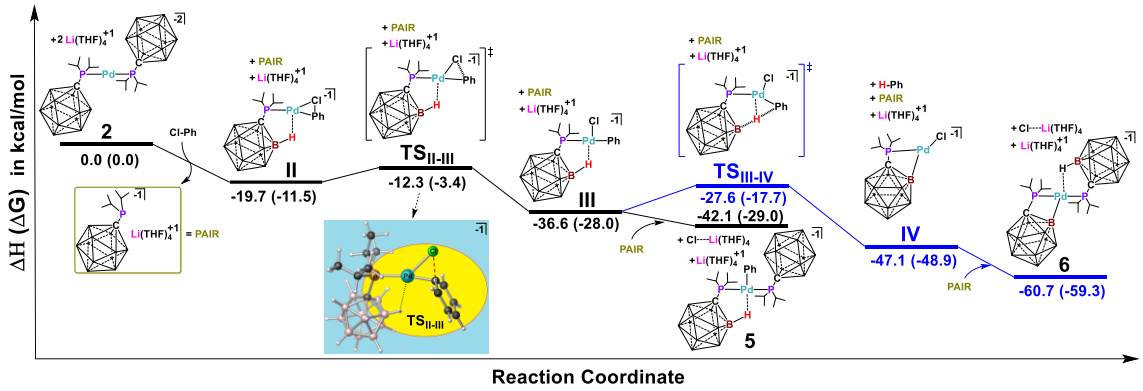

Figure 5-3 Plausible reaction profiles for the formation of the complexes **5** (black), and **6** (blue). The values in parenthesis correspond to the relative Gibbs free energies

Continuing along the reaction pathway, intermediate **III** has two options: 1) the liberated anionic carboranyl phosphine can re-associate with **III** and simultaneously extrude Cl^- to afford complex **5** (Figure 5-3). This process is barrier-less and exothermic ($\Delta H^{\ddagger}$= -5.5 kcal/mol). 2) Alternatively, intermediate **III** can cyclometalate (**TS_{III-IV}**: $\Delta H^{\ddagger}$= 9.0 kcal/mol) via a σ-bond metathesis pathway to afford intermediate **IV** (**(**$\Delta H^{\ddagger}$= -10.6 kcal/mol), which subsequently binds a liberated phosphine ligand exothermically ($\Delta H^{\ddagger}$= -13.6 kcal/mol) to afford the thermodynamic product **6**. These calculated competing reaction pathways are in agreement with the observed formation of **5** and **6** as the major and minor products, respectively. Moreover, adding excess phosphine to the reaction mixture not only slows down the rate of oxidative addition, but it also retards cyclometalation, which is in complete agreement with what one would expect from the calculations above.

In order to better understand the mechanism of the oxidative addition of chlorobenzene, the rates of reaction were studied. Various concentrations of the carboranyl phosphine was added while keeping all other variables constant. The plot of $1/k_{obs}$ versus 1/[Phosph] for various concentrations of carboranyl phosphine indicates that the reaction is inverse first order as expected from typical $Pd(0)L_2$ compelexes[41] (Figure 5-4). Also, at higher concentrations of phosphine, a new peak at 63.4 ppm appears before any oxidative addition product is observed. This is hypothesized to be some form of PdL_4 species or intermediate observed before the addition of oxidative addition. However, further investigation is needed to confirm the identity of unknown phosphine species.

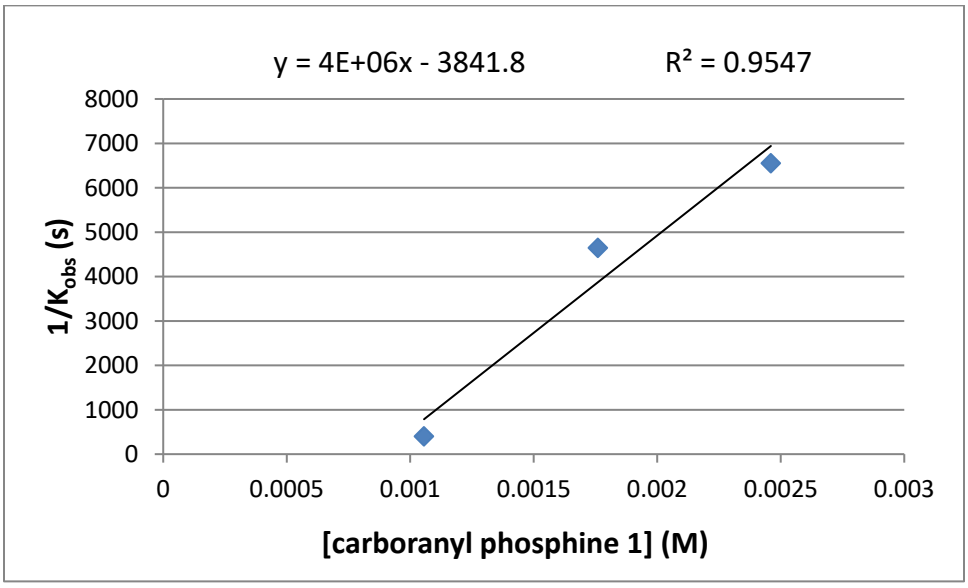

Figure 5-4 Dependence of K_{obs} on the concentration of phosphine **1** (0.001 - 0.0025 M) in 500 μl of PhCl for oxidative addition of PhCl to Pd complex **2**

In order to show that complex **2** is a competent catalyst for Pd catalyzed cross-coupling we examined its efficiency for several simple Kumada cross couplings (Table 5-1). No catalysis was observed at R.T.; However, heating the mixtures at 65°C for 15-24 hours resulted in moderate to excellent yields. Since we know that the oxidative addition of chlorobenzene to **2** occurs within minutes at R.T. the requirement of heat suggests that the slow step in the catalytic cycle is either transmetalation or reductive elimination. Both small (entries A-D) and sterically encumbered (entries E-H) Grignard reagents are effective coupling partners. With respect to electronic effects, the activity of **2** follows the typical trend observed in Pd catalyzed cross-coupling with unactivated or deactivated aryl-chlorides being more efficient substrates.

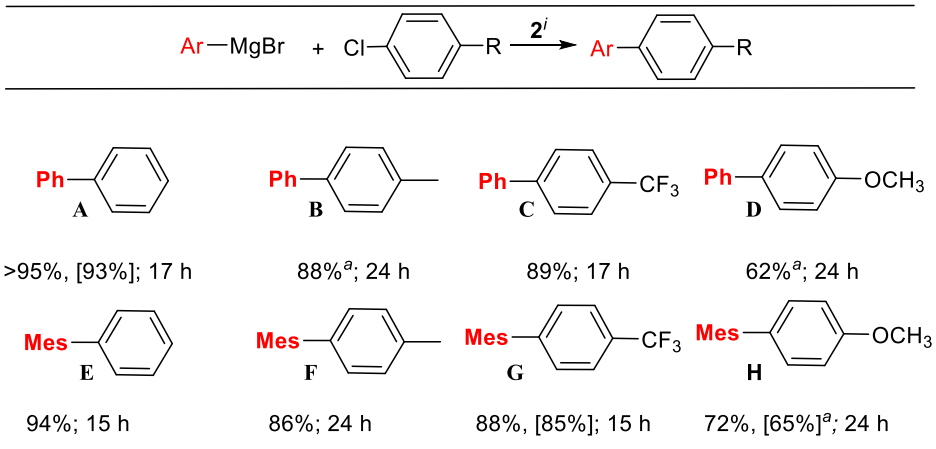

The catalyst **2** was formed in situ by premixing ligand **1** (2 eq) and $(TMSCH_2)_2Pd(COD)$ (1eq). *i* = 5 mol% **2,** 65°C, THF (1 mL) . *a* = 10 mol% **2**.Yields without brackets are calculated by integration of the ^1H NMR spectra with durene as an internal standard. Yields in brackets are isolated yields.

Table 5-1 Kumada Coupling of Simple Aryl Chlorides

From these results, we wished to pursue the hexahalogentated cluster. We hoped that the increased halogenation would prevent or reduce the amount of cyclometalation seen in the oxidative step of the reaction. Scheme 5-3 shows the synthesis of a dianionic Pd(0) complex with hexachlorinated carboranyl phosphines.

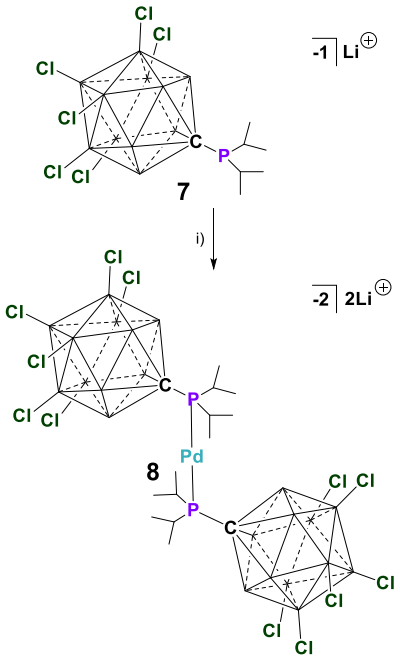

Scheme 5-3 Synthesis of dianionic Pd(0) complexes **8** with hexachlorinated carboranyl phosphine **7**, i) = $(TMSCH_2)_2Pd(COD)$ 0.5 eq., C_6D_6, R.T., 5 min. Unlabeled vertices = B-H

The structure of **8** was unambiguously determined by single crystal X-ray diffraction studies. Complex **8** was then dissolved in chlorobenzene. After 15 minute, there is a peak that corresponds to starting material, but with less of the cyclometalation species observed from the chlorobenzene reaction with complex **2**.

Though preliminary results look more promising for the hexachlorinated cluster, further investigation is necessary to study catalytic compentancy of complex **8**.

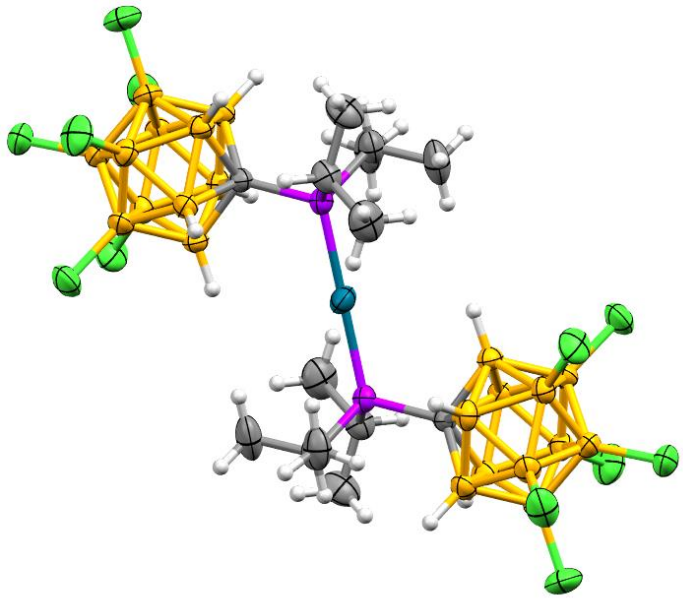

Figure 5-5 Solid-state structures of **8**. Countercations of **8** are omitted for clarity. Color code: B = brown, C = grey, Pd = blue, P = violet, Cl = green, H = white

5.3 Conclusion

This study introduces a new paradigm in Pd cross-coupling catalyst design. We have demonstrated that ligands appended to isoelectronic but charge differentiated *closo*-carboranes can induce dramatically different reactivity at metal centers. The enhanced activity of complex **2** compared to **4** can be explained by electrostatic effects that both facilitate ligand dissociation as well as oxidative addition. Importantly, the stabilizing electrostatic interactions between the carborane cage and the metal center occur both on and off cycle, which is distinct from systems based on neutral

biarylphosphines. We are currently investigating the transmetalation and reductive elimination steps in this unique catalytic system, as well as Pd(0) complexes with the hexahalogenated and perhalogenated carboranyl phosphines.

5.4 Experimental

Unless otherwise stated, all manipulations were carried out using standard Schlenk or glovebox techniques (O_2, H_2O < 1ppm) under a dinitrogen or argon atmosphere. Solvents were dried on Na, K or CaH_2, distilled under argon before use. Trimethylammonium carborane ($HNMe_3[HCB_{11}H_{11}]$), trimethylammonium hexachlorinated carborane ($HNMe_3[HCB_{11}H_5Cl_6]$), the lithium carboranyl phosphine **1** ($Li(THF)_3[P(iPr)_2CB_{11}H_{11}]$) and carboranyl phosphine **3** were prepared by literature methods[43,44]. Precursor (1,5-Cyclooctadiene)bis[(trimethylsilyl)methyl]palladium was prepared by literature method[45]. Reagents were purchased from commercial vendors and used without further purification. NMR spectra were recorded on Bruker Avance 300 MHz, Varian Inova 300 MHz, Varian Inova 400 MHz, Varian Inova 500 MHz, or Bruker Avance 600 MHz spectrometers. NMR chemical shifts are reported in parts per million (ppm). ^{1}H NMR and ^{13}C NMR chemical shifts were referenced to residual protio solvent. ^{11}B NMR chemical shifts were externally referenced to BF_3OEt_2. ^{31}P NMR chemical shifts were externally referenced to 80% H_3PO_4 in H_2O.

Synthesis and Spectroscopic Data

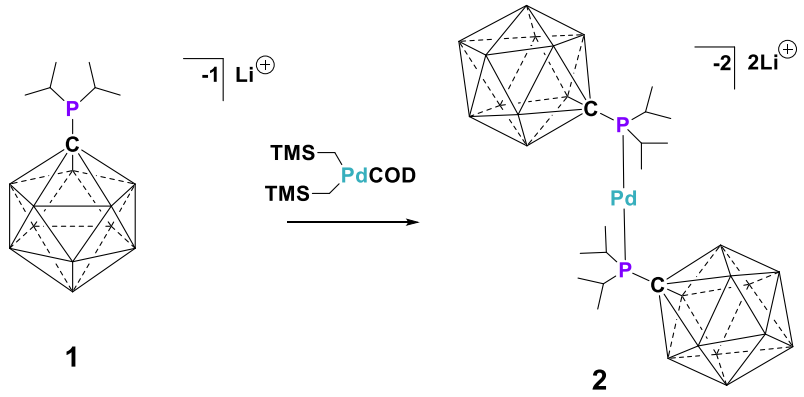

Synthesis of complex 2: Phosphine **1** (101 mg, 0.210 mmol) was dissolved in 2 ml benzene. In another vial, (1,5-Cyclooctadiene)bis[(trimethylsilyl)methyl]palladium (40.7 mg, 0.105 mmol) was dissolved in 2 mL of benzene and added drop wise to **1** and stirred for 20 minutes. An oil formed in which the benzene was removed and further washed with 4 mL of benzene. The oil was then triturated in 10 mL of hexanes, and the hexanes was subsequently removed. The product was obtained by concentrating in vacuo to afford **2** (114 mg, 98% yield) as a precipitate. ^{1}H NMR (600 MHz, CD_3CN, 25 °C) δ = 3.64 (m, 8H, THF), 1.96 (m, 4H, C*H*), 1.80 (m, 8H, THF), 1.35 (dd, 12H, CH_3, ^{3}J(P-H) = 17.9 Hz, ^{3}J(H-H) = 7.4 Hz), 1.18 (dd, 12H, CH_3, ^{3}J(P-H) = 14.8 Hz, ^{3}J(H-H) = 6.7 Hz) ppm. ^{1}H NMR (300 MHz, D_2O, 25 °C) δ = 3.71 (m, 24H, THF), 1.99 (m, 4H, C*H*),), 1.85 (m, 24H, THF), 1.34 (dd, 12H, CH_3, ^{3}J(P-H) = 19.6 Hz, ^{3}J(H-H) = 8.1 Hz), 1.19 (dd, 12H, CH_3, ^{3}J(P-H) = 14.0 Hz, ^{3}J(H-H) = 6.4 Hz) ppm. ^{13}C NMR (151 MHz, CD_3CN, 25 °C) δ = 68.2 (THF), 29.2 (*C*H),

26.2 (THF), 24.8 (CH_3), 20.1 (CH_3) ppm. ^{31}P NMR (162 MHz, CD_3CN, 25 °C) δ = 66.5 ppm. ^{11}B NMR (96 MHz, CD_3CN, 25 °C) δ = 0.2, -7.4 ppm.

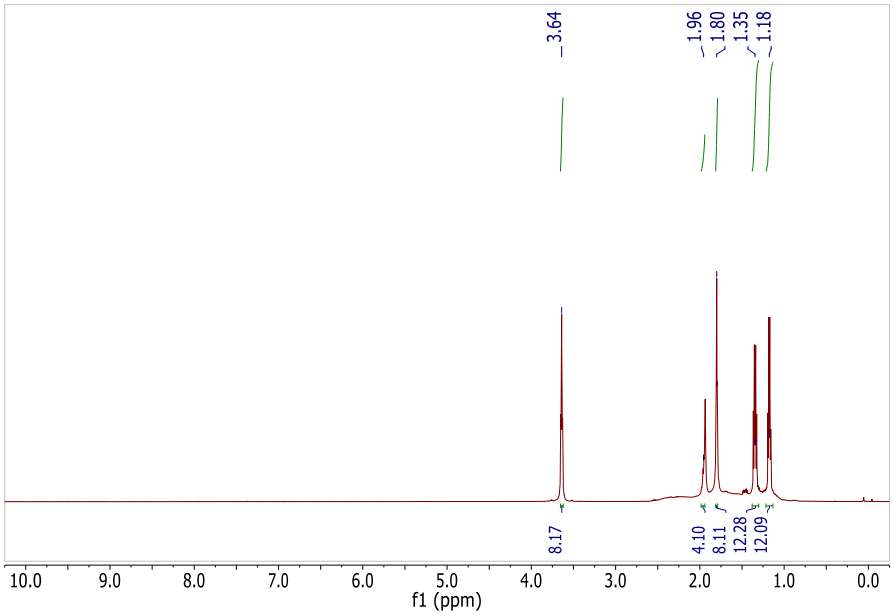

Figure 5-6 ^1H NMR of complex **2** (25°C, 600 MHz, CD_3CN)

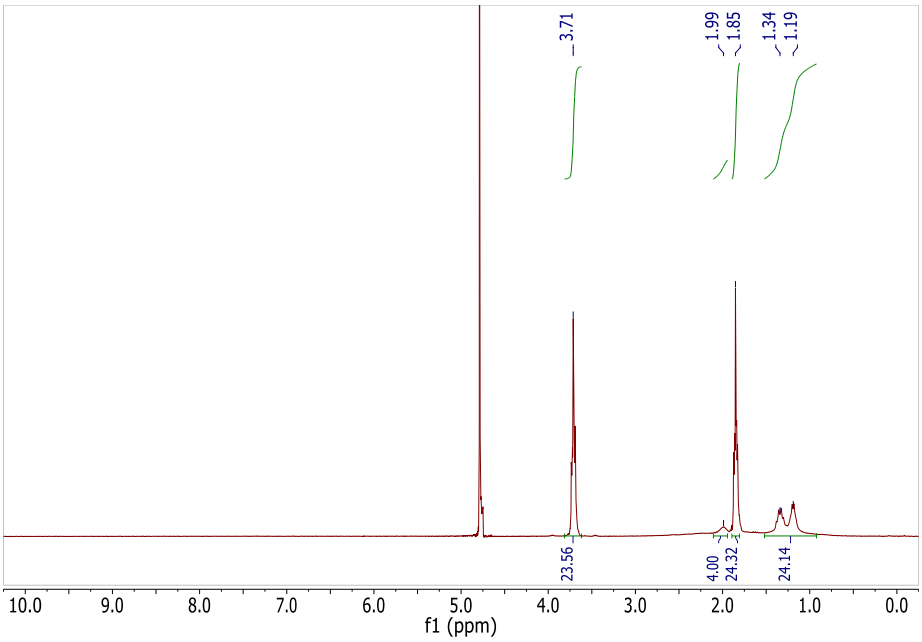

Figure 5-7 ^{1}H NMR of complex **2** (25°C, 300 MHz, D_2O)

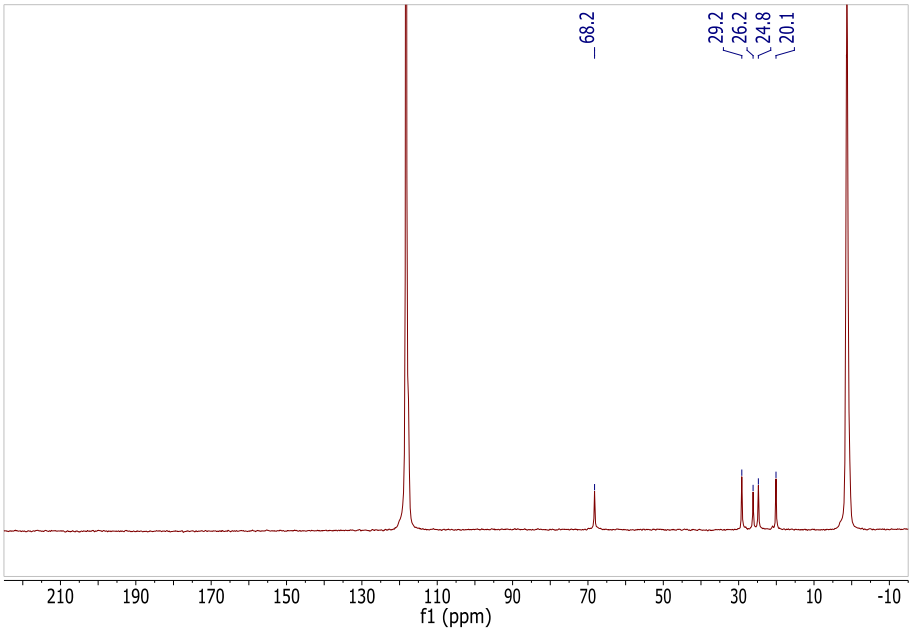

Figure 5-8 ^{13}C NMR of complex **2** (25°C, 151 MHz, CD_3CN)

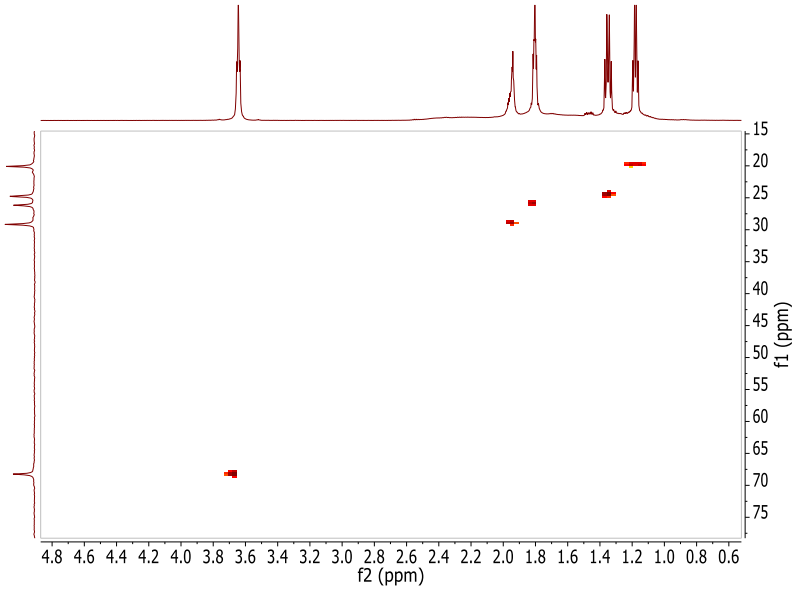

Figure 5-9 HSQC (^{13}C,^{1}H) NMR of complex **2** (25°C, 300 MHz, CD_3CN)

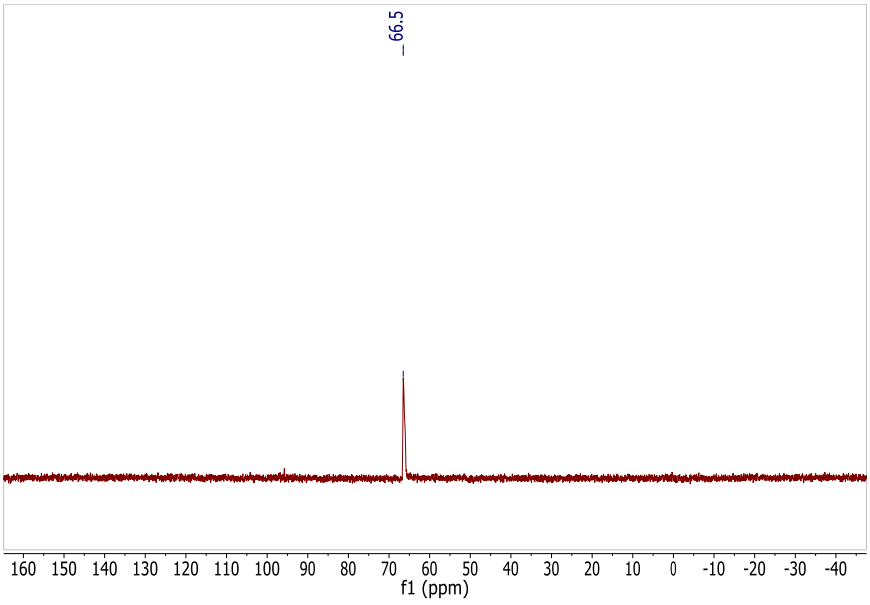

Figure 5-10 ^{31}P NMR of complex **2** (25°C, 162 MHz, CD_3CN)

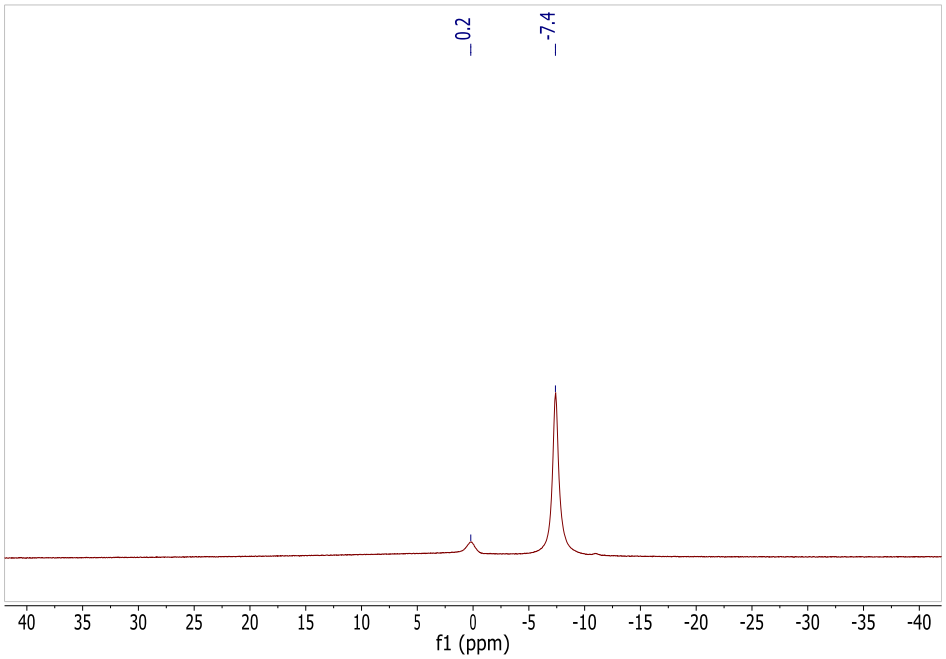

Figure 5-11 ^{11}B NMR of complex **2** (25°C, 96 MHz, CD_3CN)

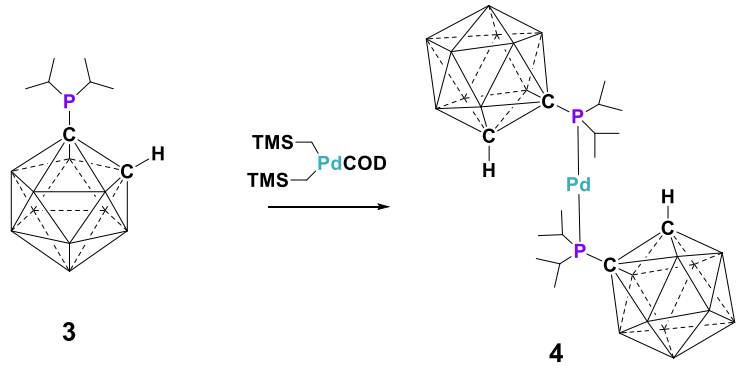

3 4

Synthesis of complex 4: A 4 mL benzene solution of (1,5-Cyclooctadiene)bis[(trimethylsilyl)methyl]palladium (20.0 mg, 0.052 mmol) was added to a 4 mL benzene solution of compound **3** (19.6 mg, .104 mmol) and stirred for 30 minutes. The resulting brown solution was pumped to dryness. The desired product was extracted with 10 mL acetonitrile and filtered. Light brown crystals were obtained upon cooling to -30 ˚C. The supernatant was decanted and the crystalline product was

washed with 1 mL of cold acetonitrile and pumped to dryness yielding complex **4** in 90% yield upon multiple crystallizations of the supernatant (22.5 mg, 0.047 mmol). ^{1}H NMR (400 MHz, C_6D_6, 25 °C) δ = 4.88 (bs, 2H, Carborane), 3.08 (bs, 1H, B*H*), 3.00 (bs, 1H, B*H*), 2.90 (bs, 2H, B*H*), 2.68 (bs, 2H, B*H*), 2.54 (bs, 2H, B*H*), 2.39 (bs, 2H, B*H*), 1.90 (m, 2H, C*H*), 1.15 (dd, ^{3}J(P-H) = 17.8, ^{3}J(H-H) = 7.5 Hz, 6H, CH_3), 0.82 (dd, ^{3}J(P-H) = 18.3, ^{3}J(H-H) = 7.1 Hz, 6H, CH_3) ppm. ^{13}C NMR (151 MHz, C_6D_6, 25 °C) δ = 74.3 (*C*H, Carborane), 71.6 (*C*P, Carborane), 28.9 (*C*H), 24.0 (*C*H_3), 19.2 (*C*H_3) ppm. ^{31}P(^{1}H) NMR (121 MHz, C_6D_6, 25 °C) δ = 81.1 ppm. ^{11}B(^{1}H) NMR (96 MHz, C_6D_6, 25 °C) δ = 3.1, 2.3, -3.6, -7.8, -8.8 ppm.

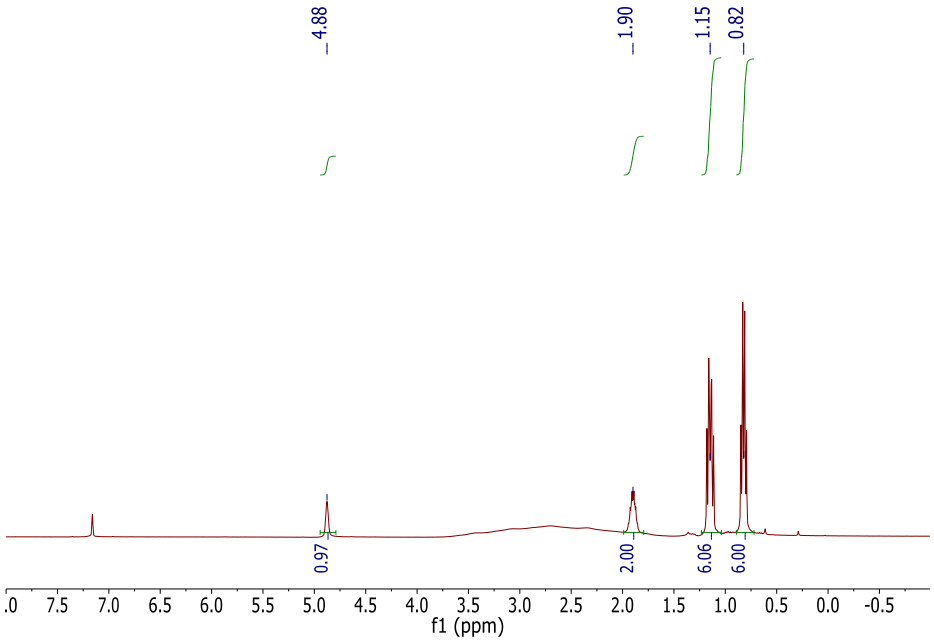

Figure 5-12 ^{1}H NMR of complex **4** (25°C, 400 MHz, C_6D_6)

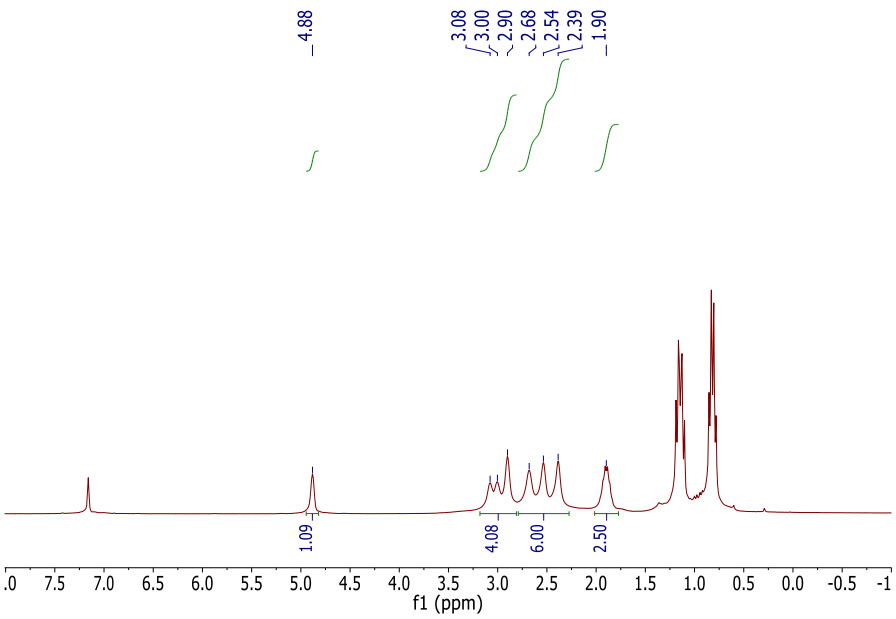

Figure 5-13 $^{1}H(^{11}B)$ NMR of complex **4** (25°C, 300 MHz, C_6D_6)

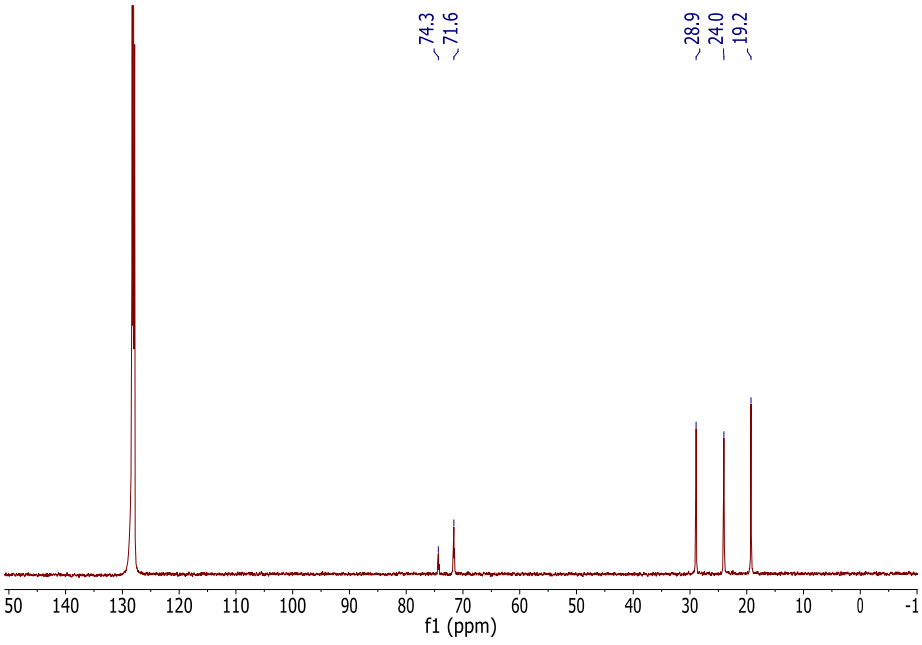

Figure 5-14 $^{13}C(^{1}H)$ NMR of complex **4** (25°C, 151 MHz, C_6D_6)

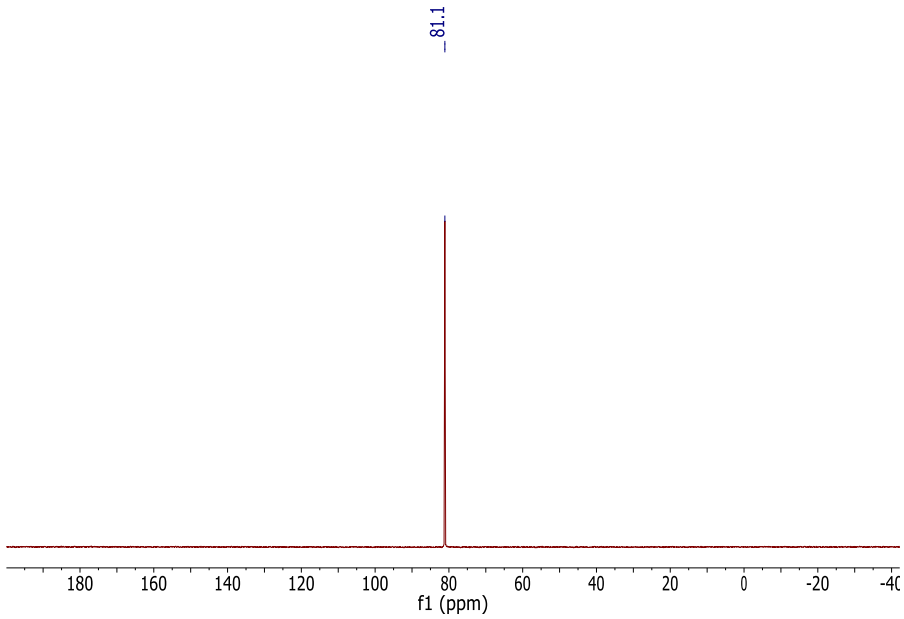

Figure 5-15 $^{31}P(^{1}H)$ NMR of complex **4** (25°C, 121 MHz, C_6D_6)

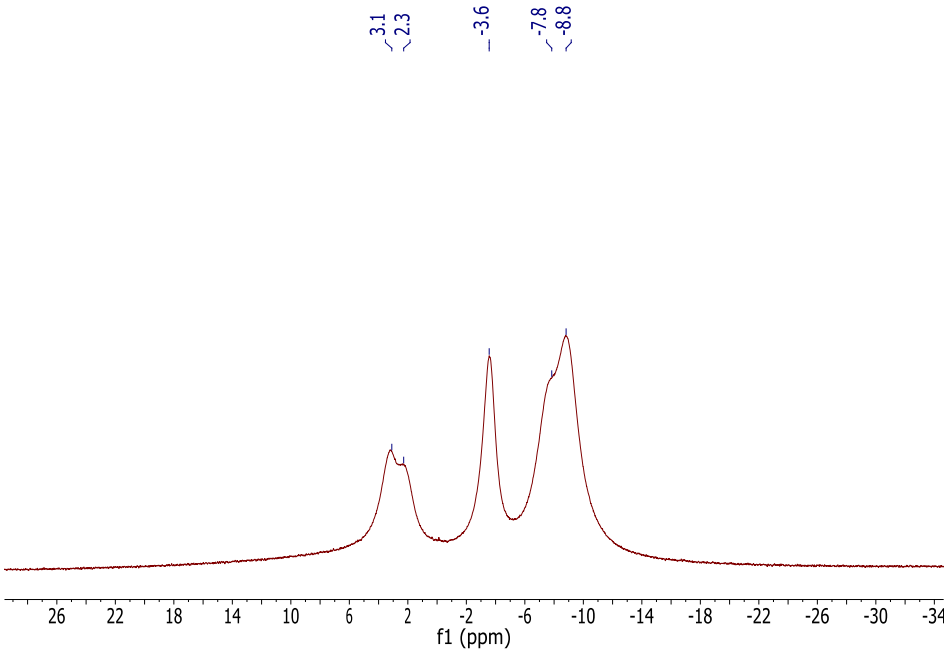

Figure 5-16 $^{11}B(^{1}H)$ NMR of complex **4** (25°C, 96 MHz, C_6D_6)

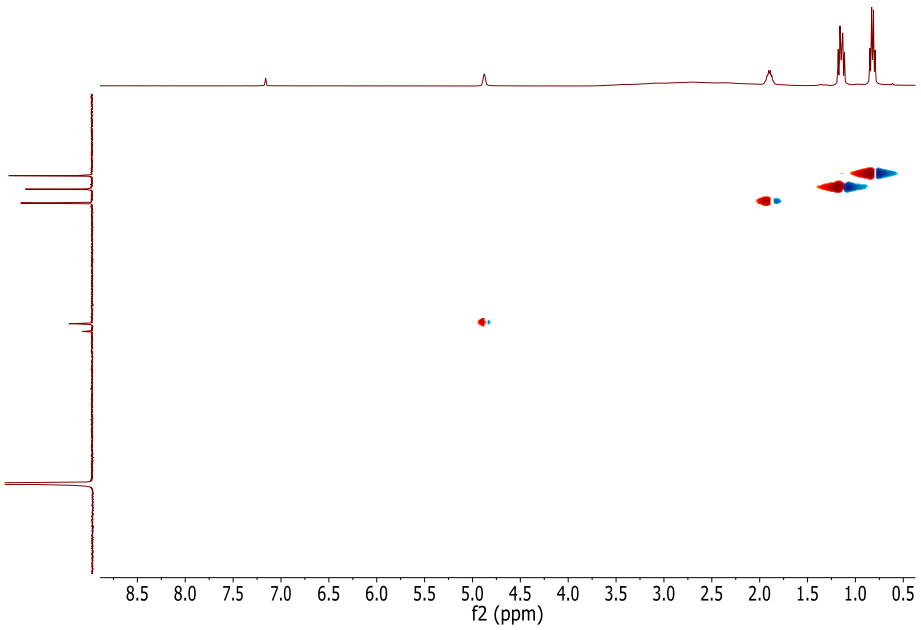

Figure 5-17 HSQC (^{13}C,^{1}H) NMR of complex **4** (25°C, 300 MHz, C_6D_6)

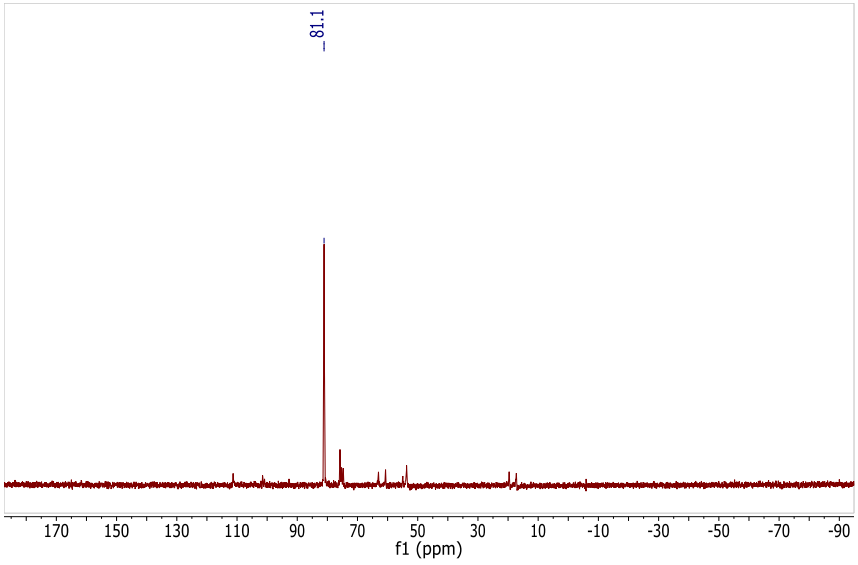

Figure 5-18 $^{31}P(^{1}H)$ NMR of complex **4** room temperature overnight in chlorobenzene. (121 MHz, C_6D_6) (Note: Primary product is the starting complex **4** at 81.1 ppm)

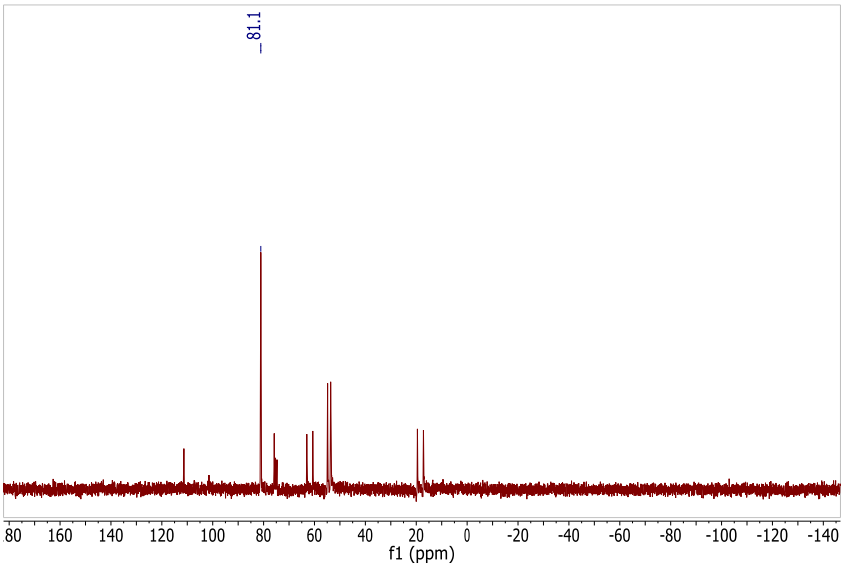

Figure 5-19 $^{31}P(^{1}H)$ NMR (121 MHz, C_6D_6) of complex **4** refluxed in chlorobenzene. (121 MHz, C_6D_6) (Note: Primary product is the starting complex **4** at 81.1 ppm)

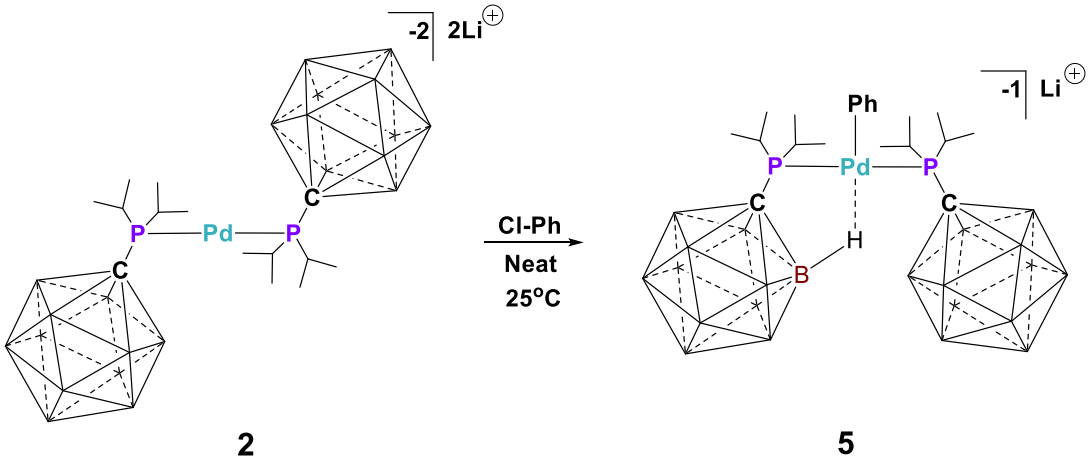

Synthesis of complex 5: Pd complex **2** (50 mg, 0.053 mmol) was dissolved in 500 μL of chlorobenzene After 9 minutes, the oxidative addition product was crashed out in 15 mL of hexanes, and the precipitate was filtered with a pipette filter and the solid was extracted with THF and pumped off. The solid residue was then dissolved in ether and placed in freezer (-30°C) overnight. ^{1}H NMR (600 MHz, THF-d8, 25 °C) δ = 7.45 (d, 2H,

C*H*, ^{3}J(H-H) = 7.9 Hz), 6.92 (dd, 2H, C*H*, ^{3}J(H-H) = 7.9 Hz, ^{3}J(H-H) = 7.2 Hz), 6.84 (t, 1H, C*H*,3J(H-H) = 7.2 Hz), 3.38 (q, 4H, ether), 2.37 (m, 4H, C*H*), 1.28 (dd, 12H, CH_3, ^{3}J(P-H) = 16.7 Hz, ^{3}J(H-H) = 7.7 Hz), 1.10 (m, 18H, CH_3 + ether) ppm. ^{13}C(^{1}H) NMR (151 MHz, THF-d8, 25 °C) δ = 139.4 (*C*H), 135.9 (quaternary *C*), 128.0(*C*H), 124.8 (*C*H), 66.3 (ether), 29.0 (*C*H), 21.3 (*C*H_3), 20.0 (*C*H_3), 15.7 (ether) ppm. ^{31}P(^{1}H) NMR (121 MHz, THF-d8, 25 °C) δ = 32.5 ppm. ^{11}B(^{1}H) NMR (96 MHz, THF-d8, 25 °C) δ = 2.2, -7.6, -10.0 ppm.

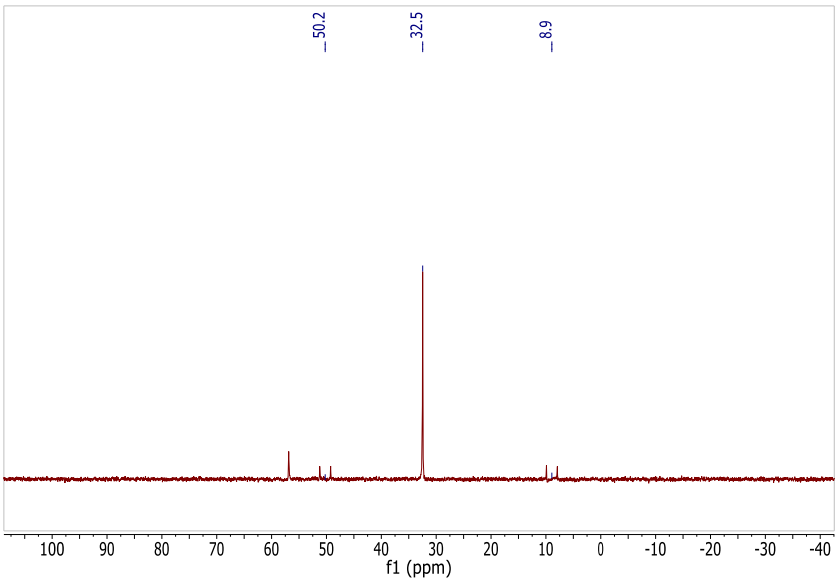

Figure 5-20 ^{31}P(^{1}H) NMR of complex **2** in chlorobenzene at room temperature. (162 MHz, C_6D_6) (Note: Primary product is complex **5** at 32.5 ppm)

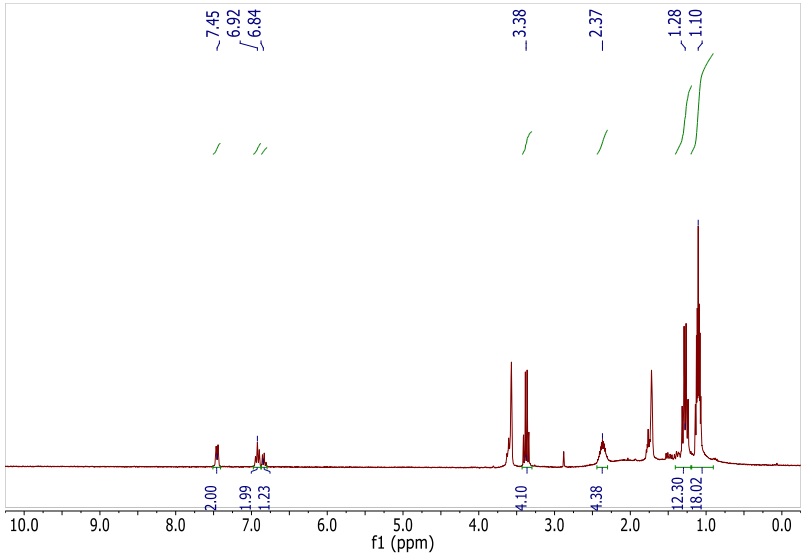

Figure 5-21 ^{1}H NMR of complex **5** (25^{o}C, 600 MHz, THF-d_8)

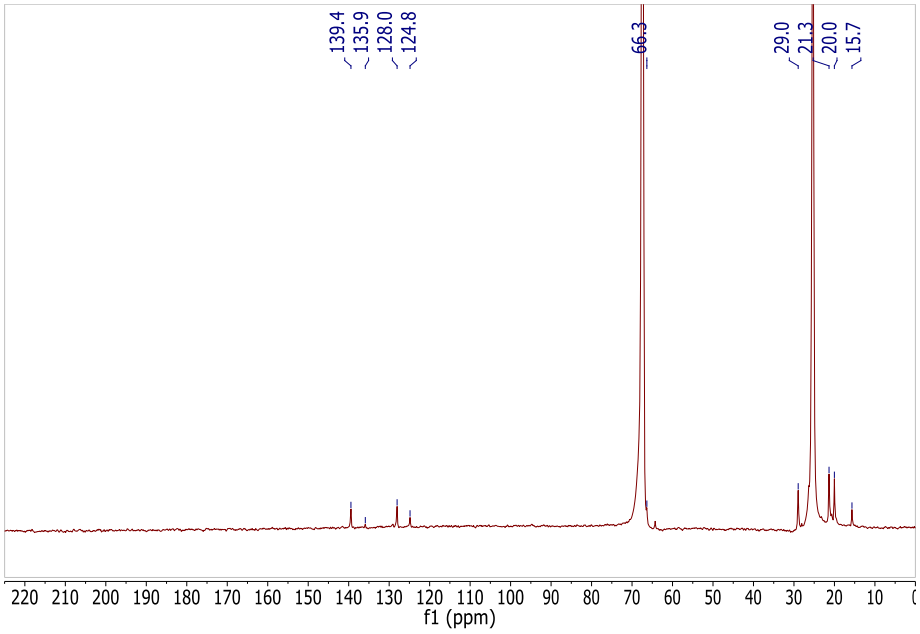

Figure 5-22 ^{13}C(^{1}H) NMR of complex **5** (25^{o}C, 151 MHz, THF-d_8)

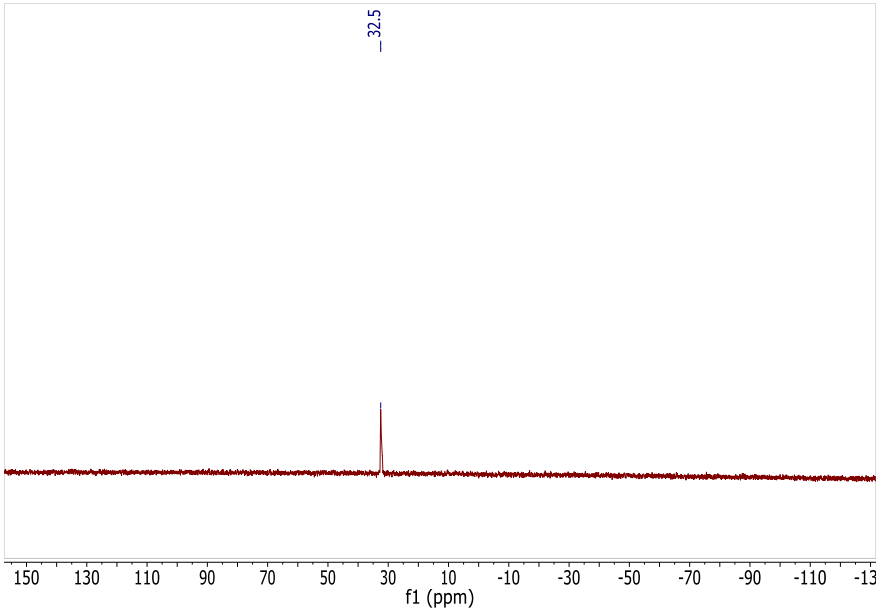

Figure 5-23 $^{31}P(^{1}H)$ NMR of complex **5** (25°C, 121 MHz, THF-d_8)

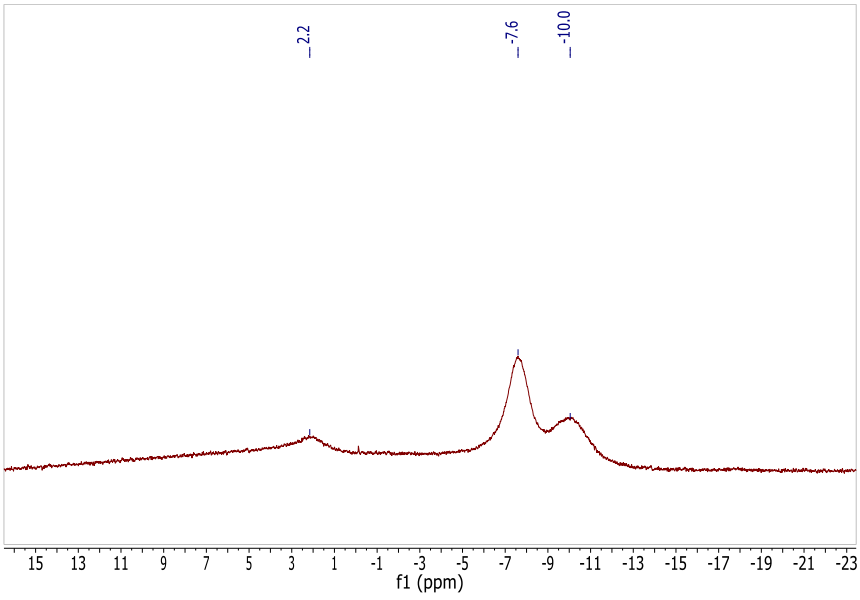

Figure 5-24 $^{11}B(^{1}H)$ NMR of complex **5** (25°C, 96 MHz, THF-d_8)

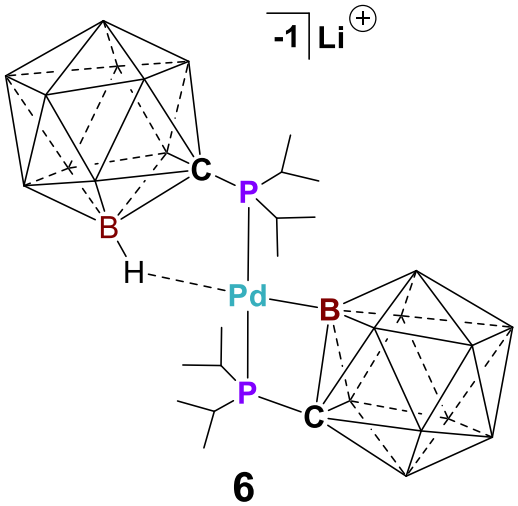

6

Cyclometalation Pd(II) Complex 6: Byproduct of oxidative addition of chlorobenzene onto complex **2**. B-cyclometalated Pd(II) complex **6** can also be made by dissolving **2** in chlorobenzene and heated at 80°C for 3 hours, then washed with hexanes, and filtered in quantitate yields. Note: In order to confirm the organic byproducts with the formation of complex **6**, an experiment was done where 1 equivalent of deuterated chlorobenzene was added to 1 equivalent of complex **2,** and the reaction was monitored by ^{1}H and ^{31}P NMR in THF-d8 over time, which indicated the formation of **6** and benzene. ^{1}H NMR (300 MHz, C_6D_6, 25 °C) δ = 3.39 (m, 8H,THF), 3.25 (q, 8H, ether), 2.48 (m, 8H, C*H*), 1.63 (dd, 12H, C*H*$_3$, ^{3}J(P-H) = 16.4 Hz, ^{3}J(H-H) = 6.9 Hz), 1.43 (m, 8H, THF), 1.26 (m, 12H, C*H*$_3$), 1.10 (t, 12H, ether) ppm. $^{13}C(^{1}H)$ NMR (151 MHz, C_6D_6, 25 °C) δ = 68.3 (THF), 65.9 (ether), 27.8 (*C*H), 25.6 (THF), 20.9 (*C*H$_3$), 20.5 (*C*H$_3$), 15.5 (ether) ppm. $^{31}P(^{1}H)$ NMR (202 MHz, THF, 25 °C) δ = 50.2 (d, ^{2}J(P-P) = 323.5 Hz), 8.9 (d, ^{2}J(P-P) = 323.5 Hz) ppm. $^{11}B(^{1}H)$ NMR (193 MHz, THF, 25 °C) δ = 2.2, -7.6, -10.0 ppm.

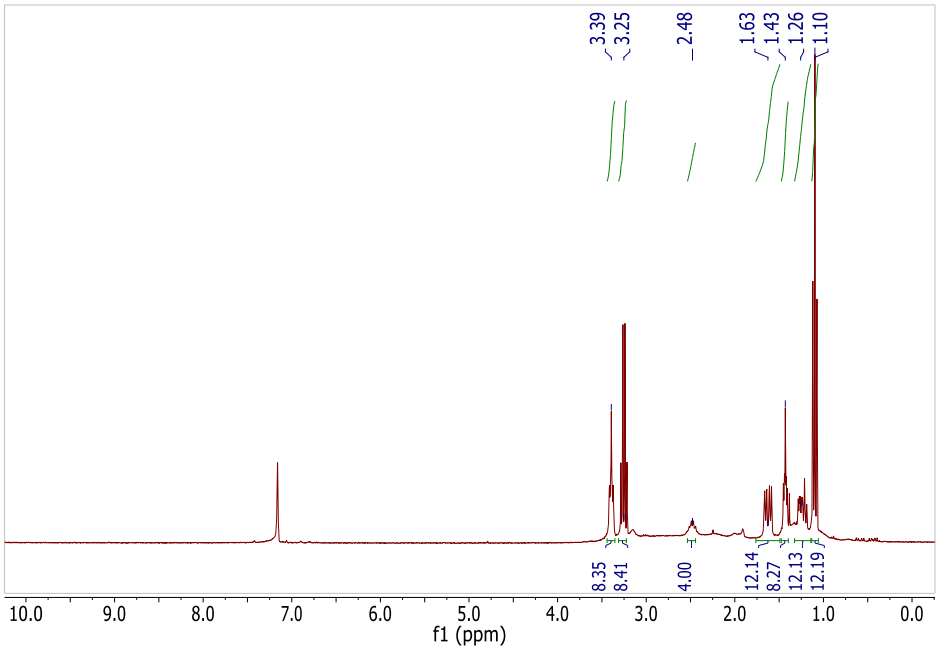

Figure 5-25 ^{1}H NMR of complex **6** (25°C, 300 MHz, C_6D_6)

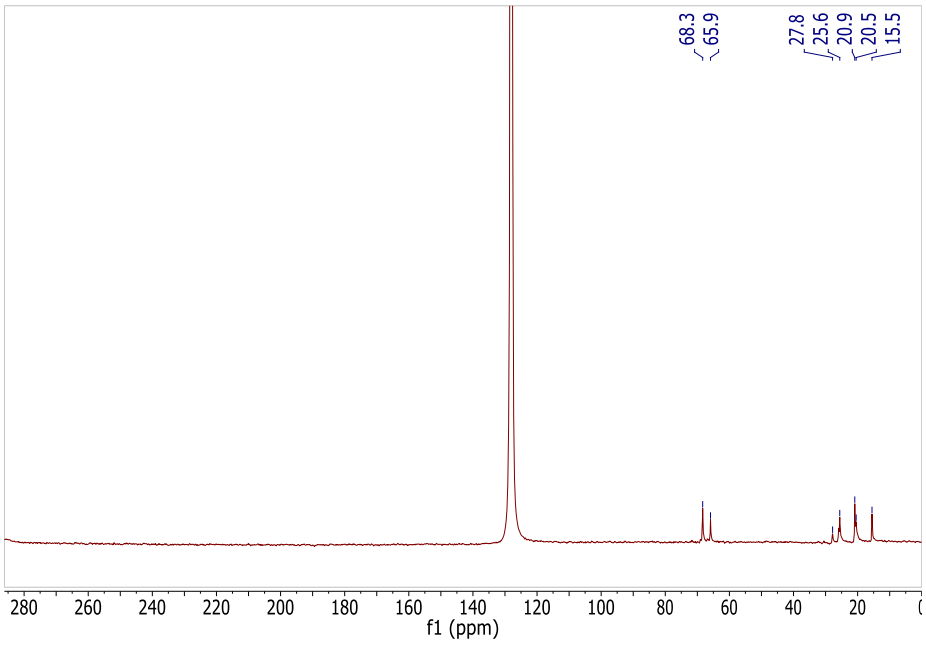

Figure 5-26 $^{13}C(^{1}H)$ NMR) of complex **6** (25°C, 151 MHz, C_6D_6)

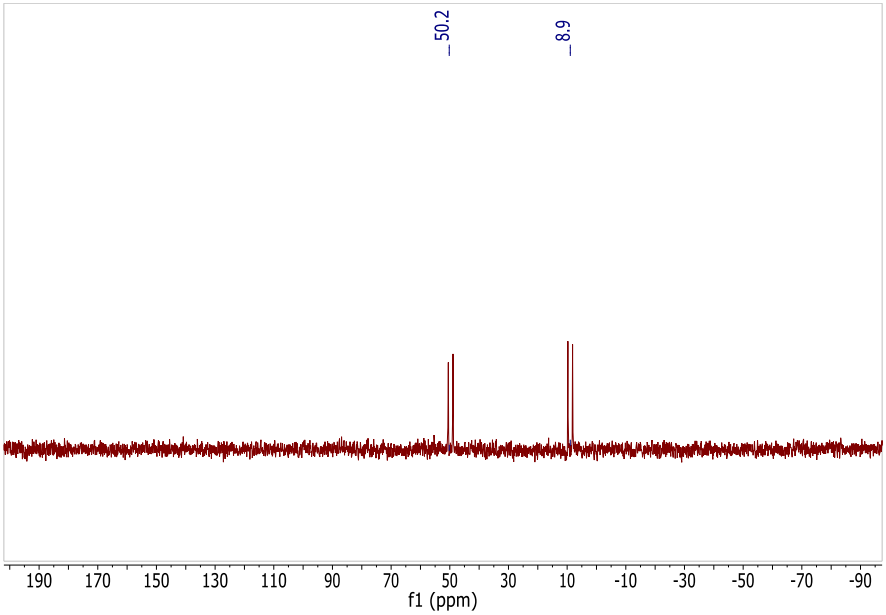

Figure 5-27 ^{31}P NMR of complex **6** (25^{o}C, 202 MHz, THF)

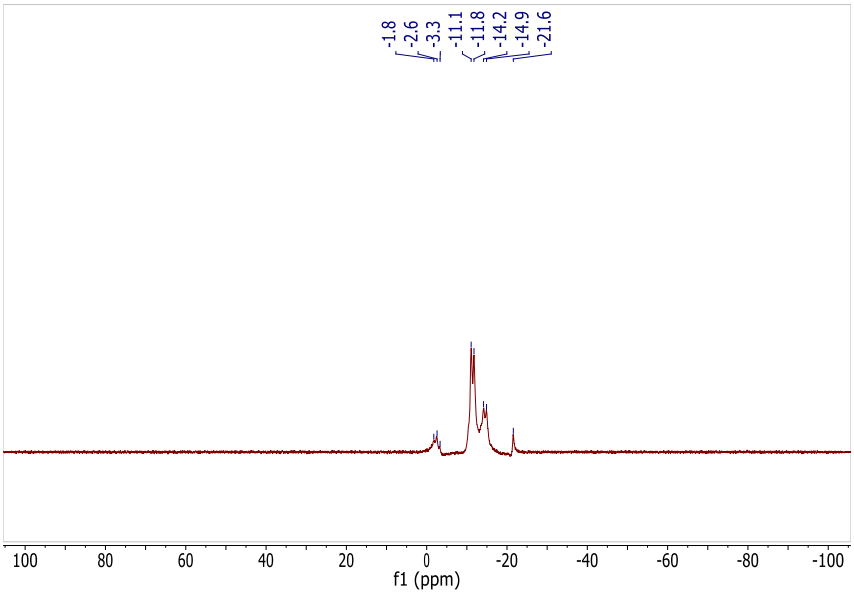

Figure 5-28 $^{11}B(^{1}H)$ NMR of complex **6** (25^{o}C, 193 MHz, THF)

Independent synthesis of $Pd(PCy_3)_2$ 8: PCy_3 (100 mg, 0.353 mmol) was dissolved in 3 mL of THF and stirred for five minutes. (1,5-Cyclooctadiene)bis[(trimethylsilyl)methyl]palladium (69 mg, 0.176 mmol) dissolved in 2 mL of THF was added to the vial containing the PCy_3 solution dropwise. The solution was then pumped off and the precipitate was crystallized from hexanes at -30°C. The crystals were then filtered off yielding complex **8** (115 mg, 95% yield). ^{31}P matched literature value[46] of $Pd(Cy_3)_2$.$^{31}P(^1H)$ NMR (121 MHz, THF, 25°C) δ = 39.8 ppm.

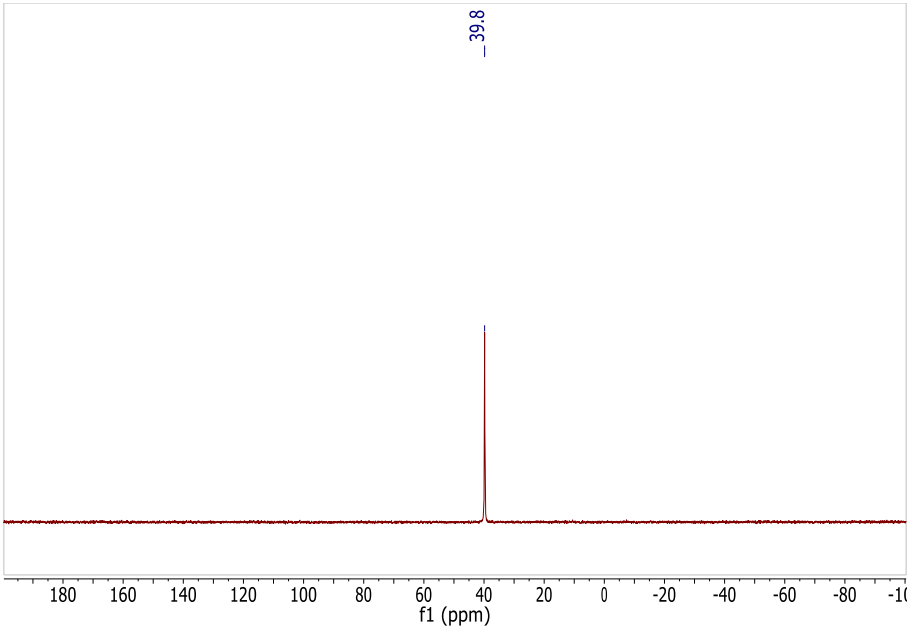

Figure 5-29 $^{31}P(^1H)$ NMR of complex **8** (25°C, 121 MHz, THF)

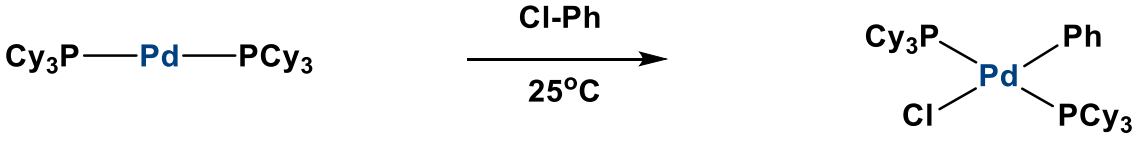

Addition of chlorobenzene to complex 8: Complex **8** (20 mg, 0.0297 mmol) was dissolved in 500 μl of chlorobenzene and monitored by ^{31}P NMR over time. After more than 28 hours, there is full conversion of complex **8** (39.8 ppm) to the oxidative addition product (21.8 ppm) which matches with literature value[47].

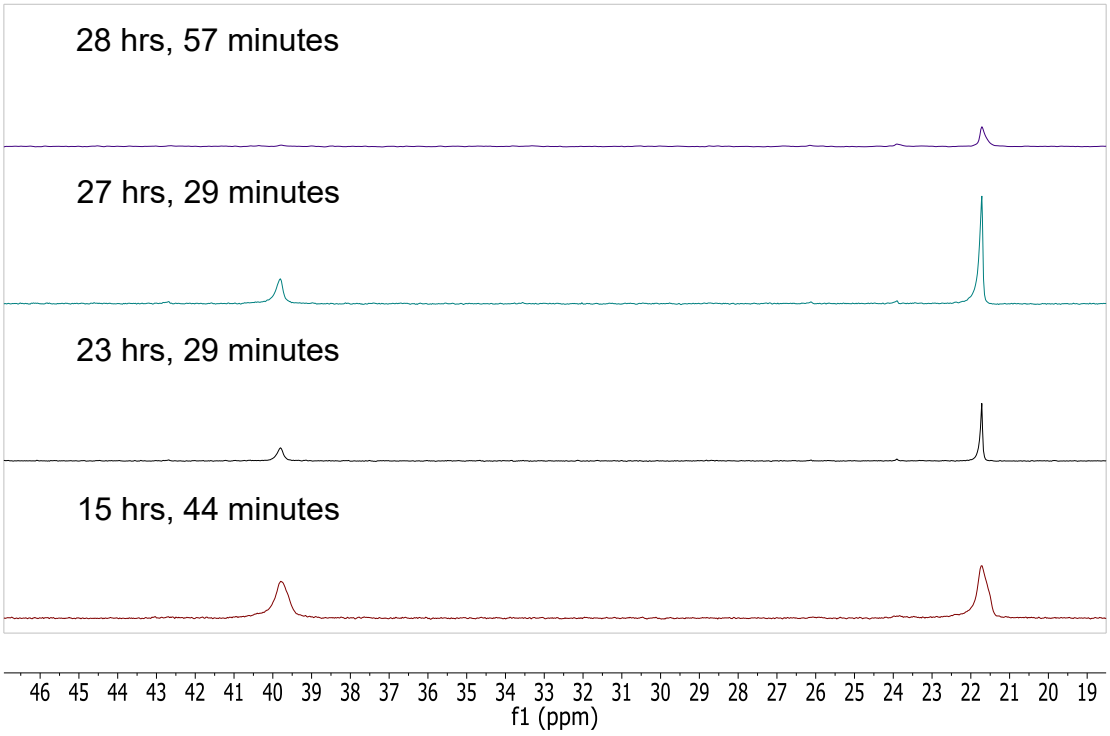

Figure 5-30 $^{31}P(^{1}H)$ NMR of complex **8** (25°C, 121 MHz, THF) in chlorobenzene over time

Independent synthesis of Pd(P(*t*-bu)$_3$)$_2$: P(*t*-bu)$_3$ (100 mg, 0.494 mmol) was dissolved in 3 mL of THF and stirred for five minutes. (1,5-Cyclooctadiene)bis[(trimethylsilyl)methyl]palladium (69 mg, 0.247 mmol) dissolved in 2 mL of THF was added to the vial containing the P(*t*-bu)$_3$ solution dropwise. The solution

was then pumped off and crystallized from hexanes at -30 °C. The crystals were then filtered off yielding Pd(P(*t*-bu)$_3$)$_2$ (125 mg, 96% yield). ^{31}P matched literature value[48] of Pd(P(*t*-bu)$_3$)$_2$. ^{31}P(^{1}H) NMR (121 MHz, THF, 25 °C) δ = 84.7 ppm.

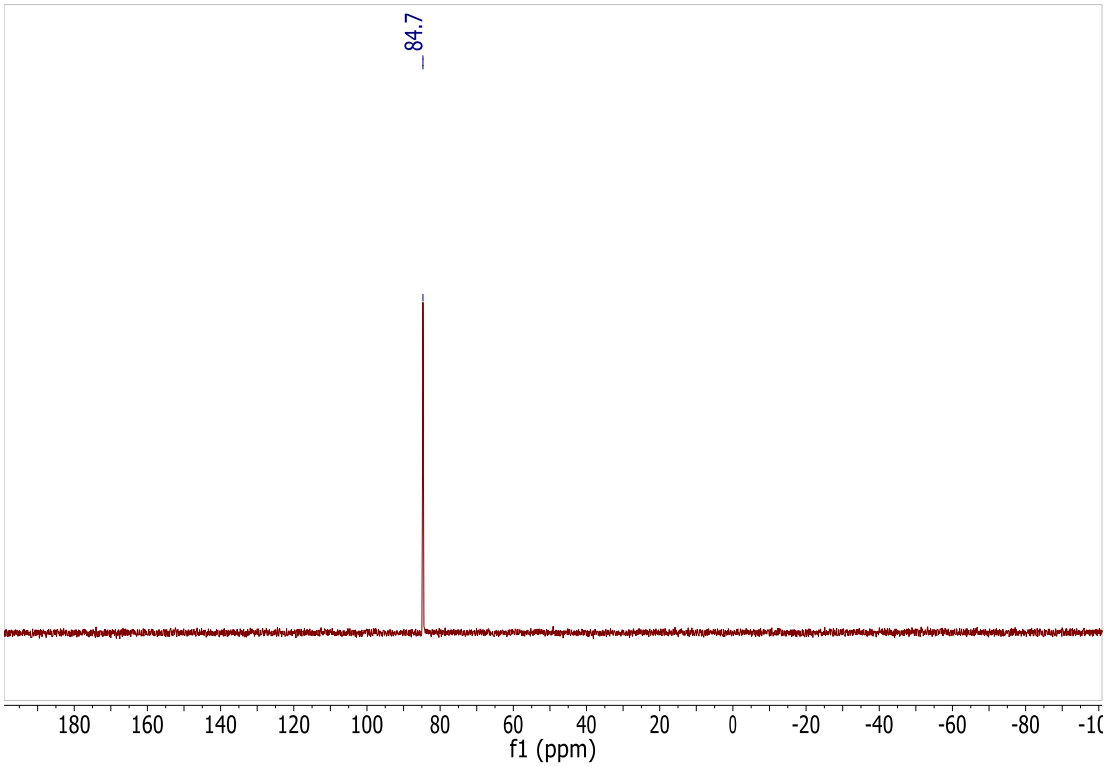

Figure 5-31 ^{31}P(^{1}H) NMR of complex **8** (25°C, 121 MHz, THF)

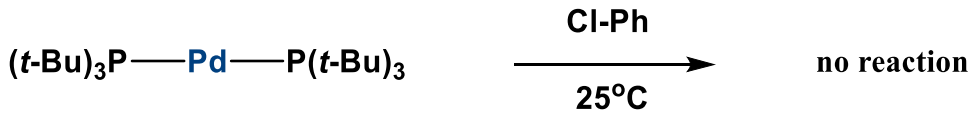

Addition of chlorobenzene to Pd(P(*t*-bu)$_3$)$_2$: Pd(P(*t*-bu)$_3$)$_2$ (15 mg, 0.0297 mmol) was dissolved in 500 μl of chlorobenzene and monitored by 31P NMR over time. After 24

hrs, there is a small peak at 81.9 ppm, but it does not correspond to the desired product[41] (72.8 ppm).

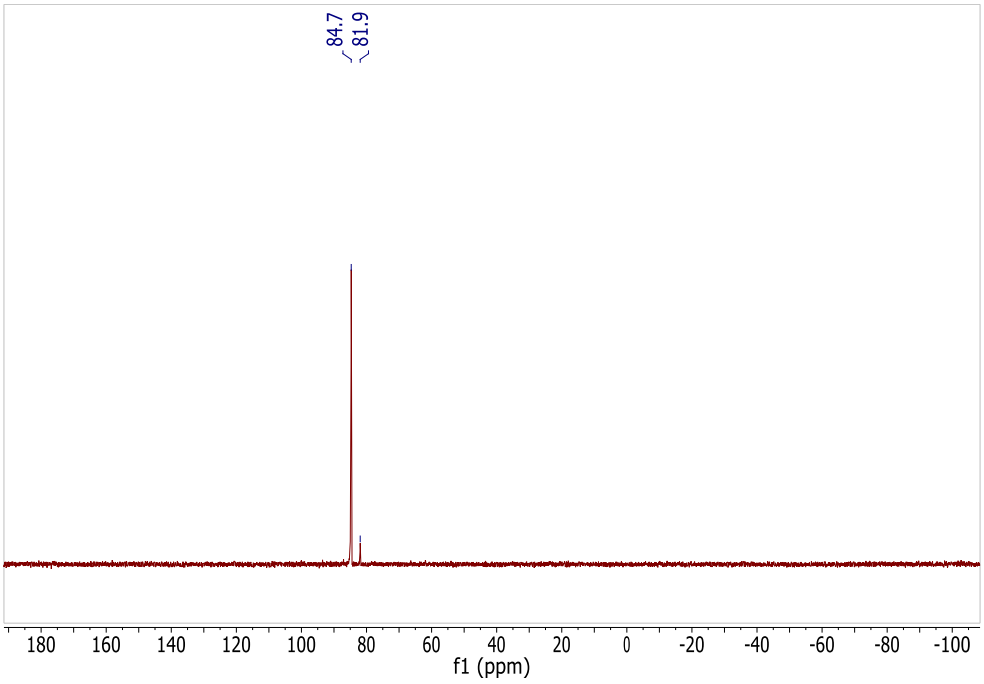

Figure 5-32 $^{31}P(^{1}H)$ NMR) of $Pd(P(t\text{-}bu)_3)_2$ in chlorobenzene (25°C, 162 MHz, THF) after 24 hours

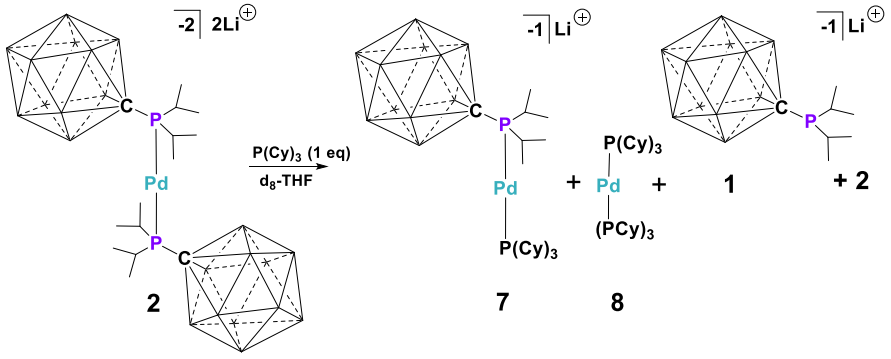

Addition of 1 eq $P(Cy_3)_3$ to Complex 2: 50 mg (0.0467 mmol) of Complex **2** was dissolved in 500 µl THF. After one minute, 13 mg (0.0467 mmol) of PCy_3 was added to

the solution. A ^{31}P NMR was taken immediately after. $^{31}P(^{1}H)$ NMR (121 MHz, THF, 25 °C) δ = 66.5, 66.1 (d, $^{2}J(P\text{-}P)$ = 254.2 Hz), 43.0, 39.8, 39.5 (d, $^{2}J(P\text{-}P)$ = 254.2 Hz) ppm.

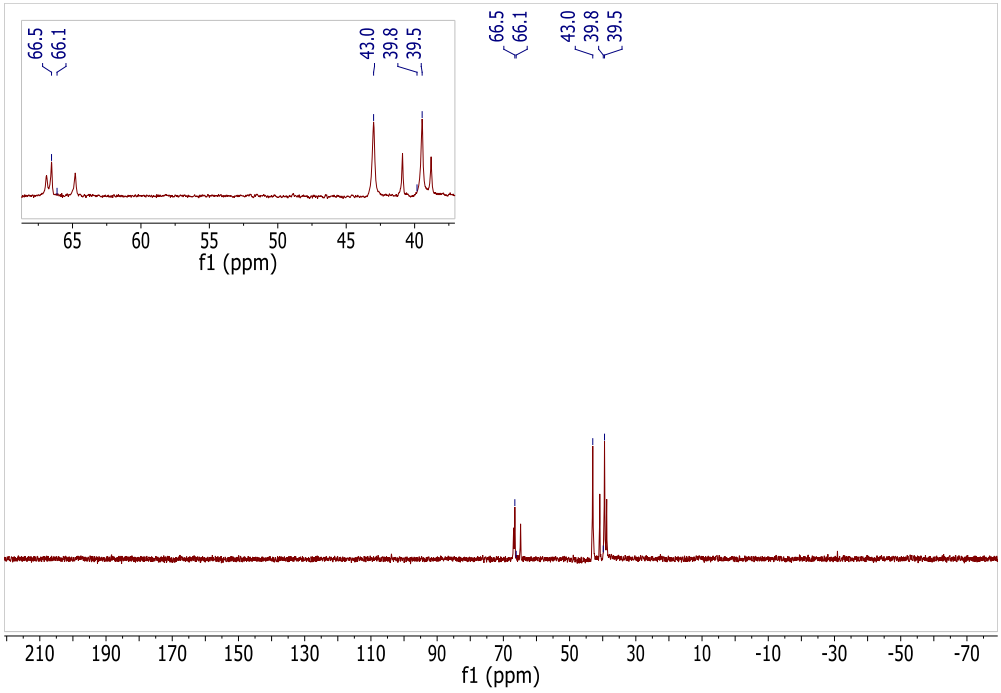

Figure 5-33 ^{31}P NMR of immediate addition of $P(Cy)_3$ to complex **2** (25°C, 121 MHz, THF). The peak at 66.5, 43.0, and 39.5 ppm correspond to complex **2**, phosphine **1**, and complex **8** respectively. Two doublets at 66.1 and 39.8 ppm ($^{2}J(P,P)$ = 254.2 Hz) correspond to complex **7**

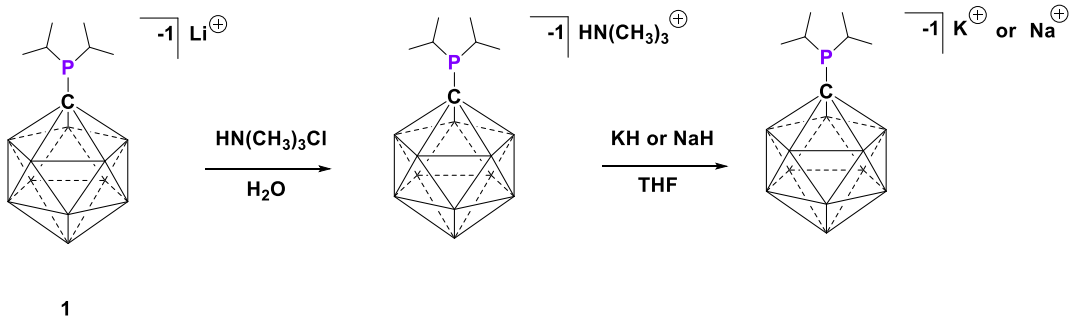

1

Synthesis of $HN(CH_3)_3[P(iPr)_2CB_{11}H_{11}]$, $K[P(iPr)_2CB_{11}H_{11}]$, $Na[P(iPr)_2CB_{11}H_{11}]$: Phosphine (1 mmol) **1** was dissolved in degassed H_2O and 3 equivalents of $HN(CH_3)_3Cl$ (3 mmol) was

added while stirring. Precipitate formed, and the precipitate was cannula filtered and vacuumed overnight at 60 ^{o}C. Excess KH or NaH was added in THF depending on the desired salt and stirred for 1 hour. Excess KH or NaH was removed by filtration and the THF was pumped off to yield the salts in quantitative yields. ^{31}P NMR for all phosphines found at 45.0 ppm. $HN(CH_3)_3[P(iPr)_2CB_{11}H_{11}]$: ^{1}H NMR (300 MHz, C_6D_6, 25 °C) δ = 5.35 (s, 1H, *H*N$(CH_3)_3$), 1.91 (m, 1H, C*H*), 1.86 (s, 8H, HN(C*H*$_3)_3$), 0.72 (dd, 12H, C*H*$_3$, ^{3}J(P-H) = 17.2 Hz, ^{3}J(H-H) = 7.3 Hz), 0.61 (dd, 12H, C*H*$_3$, ^{3}J(P-H) = 19.3 Hz, ^{3}J(H-H) = 7.3 Hz) ppm. $K[P(iPr)_2CB_{11}H_{11}]$: ^{1}H NMR (300 MHz, CD_3CN, 25 °C) δ = 1.92 (m, 1H, C*H*), 1.16 (dd, 12H, C*H*$_3$, ^{3}J(P-H) = 16.2 Hz, ^{3}J(H-H) = 7.2 Hz), 1.10 (dd, 12H, C*H*$_3$, ^{3}J(P-H) = 9.8 Hz, ^{3}J(H-H) = 7.1 Hz) ppm. $Na[P(iPr)_2CB_{11}H_{11}]$: ^{1}H NMR (300 MHz, CD_3CN, 25 °C) δ = 1.92 (m, 1H, C*H*), 1.16 (dd, 12H, C*H*$_3$, ^{3}J(P-H) = 16.3 Hz, ^{3}J(H-H) = 7.3 Hz), 1.10 (dd, 12H, C*H*$_3$, ^{3}J(P-H) = 9.8 Hz, ^{3}J(H-H) = 7.1 Hz) ppm.

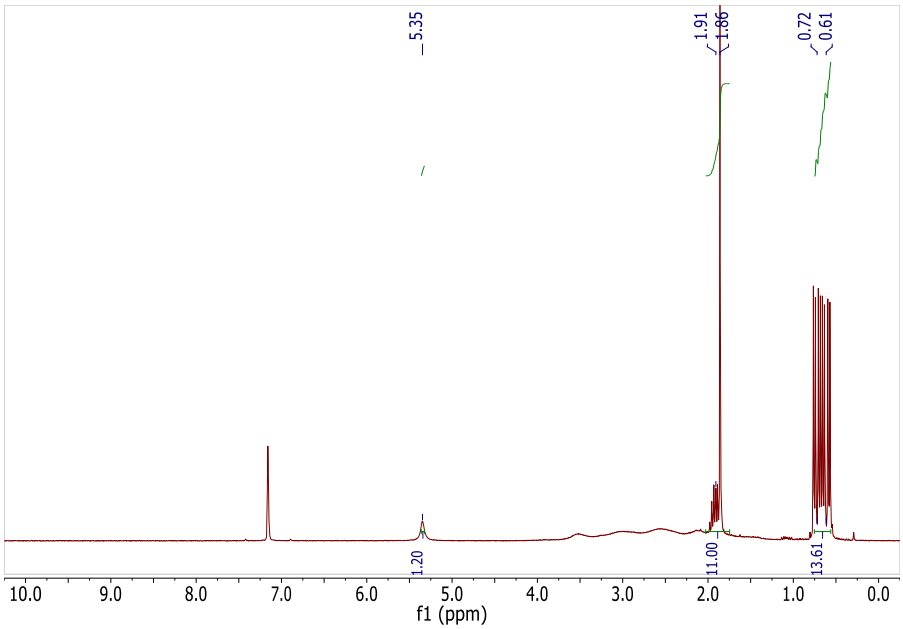

Figure 5-34 ^{1}H NMR of $HN(CH_3)_3[P(iPr)_2CB_{11}H_{11}]$ (25°C, 300 MHz, C_6D_6)

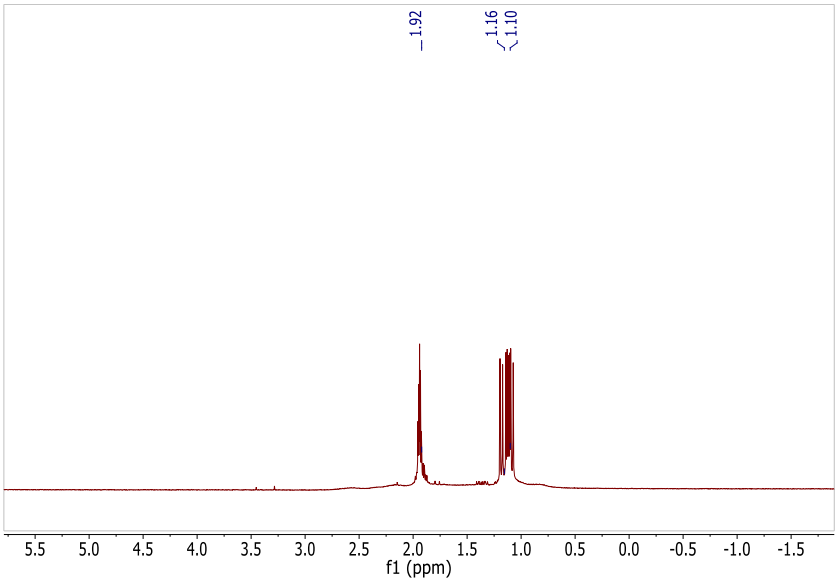

Figure 5-35 ^{1}H NMR of $K[P(iPr)_2CB_{11}H_{11}]$ (25°C, 300 MHz, CD_3CN)

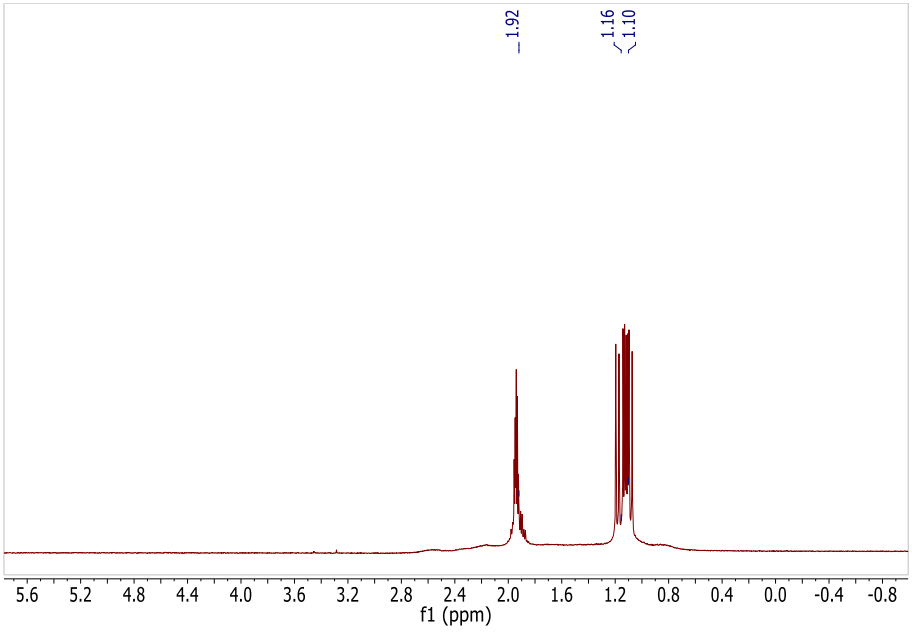

Figure 5-36 ^{1}H NMR of Na[P(iPr)$_2$CB$_{11}$H$_{11}$] (25^{o}C, 300 MHz, CD$_3$CN)

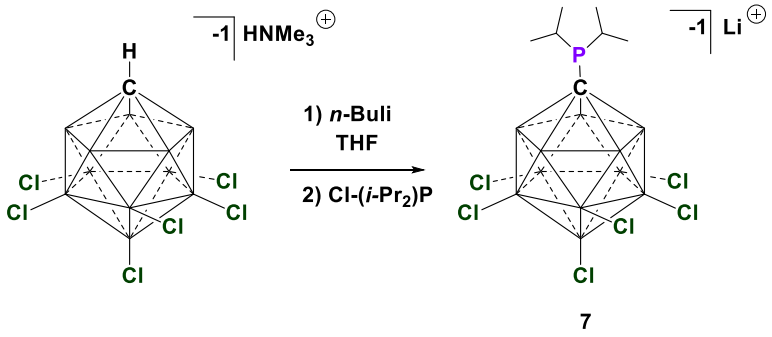

Synthesis of Phosphine 7: HNMe$_3$[HCB$_{11}$H$_5$Cl$_6$] (200 mg, 0.488 mmol) was dissolved in 3 mL of THF. 2.5M *n*-Buli (4 eq) was added slowly. After stirring for 10 minutes, precipitation was observed, and THF was added until the reaction mixture returned to a solution (ca. 5 ml). The solution was then stirred for 2 hours. 10 mL hexanes was then added, and an immediate white powder was formed. The white precipitate was filtered and washed again with 10 ml of hexanes. The white precipitated was then dried under

vacuum, and 5 mL THF was added to the precipitate. 1.1 eq of chlorodiisopropylphosphine was then added dropwise. The product was then crashed out of hexanes, filtered, and then extracted with 20 mL of fluorobenzene. The fluorobenzene was then vacuumed, and a white solid was obtained (309 mg, 92% yield).

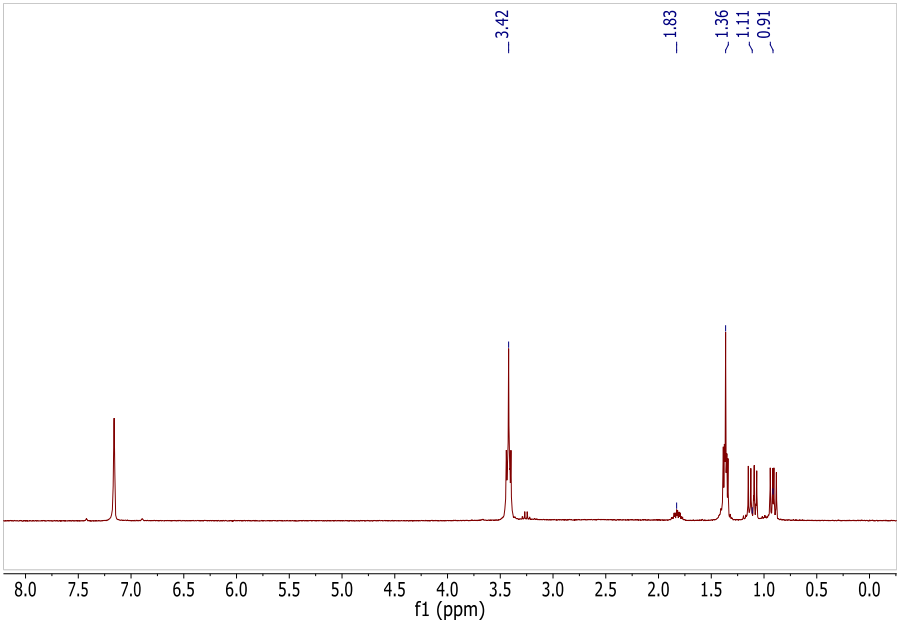

Figure 5-37 ^{1}H NMR of phosphine **7** (25^{o}C, 300 MHz, C_6D_6)

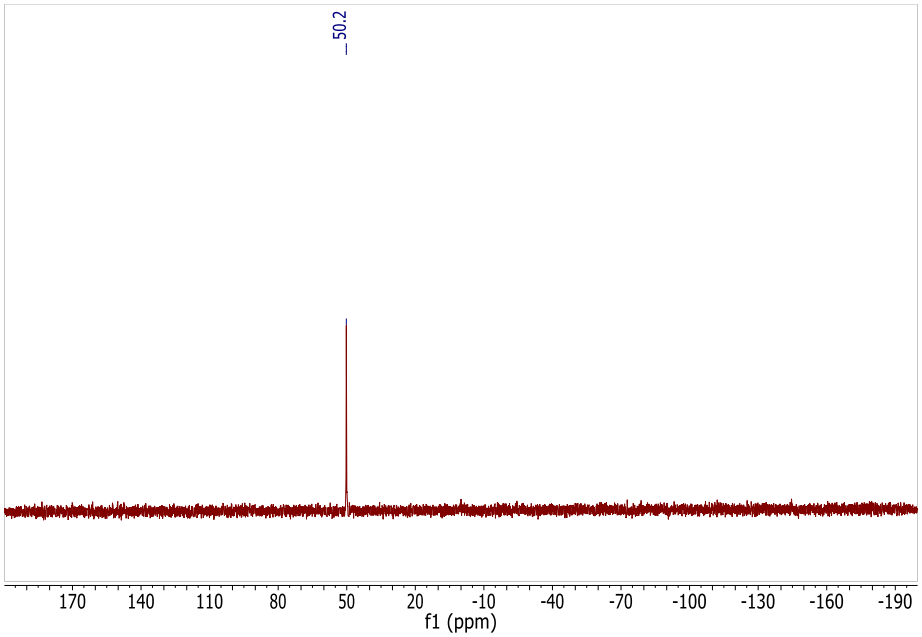

Figure 5-38 ^{31}P NMR of phosphine **7** (25^{o}C, 121 MHz, C_6D_6)

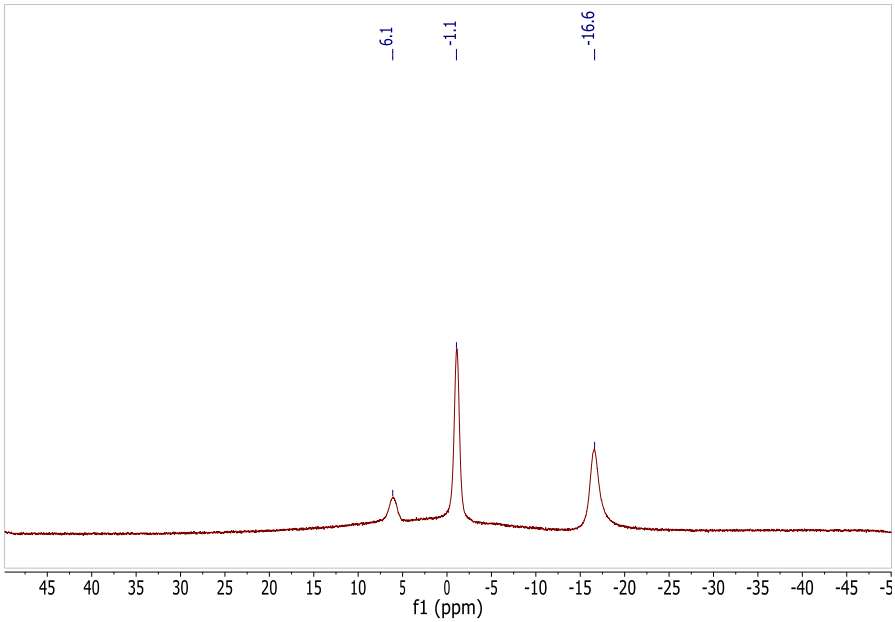

Figure 5-39 ^{11}B NMR of phosphine **7** (25^{o}C, 96 MHz, C_6D_6)

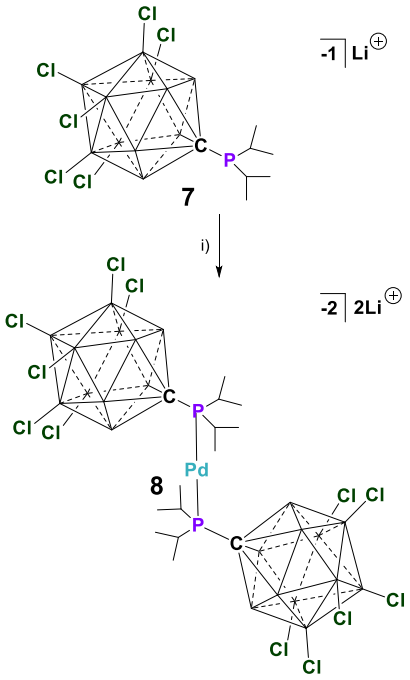

Synthesis of Complex 8: Phosphine **7** (100 mg, 0.145 mmol) and (1,5 Cyclooctadiene)bis[(trimethylsilyl)methyl]palladium (28 mg, 0.0726 mmol) was dissolved in 2 mL of benzene and added drop wise to **1** and stirred for 20 minutes. An oil formed in which the benzene was removed and further washed with 4 mL of benzene. The oil was then triturated in 10 mL of hexanes, and the hexanes was subsequently removed. The product was obtained by concentrating in vacuo to afford **2** (105 mg, 97% yield) as a precipitate.

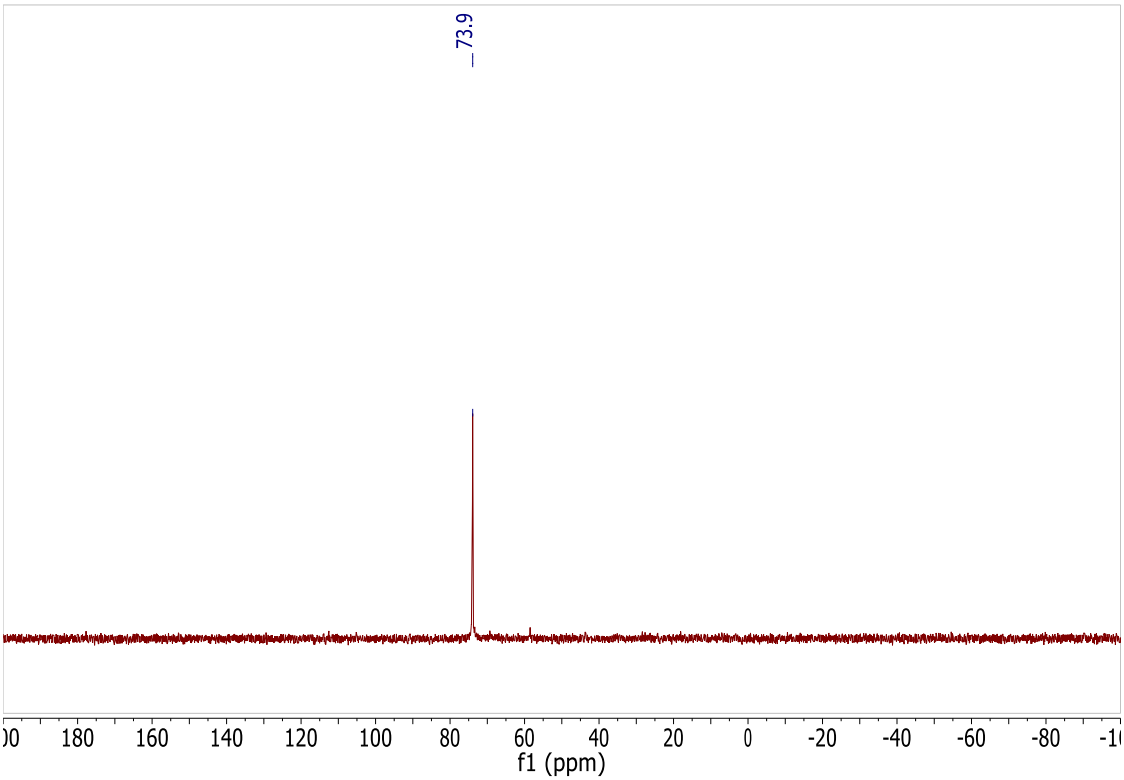

Figure 5-40 ^{31}P NMR of complex **8** (25°C, 96 MHz, C_6D_6)

Kinetic Studies

General procedure for kinetic experiments: A stock solution of phosphine **1** and complex **2** were prepared in chlorobenzene. A micropipette was used to dispense all reagents and starting materials. A sealed capillary tube with a THF solution of H_3PO_4 was placed inside the NMR tube to be used as an external standard. For heated samples, the desired temperature was stabilized before sample tube was inserted. 0.0155 mmol of Pd complex **2**, and varying mol % of phosphine **1** in 500 μl of chlorobenzene were placed in a NMR tube. ^{31}P NMR spectra were acquired at fixed time

intervals throughout the length of experiment with the aid of an automated data collection program.

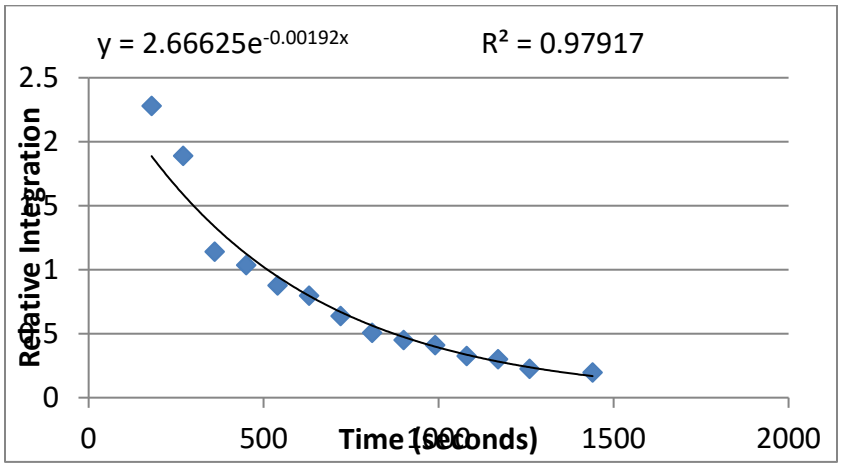

Figure 5-41 Representative decay of Pd complex **2** in the prescence of PhCl and phosphine **1** (1.5 mol %) at 50°C

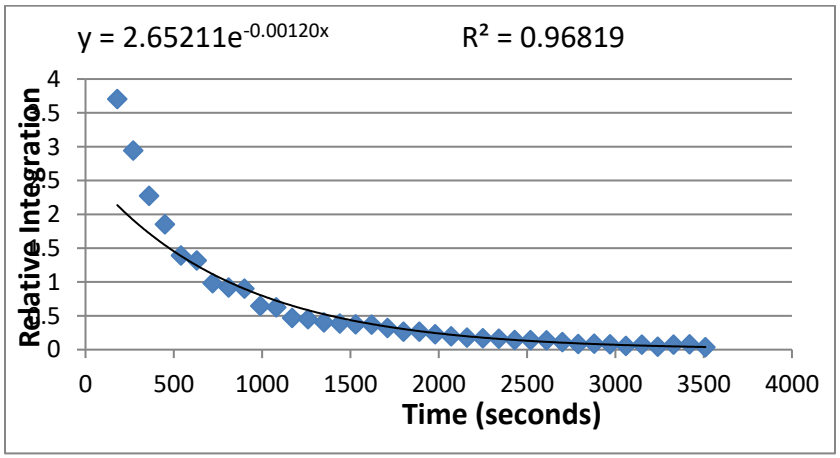

Figure 5-42 Representative decay of Pd complex **2** in the prescence of PhCl and phosphine **1** (2 mol %) at 50°C

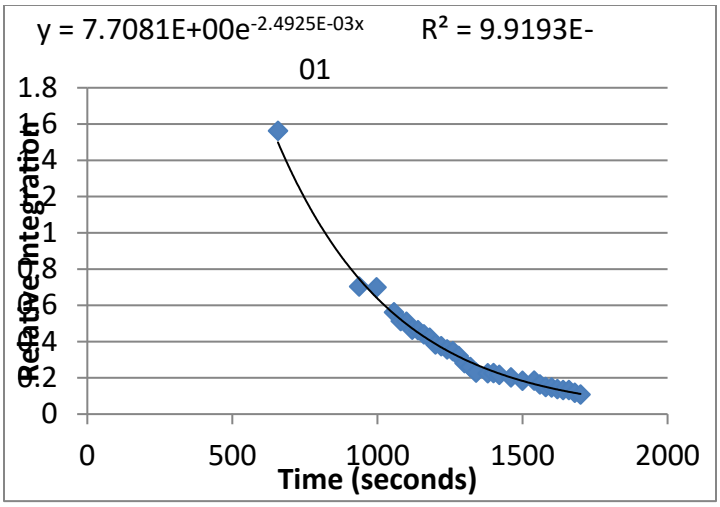

Figure 5-43 Representative decay of Pd complex **2** in the prescence of PhCl and phosphine **1** (3 mol %) at 25°C

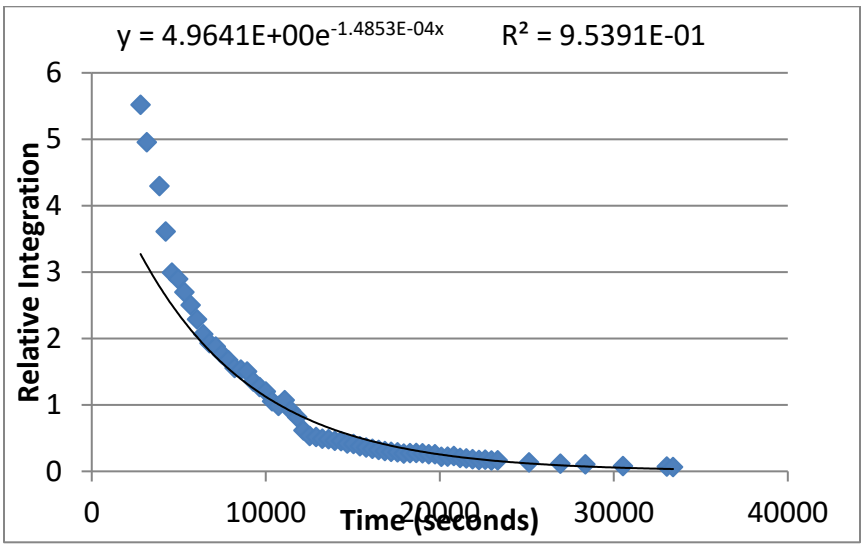

Figure 5-44 Representative decay of Pd complex **2** in the prescence of PhCl and phosphine **1** (5 mol %) at 25°C

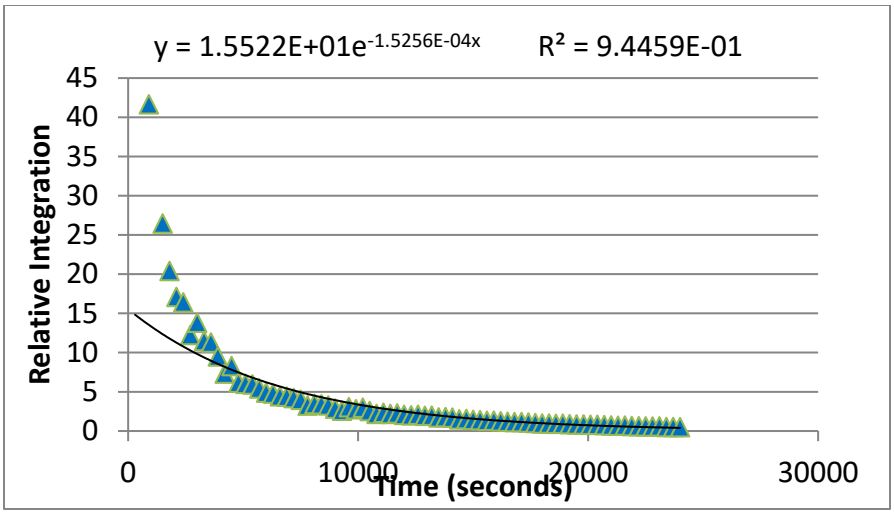

Figure 5-45 Representative decay of Pd complex **2** in the prescence of PhCl and phosphine **1** (7 mol %) at 25°C

Catalysis

General procedure for catalysis: In a glove box, a stir bar, the aryl chloride (1.1 eq), the grignard reagent (1 eq), duerene (1 eq), and the carboranyl phosphine were added in a 20 ml scintillation vial in THF (1 mL). After 5 minutes of stirring, the bis(trimethylsilylmethyl)-(cycloocta-1,5-diene) palladium(II) complex dissolved in THF (1 mL) was added to reaction mixture dropwise, and the reaction mixture was heated at 65°C on a heating block. Amount of catalyst and times are indicated in Table 5-1. At the indicated times, the solutions were then removed via high vacuum and NMRs were taken in $CDCl_3$. Yields were calculated by integration of the ^1H NMR via direct comparison of durene (internal standard) after heating. Validity of this approach was confirmed by obtaining isolated yields of several compounds. In these cases, products were isolated by water/ethyl acetate extraction and purified by flash column

chromatography in hexanes. All products have been previously reported and ^{1}H and ^{13}C NMR matched literature values[49-58].

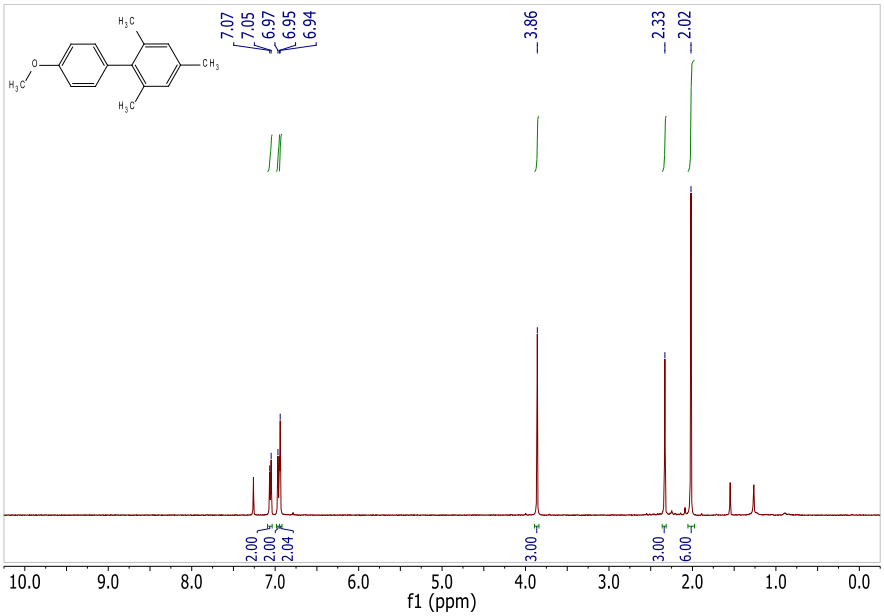

Figure 5-46 ^{1}H NMR (25°C, 300 MHz, $CDCl_3$)

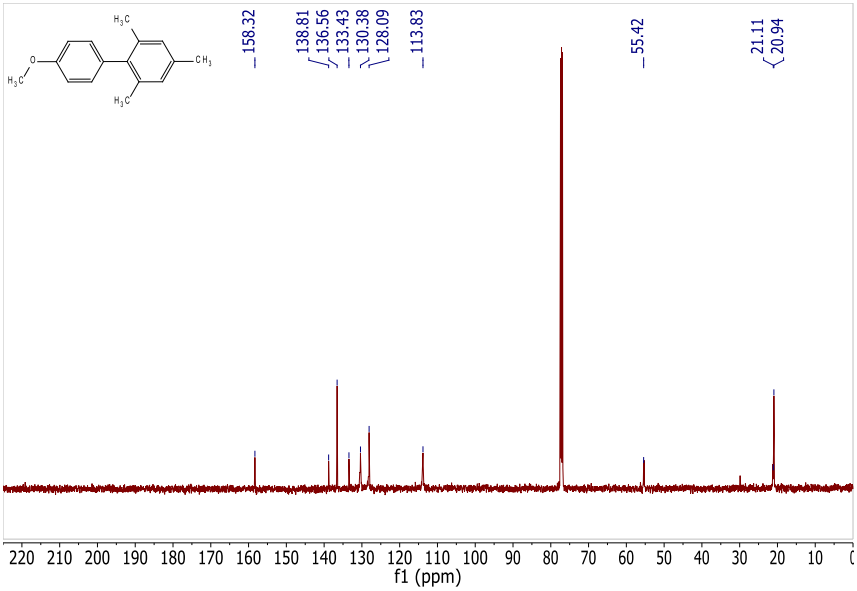

Figure 5-47 $^{13}C(^{1}H)$ NMR (25°C, 126 MHz, $CDCl_3$)

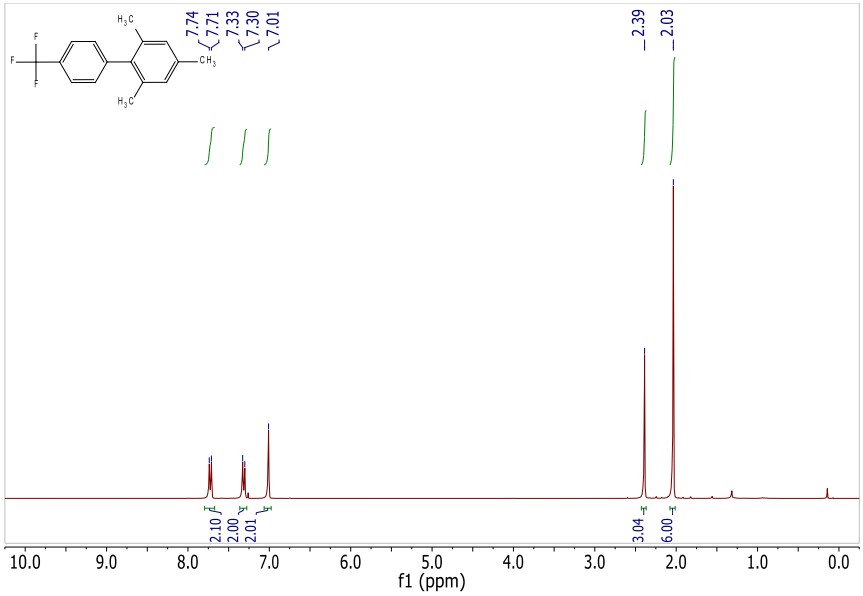

Figure 5-48 ^{1}H NMR (25°C, 300 MHz, $CDCl_3$)

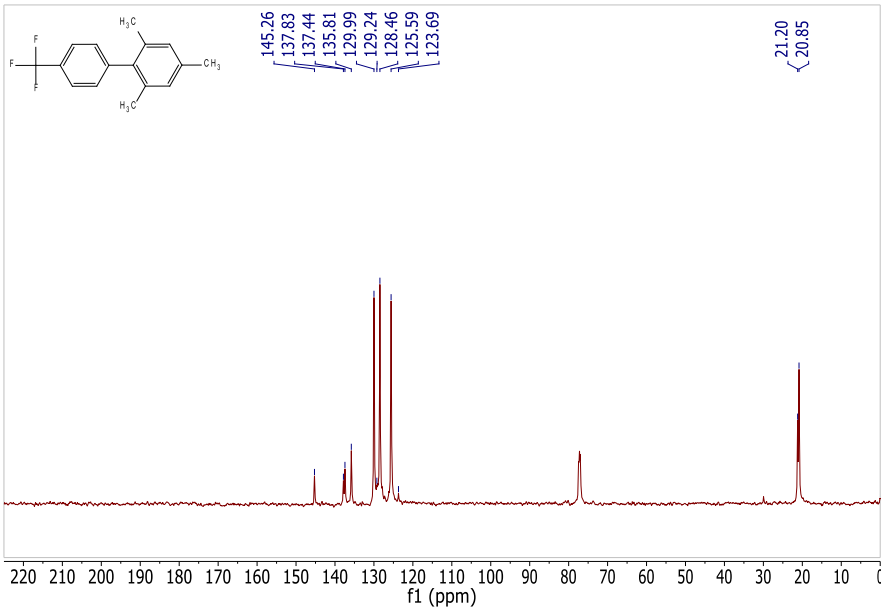

Figure 5-49 $^{13}C(^{1}H)$ NMR (25°C, 151 MHz, $CDCl_3$)

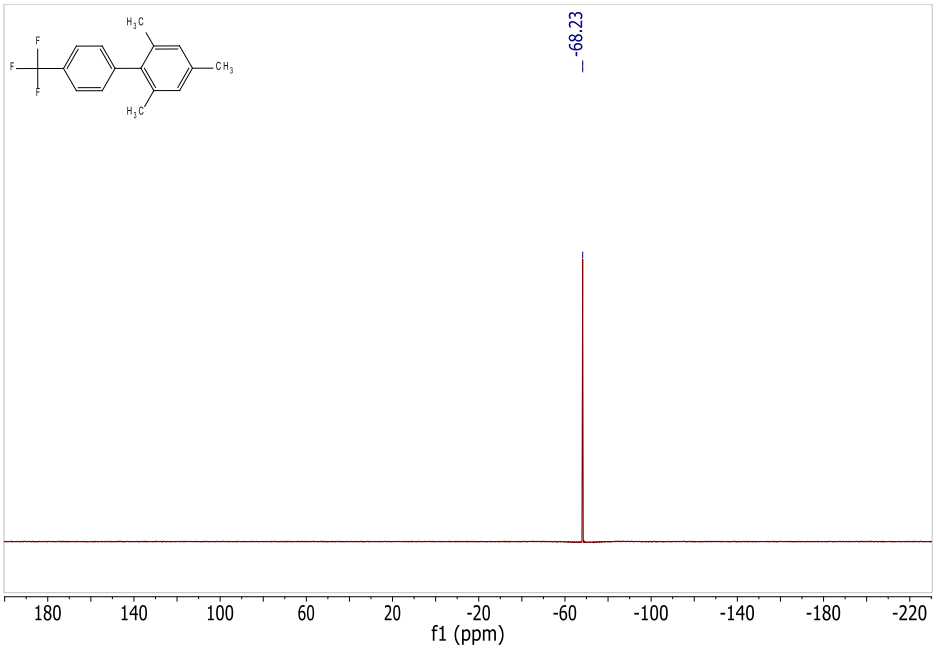

Figure 5-50 ^{19}F NMR (25°C, 283 MHz, $CDCl_3$)

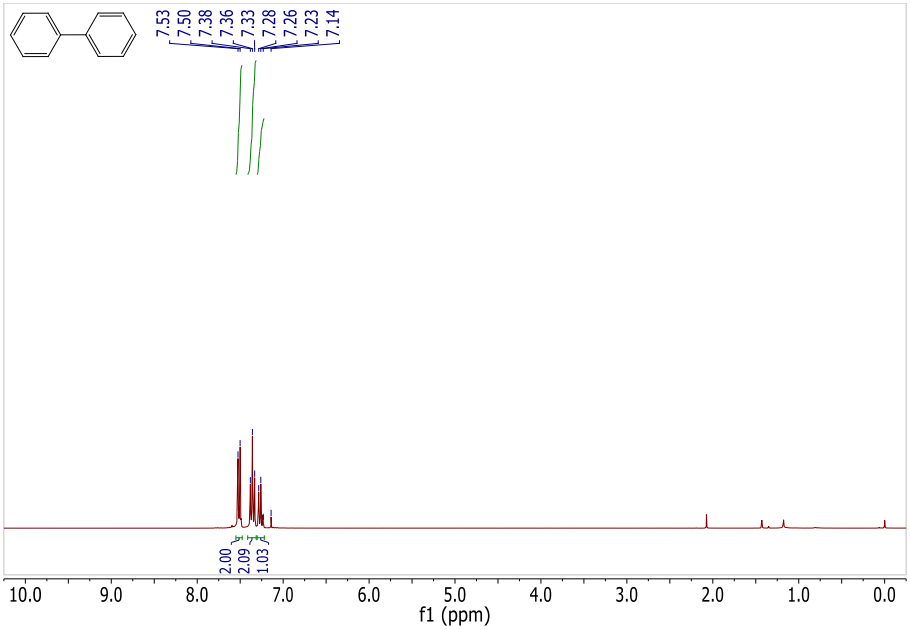

Figure 5-51 ^{1}H NMR (25°C, 300 MHz, $CDCl_3$)

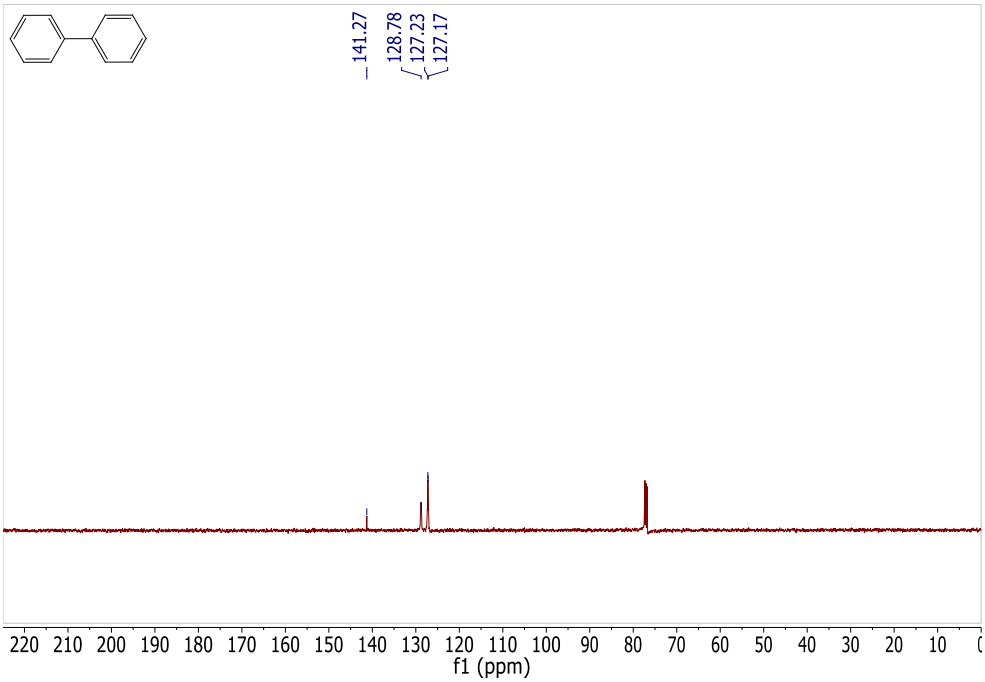

Figure 5-52 $^{13}C(^{1}H)$ NMR (25°C, 126 MHz, $CDCl_3$)

X-Ray Diffraction Studies

X-Ray Structure Determination for complex **2** (CCDC: 1489627)

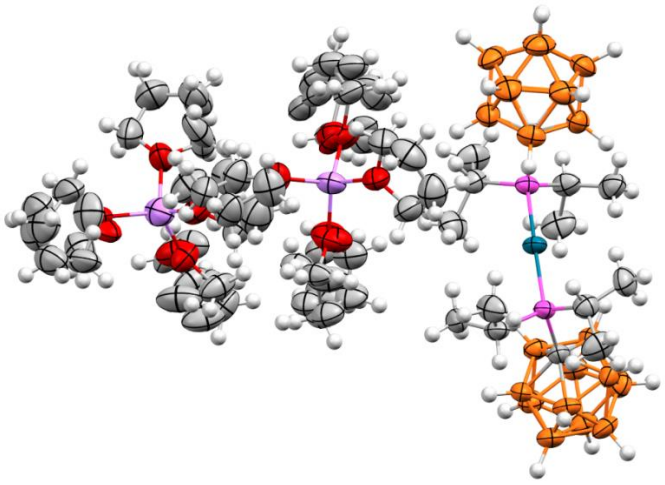

Figure 5-53 Solid-state structure of complex **2**

A colorless thin plate fragment (0.403 x 0.209 x 0.028 mm^3) was used for the single crystal x-ray diffraction study of $[Li[C_4H_8O]_4]_2.[CH_{11}B_{11}]_2[C_3H_7]_4P_2Pd$ (complex **2**). The crystal was coated with paratone oil and mounted on to a cryo-loop glass fiber. X-ray intensity data were collected at 250(2) K on a Bruker APEX2 platform-CCD x-ray diffractometer system (fine focus Mo-radiation, λ = 0.71073 Å, 50KV/30mA power). The CCD detector was placed at a distance of 5.0600 cm from the crystal.

A total of 2400 frames were collected for a sphere of reflections (with scan width of 0.3° in ω, starting ω and 2θ angles of -30°, and ϕ angles of 0°, 90°, 120°, and 240° for every 600 frames, 100 sec/frame exposure time). The Bruker Cell Now program was used to obtain the two different orientation matrices of the rotational twin components

(Twin law is 180^o rotation about the 0 1 0 reciprocal axis). These matrices were imported into the APEX2 program for Bravais lattice determination and initial unit cell refinement. The frames were integrated using the Bruker SAINT software package and using a narrow-frame integration algorithm. Based on a triclinic crystal system, the integrated frames yielded a total of 23159 reflections at a maximum 2θ angle of 50.700^o (0.83 Å resolution), of which 12756 were independent reflections (R_{int} = 0.0248, R_{sig} = 0.0562, redundancy = 1.8, completeness = 99.3%) and 9320 (73.1%) reflections were greater than 2σ(I). The unit cell parameters were, **a** = 11.1686(26) Å, **b** = 17.0277(39) Å, **c** = 18.8242(44) Å, **α** = 79.8723(42) **β** = 89.3161(44)^o**, γ** = 83.8763(39) V = 3503.9(14) Å^3, Z = 2, calculated density D_c = 1.152 g/cm^3. Absorption corrections were applied (absorption coefficient μ = 0.353 mm^{-1}; min/max transmission = 0.871/0.990) to the raw intensity data using the TWINABS program.

The Bruker SHELXTL software package was used for phase determination and structure refinement. The distribution of intensities (E^2-1 = 0.878) and no systematic absent reflections indicated two possible space groups, P-1and P1. The space group P-1 (#2) was later determined to be correct. Direct methods of phase determination followed by two Fourier cycles of refinement led to an electron density map from which most of the non-hydrogen atoms were identified in the asymmetric unit of the unit cell. With subsequent isotropic refinement, all of the non-hydrogen atoms were identified. The combined (major and minor components) HKLF 5 intensity dataset was used in the final structure refinement. There were two disordered cations of $Li[C_4H_8O]_4$ and one anion of $[CH_{11}B_{11}]_2[C_3H_7]_4P_2Pd$ present in the asymmetric unit of the unit cell. Five of the eight

THF molecules of the cations were modeled with disordered (The THF disordered site occupancy ratios were 63%/37%, 58%/42%, 53%/47%, 58%/31%/11%, 44%/34%/22%). The rotational twin law was 180^o rotation about the 0 1 0 reciprocal axis. The major/minor component twin ratio was 75%/25%. The crystal went through phase transition at about 230K and data were collected at 250K.

Atomic coordinates, isotropic and anisotropic displacement parameters of all the non-hydrogen atoms were refined by means of a full matrix least-squares procedure on F^2. The H-atoms were included in the refinement in calculated positions riding on the atoms to which they were attached. The refinement converged at R1 = 0.0484, wR2 = 0.1008, with intensity I>2σ (I). The largest peak/hole in the final difference map was 0.408/-0.317 e/Å^3.

Crystal data and structure refinement complex **2** (CCDC: 1489627)

Identification code	vL130AC_2_0m-5	
Empirical formula	C46 H114 B22 Li2 O8 P2 Pd	
Formula weight	1215.41	
Temperature	250(2) K	
Wavelength	0.71073 Å	
Crystal system	Triclinic	
Space group	P -1 (#2)	
Unit cell dimensions	a = 11.169(3) Å	α= 79.872(4)°.
	b = 17.028(4) Å	β= 89.316(4)°.
	c = 18.824(4) Å	γ = 83.876(4)°.
Volume	3503.9(14) Å^3	
Z	2	

Density (calculated)	1.152 Mg/m^3
Absorption coefficient	0.353 mm^{-1}
F(000)	1292
Crystal size	0.403 x 0.209 x 0.028 mm^3
Theta range for data collection	1.493 to 25.350°.
Index ranges	-13<=h<=13, -20<=k<=20, 0<=l<=22
Reflections collected	23159
Independent reflections	12756 [R(int) = 0.0248]
Completeness to theta = 25.242°	99.9 %
Absorption correction	Semi-empirical from equivalents
Refinement method	Full-matrix least-squares on F^2
Data / restraints / parameters	12756 / 1408 / 1000
Goodness-of-fit on F^2	1.015
Final R indices [I>2sigma(I)]	R1 = 0.0484, wR2 = 0.1008
R indices (all data)	R1 = 0.0810, wR2 = 0.1135
Extinction coefficient	n/a
Largest diff. peak and hole	0.408 and -0.317 $e.Å^{-3}$

X-Ray Structure Determination for complex **4** (CCDC: 1489626)

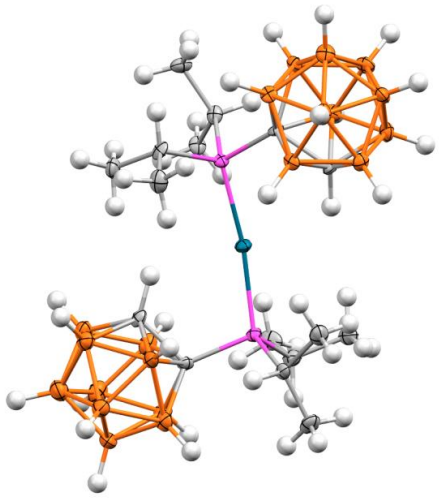

Figure 5-54 Solid-state structure of complex **4**

A light grey thin needle fragment (0.488 x 0.049 x 0.010 mm^3) was used for the single crystal x-ray diffraction study of $C_{16}H_{50}B_{20}P_2Pd$ (complex **4**). The crystal was coated with paratone oil and mounted on to a cryo-loop glass fiber. X-ray intensity data were collected at 100(2) K on a Bruker APEX2 platform-CCD x-ray diffractometer system (fine focus Mo-radiation, λ = 0.71073 Å, 50KV/30mA power). The CCD detector was placed at a distance of 5.0600 cm from the crystal.

A total of 2400 frames were collected for a hemisphere of reflections (with scan width of 0.3° in ω, starting ω and 2θ angles at -25°, and ϕ angles of 0°, 90°, 120°, and 180° for every 600 frames, 120 sec/frame exposure time). The frames were integrated using the Bruker SAINT software package and using a narrow-frame integration algorithm. Based on an orthorhombic crystal system, the integrated frames yielded a total of 139053 reflections at a maximum 2θ angle of 50.700° (0.83 Å resolution), of which 11980 were independent reflections (R_{int} = 0.1783, R_{sig} = 0.0808, redundancy = 11.6,

completeness = 99.9%) and 8483 (70.8%) reflections were greater than $2\sigma(I)$. The unit cell parameters were, **a** = 13.7415(10) Å, **b** = 22.9967(17) Å, **c** = 41.3835(31) Å, $\alpha = \beta = \gamma = 90^{o}$, V = 13077.6(17) $Å^3$, Z = 16, calculated density D_c = 1.274 g/cm^3. Absorption corrections were applied (absorption coefficient μ = 0.676 mm^{-1}; max/min transmission = 0.993/0.734) to the raw intensity data using the SADABS program.

The Bruker SHELXTL software package was used for phase determination and structure refinement. The distribution of intensities (E^2-1 = 0.883) and systematic absent reflections indicated one possible space group, Pbca. The space group Pbca (#61) was later determined to be correct. Direct methods of phase determination followed by two Fourier cycles of refinement led to an electron density map from which most of the non-hydrogen atoms were identified in the asymmetric unit of the unit cell. With subsequent isotropic refinement, all of the non-hydrogen atoms were identified. There were two molecules of $C_{16}H_{50}B_{20}P_2Pd$ present in the asymmetric unit of the unit cell. The hight R(int) value for the equivalent reflections was due to the weakly diffracting poor quality crystal and the difficulty of getting suitable absorption correction parameters for a very thin needle fragment. The connectivities of the molecule are accurate but the bond distances and angles have high degree of standard uncertainty.

Atomic coordinates, isotropic and anisotropic displacement parameters of all the non-hydrogen atoms were refined by means of a full matrix least-squares procedure on F^2. The H-atoms were included in the refinement in calculated positions riding on the atoms to which they were attached. The refinement converged at R1 = 0.0718, wR2 =

0.1329, with intensity, I>2σ(I). The largest peak/hole in the final difference map was 1.367/-1.109 e/Å^3.

Crystal data and structure refinement for complex **4**. (CCDC: 1489626)

Identification code	vL172JE_0m	
Empirical formula	C16 H50 B20 P2 Pd	
Formula weight	627.10	
Temperature	100(2) K	
Wavelength	0.71073 Å	
Crystal system	Orthorhombic	
Space group	P b c a	
Unit cell dimensions	a = 13.7415(10) Å	α= 90°.
	b = 22.9967(17) Å	β= 90°.
	c = 41.383(3) Å	γ = 90°.
Volume	13077.6(17) Å^3	
Z	16	
Density (calculated)	1.274 Mg/m^3	
Absorption coefficient	0.676 mm^{-1}	
F(000)	5152	
Crystal size	0.488 x 0.049 x 0.010 mm^3	
Theta range for data collection	1.771 to 25.350°.	
Index ranges	-16<=h<=16, -27<=k<=27, -46<=l<=49	
Reflections collected	139053	
Independent reflections	11980 [R(int) = 0.1783]	
Completeness to theta = 25.242°	99.9 %	
Absorption correction	Semi-empirical from equivalents	
Refinement method	Full-matrix least-squares on F^2	

Data / restraints / parameters	11980 / 0 / 719
Goodness-of-fit on F^2	1.156
Final R indices [I>2sigma(I)]	R1 = 0.0718, wR2 = 0.1329
R indices (all data)	R1 = 0.1116, wR2 = 0.1449
Extinction coefficient	n/a
Largest diff. peak and hole	1.367 and -1.109 e.$Å^{-3}$

X-Ray Structure Determination for complex **5** (CCDC: 1489629)

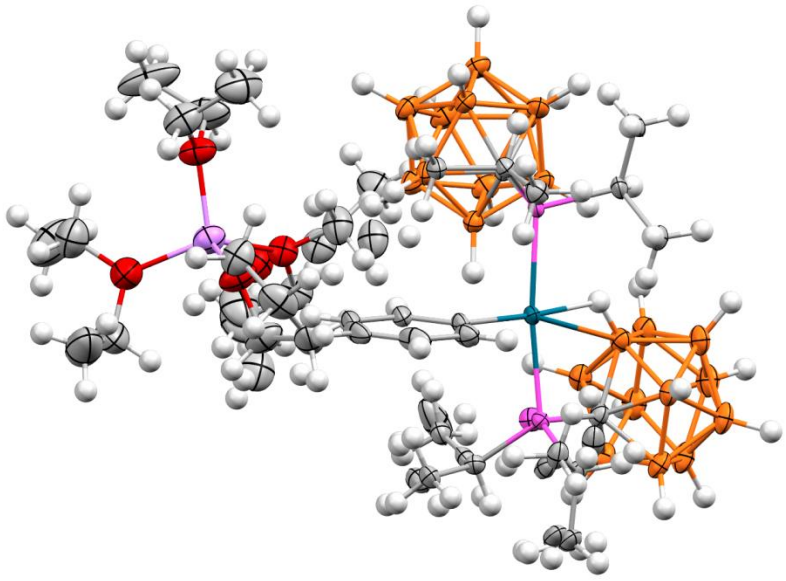

Figure 5-55 Solid-state structure of complex **5**

A colorless needle fragment (0.556 x 0.144 x 0.054 mm^3) was used for the single crystal x-ray diffraction study of $[CB_{11}H_{11}]_2[P[C_3H_7]_2]_2C_6H_5Pd.Li[C_4H_{10}O]_3[C_4H_8O]$ (complex **5**). The crystal was coated with paratone oil and mounted on to a cryo-loop glass fiber. X-ray intensity data were collected at 100(2) K on a Bruker APEX2 platform-CCD x-ray diffractometer system (fine focus Mo-radiation, λ = 0.71073 Å, 50KV/30mA power). The CCD detector was placed at a distance of 5.0600 cm from the crystal.

A total of 8400 frames were collected for a sphere of reflections (with scan width of 0.3° in ω and ϕ, starting ω and 2θ angles of -30°, and ϕ angles of 0°, 45°, 90°, 120°, 135°, 180°, 215°, 240°, 270°, and 305° for every 600 frames, two sets of 1200 frames with ϕ-scan from 0-360° (starting $\omega/2\theta$ angles of -10°/-10° and -30°/-30°), 60 sec/frame

exposure time). The frames were integrated using the Bruker SAINT software package and using a narrow-frame integration algorithm. Based on a monoclinic crystal system, the integrated frames yielded a total of 242731 reflections at a maximum 2θ angle of 56.564° (0.75 Å resolution), of which 13958 were independent reflections (R_{int} = 0.0420, R_{sig} = 0.0172, redundancy = 17.4, completeness = 99.9%) and 11862 (85.0%) reflections were greater than $2\sigma(I)$. The unit cell parameters were, **a** = 19.1204(4) Å, **b** = 16.5121(4) Å, **c** = 19.7932(4) Å, β = 115.8275(7)°, V = 5624.8(2) Å^3, Z = 4, calculated density D_c = 1.185 g/cm^3. Absorption corrections were applied (absorption coefficient μ = 0.422 mm^{-1}; min/max transmission = 0.799 /0.978) to the raw intensity data using the SADABS program.

The Bruker SHELXTL software package was used for phase determination and structure refinement. The distribution of intensities (E^2-1 = 0.937) and systematic absent reflections indicated one possible space group, P2(1)/c. The space group P2(1)/c (#14) was later determined to be correct. Direct methods of phase determination followed by two Fourier cycles of refinement led to an electron density map from which most of the non-hydrogen atoms were identified in the asymmetric unit of the unit cell. With subsequent isotropic refinement, all of the non-hydrogen atoms were identified. There was one disordered anion of $[CB_{11}H_{11}]_2[P[C_3H_7]_2]_2C_6H_5Pd$ and one disordered cation of $Li[C_4H_{10}O]_3[C_4H_8O]$ present in the asymmetric unit of the unit cell. The disorder of the anion was at one of the two $P[C_3H_7]_2$-groups (disordered site occupancy ratios was

75%/25%). The disorder of the cation was at one of the three $C_4H_{10}O$-groups (disordered site occupancy ratios was 80%/20%).

Atomic coordinates, isotropic and anisotropic displacement parameters of all the non-hydrogen atoms were refined by means of a full matrix least-squares procedure on F^2. The H-atoms were included in the refinement in calculated positions riding on the atoms to which they were attached. The refinement converged at R1 = 0.0382, wR2 = 0.1006, with intensity $I>2\sigma$ (I). The largest peak/hole in the final difference map was 1.122/-0.647 e/Å^3. The high residual electron density peak/hole is probably due to absorption correction errors and unresolved possible disorder near one of the three $C_4H_{10}O$-groups.

Crystal data and structure refinement for complex **5**. (CCDC: 1489629)

Identification code	vL129AC_0m	
Empirical formula	C36 H93 B22 Li O4 P2 Pd	
Formula weight	1003.20	
Temperature	100(2) K	
Wavelength	0.71073 Å	
Crystal system	Monoclinic	
Space group	P 21/c (#14)	
Unit cell dimensions	a = 19.1204(4) Å	α= 90°.
	b = 16.5121(4) Å	β= 115.8275(7)°.
	c = 19.7932(4) Å	γ = 90°.
Volume	5624.8(2) Å^3	
Z	4	

Density (calculated)	1.185 Mg/m^3
Absorption coefficient	0.422 mm^{-1}
F(000)	2120
Crystal size	0.556 x 0.144 x 0.054 mm^3
Theta range for data collection	1.709 to 28.282°.
Index ranges	-25<=h<=25, -22<=k<=22, -26<=l<=26
Reflections collected	242731
Independent reflections	13958 [R(int) = 0.0420]
Completeness to theta = 25.242°	99.9 %
Absorption correction	Semi-empirical from equivalents
Refinement method	Full-matrix least-squares on F^2
Data / restraints / parameters	13958 / 87 / 701
Goodness-of-fit on F^2	1.057
Final R indices [I>2sigma(I)]	R1 = 0.0382, wR2 = 0.1006
R indices (all data)	R1 = 0.0485, wR2 = 0.1085
Extinction coefficient	n/a
Largest diff. peak and hole	1.122 and -0.647 $e.Å^{-3}$

X-Ray Structure Determination for complex **6** (CCDC: 1489628)

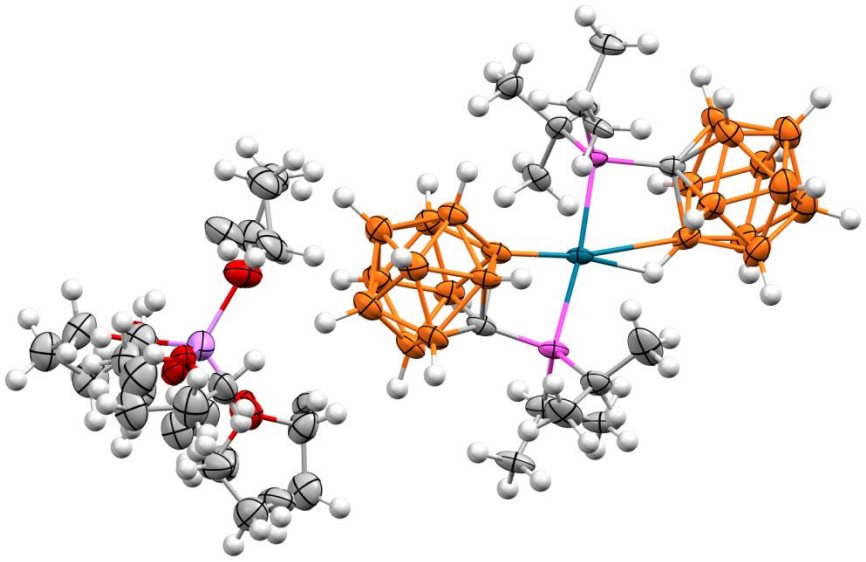

Figure 5-56 Solid-state structure of complex **6**

A colorless thin needle fragment (0.545 x 0.096 x 0.046 mm^3) was used for the single crystal x-ray diffraction study of $[Li[C_4H_8O]_4]^+.[C_{14}H_{49}B_{22}P_2Pd]^-$ (complex **6**). The crystal was coated with paratone oil and mounted on to a cryo-loop glass fiber. X-ray intensity data were collected at 100(2) K on a Bruker APEX2 platform-CCD x-ray diffractometer system (fine focus Mo-radiation, λ = 0.71073 Å, 50KV/30mA power). The CCD detector was placed at a distance of 7.1000 cm from the crystal.

A total of 1323 frames were collected for a hemisphere of reflections (with scan width of 0.3° in ω). The starting ω and 2θ angles were set to -22°, -26°, and, -24° with ϕ angles of 0° (600 frames), 90° (600 frames), and 45° (123 frames), respectively. The exposure time was at 120 sec/frame. The frames were integrated using the Bruker SAINT software package and using a narrow-frame integration algorithm. Based on a monoclinic crystal system, the integrated frames yielded a total of 34843 reflections at a

maximum 2θ angle of 46.514° (0.90 Å resolution), of which 13797 were independent reflections (R_{int} = 0.0792, R_{sig} = 0.1193, redundancy = 2.5, completeness = 95.5%) and 9096 (65.9%) reflections were greater than 2σ(I). The unit cell parameters were, **a** = 20.296(3) Å, **b** = 8.3209(11) Å, **c** = 59.641(7) Å, **β** = 93.7182(18)°, V = 10051(2) Å^3, Z = 8, calculated density D_c = 1.215 g/cm^3. Absorption corrections were applied (absorption coefficient μ = 0.466 mm^{-1}; max/min transmission = 0.979/0.785) to the raw intensity data using the SADABS program.

The Bruker SHELXTL software package was used for phase determination and structure refinement. The distribution of intensities (E^2-1 = 0.807) and systematic absent reflections indicated one possible space group, P2(1)/c. The space group P2(1)/c (#14) was later determined to be correct. Direct methods of phase determination followed by two Fourier cycles of refinement led to an electron density map from which most of the non-hydrogen atoms were identified in the asymmetric unit of the unit cell. With subsequent isotropic refinement, all of the non-hydrogen atoms were identified. There were two disordered cation of $[Li[C_4H_8O]_2]^+$ and two anions of $[C_{14}H_{49}B_{22}P_2Pd]^-$ present in the asymmetric unit of the unit cell. Five of the eight THF molecules of the two cations were modeled with disorder (disordered site occupancy ratios were 82%/18%, 61%/39%, 57%/43%, 56%/44%, and 55%/45%). The check cif B C and G-levels alert were mostly due to the poor quality crystal where only low resolution data can be collected. Possible non-merohedral twinning was observed but the final integration was done using the matrix of the major component only. The atoms connectivity is accurate but

the standard uncertainty for the bond lengths and angles are high due to the poor quality crystal and unresolved twinning.

Atomic coordinates, isotropic and anisotropic displacement parameters of all the non-hydrogen atoms were refined by means of a full matrix least-squares procedure on F^2. The H-atoms were included in the refinement in calculated positions riding on the atoms to which they were attached. The refinement converged at R1 = 0.0810, wR2 = 0.1612, with intensity $I>2\sigma$ (I). The largest peak/hole in the final difference map was 1.375/-0.959 e/Å^3. The high peak/hole from the electron density map is probably due to absorption corrections error.

Crystal data and structure refinement for complex **6**. (CCDC: 1489628)

Identification code	vL115AC_70A_0m	
Empirical formula	C30 H81 B22 Li O4 P2 Pd	
Formula weight	919.04	
Temperature	100(2) K	
Wavelength	0.71073 Å	
Crystal system	Monoclinic	
Space group	P 21/c	
Unit cell dimensions	a = 20.296(3) Å	α= 90°.
	b = 8.3209(11) Å	β= 93.7182(18)°.
	c = 59.641(7) Å	γ = 90°.
Volume	10051(2) Å^3	
Z	8	
Density (calculated)	1.215 Mg/m^3	
Absorption coefficient	0.466 mm^{-1}	

F(000)	3856
Crystal size	0.545 x 0.096 x 0.046 mm^3
Theta range for data collection	1.645 to 23.257°.
Index ranges	-22<=h<=19, -9<=k<=8, -65<=l<=55
Reflections collected	34843
Independent reflections	13797 [R(int) = 0.0792]
Completeness to theta = 25.242°	76.0 %
Absorption correction	None
Refinement method	Full-matrix least-squares on F^2
Data / restraints / parameters	13797 / 1899 / 1255
Goodness-of-fit on F^2	1.084
Final R indices [I>2sigma(I)]	R1 = 0.0810, wR2 = 0.1612
R indices (all data)	R1 = 0.1300, wR2 = 0.1776
Extinction coefficient	n/a
Largest diff. peak and hole	1.375 and -0.959 e.$Å^{-3}$

Computational Details

All DFT calculations were carried out using the Gaussian09 program suite, at the B3PW91 level of theory[59,60]. Pd, Cl, and P were treated with the corresponding Stuttgart-Dresden RECP (relativistic effective core potential) in combination with their adapted basis sets[61-63], each one augmented by an extra set of polarization functions[64]. The remaining atoms were represented by a 6-31G(d,p) basis set[65]. In addition, solvent

effects were considered throughout the optimizations herein by using the SMD solvation model (solvent=benzene)[66]. The nature of the species connected by a given transition state structure was confirmed by intrinsic reaction coordinate (IRC) calculations, while intrinsic reaction paths (IRPs)[67] were traced from the various transition structures to make sure that no further intermediates exist. Analysis of the electron distribution function was made on the basis of QTAIM (Quantum Theory of Atoms In Molecules), with the search and topological analysis of bond critical points (BCPs) done by using the Multiwfn program[68].

Potential addition of phosphine to intermediate **III**.

From intermediate **III**, a possible outcome besides a chloride abstraction or σ-bond metathesis step is the re-association of the phosphine to afford a putative species **V**. However, **V** is 33 kcal/mol less stable than **III** and henceforth unlikely to exist. This destabilization is most likely due to the loss of the electrostatic interactions between the carborane fragment and the metal center. It should be noted that in the square-planar geometry of **V**, the two phosphines are *trans*- to each other (Figure 5-57).

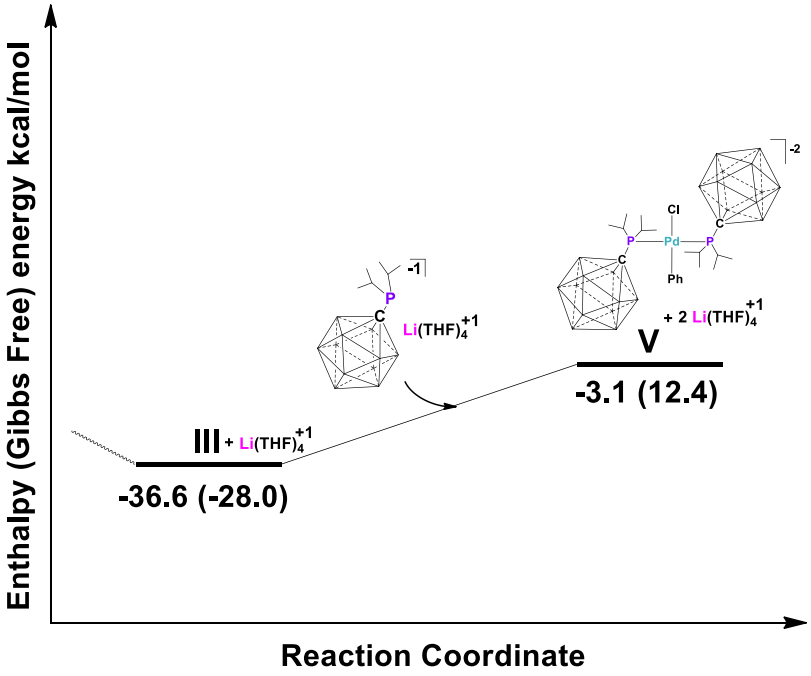

Figure 5-57 Probable re-association of the phosphine to intermediate **III**

Alternative reaction pathway for the formation of complex **6**

From intermediate **5** to complex **6**, a transition state $\mathbf{TS_{5\text{-}6}}$ is located on the PES but stands at almost 43 kcal/mol higher than **5**, making this process kinetically inaccessible and excluded from further consideration (Figure 5-58). The latter high activation barrier is probably the result of the increased steric bulk induced by the carboranyl phosphine in order for σ-bond metathesis to be accomplished, but also from the loss of the hydrogen ionic interaction between the carboranyl phosphine with the palladium center. This interaction is present in **5** and **6** as well, contributing considerably in their total energy stabilization.

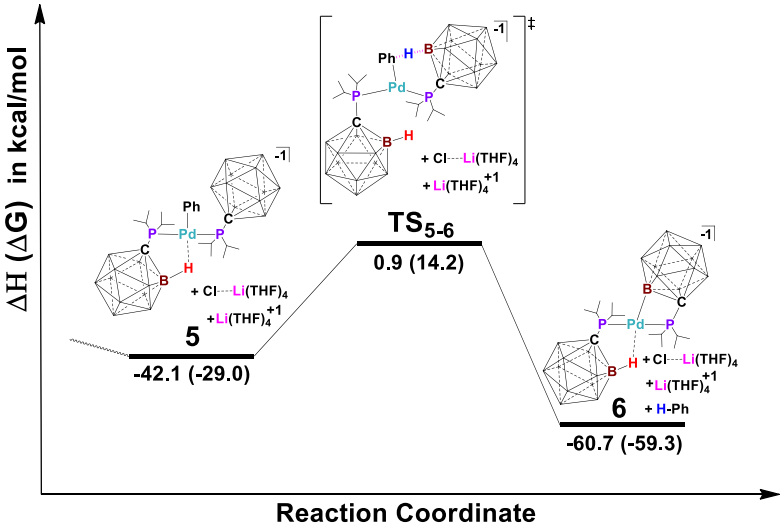

Figure 5-58 Formation of complex **6** from **5** in one step

Figure 5-59 shows an alternative reaction pathway from complex **5** to complex **6**. Instead of passing through the $\mathbf{TS_{5\text{-}6}}$ which showed orientation of the carboranyl phosphine group closest to the phenyl group to undergo cyclometalation, $\mathbf{TS_{VI\text{-}VII}}$ shows rotation of the other carbonayl phosphine around the Pd-P axis to adopt a geometry for σ-bond metathesis to take place. However, this alternative reaction pathway is also found not to be plausible. After phosphine rotation, intermediate **VI** is higher in energy by almost 20 kcal/mol with respect to **5.** Though an agostic interaction is present, the carboranyl phosphine steric bulk decreases its stability relative to **5**, pointing out that steric effects govern the energy destabilization observed over electronic effects. From intermediate **VI** to intermediate **VII**, the transition requires an activation barrier of 10 kcal/mol to give a relative stable intermediate **VII** where benzene is formed and a B-H agostic bond is present. The overall enthalpy change of +30 kcal/mol is prohibitive for

this reaction route to occur. Plausible rotation of the carboranyl phosphine that has agostic interaction with the metal center can give the more thermodynamically stable complex **6**. However, this rotation can be energetically very demanding to be accomplished, since the agostic interaction has to be broken. Unfortunately, this kind of transition state was not found after numerous attempts.

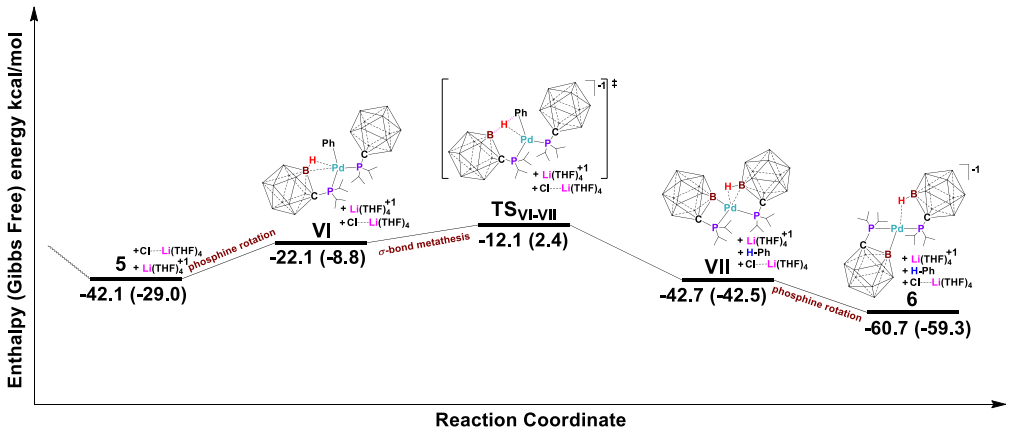

Figure 5-59 Alternative mechanistic pathway for the formation of **6** starting from **5**

A different type of reaction pathway that leads to complex **6** was considered (Figure 5-60). From intermediate **III**, a chloride abstraction from the palladium center occurs, facilitated by ionic interaction between $[Li(THF)_4]^+$ and the palladium complexes to give a coordinatively unsaturated T-shaped palladium complex intermediate **VIII**. **VIII** is located at 16.0 kcal/mol above **III** on the PES, even though there is a stabilizing electrostatic interaction between the carborane cluster and the Pd center. The activation barrier for the following transition state is almost zero, corresponding to a

barrier-less process with respect to intermediate **VIII**. Then, the resulting highly unsaturated intermediate complex upon coordination of the remaining phosphine will afford complex **6**.

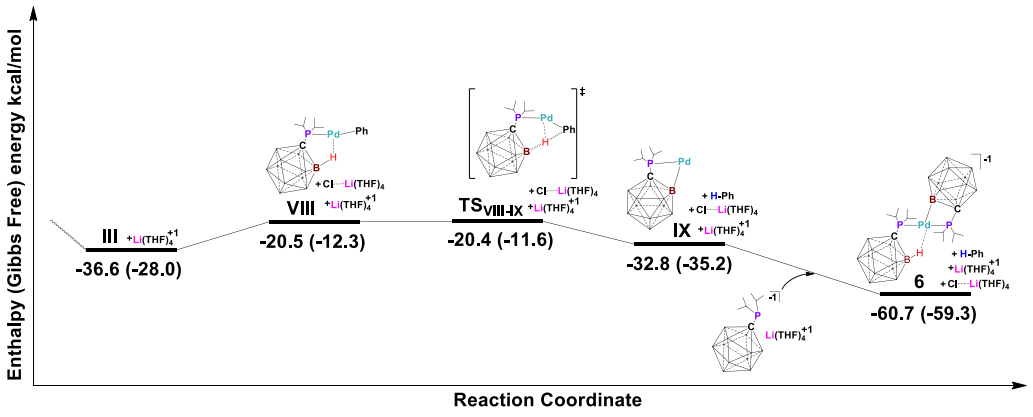

Figure 5-60 Alternative mechanistic profile for the formation of complex **6** from intermediate **III**

Various plausible equilibria for complexes **3** and **4**

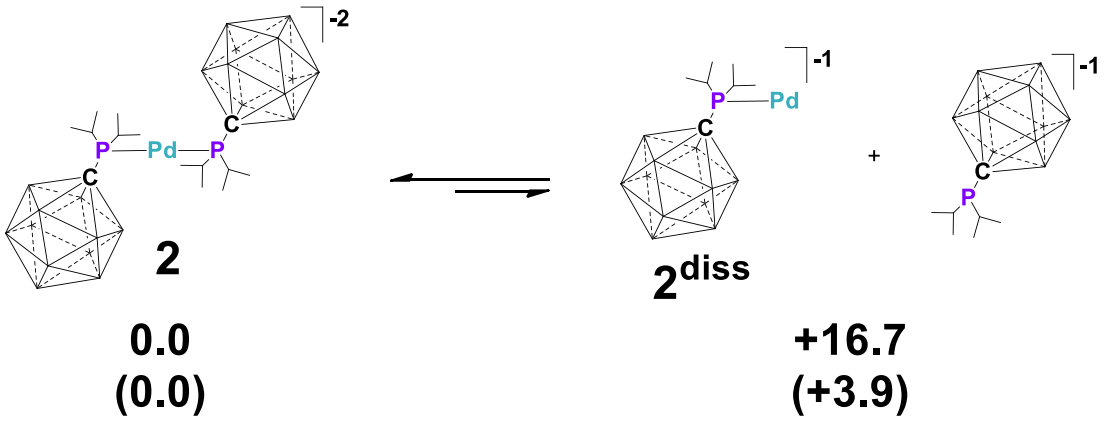

Figure 5-61 Equilibria between complex **2** and the dissociation fragment without considerating the cations. Energy differences correspond to enthalpies and in parenthesis correspond to relative Gibbs free energies. Unlabeled vertices = B-H

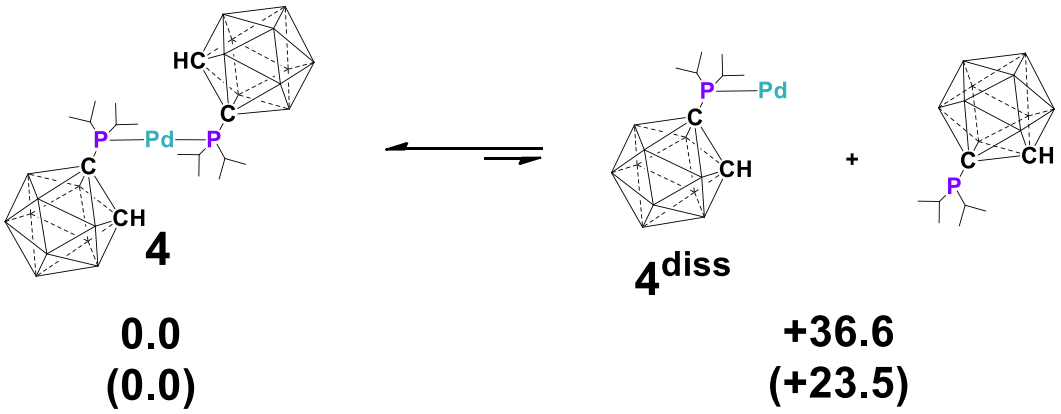

Figure 5-62 Equilibria between complex **4** and the fragments resulted from the dissociation of one phosphine. Energy differences correspond to enthalpies and in parenthesis correspond to relative Gibbs free energies. Unlabeled vertices = B-H

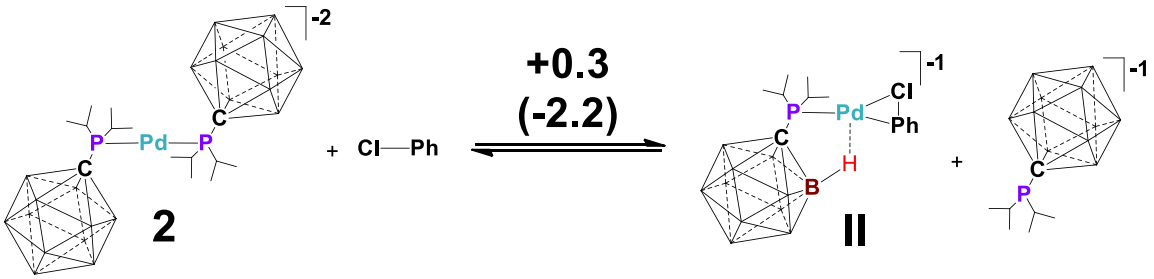

Figure 5-63 Equilibria between complex **2** and pre-complex **II** without considering the cations. Energy differences correspond to enthalpies and in parenthesis correspond to relative Gibbs free energies. Unlabeled vertices = B-H

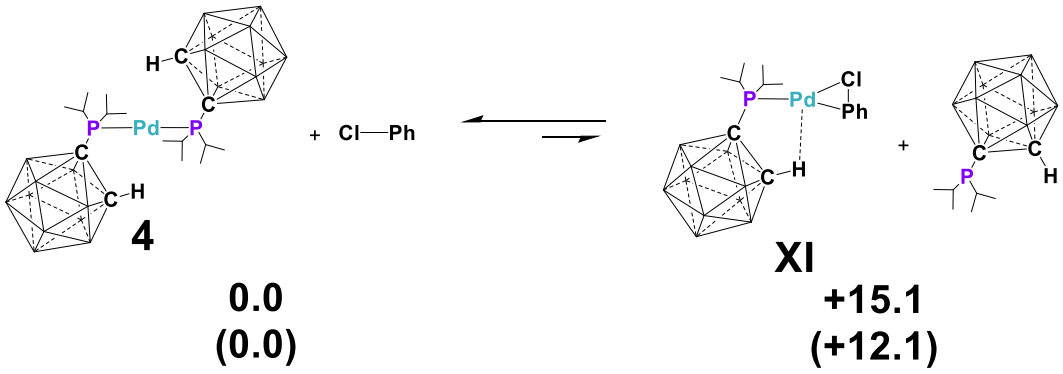

Figure 5-64 Equilibria between complex **4** and pre-complex **XI** without considering the cations. Energy differences correspond to enthalpies and in parenthesis correspond to relative Gibbs free energies. Unlabeled vertices = B-H

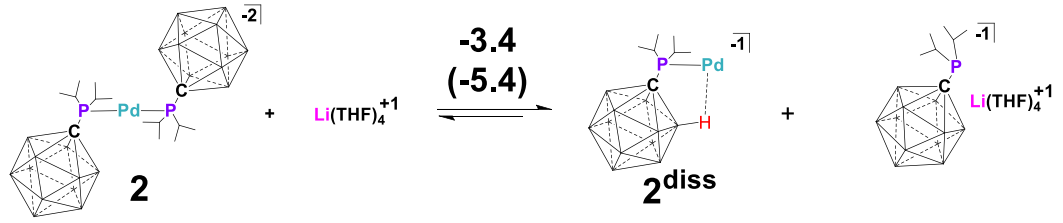

Figure 5-65 Equilibria between complex **2** and the resulting dissociation fragments. Energy differences correspond to enthalpies and in parenthesis correspond to relative Gibbs free energies. Unlabeled vertices = B-H

Plausible oxidative addition of Cl-Ph to complex **4**

As shown independently by Hartwig et al.[41] and Baird et al.[69] through detailed kinetic studies, the first necessary step for the oxidative addition step to occur in a bis-phosphine palladium complex is the dissociation of one of the phosphine ligands. This is also true in our case here, where any attempt to locate a transition state where both bulky phosphines were present was unsuccessful. The substitution of the dissociated phosphine by chlorobenzene corresponds to an exothermic process due to the availability of $[Li(THF)_4]^+$ which will stabilize the dissociated phosphine to form a pair.

This is not the case for the analogous *ortho*-carboranyl phosphine neutral complex, where the substitution reaction costs a noticeable amount of energy (being 15.1 kcal/mol in terms of enthalpy) followed by an activation barrier of almost 11 kcal/mol, making consequently this process extremely kinetically demanding at room temperature. Although the latter activation barrier is very close to the typical activation energy for other related oxidative addition reactions involving coordinated conventional phosphines on palladium complexes, in the case of the dianionic complex **2** the activation barrier is found to be lower by 4.0 kcal/mol, being reminiscent of that calculated in the case of using Ph-Br instead, with the use of the latter corresponding to a kinetically more easily accessible process[70].

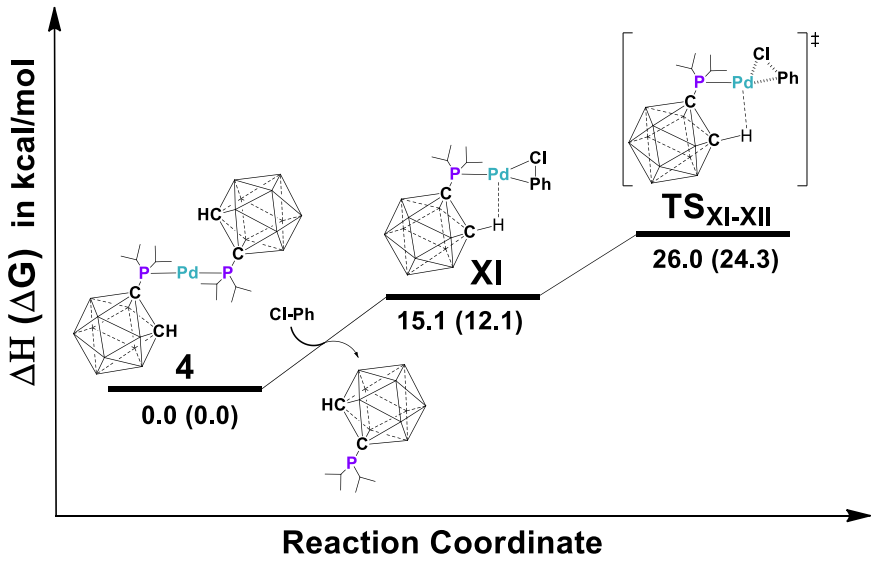

Figure 5-66 Plausible reaction profile for the oxidative addition of Cl-Ph to complex **4.** Energy reaction profiles for the formation of complexes **5** and **6** without the consideration of any ionic pair

The energy reaction profiles depicted in Figure 5-67 correspond to the formation of the complexes **5** and **6** (underlined in black and blue respectively) without consideration of the formation of any plausible pair of ions. Assuming an absence of zwitterions, we observe surprisingly that for the case of the substitution of the phosphine by Cl-Ph, it corresponds to an thermoneutral process and slightly exoergic one, in line with the experimental observations. Also, the significance of electrostatic and stabilizing interactions are shown clearly by the lack of the stabilization of product **5**, which is isoenergetic with respect to **III** (-16.5 kcal/mol). It should be noted that apart from the formation of monoanionic complex **5**, we have considered energetically two molecules of $[Li(THF)_4]^+$ and a "nude" anion of chloride.

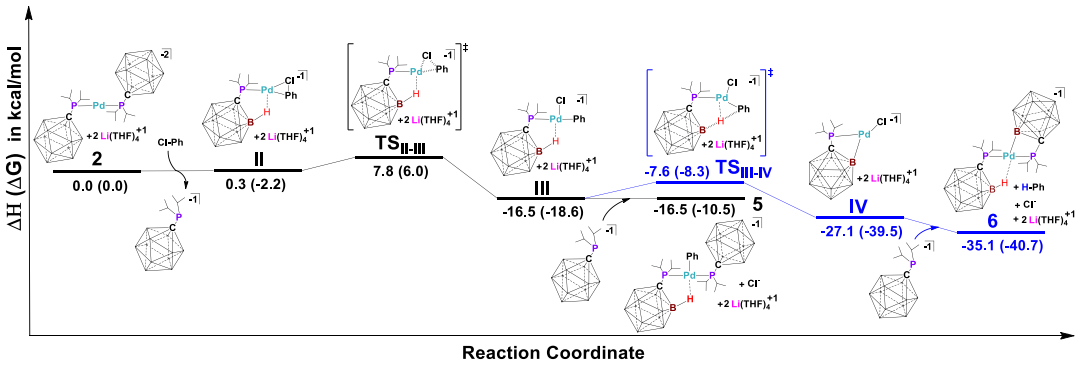

Figure 5-67 Plausible reaction profiles for the formation of the complexes **5** (coloured in black), and 6 (coloured in blue) without consideration of any plausible pair of ions. The values in parenthesis correspond to the relative Gibbs free energies

AIM analysis of the **II**, $\mathbf{TS_{II-III}}$ and **III**

The calculated electron density properties of **II**, **TS_{II-III}** and **III** show that all the Pd···H interactions have low $\boldsymbol{\rho_b}$ for the first two and much bigger value for the third respectively. Also, the Laplacian ($\boldsymbol{\nabla^2\rho_b}$) values are all positive. It should be noted, that the magnitude of both values at the bond critical points (BCPs) gives further information about the nature of the interaction between the two atoms. In particular, the positive values of the Laplacian are characteristic of ionic bonds, and the electron density value between the two atoms falls in the range for ionic and hydrogen bonds. Having this in mind, and based on the calculated values for the BCP of Pd···H bond, quantifies this bond as a weak hydrogen bond with electrostatic character[71-74].

	$\boldsymbol{\rho_b}$	$\boldsymbol{\nabla^2\rho_b}$
II	0.010	0.026
TS_{II-III}	0.012	0.034
III	0.080	0.244

Table 5-2 Properties of the electron density at bond critical point located at the interatomic distance of Pd···H, ρ_b and $\nabla^2\rho_b$ (a.u.) for **II**, **TS_{II-III}** and **III**, calculated at the B3PW91 level of theory

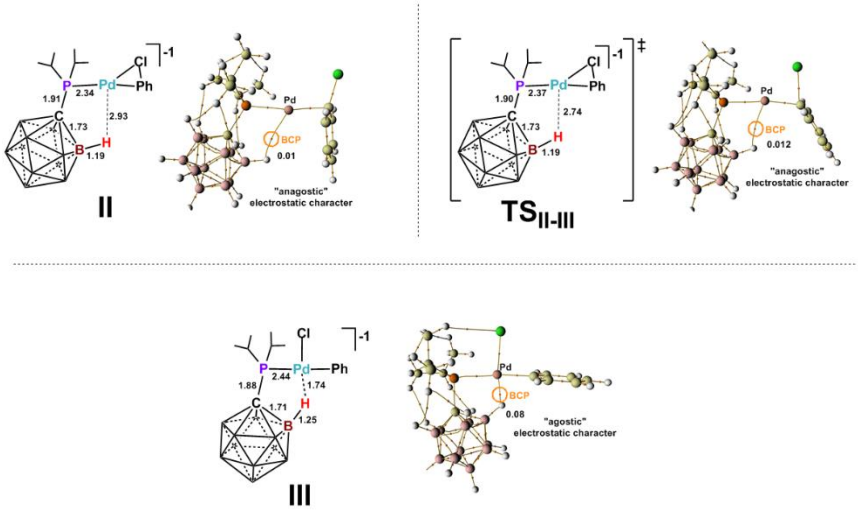

Figure 5-68 Bond critical points (BCP) colored in orange, along with some selected bond distances for the intermediate **II**, TS_{II-III} and intermediate **III**. Unlabeled vertices= B-H

5.5 References

(1) Hanna, L. E.; Jarvo, E. R. *Angewandte Chemie International Edition* **2015**, *54*, 15618.

(2) Girard, S. A.; Knauber, T.; Li, C. J. *Angewandte Chemie International Edition* **2014**, *53*, 74.

(3) Jahn, E.; Jahn, U. *Angewandte Chemie International Edition* **2014**, *53*, 13326.

(4) Vlaar, T.; Ruijter, E.; Maes, B. U. W.; Orru, R. V. A. *Angewandte Chemie International Edition* **2013**, *52*, 7084.

(5) Lennox, A. J.; Lloyd-Jones, G. C. *Angewandte Chemie International Edition* **2013**, *52*, 7362.

(6) Xuan, J.; Zhang, Z. G.; Xiao, W. J. *Angewandte Chemie International Edition* **2015**, *54*, 15632.

(7) Leonori, D.; Aggarwal, V. K. *Angewandte Chemie International Edition* **2015**, *54*, 1082.

(8) Hartwig, J. F. *Accounts of Chemical Research* **2008**, *41*, 1534.

(9) Martin, R.; Buchwald, S. L. *Accounts of Chemical Research* **2008**, *41*, 1461.

(10) Chen, T.; Han, L. B. *Angewandte Chemie International Edition* **2015**, *54*, 8600.

(11) Garcia-Melchor, M.; Braga, A. A.; Lledos, A.; Ujaque, G.; Maseras, F. *Accounts of Chemical Research* **2013**, *46*, 2626.

(12) Surry, D. S.; Buchwald, S. L. *Chemical Science* **2011**, *2*, 27.

(13) Hartwig, J. F. *Accounts of Chemical Research* **2008**, *41*, 1534.

(14) Chen, L.; Ren, P.; Carrow, B. P. *Journal of the American Chemical Society* **2016**, *138*, 6392.

(15) Martin, R.; Buchwald, S. L. *Accounts of Chemical Research* **2008**, *41*, 1461.

(16) Strieter, E. R.; Buchwald, S. L. *Angewandte Chemie* **2006**, *118*, 939.

(17) Barder, T. E.; Biscoe, M. R.; Buchwald, S. L. *Organometallics* **2007**, *26*, 2183.

(18) Estrada, J.; Lugo, C. A.; McArthur, S. G.; Lavallo, V. *Chemical Communications* **2016**, *52*, 1824.

(19) Estrada, J.; Lee, S. E.; McArthur, S. G.; El-Hellani, A.; Tham, F. S.; Lavallo, V. *Journal of Organometallic Chemistry* **2015**, *798, Part 1*, 214.

(20) Estrada, J.; Woen, D. H.; Tham, F. S.; Miyake, G. M.; Lavallo, V. *Inorganic Chemistry* **2015**, *54*, 5142.

(21) El-Hellani, A.; Kefalidis, C. E.; Tham, F. S.; Maron, L.; Lavallo, V. *Organometallics* **2013**, *32*, 6887.

(22) Lavallo, V.; Wright, J. H.; Tham, F. S.; Quinlivan, S. *Angewandte Chemie International Edition* **2013**, *52*, 3172.

(23) Drisch, M.; Sprenger, J. A. P.; Finze, M. *Zeitschrift für anorganische und allgemeine Chemie* **2013**, *639*, 1134.

(24) Fisher, S. P.; El-Hellani, A.; Tham, F. S.; Lavallo, V. *Dalton Transactions* **2016**, *45*, 9762.

(25) Asay, M. J.; Fisher, S. P.; Lee, S. E.; Tham, F. S.; Borchardt, D.; Lavallo, V. *Chemical Communications* **2015**, *51*, 5359.

(26) El-Hellani, A.; Lavallo, V. *Angewandte Chemie International Edition* **2014**, *53*, 4489.

(27) Zhang, J.; Xie, Z. *Accounts of Chemical Research* **2014**, *47*, 1623.

(28) Popescu, A. R.; Teixidor, F.; Viñas, C. *Coordination Chemistry Reviews* **2014**, *269*, 54.

(29) Olid, D.; Nunez, R.; Vinas, C.; Teixidor, F. *Chemical Society Reviews* **2013**, *42*, 3318.

(30) Spokoyny, A. M. *Pure Appl. Chem.* **2013**, *85*, 903.

(31) Douvris, C.; Michl, J. *Chemical Reviews* **2013**, *113*, PR179.

(32) Reed, C. A. *Accounts of Chemical Research* **2009**, *43*, 121.

(33) Li, Y.; Carroll, P. J.; Sneddon, L. G. *Inorganic Chemistry* **2008**, *47*, 9193.

(34) Douvris, C.; Ozerov, O. V. *Science* **2008**, *321*, 1188.

(35) Gutsulyak, D. V.; Gott, A. L.; Piers, W. E.; Parvez, M. *Organometallics* **2013**, *32*, 3363.

(36) Kolychev, E. L.; Kronig, S.; Brandhorst, K.; Freytag, M.; Jones, P. G.; Tamm, M. *Journal of the American Chemical Society* **2013**, *135*, 12448.

(37) Kronig, S.; Theuergarten, E.; Daniliuc, C. G.; Jones, P. G.; Tamm, M. *Angewandte Chemie International Edition* **2012**, *51*, 3240.

(38) Kim, Y.; Jordan, R. F. *Organometallics* **2011**, *30*, 4250.

(39) Thomas, C. M.; Peters, J. C. *Inorganic Chemistry* **2004**, *43*, 8.

(40) Spokoyny, A. M.; Lewis, C. D.; Teverovskiy, G.; Buchwald, S. L. *Organometallics* **2012**, *31*, 8478.

(41) Barrios-Landeros, F.; Carrow, B. P.; Hartwig, J. F. *Journal of the American Chemical Society* **2009**, *131*, 8141.

(42) Biscoe, M. R.; Fors, B. P.; Buchwald, S. L. *Journal of the American Chemical Society* **2008**, *130*, 6686.

(43) El-Hellani, A.; Kefalidis, C. E.; Tham, F. S.; Maron, L.; Lavallo, V. *Organometallics* **2013**, *32*, 6887.

(44) Nunez, R.; Vinas, C.; Teixidor, F.; Sillanpaa, R.; Kivekas, R. *Journal of Organometallic Chemistry* **1999**, *592*, 22.

(45) McAtee, J. R.; Martin, S. E. S.; Ahneman, D. T.; Johnson, K. A.; Watson, D. A. *Angewandte Chemie International Edition* **2012**, *51*, 3663.

(46) Mann, B. E.; Musco, A. *Journal of the Chemical Society, Dalton Transactions* **1975**, 1673.

(47) Huser, M.; Youinou, M.-T.; Osborn, J. A. *Angewandte Chemie International Edition* **1989**, *101*, 1427.

(48) Mitchell, E. A.; Baird, M. C. *Organometallics* **2007**, *26*, 5230.

(49) Sun, C. L.; Li, H.; Yu, D. G.; Yu, M.; Zhou, X.; Lu, X. Y.; Huang, K.; Zheng, S. F.; Li, B. J.; Shi, Z. J. *Nature Chemistry* **2010**, *2*, 1044.

(50) Ke, H.; Chen, X.; Zou, G. *The Journal of Organic Chemistry* **2014**, *79*, 7132.

(51) Paira, R.; Singh, B.; Hota, P. K.; Ahmed, J.; Sau, S. C.; Johnpeter, J. P.; Mandal, S. K. *The Journal of Organic Chemistry* **2016**, *81*, 2432.

(52) Lee, H. W.; Lam, F. L.; So, C. M.; Lau, C. P.; Chan, A. S.; Kwong, F. Y. *Angewandte Chemie International Edition* **2009**, *48*, 7436.

(53) Liu, L.; Zhang, Y.; Wang, Y. *The Journal of Organic Chemistry* **2005**, *70*, 6122.

(54) Ackermann, L.; Potukuchi, H. K.; Althammer, A.; Born, R.; Mayer, P. *Organic Letters* **2010**, *12*, 1004.

(55) Limmert, M. E.; Roy, A. H.; Hartwig, J. F. *The Journal of Organic Chemistry* **2005**, *70*, 9364.

(56) Ohtaka, A.; Teratani, T.; Fujii, R.; Ikeshita, K.; Kawashima, T.; Tatsumi, K.; Shimomura, O.; Nomura, R. *The Journal of Organic Chemistry* **2011**, *76*, 4052.

(57) Wen, J.; Zhang, J.; Chen, S. Y.; Li, J.; Yu, X. Q. *Angewandte Chemie International Edition* **2008**, *47*, 8897.

(58) Iosub, A. V.; Stahl, S. S. *Journal of the American Chemical Society* **2015**, *137*, 3454.

(59) Becke, A. D. *The Journal of Chemical Physics* **1993**, *98*, 5648.

(60) Perdew, J. P.; Wang, Y. *Physical Review B* **1992**, *45*, 13244.

(61) Andrae, D.; Häußermann, U.; Dolg, M.; Stoll, H.; Preuß, H. *Theoretica Chimica Acta* **1990**, *77*, 123.

(62) Bergner, A.; Dolg, M.; Kuchle, W.; Stoll, H.; Preuss, H. *Molecular Physics* **1993**, *80*, 1431.

(63) Martin, J. M. L.; Sundermann, A. *The Journal of Chemical Physics* **2001**, *114*, 3408.

(64) Ehlers, A. W.; Böhme, M.; Dapprich, S.; Gobbi, A.; Höllwarth, A.; Jonas, V.; Köhler, K. F.; Stegmann, R.; Veldkamp, A.; Frenking, G. *Chemical Physics Letters* **1993**, *208*, 111.

(65) Hariharan, P. C.; Pople, J. A. *Theoretica Chimica Acta* **1973**, *28*, 213.

(66) Marenich, A. V.; Cramer, C. J.; Truhlar, D. G. *The Journal of Physical Chemistry. B* **2009**, *113*, 6378.

(67) Gonzalez, C.; Schlegel, H. B. *The Journal of Chemical Physics* **1989**, *90*, 2154.

(68) Lu, T.; Chen, F. *Journal of Computational Chemistry* **2012**, *33*, 580.

(69) Mitchell, E. A.; Jessop, P. G.; Baird, M. C. *Organometallics* **2009**, *28*, 6732.

(70) Rousseaux, S.; Davi, M.; Sofack-Kreutzer, J.; Pierre, C.; Kefalidis, C. E.; Clot, E.; Fagnou, K.; Baudoin, O. *Journal of the American Chemical Society* **2010**, *132*, 10706.

(71) Brookhart, M.; Green, M. L. H. *Journal of Organometallic Chemistry* **1983**, *250*, 395.

(72) Braga, D.; Grepioni, F.; Tedesco, E.; Biradha, K.; Desiraju, G. R. *Organometallics* **1997**, *16*, 1846.

(73) Brookhart, M.; Green, M. L. H.; Parkin, G. *Proceedings of the National Academy of Sciences* **2007**, *104*, 6908.

(74) Stambuli, J. P.; Incarvito, C. D.; Bühl, M.; Hartwig, J. F. *Journal of the American Chemical Society* **2004**, *126*, 1184.